



AIRCRAFT CAPSTONE: DACION FALCO E-1

April 4, 2019

Department of Aerospace Engineering
Ryerson University

CAPSTONE FINAL REPORT

CAPSTONE FINAL REPORT



DACION



FALCO E-1

Nikola Doric	Avionics	Chief Coordinator
Kelvin Tam	Aerodynamics	Co-Coordinator
Issa Baidoun	Propulsion	
Ahmed Elrufaie	Stability	
Sevag Gaprielian	Structures	
Kevin Kan	Aerodynamics	
William Ching Hin Lo	Structures	
Mohamed Nayeem	Avionics	
Niyant Narayan	Structures	
Alana Pitamber	Stability	
Walid Rutagari	Propulsion	
Zi Lin Wang	Propulsion	

Contents

I Book I: DACION FALCO E-1 Overview	1
1 Project Overview	1
2 Project Description with Requirements & Objectives	1
3 Executive Summary	2
3.1 Aerodynamics	2
3.2 Propulsion and Performance	2
3.2.1 Propeller Design	2
3.3 Structures	3
3.3.1 Fuselage	3
3.3.2 Wing Structure	3
3.3.3 Landing Gear	3
3.4 Stability and Control	4
3.5 Cabin Interior	4
3.6 Avionics	4
4 Aircraft Designs	5
II Book II: Aerodynamics Design and Analysis of FALCO E-1	8
1 Aerodynamics Design Criteria & Initial Considerations	8
2 Airfoil Selection	8
3 Final Wing Geometry	11
4 Flaps and Ailerons Sizing	18
4.1 Aileron Sizing	18
4.2 Flap Sizing	20
4.3 Wing Tip Device Considerations	21
5 Computational Fluid Dynamics on FALCO E-1	25
5.1 Analysis Method on Using ANSYS Fluent	25
5.2 FALCO E-1 Clean Configuration Wing CFD Analysis	27
5.3 FALCO E-1 Wing CFD Analysis at Max Flaps Down Configuration	32
5.4 FALCO E-1 Aircraft Analysis	36
5.5 XFLR5 Analysis vs ANSYS Fluent Analysis	38
6 Aerodynamics Conclusion	39
III Book III: Structural Analysis of FALCO E-1	40

1 Material Selection	40
2 Fuselage Design	41
2.1 Stringers and Bulkheads	42
2.2 Firewall	44
2.3 Windscreen and Doors	45
2.4 Skin Panels	47
3 Boom Design	48
4 Structural Analysis	50
4.1 First Iteration	50
4.2 Final Design	51
4.3 Maneuvering Loads	53
5 Landing Gear	56
5.1 Landing Gear Introduction	56
5.2 Design Requirement	56
5.3 Landing Gear Geometry Layout	57
5.4 Static loads and Tire Selection	59
5.5 Tire Selection	59
5.6 Growth and Minimum Clearance Allowance	60
5.7 Material Selection	62
5.8 Nose Landing Gear	62
5.9 Stroke Calculation	63
5.10 Strut Diameter and Piston Diameter	63
5.11 Performance Characteristics of the Shock Absorber	64
5.12 CAD Model	67
5.13 Stress Analysis	69
6 Main Landing Gear	70
6.1 Stroke Calculation	71
6.2 Breaking Energy	73
6.3 CAD Model	74
6.4 Stress Analysis	75
7 Cabin Interior Design	78
7.1 Cabin Front and Rear Seat	80
7.2 Cabin Interior Materials	83
8 Wing Structures	85
8.1 Wing Spars	85
8.2 Wing Ribs	86
8.3 Wing Stiffeners	86
9 Load Analysis	86
9.1 V-n Diagram/Flight Envelope	86

9.2 Load Analysis for Lift	87
9.3 Structural load	88
9.4 Resultant Load Distribution	89
10 Wingbox Design	91
10.1 Structural Idealization	91
10.2 Shear Flow Calculations and Analysis	94
11 Material Selection	96
12 Discussion and Conclusion	98
12.1 Stringer Design and Rib Spacing	98
12.2 Wingbox Design	98
13 Appendix	99
13.1 Wing Load distribution	99
13.2 7.2 Shear Flow Calculations	107
IV Book IV: Avionics Systems for FALCO E-1	118
1 Introduction	118
2 Instruments Panel Design	118
2.1 Design Parameters	118
2.2 Final Instrument List	122
2.3 Instrument Panel Design	124
3 Instruments and Crew-Plane Interface	126
3.1 Glass Cockpit	126
3.2 Six Pack Instruments	127
3.3 Autopilot	128
3.4 Flight management system	129
3.5 Audio Panel	129
3.6 Switches	130
4 Avionics System Design and Framework	131
5 Avionics Engine Control System	132
5.1 Speed Controller	132
5.2 Battery Management System	133
5.3 Battery Charging Station	135
5.4 Portable Battery Charger	136
6 Environmental Control	137
6.1 Aircraft Cooling	137
6.2 Aircraft Heating	138

7 Flight Control System	139
8 Hydraulics	141
9 Exterior Lighting	142
9.1 Strobe Lights & Anti-Collision Lights	142
9.2 Taxi Lights	142
9.3 Wing Inspection Lights	143
9.4 Landing Lights	143
V Book V: Propulsion	144
1 Propulsion Design Parameters & Initial Considerations	144
2 Flight Performance & Range	144
2.1 Mission Profile & Power Requirements	144
2.1.1 Cruise	144
2.1.2 Takeoff	145
2.1.3 Climb	146
2.1.4 Landing	146
2.1.5 Power Requirements & Range Calculation	147
3 Battery Selection	149
3.1 Project Constraints	149
3.2 Selection Process	149
3.2.1 Specific Capacity	150
3.2.2 Life Span	151
3.2.3 Charge and Discharge Rates	152
3.2.4 Operating Conditions	152
3.2.5 Airworthiness & Market Availability	152
3.2.6 In-built Features	153
3.2.7 Battery Cell Chosen	154
3.2.8 Late Battery Change	154
3.3 Layout and Structural Design	155
3.3.1 Positioning & Mass Balance	156
3.3.2 Cooling	158
3.3.3 Safety Considerations	160
3.3.4 Geometry & Stress Analysis	161
3.3.5 In-Depth Stress Analysis	162
3.3.6 Jig Assembly & Changeover Time	163
4 Motor	164
4.1 Propulsion Overview	164
4.2 Motor Selection	165
4.3 Motor Calculation	170
4.4 ENGINE FAILURE PROCEDURE	173

5 Propeller Design Criteria and Initial Consideration	173
5.1 Propeller Material Selection	174
5.2 Propeller Blade Sizing	177
5.3 Contra Rotating Propeller Propulsive System	177
5.4 Propeller Noise Estimation	182
VI Book VI: Stability & Control Analysis	184
1 Theory	184
1.1 Center of Gravity	184
1.2 Static Stability	184
1.3 Wing Contribution	184
1.4 Tail Contribution	185
1.5 Steps for designing the horizontal tail	185
1.6 Steps for designing the vertical tail	189
1.7 Other Considerations	191
1.8 Dynamic Stability	192
2 Results and Discussion	193
2.1 Center of Gravity	193
2.2 Aircraft Weight Optimization	196
2.3 AVL Stability Analysis	198
2.4 Roll Control	205
2.5 Spiral Stability	205
2.6 Tail Sizing and Airfoil Selection	208
2.6.1 Initial design considerations	208
2.6.2 Horizontal and vertical tail initial s	208
2.7 Dynamic Longitudinal Analysis	210
2.7.1 Xflr5 short period longitudinal stability analysis	212
2.7.2 Xflr5 long period motion longitudinal stability analysis	216
2.7.3 AVL short period motion	217
2.7.4 AVL long period motion	219
3 Stability Conclusion	221
VII Book VII: Airworthiness	222
1 Subpart B – Flight	222
1.1 Performance	222
1.1.0.1 Weight and center of gravity	222
1.1.0.2 Performance data	222
1.1.0.3 Stall speed	222
1.1.0.4 Takeoff performance	222
1.1.0.5 Climb requirements	222

1.1.0.6	Climb information	222
1.1.0.7	Landing	222
1.2	Flight Characteristics	222
1.2.0.1	Controllability	222
1.2.0.2	Trim	223
1.2.0.3	Stability	223
1.2.0.4	Stall characteristics, stall warning and spins	223
1.2.0.5	Ground and water handling characteristics	223
1.2.0.6	Vibration, buffeting and highspeed characteristics	223
1.2.0.7	Performance and flight characteristics requirements for flight in icing conditions	223
2	Subpart B-Structures	223
2.1	Structure design envelope	223
2.2	Interaction of systems and structures	223
2.3	Structural loads	224
2.3.1	Flight load conditions	224
2.3.2	Ground Load conditions	224
2.3.3	Level Landing Conditions:	224
2.3.4	One-wheel Landing Conditions:	224
2.3.5	Side Load Conditions:	224
2.3.6	Braked Roll Conditions	225
2.3.7	Supplementary Conditions for Nose Wheels	225
2.3.8	Towing Loads	226
2.4	Structural performance	226
2.4.1	Structural strength	226
3	Subpart D—Design and Construction	227
3.1	Flight control systems	227
3.2	Landing gear systems	227
3.3	Fire protection	227
3.3.1	Lightning protection	227
4	Subpart E—Powerplant	227
4.1	Powerplant installation	227
4.2	Powerplant installation hazard assessment	228
4.3	Powerplant ice protection	228
4.4	Reversing systems	228
4.5	Powerplant operational characteristics	228
5	Subpart F – Equipment	228
5.1	Airplane level systems requirements	228
5.2	Function and installation	228
5.3	Equipment, systems and installations	229
5.4	System power generation, storage and distribution	229
5.5	External and cockpit lighting	229

5.6 Safety equipment	229
5.7 Equipment containing high energy rotors	229
6 Subpart G – Flightcrew Interface and Other Information	229
6.1 Flightcrew interface	229
6.2 Installation and operation	230
6.3 Instrument markings, control markings, and placards	230
6.4 Flight, navigation, and powerplant instruments	230
VIII Book VIII: Cost and Budgeting	231
1 Project Development Costs	231
2 Operational Costs	234
3 Master Cost Structure for FALCO E-1	236
IX Book X: Marketing	237
1 Electric Aircraft Market Overview	237
2 Marketing Strategy	237
3 The Product	237
4 Location & Place	238
5 Promotion	238
6 Price	238
7 Appendices	243
A Preliminary Designs	243
B Avionics	246
C Aerodynamics	250
C.1 Additional Graphs	250
D Propulsion	252
D.1 Motor Technical Data	252
E MATLAB	253
E.1 Aerodynamics	253
E.2 Stability	255
E.3 Landing Gear Stroke MATLAB Code	264
Stroke MATLAB Code	264

E.4	Landing Gear Tire Clearance MATLAB Code	268
	Tire Clearance MATLAB Code	268
E.5	Wing Boom Idealization and Stresses Code	270
E.6	Range MATLAB Code	274
	Range MATLAB Code	274
E.7	Battery Sizing and Positioning MATLAB Code	281
	Battery Sizing and Positioning MATLAB Code	281
F	CATIA Drawings	286
	CATIA DRAWINGS	286
F.1	Landing Gear Drawings	286
F.2	Wing Structure Drawing	303
F.3	Fuselage Structure and Assembly Drawings	304
F.4	Propeller Drawing	306
G	ANSYS Results	311
	ANSYS Results	311
G.1	Landing Gear	311

List of Figures

2.1	DAC-Hybrid Component Composition Airfoils Geometry	9
2.2	DAC-Hybrid Airfoil Geometry	9
2.3	DAC-Hybrid Cl VS Alpha Polar Graph	10
2.4	DAC-Hybrid Cl VS Cd Polar Graph	10
2.5	DAC-Hybrid Cl/Cd VS Alpha Polar Graph	11
3.1	FALCO E-1 Final Wing Geometry	12
3.2	Finalized Wing Lift Curve Polar Graphs	13
3.3	Finalized Wing Drag Curve Polar Graphs	14
3.4	Finalized Wing Moment Curve Polar Graphs	15
3.5	Finalized Wing Viscous Drag Polar Graphs	16
3.6	Finalized Wing Induced Drag Polar Graphs	17
4.1	Lift Distribution of Finalized Clean Wing	19
4.2	Distribution of Sectional Moments along the Wing	19
4.3	Hoerner Wing Tips [1]	21
4.4	Winglets [2]	22
4.5	FALCO E-1 Analysis with Implemented Winglets 80 <i>deg</i>	22
4.6	Comparison of Clean Wing and Implemented Winglets on FALCO E-1	23
4.7	Raked Wing Tips [3]	24
4.8	Vortex Generator [4]	25
5.1	Enclosure Mesh of Wing at Cruise Conditions	28
5.2	Cross Section of Wing Mesh at Cruise Conditions	29
5.3	Close Up of Wing Mesh Cross-Section	29
5.4	Wing Boundary Layer At Cruise Conditions	30
5.5	Residuals for Cruise Analysis Clean Wing Configuration	30
5.6	Clean Wing Configuration Top Pressure Gradient	31
5.7	Clean Wing Configuration Bottom Pressure Gradient	31
5.8	Enclosure Mesh at Flaps Down Configuration Wireframe View	33
5.9	Cross Section at Flaps Down Configuration Wireframe View	34
5.10	Boundary Layer at Flaps Down Configuration Wireframe View	35
5.11	FALCO E-1 in Design Modeller	36
5.12	FALCO E-1 Mesh Wire-Frame View	37
5.13	FALCO E-1 Mesh Cross Section	37
5.14	FALCO E-1 Mesh Analysis Residuals	38
2.1	Falco E-1 Fuselage	41
2.2	Fuselage Structure with Square Bulkheads	42
2.3	Complete Fuselage Structures	43
2.4	Front Firewall	44
2.5	Rear Firewall	44
2.6	Pipistrel Virus Aircraft [5]	45
2.7	Merged Windscreen and Door	46
2.8	Outer Skin	47
2.9	Inner and Outer Skin	48
3.1	Boom Structures With Batteries	48

3.2 Boom Structure With Skin and Batteries (transparent to allow visibility of batteries in figure)	49
4.1 First Iteration - Stress	50
4.2 First Iteration - Deformation	51
4.3 Loading for Final Design	51
4.4 Final Design - Stress	52
4.5 Final Design - Deformation	53
4.6 Maneuvering Loading Final Design	53
4.7 Final Design - Maneuvering Stress	54
4.8 Final Design - Maneuvering Deformation	54
5.1 Landing Gear Layout [6]	57
5.2 Landing Gear Geometry Location [6]	58
5.3 Growth and Minimum Clearance Allowance [7]	60
5.4 Load vs Stroke Curve	66
5.5 Nose Landing Gear CAD Model	68
5.6 Nose Landing Gear	69
5.7 Nose Landing Gear Total Deformation	69
5.8 Nose Landing Gear Equivalent Stress	70
6.1 leaf spring gear [6]	71
6.2 leaf spring gear beam width [6]	72
6.3 leaf spring sizing [6]	72
6.4 Finalized leaf spring	73
6.5 Main Landing Gear Assembly View	74
6.6 Main Landing Gear CAD Model Front View	75
6.7 Main Landing Gear CAD Model Rear View	75
6.8 Main Landing Gear Load Layout	76
6.9 Main Landing Gear Total Deformation	76
6.10 Main Landing Gear Equivalent Stress	77
7.1 Cabin Layout (Side View)	78
7.2 Cabin Layout (Top View) - Tentative	79
7.3 Rear Seat	80
7.4 Front seat	80
7.5 Rear Seat with Cup holder and Armrest	81
7.6 USB Port on the Rear Seat	81
7.7 Foldable Rear Seat	82
7.8 Cabin Seat Assembly View	82
7.9 Cabin Seat Front View	83
8.1 Wingbox Structural Components	85
9.1 V-n Diagram at equivalent speeds	86
9.2 Lift Distribution	88
9.3 Wing Structural Load Distribution	89
9.4 PHAA Resultant Load Distribution	89
9.5 PLAA Resultant Load Distribution	90
10.1 Spar and stringer locations	92
12.1 Shear Buckling coefficient	99

2.1	Cessna 172 Instrument Panel Diagram[8]	119
2.2	Instrument Panel Dimensions[9]	121
2.3	Instrument Panel Initial Design CAD	124
2.4	Final Design of the Instrument Panel	125
2.5	Final Design Instrument Panel II	125
3.1	Aspen Avionics Evolution 1000 Pro MAX[10]	126
3.2	6-Pack Arrangement	127
3.3	Genesys System 55X Digital Autopilot[11]	128
3.4	Avidyne IFD550[12]	129
3.5	AMX240 Audio Panel	130
3.6	Rocker Panel[13]	130
4.1	Ballard :AB2000	131
5.1	Motor Controller[14]	132
5.2	Motor Controller PCB[14]	133
5.3	Cell Balancer	133
5.4	Charging Station	135
5.5	Charging Station Specifications	135
5.6	Charging Station Portable	136
5.7	Portable charger functions	136
6.1	Pneumatic Valves	137
6.3	DC heater by Aircraft Spruce[15]	138
7.1	Cessna 172 Aileron Control Mapping[9]	139
7.2	Cessna 172 Elevator Control Mapping[9]	139
7.3	Cessna 172 Elevator Trim Control Mapping[9]	140
7.4	Cessna 172 Rudder Control[9]	140
9.1	Strobe and Anti-Collision lights	142
9.2	Taxi Lights	142
9.3	Taxi Lights	143
9.4	Landing Lights	143
2.1	Common Takeoff Angles	147
3.1	Licerion Battery Module	149
3.2	UN 38.3 Certification Badge	152
3.3	Future Licerion High Capacity Cell	155
3.4	Module Specifications	155
3.5	Side View of Battery Available Space	156
3.6	Top View of Battery Available Space	157
3.7	Battery Section Sizing Code Algorithm	157
3.8	Battery CG with Respect to Pack Positioning	158
3.9	Battery CG Controller Code Algorithm	159
3.10	Front View of the Nose Intakes	159
3.11	Isometric View of the Nose Intakes and Open Engine Bay	160
3.12	Isometric View of Left Rear Intake	160
3.13	Front and Rear Firewalls	161
3.14	Nose Gear Clearance Area	161
3.15	Cessna 172 Engine Mount and Firewall	162

3.16	Front Battery Section Truss Structure	162
3.17	Rear Battery Section Truss Structure	163
3.18	Front Battery Section Truss Structure	163
3.19	Rear Battery Section Truss Structure	164
3.20	Rear Battery Section Truss Structure	164
4.1	Nose Air Intake	168
4.2	NEC Article 430 Motor Branch Circuit Requirements	169
4.3	EMRAX268 Motor	171
4.4	EMRAX228 Motor	171
4.5	EMRAX268 & 228 Motor Placement in Nose	172
5.1	Wood Propeller Analysis	175
5.2	Aluminum Propeller Analysis	176
5.3	Contra Rotating Propeller [16]	178
5.4	Torque, Thrust VS. Speed [16]	181
5.5	Contra Rotating Propeller CAD (Front view)	182
5.6	Contra Rotating Propeller CAD (Top view)	182
1.1	Cm α Graph	189
1.2	Cn β stability graph showing a positive value as stable	191
2.1	Wing Geometry using AVL	198
2.2	Downwash Angle using AVL	199
2.3	Wing Loading Forces using AVL	200
2.4	Forces in Run Case using AVL	201
2.5	Trailing Edges and Normal Vector using AVL	202
2.6	Coefficient of Lift vs Angle of Attack	203
2.7	Yaw Moment Analysis	204
2.8	First Iteration of XFLR Stability Calculation	206
2.9	Second Iteration of XFLR Stability Calculation	207
2.10	Saab 37 Viggen, aft horizontal tail, canard configuration	209
2.11	B2 spirit bomber Tailless aircraft	209
2.12	Different Cases for Tail Designs	210
2.13	Different initial Geometry Configurations	211
2.14	Short Period Cruise at 0 degrees	212
2.15	Short period motion at climb of 7 degrees AoA	213
2.16	Short period motion for descent of -0.5 degrees	214
2.17	Short period motion at max AoA 14 degrees	215
2.18	Long period motion error on Xflr5	216
2.19	Short period motion Position 1 AVL	217
2.20	Short period motion Position 2 AVL	217
2.21	Short period motion Position 3 AVL	218
2.22	Short period motion Position 4 AVL	218
2.23	Long period motion Position 1 AVL	219
2.24	Long period motion Position 2 AVL	219
2.25	Long period motion Position 3 AVL	220
2.26	Long period motion Position 4 AVL	220
2.1	Prescribed Towing Loads Given by CAR	226

A.1	Concept Design 1	243
A.2	Concept Design 2	244
A.3	Final Preliminary Sketch	245
C.1	Clark Y Airfoil Geometry	250
C.2	Airfoil Outlines of	251
C.3	Airfoil Outlines of	251
D.1	EMRAX268 Technical Data Table	252
D.2	EMRAX228 Technical Data Table	253
G.1	MLG Total Deformation with 1.33 limit vertical load factor	311
G.2	MLG Equivalent Stress with 1.33 limit vertical load factor	311
G.3	MLG Total Deformation with 0.5W on one side	312
G.4	MLG Equivalent Stress with 0.5W Acting on One Side	312
G.5	MLG Total Deformation with 0.33W Acting Outboard on On Side	313
G.6	MLG Equivalent Stress with 0.33W Acting Outboard on On Side	313
G.7	NLG Layout with 0.8 Drag Component	314
G.8	NLG Total Deformation with 0.8 Drag Component	314
G.9	NLG Equivalent Stress with 0.8 Drag Component	315
G.10	NLG Layout with Foward Component of 0.4	316
G.11	NLG Total Deformation with Foward Component of 0.4	316
G.12	NLG Equivalent Stress with Foward Component of 0.4	317
G.13	NLG Layout with Side Component of 0.7	317
G.14	NLG Total Deformation with Side Component of 0.7	318
G.15	NLG Equivalent Stress with Side Component of 0.7	318
G.16	Total Deformation of Swivelled Forward with 0.3W Load	319
G.17	Equivalent Stress of Swivelled Forward with 0.3W Load	319
G.18	Total Deformation of Swivelled 45 deg Forward with 0.15W Load	320
G.19	Equivalent Stress of Swivelled 45 deg Forward with 0.15W Load	320

List of Tables

3.1	Final Wing Design Geometric Parameters	11
3.2	Final Interpolated Airfoil Coefficients at Major Angles of Attack Estimated from XFLR5	17
5.1	Aerodynamic Characteristics of FALCO E-1 Wing at Required Cruise Conditions . .	32
5.2	Aerodynamic Characteristics of FALCO E-1 Wing with Max Flap Deflection at Required Cruise Conditions	35
5.3	FALCO E-1 CFD Crusie Analysis	38
1.1	Material Selection for Structural Components of the Air-Frame [17]	40
1.2	Material Selection for Windscreen and Windows [18]	40
2.1	Bulkhead Dimension	42
2.2	Stinger Dimensions	43
2.3	Dimensions of Firewall	45
2.4	Dimensions of Windscreen and Door	46
2.5	Dimensions of Skin Panels	47
3.1	Boom Rib Dimensions	49
3.2	Boom Stinger Dimensions	50
4.1	Fuselage Loading	52
4.2	Fuselage Maneuvering Loading	54
5.1	Given Design Requirement	56
5.2	Aircraft's Weight On Gear and Geometry Layout	58
5.3	Maximum and Minimum Gear Load	59
5.4	Static Load Per Tire	59
5.5	Tire Selection	60
5.6	Minimum Clearance and Tire Deflection Data	61
5.7	Data of Selected Materials	62
5.8	Stroke Calculation Data	63
5.9	Diameter of the strut and Piston	64
5.10	Two Compression Ratio	64
5.11	Calculated Loads at Different Position	64
5.12	Calculation of Isothermal Compression	65
5.13	Selected Material for Each Component on NLG	67
6.1	Leaf Spring Calculation Data	71
6.2	Selected Material for Each Component on MLG	74
7.1	MR&O Requirements Compared to Designed Values [1]	78
7.2	Baggage Dimensions [19]	79
9.1	V-n Diagram Speeds and Mach Numbers	87
9.2	PHAA and PLAA Shear Loads and Moments	91
10.1	Root Dimensions	92
10.2	Wing box Properties	93
10.3	Final Boom Areas and Direct Stresses	94
10.4	Shear stress distribution	96
11.1	Material Selection chart	97
11.2	7175 Aluminum Material Properties	97

13.1 Wing Load Distribution Part 1	99
13.2 Wing Load Distribution Part 2	100
13.3 Wing Load Distribution Part 3	100
13.4 Wing Load Distribution Part 4	101
13.5 Wing Distribution Part 5	101
13.6 Wing Distribution Part 6	102
13.7 Wing Distribution Part 7	103
13.8 Wing Distribution Part 8	103
13.9 Wing Distribution Part 9	104
13.10 Wing Distribution Part 10	105
13.11 Wing Distribution Part 11	106
13.12 Shear FFlow Calculations Part 1	107
13.13 Shear FFlow Calculations Part 2	108
13.14 Shear FFlow Calculations Part 3	109
13.15 Shear FFlow Calculations Part 4	110
13.16 Shear FFlow Calculations Part 5	110
13.17 Shear FFlow Calculations Part 6	111
13.18 Shear FFlow Calculations Part 7	112
13.19 Shear FFlow Calculations Part 8	113
13.20 Shear FFlow Calculations Part 9	113
13.21 Shear FFlow Calculations Part 10	114
13.22 Shear FFlow Calculations Part 11	115
13.23 Shear FFlow Calculations Part 12	116
13.24 Shear FFlow Calculations Part 13	116
13.25 Shear FFlow Calculations Part 14	117
2.1 Instrument Panel Checklist	120
2.2 Final Equipment List	123
3.1 Initial Mass Allocation Estimate	150
3.2 Candidate Battery Ranking Matrix	154
4.1 Table of Objectives and Requirements	165
4.2 Pros and Cons of Each Motor	166
4.3 Electric Motor Trade Study	166
5.1 Fix Pitch Propeller [20]	174
5.2 Variable/Constant Pitch Propeller [20]	174
5.3 Composite Propeller Analysis [21]	176
5.4 Factor K_p for Typical Propeller Types[20]	177
5.5 Propeller Initial Sizing	177
1.1 Ranges of Lateral Stability for Tails	191
2.1 Configuration 1	193
2.2 Configuration 2	194
2.3 Configuration 3	194
2.4 Configuration 4	194
2.5 Configuration 5: Nose Batteries out	195
2.6 Configuration 6: Fuselage Batteries out	196
2.7 Aircraft Weight Optimization	197

2.8	Typical values for horizontal and vertical tail volume coefficients	208
2.9	Chosen tail geometry with stability values	210
1.1	Avionics System Cost Analysis	233
1.2	Structural Raw Material Cost Breakdown	234
1.3	Propulsion System Cost Breakdown	234
3.1	DACION Project Development Cost Analysis	236
3.2	DACION Operational Cost Analysis	236

Nomenclature

α	angle of attack
α_f	Fuselage angle of attack
α_t	Tail angle of attack
h	Horizontal tail efficiency
v	Vertical tail efficiency
Λ	Sweep angle
λ	Wing taper ratio
λ_h	Horizontal tail taper ratio
λ_v	Vertical tail taper ratio
\bar{C}	Mean aerodynamic chord
\bar{C}_h	Horizontal tail MAC
ρ	Air density
σ_β	
AR	Aspect ratio of the wing
AR_h	Horizontal tail aspect ratio
AR_v	Vertical tail aspect ratio
b	Wing span
b_h	Horizontal tail span
b_v	Vertical tail span
c	Speed of light in a vacuum inertial frame
C_L	Coefficient of lift
$C_L\alpha$	Lift curve slope

C_L	Lift curve slope for horizontal tail
C_L	Vertical tail lift curve slope
C_{Lh}	Lift coefficient of horizontal tail
$C_m\alpha$	moment curve slope
C_m	Moment curve slope of the fuselage
C_{mowf}	0 angle of attack moment coefficient of wing-fuselage combination
$C_n\beta$	Directional stability derivative
C_{hroot}	Horizontal tail root chord length
C_{htip}	tip chord length
$C_{l_{\delta_a}}$	Roll Authority
C_{l_p}	Roll Dampening
C_{vroot}	Vertical tail root chord length
C_{vtip}	Vertical tail tip chord length
CG	Center of gravity
D	Drag
D_f	Max fuselage diameter
E	Downwash
E_α	Downwash curve slope
E_o	Reference Downwash
h	Distance between leading edge and cg location
h	Planck constant
h_o	Distance from leading edge to neutral point
i_h	Horizontal tail incidence angle
K_c	Correction factor for different aircraft configurations
K_{fl}	Correction factor

L	Lift
l	boom length
l_h	Boom length with respect to the horizontal tail mean aerodynamic chord
l_v	length between wing MAC and vertical tail MAC
MAC	Mean Aerodynamic Chord
S	Wing planform area
S_h	Horizontal tail planform area
S_v	Vertical tail planform area
V	Velocity
V_c	Cruise velocity
W	Aircraft weight in kilogram
X_{cg}	CG location in terms of MAC
\overline{V}_V	Vertical tail volume coefficient

Part I

Book I: DACION FALCO E-1 Overview

1 Project Overview

DACION is a Canadian based aerospace company that pursues the advancement in greener aviation alternatives. The client, Ryerson University has approached DACION for a partnership to design a general aviation aircraft (similar to the Cessna 172) that shall incorporate a pure electric propulsion system. The team will follow aircraft design regulations by FAR, CAR, FAA and EASA with the purpose to be certified for training, recreational and private use domestically and internationally.

2 Project Description with Requirements & Objectives

The designed aircraft will provide excellent value for the client with lower operating and acquisition cost than a new Cessna 172. A quiet, naturally well lit signature cabin with exceptional interior ergonomics design optimized for training purposes is to be expected with the FALCO E-1. As a replacement to the fuel system, a rechargeable Li-ion battery system will have a turnover time of twenty minutes between flights. As outlined in the project description provided by Ryerson University, a series of flight mission requirements and objectives were provided as direct competition to the Cessna 172's capabilities. In terms of cabin specific requirements, accessibility for luggage will be a unique objective given the size of the referenced aircraft. When taking into consideration the passengers and pilot, an assumed weight for all persons is 200lb, 170lb for body weight, 30lb for luggage.

Ramp appeal must be taken into heavy consideration to not only be visually attractive but also provide functional usability. This includes everything from visibility, visual appeal, comfort, amongst many other aspects. FAR23 and CAR523 regulations will be closely referenced with every design decision made as a team. The maximum empty weight is 1750lbs, but when payload (passengers) is reduced to 500lbs, the empty weight can be increased to 2050lbs to allow for 300lbs more of batteries. Designs other than fixed wing are prohibited and along with meeting all the requirements and/or objectives, it must be shown that the plane will have a return on investment for the OEM as well as the customers that use the aircraft. The aircraft won't be monetizable if the aircraft isn't suitable for flight. Therefore, following the FAA regulations and ensuring the passing of airworthiness tests is crucial.

Since the task at hand is to design a fully electric aircraft, choosing the right power plant components (battery, motor and propeller) will make the FALCO E-1 competitive within its class. The handling characteristics of the aircraft can be aided by an autopilot, although it is an objective, having autopilot helps with marketing, and stability. Passenger comfort is key in

building brand status and helping the reputation of the company. Therefore, compliance to the given list of requirements and objectives will be of DACION's top priority.

Tasks were distributed such that each team member will be involved in one of the core disciplines including: Structural Design and Analysis, Performance/Propulsion, Aerodynamics, Stability and Control, and/or Avionics. It is not necessary for everyone to participate in the non-core subjects but multiple members will have tasks in both core and non-core. Non-core subjects include: Airworthiness, Marketing, Economics, Cabin Interior, etc.

In the end, groups will use their knowledge in all core and non-core subjects, design the aircraft in accordance to the customer requirements and offer desirable features which are competitive, allow for easy maintenance, and make the aircraft suitable for both leisure flying and for training.

3 Executive Summary

3.1 Aerodynamics

In order to fulfill DACION's mission of achieving the best in-class range in electric aircraft performance, the wing design was completely tailored to maximizing aerodynamic efficiency at cruise. By using XFLR5 and ANSYS Fluent, the aerodynamics team was able to refine the airfoil and wing geometry to exceed performance required for mission objectives. The DAC-Hybrid airfoil, the final airfoil selected for the FALCO E-1, was interpolated from the following three existing airfoils: Clark-Y airfoil, SM 701 airfoil, and NASA Prantdl-D Low Drag Root airfoil. The final wing geometry incorporates a compound taper with a taper ratio of 0.59. The wing root has a chord length of 1.35 m, decreasing linearly to a wing tip chord length of 0.8 m. The geometric configuration includes a full wingspan of 13 m with an area of 13.975 m². To improve stalling characteristics and reduce the induced drag, the FALCO E-1 has an aspect ratio of 12.09 and a wing root washout angle of 2.5 degrees. All of the design decisions were made to improve aerodynamic efficiency while keeping stability parameters at an acceptable level. The aerodynamic efficiency of the FALCO E-1 at cruise conditions peak at 15 at 0 °degrees - 0.5 °degrees angle of incidence.

3.2 Propulsion and Performance

3.2.1 Propeller Design

A technical and scientific approach was conducted to design the propeller. The propeller type, material, and blade size were all listed and analyzed in the main content of the propeller section. Since the all the information such as, blade geometry, pitch angle, and thrust produced were difficult to find and proprietary. After collecting the basic data on the existing propeller model, the propeller was selected and the basic parameters were analyzed and discussed. The propeller for DACION FALCO E-1 was determined as contra rotating propeller from CONTRA ELECTRIC PROPULSION LTD. which had two two-balanced composite material propeller (one pull propeller

with the diameter of 178 cm in the front and one push propeller with diameter of 170 cm behind). By doing more research and using a software called OPENVSP, the propeller geometry was designed, and a CATIA model was built for overall aircraft simulation.

3.3 Structures

3.3.1 Fuselage

A technical and aesthetic approach was taken to design the fuselage, boom, windscreens, and firewall. The fuselage was designed to have a circular outside with a square cross section to allow for better comfort for passengers. The boom was designed to house the additional batteries needed to meet the set out MR&O, which can be adjusted to accommodate for the various flying configurations. The windscreens were designed with maximum visibility in mind, as it would appeal to new pilots and trainees. Structural analysis on the structures was successful under normal flight, as well as extreme maneuvering conditions set out by FAR. The maximum stress experienced by the fuselage was 73.9 MPa with a deformation of 0.012 m, under normal loading conditions of 4 passengers and a lower battery configuration. Taking into account the 3.8 maneuvering loading factor, the maximum stress was 133.9 MPa with a maximum deformation of 0.018 m. A factor of safety of 1.5 was used, making the maximum allowable stress 160 MPa. Under both loading conditions, the stress was maintained under the allowable maximum stress of 160 MPa. There is a slight margin in both configurations, allowing for slight errors in flight for new pilots.

3.3.2 Wing Structure

The wingbox was designed with 2 spars and 6 stringers. The material chosen was 7175 Aluminum Alloy with a yield strength of 435 MPa. The direct stresses were calculated using boom structural idealization and a factor of safety of 1.5 was applied in order to make sure the stresses were below 290 MPa. The wingbox was also designed at a maneuvering load factor of +3.8g, in accordance with the FAR part 23 and CAR Chapter 523. The shear flow was also calculated at the root with a factor of safety of 1.5 as well. The wing weight was determined by uploading the CAD CATIA model into ANSYS. The total wing weight was determined to be 172 kg which is a sensible number given the larger size of the wing in comparison to the Cessna 172. Skin panel thickness is 1.1mm from 0m to 2m half span, followed by 0.8mm for the rest of the wing.

3.3.3 Landing Gear

The landing gear was followed the design requirement with a tricycle fixed landing gear configuration. The shock absorber chosen for nose landing gear is oleo-pneumatic shock absorber and main landing gear is leaf spring shock absorber. Through the stroke calculation, the NLG stroke is 20.9931 cm and the MLG stroke is 30.38 cm. The main landing gear was tested in ansys with safety factor of 1.5 and reinforced with a c-beam to make the MLG more stronger.

The materials chosen for all the components of both main and nose landing gear is Titanium Ti-10V-2Fe-3Al, Aluminum A356.0-T6, Aluminum 7075-T6 and 4340 Alloy Steel. The landing gear weight was determined in CATIA, the total weight of the NLG is 25.40 kg and two MLG is 22.3296. Both landing gear was tested in ANSYS for stress analysis with 1.5 safety factor and the required factor (2.25 for NLG and 1.33 for MLG) from CAR 523, and the results shown that it can support the aircraft maximum weight and the impact force from landing.

3.4 Stability and Control

To ensure the safety and comfort of the passengers and crew, DACION made sure the longitudinal and lateral stability of the aircraft is within an acceptable range for different CG locations and angles of attack. With a static margin of 0.3 to 0.6 throughout the flight mission, the aircraft shall be stable throughout this range. This makes the aircraft recover from any destabilizing motion such as long period, phugoid and dutch roll, such that the aircraft returns to its steady state within seconds for short period motion and within a minute for long period motion.

The CG was found by allocating the masses of the aircraft carefully to obtain the desired range of CG. This creates a stable aircraft that is resistant to gust, several disturbances and that is safe.

The tail was designed to specifically withstand any disturbances within the flight envelope and trim the aircraft for a stable flight and to reduce the pilot's fatigue by emphasizing the use of vertical and horizontal tabs. These tabs allow the pilot to pinpoint slight trim angles that increase the aircraft's stability and improve the pilots well being. The tail is also assembled in a way to counteract the propeller's yaw inducing moment by having the incidence of the vertical tail to be -1.5 degrees. An asymmetrical tab, only on the right side, was implemented to also counteract this yaw inducing moment.

3.5 Cabin Interior

Cabin layout was solely based on the MR&O, and the team was able to make a cabin smaller than that of the Cessna 172. The cabin was designed with a minimum cabin width of 50 inch, a minimum cabin height of 46 inch, a cabin seating length of 34 inch in-seat pitch, a cabin length of 96.5 inch, and a baggage area of 17.19 inch.

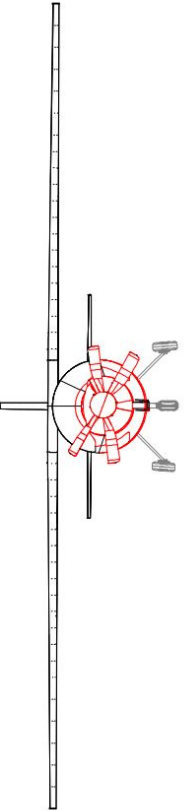
3.6 Avionics

Falco E-1 Avionics was based on the MR&O, the avionics team chose the right equipment based on similar models to Cessna 172. The instrument panel dimensions used were 1000mm in width and 500mm in height to be similar to match the dimensions most manufacturers of instrument panels use for trainer aircraft. A custom manufacturer for the instrument panel cover was used to accommodate for the different instruments used for a fully electric aircraft. All components from the state-of-the-art glass cockpits to the exterior lights is FAA approved or follows the rules and regulations of the FAA.

4 Aircraft Designs

REV.	DATE	BY	REVISION DESCRIPTION

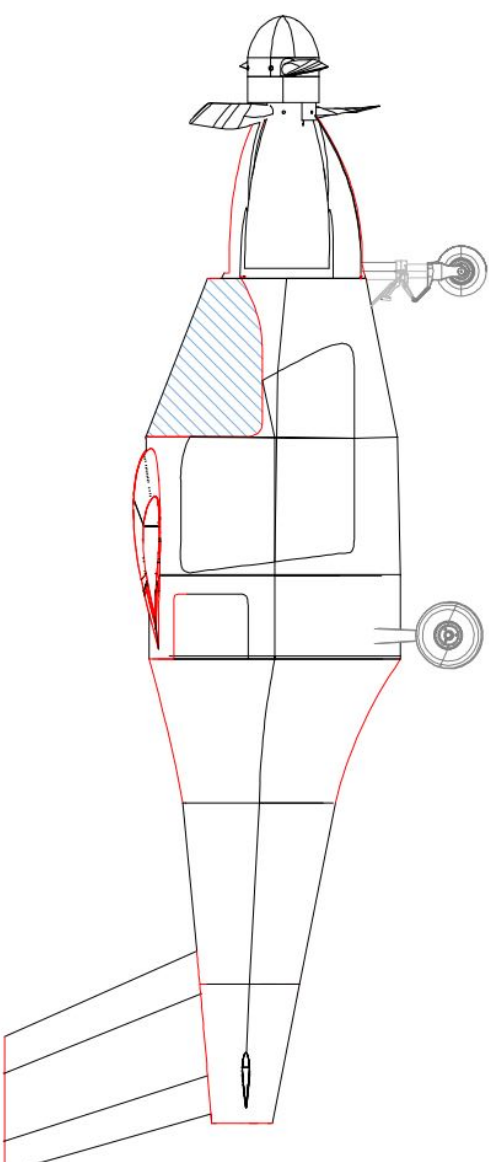
	MATERIAL: Composites	TITLE: Falcon E-1 DACION		
FALCON E-1	NOTICE : This technical drawing of Falcon E-1 is furnished by DACION INC. & is intended for use in aircraft design & development only. It is not to be reproduced, copied or used except for the purpose of producing tools or products exclusively for DACION INC. Copies of this drawing are to be made only when necessary for the purpose stated above & all copies must contain this notice.	SCALE: FULL	PRINTED BY: NASEH NAYEM	REFERENCE: CAB 1.2.3 STOCK DRAW NO: APR-4-2019 DRAWING/MATERIAL NUMBER:



REV.	DATE	BY	REVISION DESCRIPTION

		TITLE: FALCO E-1 DACION	
 FALCO E-1		MATERIAL: Composites	SHEET: 1 of 1 SCALE: FULL APPROVED BY: Naseem Naseem DRAWN BY: NASEEM NAYEEM DATE: APR-4-2019

NOTICE : The drawing is the exclusive property of DACION, INC. & is disclosed to you in strict confidence & with the understanding that it is not to be reproduced, copied, or used except for the purpose of producing tools or products exclusively for DACION, INC. Copies of this drawing one to be made only when necessary for the purpose stated above & all copies must contain this notice.	
REFERENCE: CAB-123 STOCK ROOM NO: DRAWN BY: DRAWN/NAYEEM	

REV.	DATE	BY	REVISION DESCRIPTION
FALCO E-1			
NOTICE :			<p>This drawing is the exclusive property of DACON INC. & is disclosed to you in strict confidence & with the understanding that it is not to be reproduced, copied, or used except for the purpose of producing tools or products exclusively for DACON INC. Copies of this drawing are to be made only when necessary for the purpose stated above & all copies must contain this notice.</p>
MATERIAL:			TITLE: Falco E-1 DACON 
SOLNS:			SCALE: FULL WORKED BY: <input checked="" type="checkbox"/> NASEH NAYEM COPY TO: <input checked="" type="checkbox"/> NASEH NAYEM PART: <input checked="" type="checkbox"/> NASEH NAYEM DRAWING/PART NUMBER: APR-4-2019
REFERENCE:			REF. NO.: C10 1,2,3 WORK SPOT: SHOCK DOOR INC
SHEETS:			1 of 1

Part II

Book II: Aerodynamics Design and Analysis of FALCO E-1

1 Aerodynamics Design Criteria & Initial Considerations

The design process of the wing began with an approximate wing area of 15 m^2 using an estimated V-N diagram and the Cessna 172 Skyhawk as a reference. Using this, the initial wing's aerodynamic criteria was designed for MR&O objective cruise conditions as well as DACION's objective of maximum endurance. The MR&O cruise altitude is 10,000 feet and the objective cruise velocity is 135 KIAS. Using the basic lift equation, the design coefficient of lift (c_L) was calculated as

$$c_L = \frac{L}{\frac{1}{2}\rho V_{cruise}^2 S} = 0.343 \quad (1.1)$$

To account for the tail down-force and other factors that may cause a decrease in lift, the design cruise lift coefficient was determined to be 0.4. Since DACION's objective was to maximize endurance, a high lift-to-drag ratio or aerodynamic efficiency was required. Aside from the performance objective, the airfoil shape shall be thick enough to implement flaps (without the use of slotted flaps beneath) and must be easily manufactured. An airfoil was selected based on the above criteria ensuring favourable aerodynamic characteristics.

2 Airfoil Selection

As mentioned above in Section 1, the airfoil selected must have a lift coefficient near 0.4 and high aerodynamic efficiency between $0^\circ - 5^\circ$ angle of attack (AOA) or incidence angle. The FALCO E-1 utilizes a modified version of the Clark-Y airfoil.

To achieve lower drag the Clark Y airfoil, many iterations of interpolating the Clark Y airfoil with low drag airfoils were done. Through these iterations, a cross product between the Clark Y, SM701, and NASA Prantl-D Low Drag Root airfoil was found to produce the lowest drag while maintaining the required lift. The optimum configuration with the interpolated airfoil consists of a 50/50 split between the Clark Y and SM701, followed by a 70/30 interpolation with the former. This hybrid airfoil named "DAC-Hybrid", is what the FALCO E-1 uses throughout its entire wing. Airfoil outlines of the Clark Y, SM701, and NASA Prantl-D are shown in Figure 2.1 while the airfoil used on the FALCO E-1 is shown in Figure 2.2.

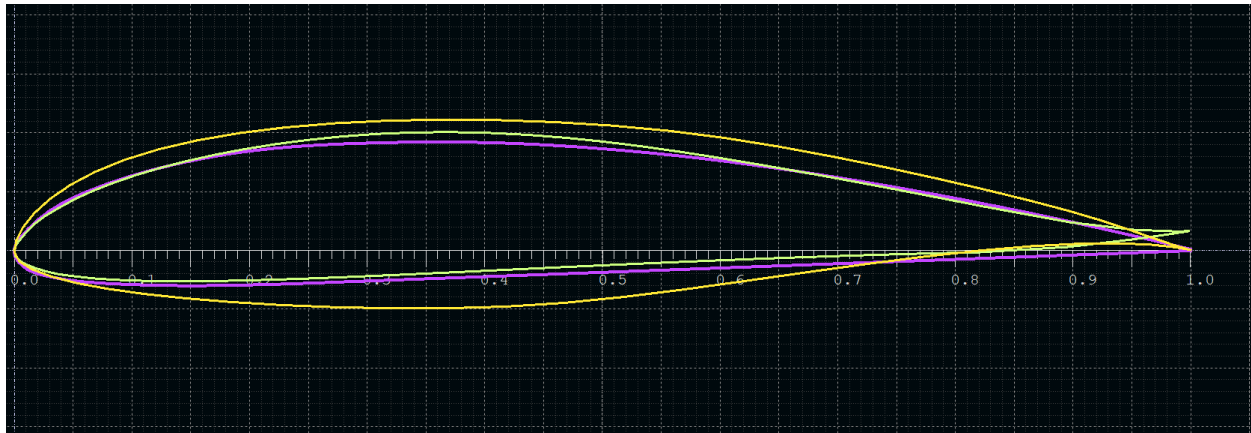


Figure 2.1: DAC-Hybrid Component Composition Airfoils Geometry

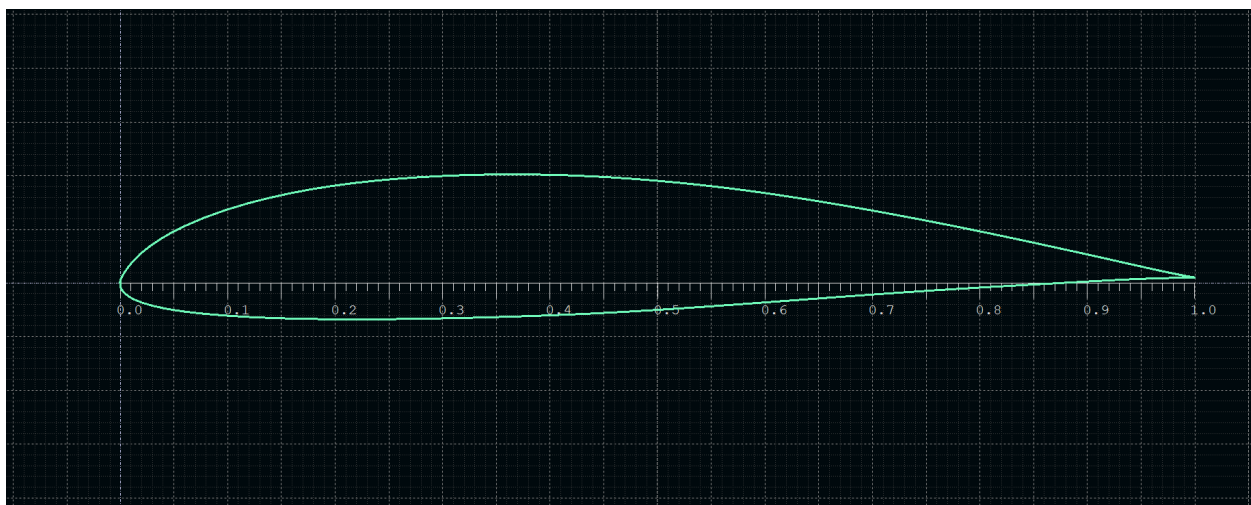


Figure 2.2: DAC-Hybrid Airfoil Geometry

The DAC-Hybrid airfoil was analyzed on XFLR5. The analysis of the airfoil simulated through Reynolds number range of 50000 to 10 million at angle of attack range of -20 to 20 degrees. The large range of Reynolds number ensures a better converging wing during wing analysis. Aerodynamic characteristics of the DAC airfoil are given in the polars shown below in Figure 2.3.

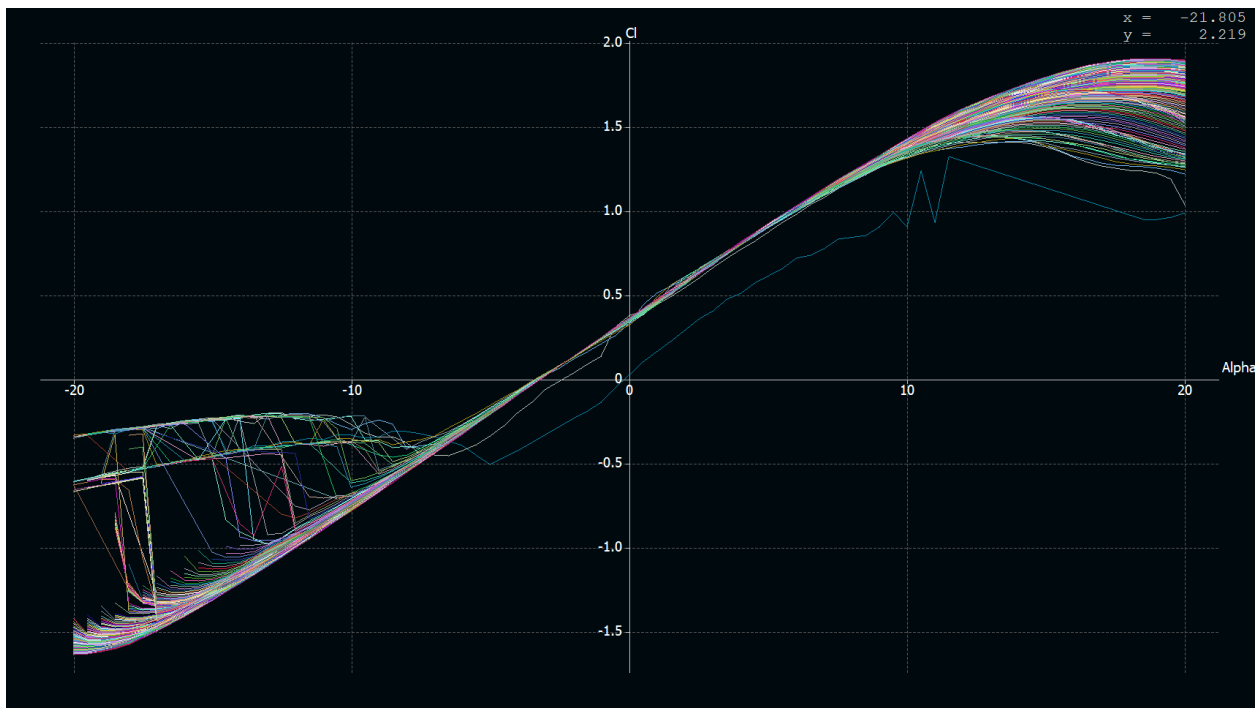


Figure 2.3: DAC-Hybrid Cl VS Alpha Polar Graph

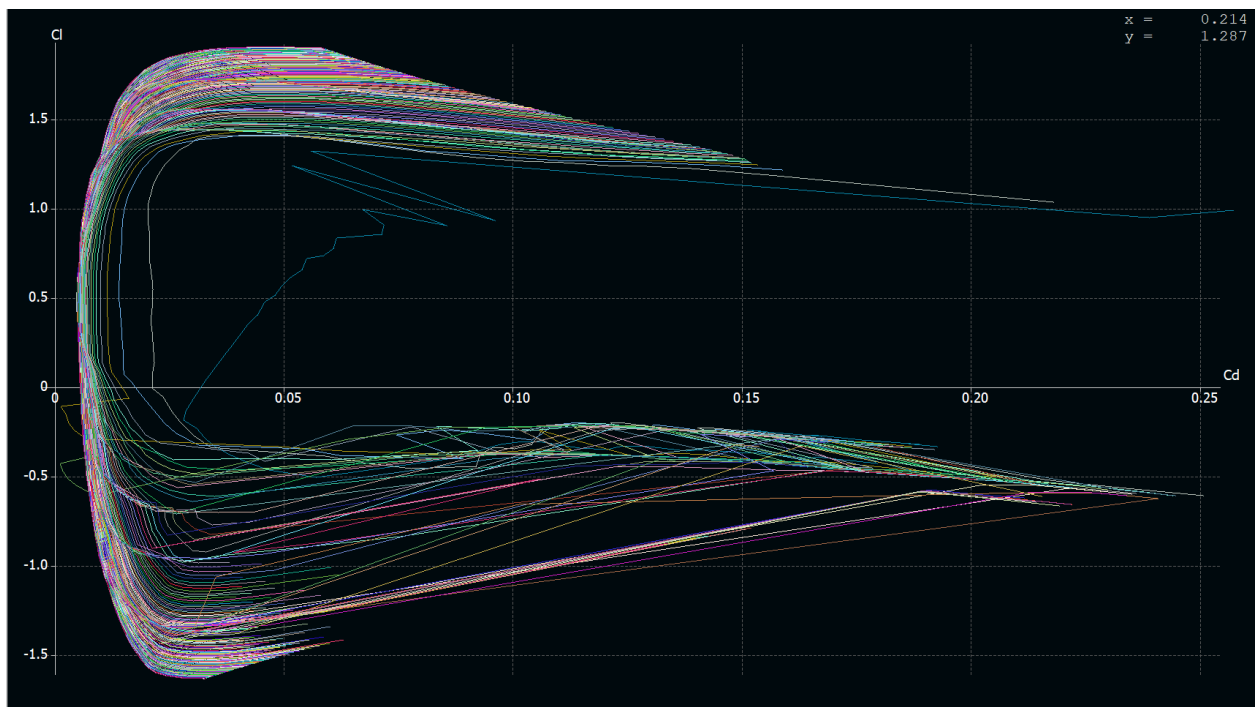


Figure 2.4: DAC-Hybrid Cl VS Cd Polar Graph

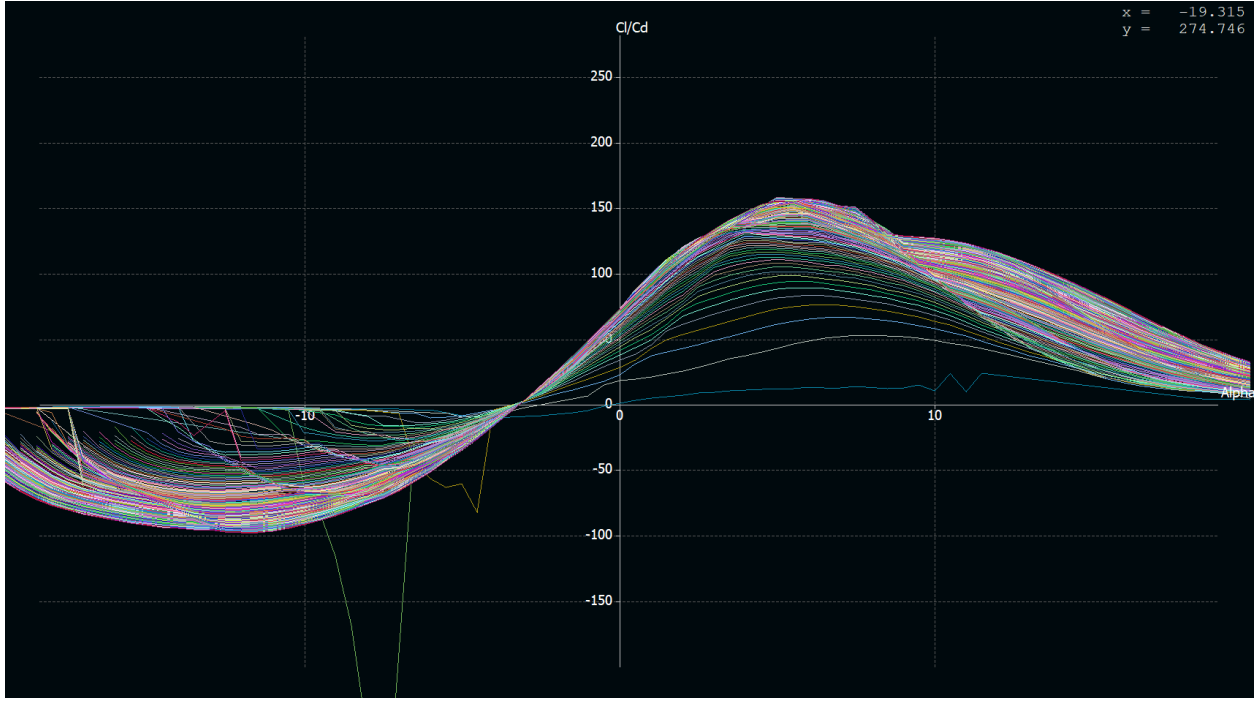


Figure 2.5: DAC-Hybrid Cl/Cd VS Alpha Polar Graph

3 Final Wing Geometry

The final wing was designed with the objective to maximize endurance by increasing the aerodynamic efficiency by doing a compound taper on the wing with a relatively higher aspect ratio. The higher aspect ratio and a compound tapered wing increases Oswald efficiency by making the wing planform and lift distribution elliptical. The compound tapering of the wing also effectively decreases tip vortices and reduces induced drag. A wing root washout angle was implemented to further improve roll stability and allows for the root to stall before the wing tips. Furthermore, the washout shifts the lift-curve slope of the wing to the left, allowing the FALCO E-1 to cruise at 0°- 0.5° thus minimizing fuselage drag. Using XFLR5, the wing geometry was simulated with the DAC-Hybrid airfoil. Below outlines the overall geometry of the final wing:

Table 3.1: Final Wing Design Geometric Parameters

Wing Area	13.98 m^2
Wing Span	13 m
Mean Aerodynamic Center	1.10 m
Aspect Ratio	12.09
Taper Ratio	0.59
Root to Tip Sweep	0 Deg
Wing Root Washout	2.5° Deg
Wing Neutral Point	0.335 m

Figure 3.1 below presents the 3D geometry of the FALCO E-1 wing.

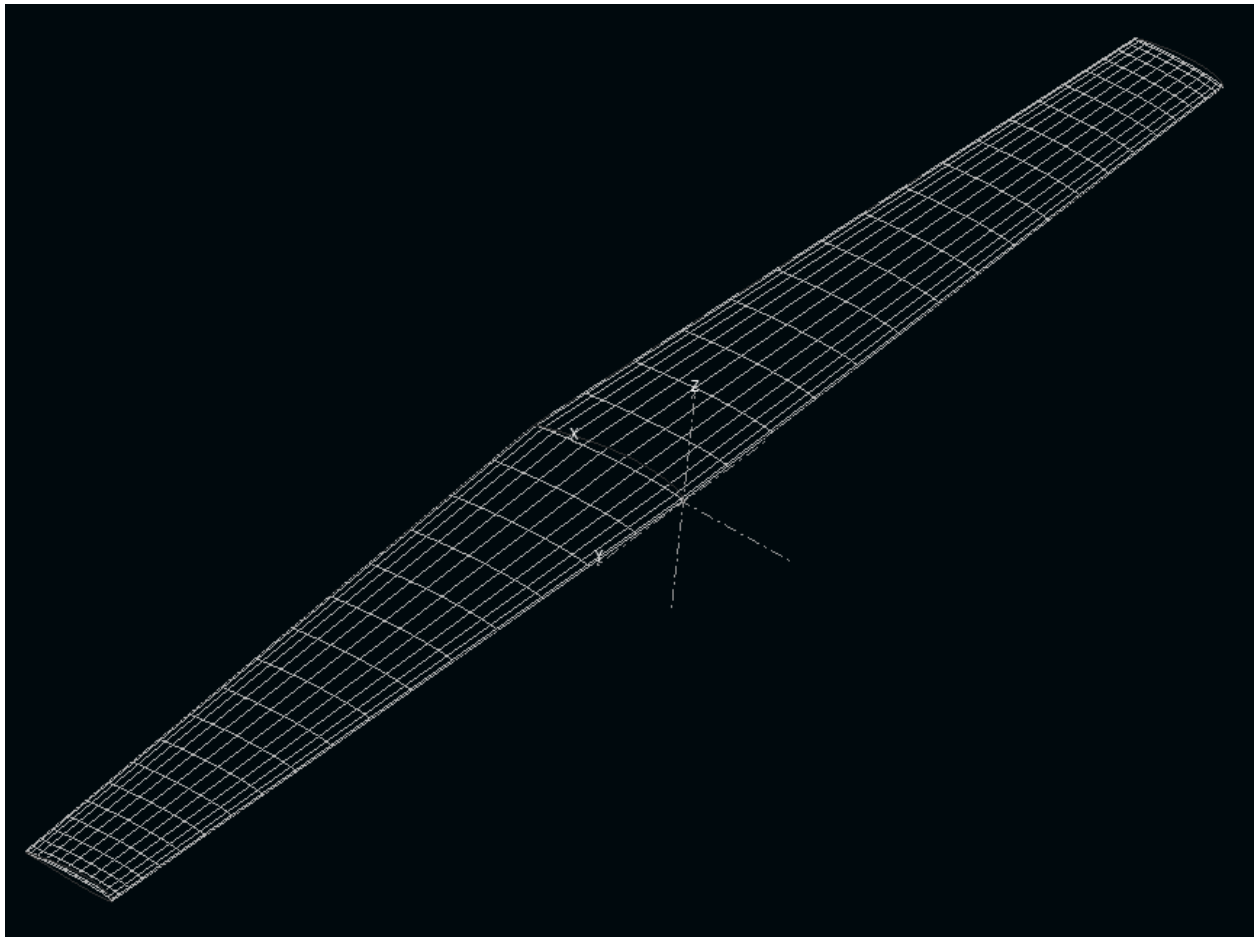


Figure 3.1: FALCO E-1 Final Wing Geometry

A 3-dimensional vortex lattice method wing analysis was completed for cruise velocity equivalent to sea level at angle of attacks ranging from -5 degrees to 17 degrees. This analysis calculates lift, induced drag and pressure distribution on the wing model disregarding viscosity conditions and skin thickness. Important aerodynamic characteristics of the airfoil are detailed in the polars shown in Figures 3.2 to 3.6.

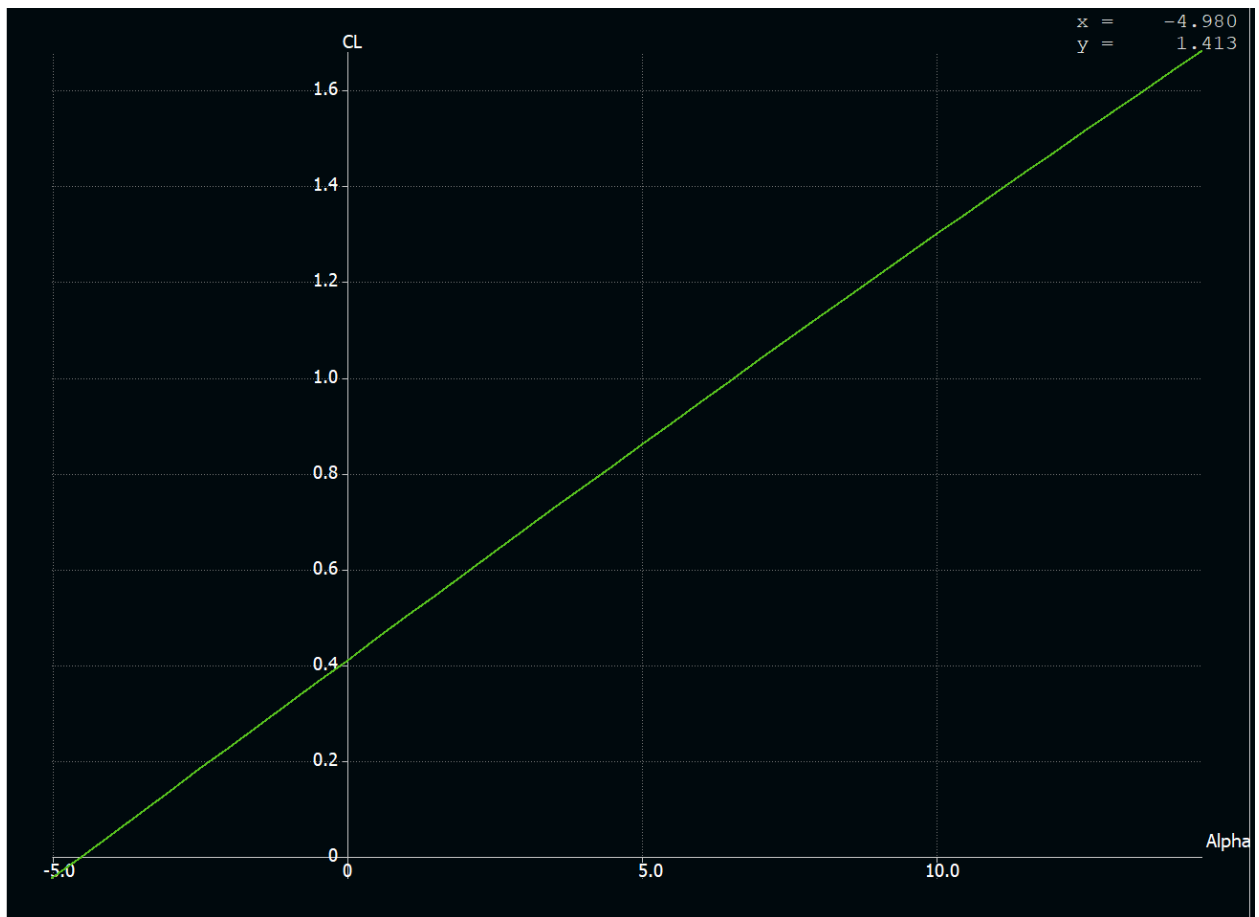


Figure 3.2: Finalized Wing Lift Curve Polar Graphs

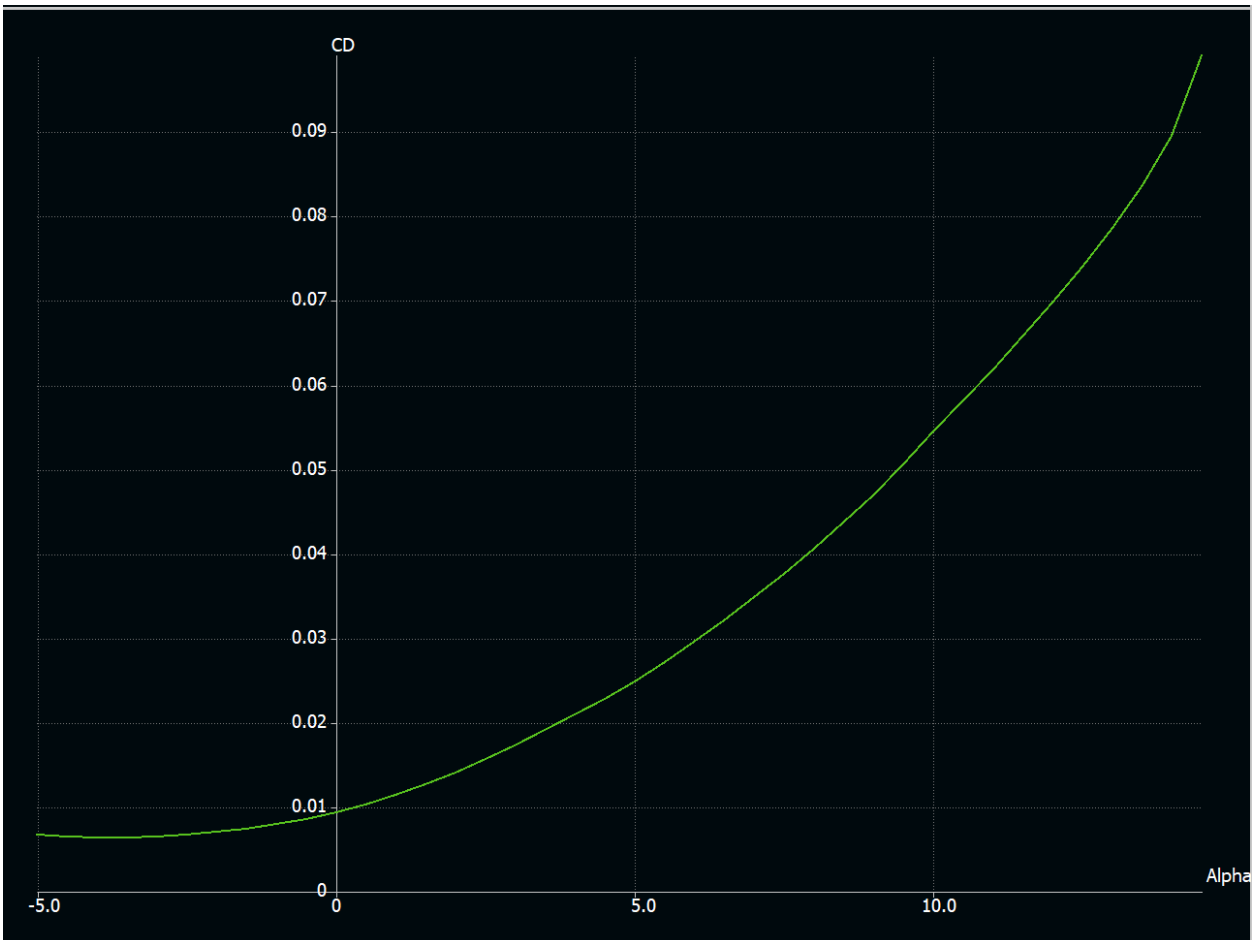


Figure 3.3: Finalized Wing Drag Curve Polar Graphs

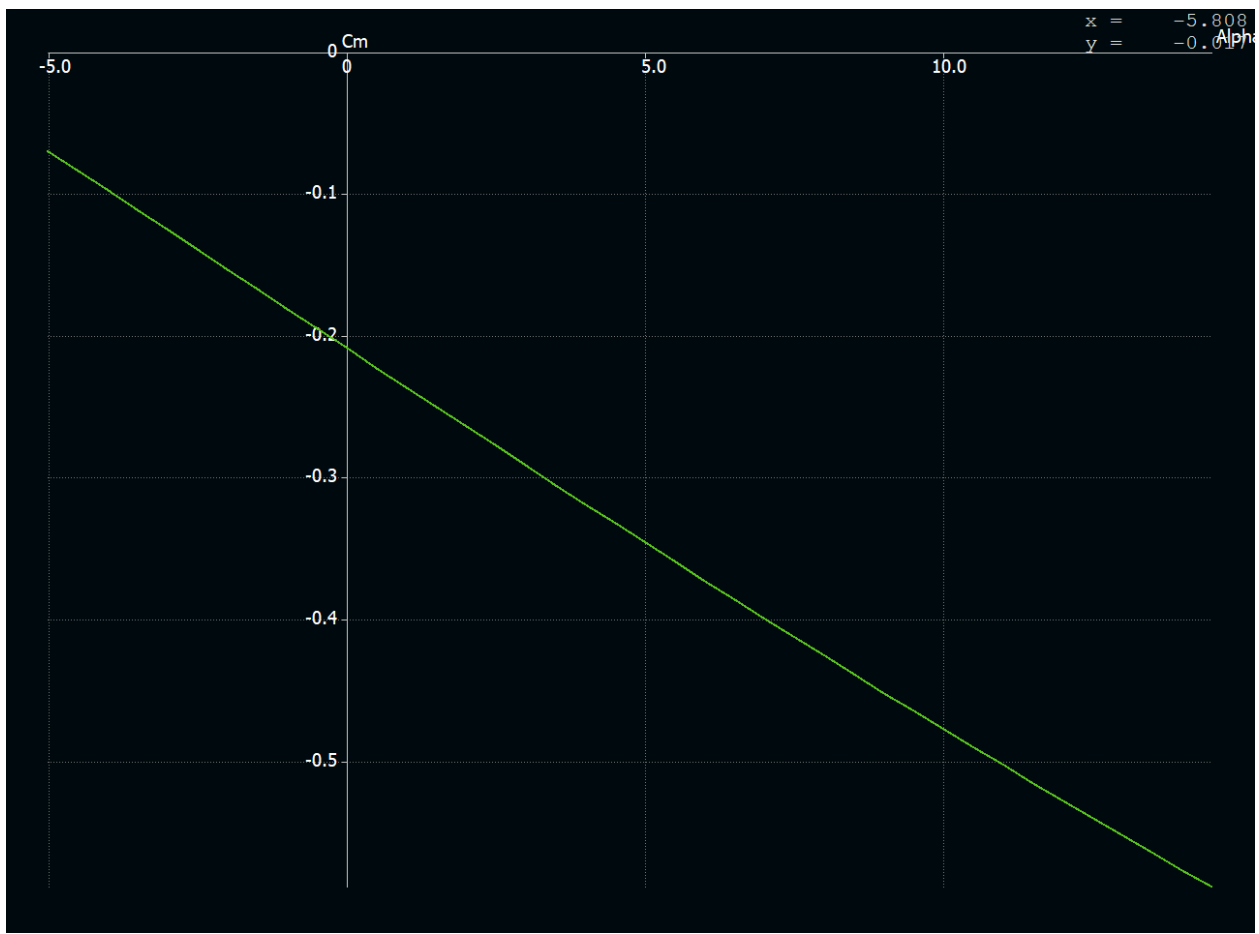


Figure 3.4: Finalized Wing Moment Curve Polar Graphs

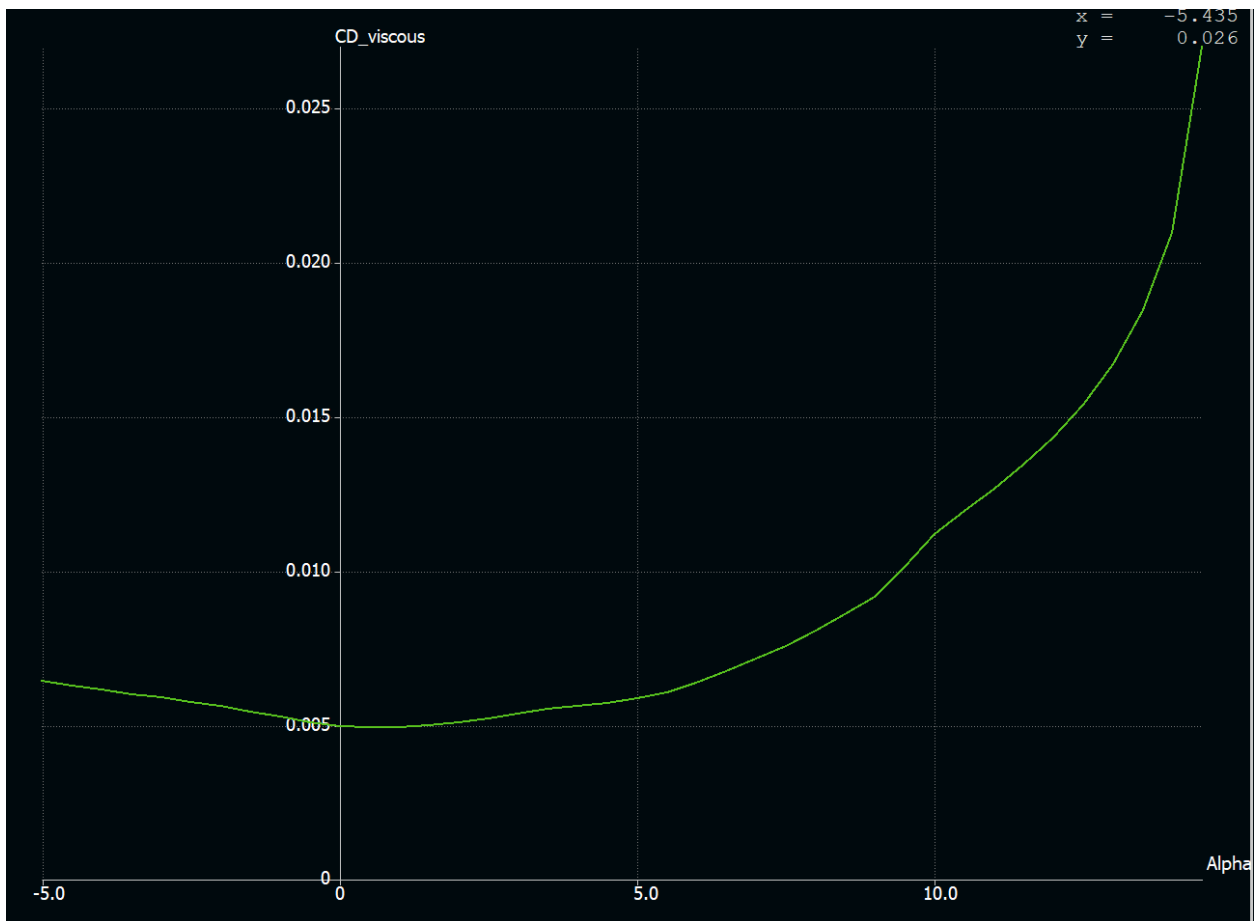


Figure 3.5: Finalized Wing Viscous Drag Polar Graphs

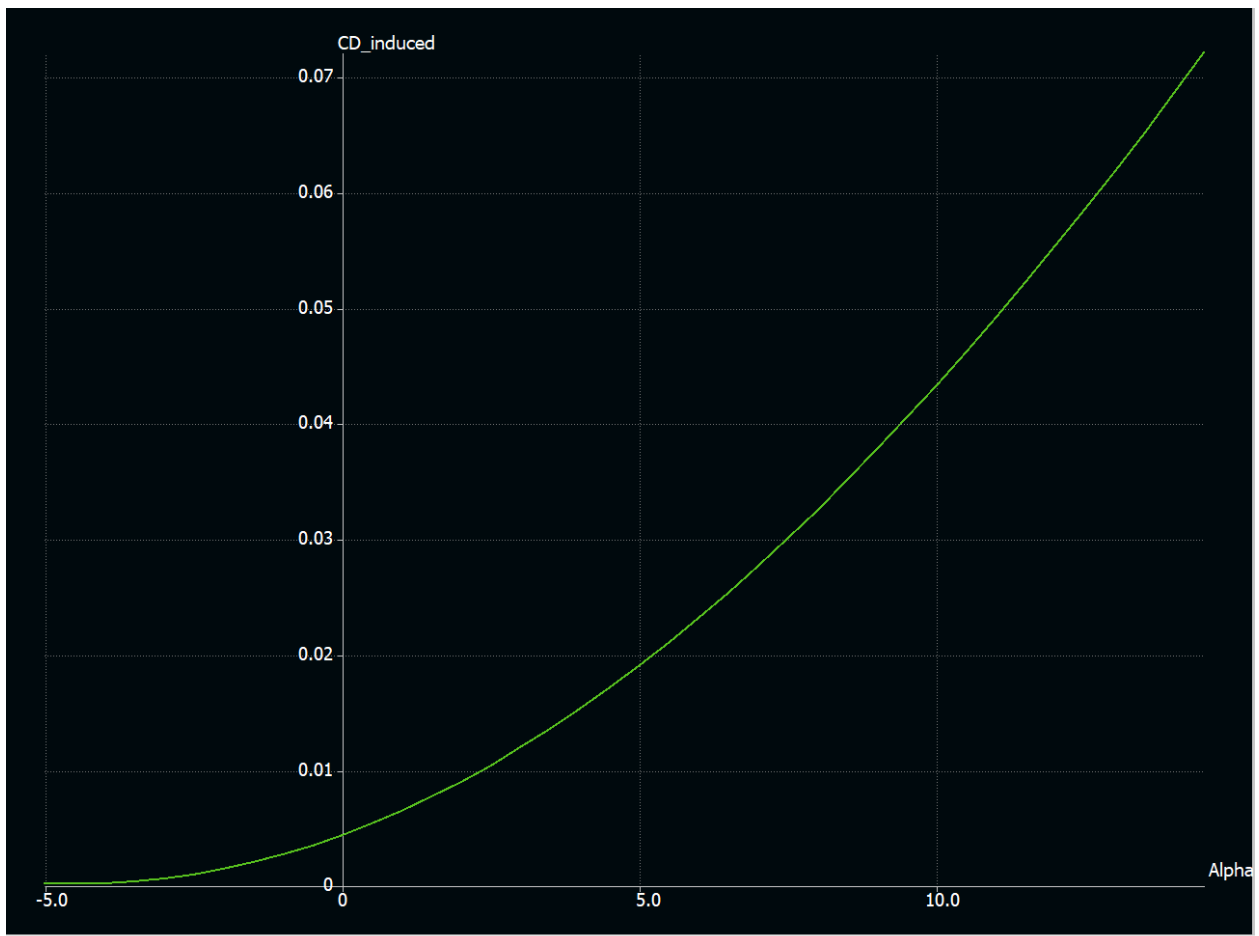


Figure 3.6: Finalized Wing Induced Drag Polar Graphs

Table 3.2: Final Interpolated Airfoil Coefficients at Major Angles of Attack Estimated from XFLR5

Angle of Attack (Deg)	Lift Coefficient	Drag Coefficient	Moment Coefficient
0	0.409	0.009	-0.209
0.5	0.454	0.010	-0.222
5	0.859	0.025	-0.346
13 (Climb)	1.642	0.094	-0.886
14.5 (Max)	1.74	0.099	-0.589

Based on table above, the design cruise coefficient of lift was achieved at 0 degree angle of attack. XFLR5's prediction on wing peak aerodynamic efficiency also occurs between 0 °degrees and 0.5 °degrees thus extending the range and endurance of the FALCO E-1.

4 Flaps and Ailerons Sizing

4.1 Aileron Sizing

Part 5 of the Canadian Aviation Regularions (CARs) details the required rolling capabilities any airworthy aircraft must have:

- *At Takeoff,*

for an aircraft of 6000 *lbs* or less, the aircraft must be able to roll from a steady 30-degree banked turn through an angle of 60 degrees, so as to reverse the direction of the turn within 5 seconds from initiation of roll [22]

- *Approach,*

for an aircraft of 6000 *lbs* or less, the aircraft must be able to roll from a steady 30-degree banked turn through an angle of 60 degrees, so as to reverse the direction of the turn within 4 seconds from initiation of roll, using landing configuration (flaps down, landing gear extended) [22]

To design the ailerons so that the FALCO E-1 would meet the above mentioned CAR requirements, aileron placement to determine maximum responsiveness was first established. Using the lift distribution's operating points from XFLR5, the data was exported to excel and the lift distribution was re-plotted and show in Figure 4.1. The lift distribution was used to create an unaccumulated sectional moment contribution graph. Using the distribution of sectional moments as shown below in Figure 4.2, one can determine where the ailerons should be placed for maximum responsiveness [23]. The ailerons for the FALCO E-1 end at 6.1 *m* half-span. Using MATLAB, an iteration process was used to determine where the ailerons should begin to meet CAR requirements.

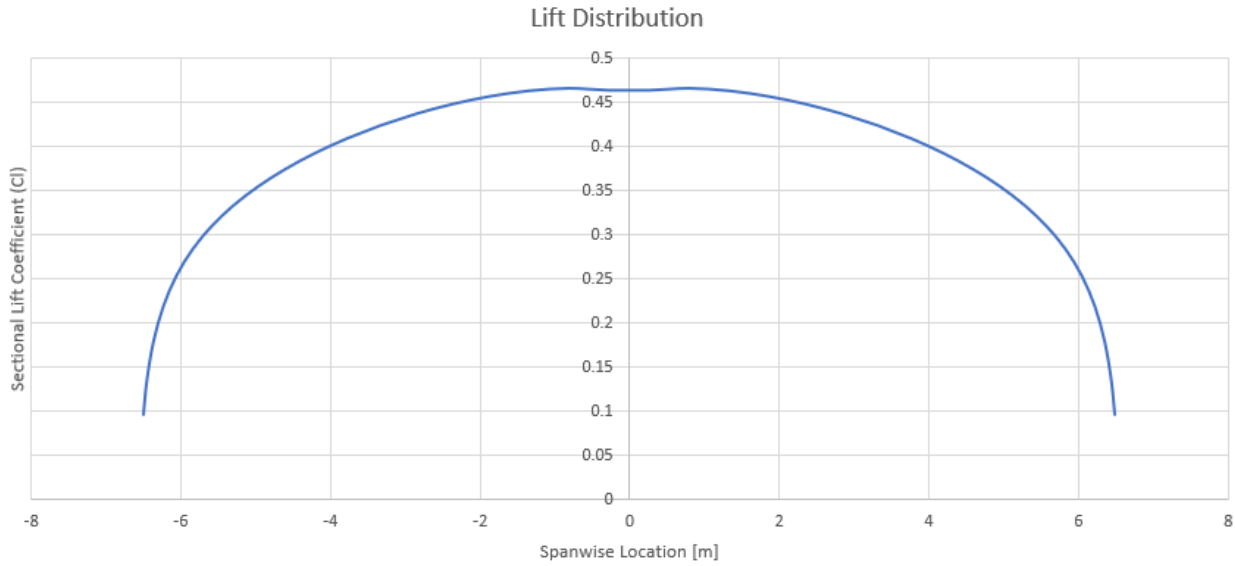


Figure 4.1: Lift Distribution of Finalized Clean Wing

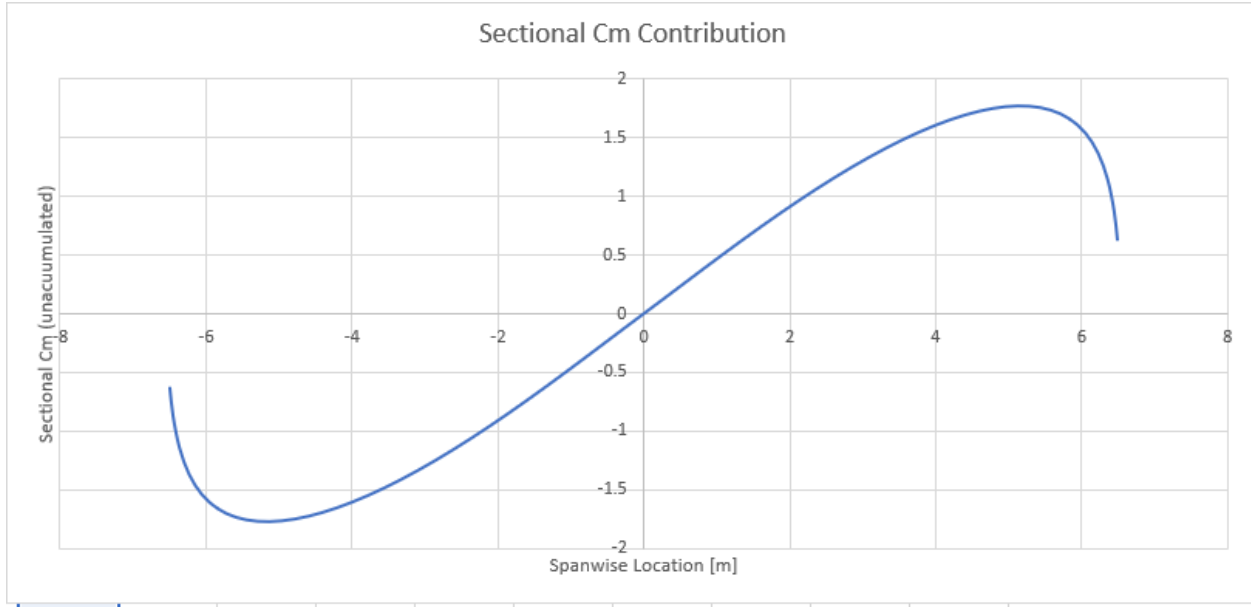


Figure 4.2: Distribution of Sectional Moments along the Wing

The MATLAB code used to find the minimum required aileron size and design for a specific roll rate is shown in Section C in the Appendices. Before beginning the MATLAB code, some parameters were found using XFLR5. The lift-curve slope (a) of the wing, zero-lift drag coefficient, and sectional roll authority ($c_{l\delta_a}$) of the airfoil were prerequisites.

Based on the structural design of the wing, the ailerons start at 75% wing chord due to the rear spar location and would be able to deflect 20 deg in both directions.

The basic idea behind the MATLAB code was to use roll authority for a linearly tapered wing, defined by [23]

$$C_{l_{\delta\alpha}} = \frac{c_{l_{\delta\alpha}} C_R}{SB} \left[(b_2^2 - b_1^2) + \frac{4(\lambda - 1)}{3b} (b_2^3 - b_1^3) \right] \quad (4.1)$$

and roll dampening defined by [23] ,

$$C_{l_p} = -\frac{(c_{l_a} + c_{d0}) C_R b}{24S} \left[1 + 3\lambda \right] \quad (4.2)$$

to calculate the aircraft's roll rate [23]

$$p = -\frac{2V}{b} \frac{C_{l_{\delta\alpha}}}{C_{l_p}} \delta_\alpha \quad (4.3)$$

To achieve a minimum roll rate of 15 deg/s as required by CAR during approach, the aileron would have to span from from 5.28 m to 6.1 m half-span. However, this method does not take roll acceleration into consideration as the roll inertia of the FALCO E-1. Therefore, the actual required aileron size is slightly bigger. This is not of any significant concern as the ailerons were designed to be much bigger than this.

To match the maximum roll rate of 34.8 deg/s of the Cessna Citation (also made to replace the Cessna 172) the FALCO E-1's ailerons span from 4 m to 6.1 m [24]. The maximum roll rate of the FALCO E-1 is 36 deg/s .

4.2 Flap Sizing

To decrease stall speed, the flaps were designed as large as reasonably possible to increase lift. Like the ailerons, the flaps begin at 75% wing chord and span from 0 m to 3.8 m half-span, and has a maximum deflection of 30 deg downwards.

The increase in lift due to flap deflection is difficult to accurately estimate. Instead analysis using computational fluid dynamic (CFD) was used. Data from CFD analysis is discussed in Section 5.

From Table 5.2 from Section 5.3, using a stall angle of 12° degrees incidence and the maximum flap deflection of 30° degree, the stall speed of the FALCO E-1 is approximately 23.32 m/s .

$$L = W = \frac{1}{2} \rho V_{stall}^2 Sc_L \quad (4.4)$$

$$V_{stall} = \sqrt{\frac{2W}{\rho Sc_L}} = 23.32 \text{ m/s} = 45.330454 \text{ knots} \quad (4.5)$$

4.3 Wing Tip Device Considerations

To provide the FALCO E-1 with better performance, several wing devices were considered.

1. Hoerner Wing Tips

A diagram of Hoerner wing tips and how they reduce drag are shown in Figure 4.3 below.

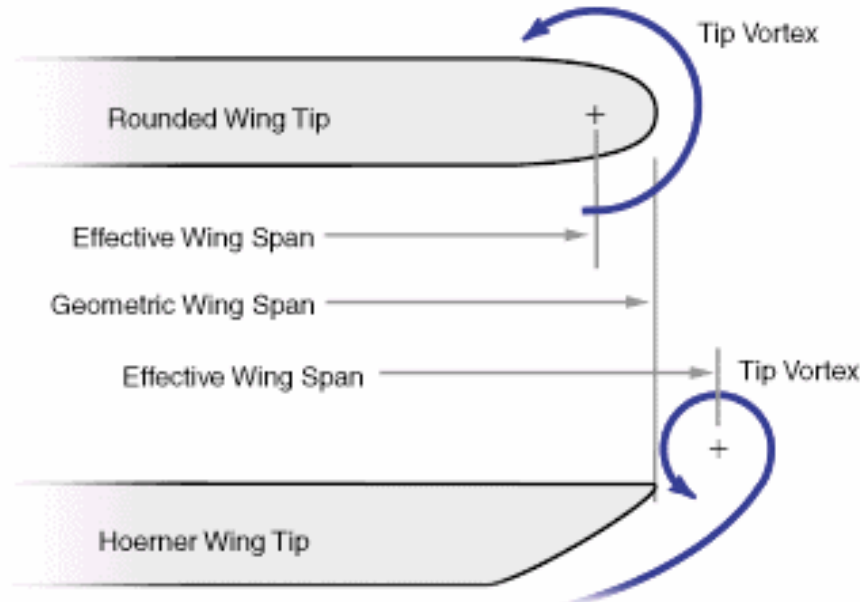


Figure 4.3: Hoerner Wing Tips [1]

Hoerner wing tips function by shifting the tip vortices away from the wing, smoothing the flow around the wing, increasing effective wing span, and reducing drag. Hoerner wing tips generally increase the range of the aircraft and lower the stall speed. Currently, the FALCO E-1 does not have Hoerner wing tips. Implementing Hoerner wing tips may be implemented into a FALCO E-1 variant and not the baseline model.

2. Winglets

Like Hoerner wing tips, winglets weaken the tip vortices. A diagram of winglets is shown below in Figure 4.4.

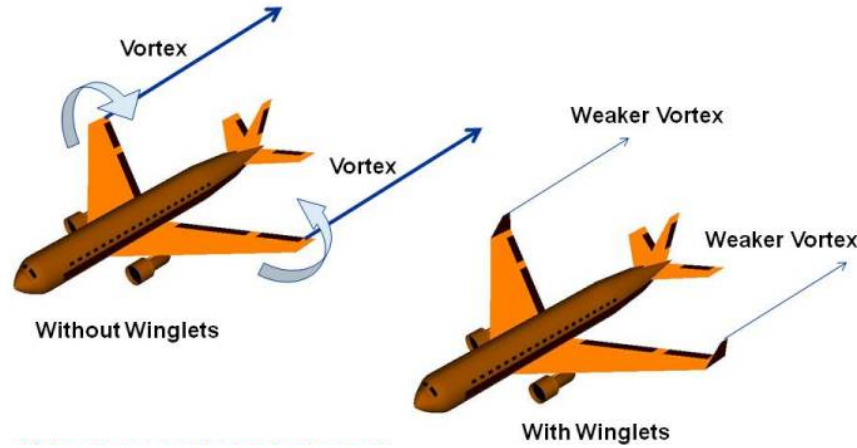


Figure 4.4: Winglets [2]

From analysis using XFLR5, implementing winglets into the FALCO E-1's wing design only very slightly decreased the induced drag as shown in Figure 4.6. Therefore the winglets were deemed unworthy of being implemented onto the design as the higher manufacturing complexity, cost, and additional weight do not outweigh the slight decrease in induced drag. The 3D model analysis at 0 AOA is shown in Figure 4.5 and the polars comparing the FALCO E-1's clean wing to the same wing with implemented winglets with a max dihedral of 80 *deg* is shown in Figure 4.6.

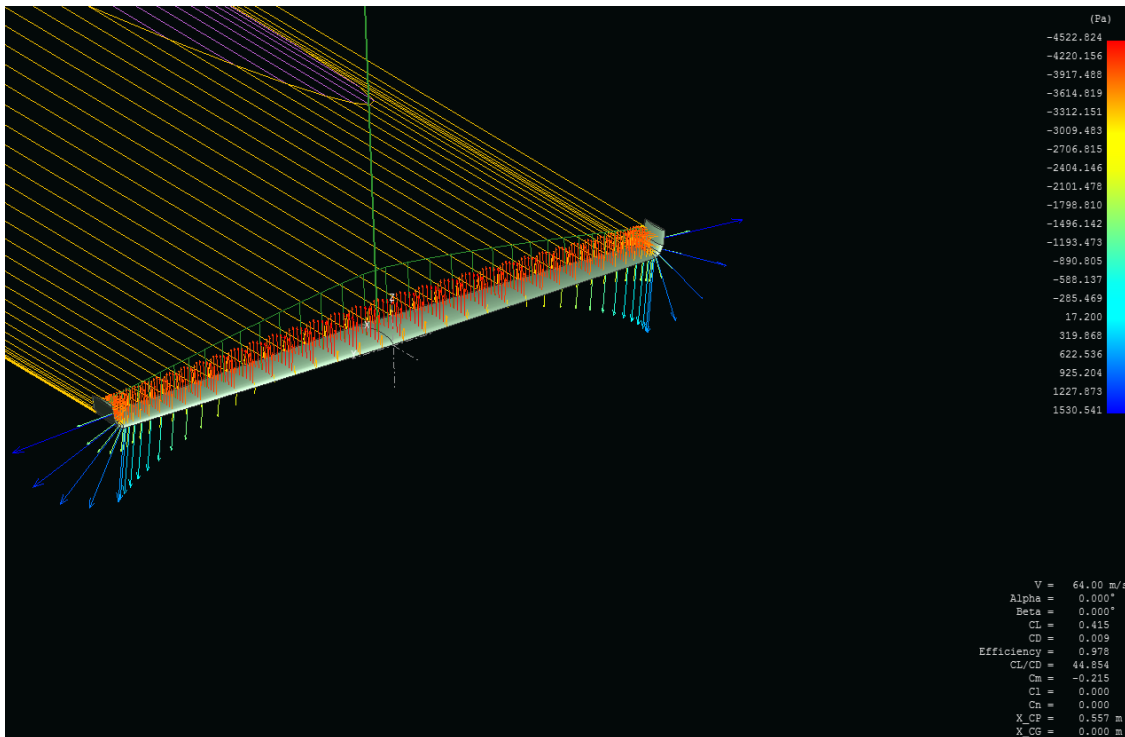


Figure 4.5: FALCO E-1 Analysis with Implemented Winglets 80 *deg*

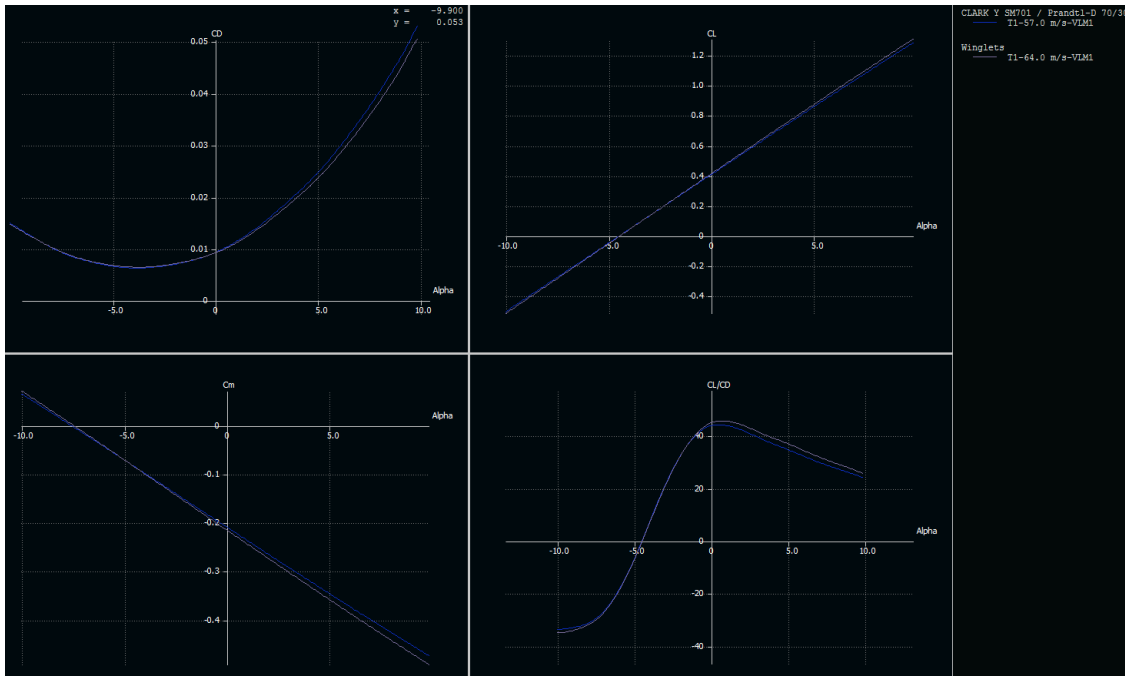


Figure 4.6: Comparison of Clean Wing and Implemented Winglets on FALCO E-1

3. Raked Wing Tips

One of the most well known twin-engine jet airliner, the Boeing 787, utilizes raked wing tips. Like almost all other wing tip devices, they reduce the effect of the tip vortices. Like Hoerner wing tips, implementation of raked wing tips may be considered in future variants of the FALCO E-1. Figure 4.7 below is a picture of a jet airliner with raked wing tips.



Figure 4.7: Raked Wing Tips [3]

4. Vortex Generator

Vortex generators are implemented onto the FALCO E-1. Vortex generators create mini vortices near the surface of the wing that delay flow separation. By using vortex generators, the critical angle of attack can be increased, thus increasing the maximum lift the aircraft can produce, and decreasing the stall speed.



Figure 4.8: Vortex Generator [4]

5 Computational Fluid Dynamics on FALCO E-1

To produce more accurate analysis and to verify the accuracy of the estimates XFLR5 produced, computational fluid dynamic (CFD) analysis on the FALCO E-1 wing was performed. Additionally, another fluid flow program was required as XFLR5 cannot produce accurate estimates for any geometry other than the wing and tail. The main program used for CFD analysis was ANSYS Fluent. The wing at multiple configurations, and fuselage along with the entirety of the FALCO E-1 aircraft, was simulated using ANSYS Fluent. ANSYS Fluent Versions 18.2 and 19.2 were used.

5.1 Analysis Method on Using ANSYS Fluent

The following is the general procedure that was used to perform computational fluid dynamic analysis on FALCO E-1 main components.

1. **Geometry - Import geometry as a .stp file into ANSYS Workbench Design Modeller**

The model to be analyzed was created using CATIA and imported as a .stp file. ANSYS Fluent requires a solid geometry with no empty spaces for the next steps.

2. Geometry - Create an enclosure/enclosures around the model

Depending on how the mesh needs to be designed, a single or multiple enclosures can be used. For the analysis done on the FALCO E-1, either box enclosures or a box enclosure containing a smaller spherical enclosure was used.

3. Geometry - Boolean subtraction

The inner enclosure (if there are multiple enclosures) and the part geometry to be analyzed is boolean cut so that a mould of the part geometry is created.

4. Meshing - Open the newly defined geometry in ANSYS Fluent Meshing

The geometry is loaded into ANSYS Fluent Meshing.

5. Meshing - Naming Geometry

Important surfaces such as the part surface, inlet, outlet, part surface, and enclosure walls (not inlet or outlet) were named for later convenience.

6. Meshing - Insert Meshing Method

A meshing method of using tetrahedrons was inserted using a patch conforming method. This helps to ensure a more accurate mesh.

7. Meshing - Insert Body Sizing (if using more than one enclosure)

If a spherical enclosure was used inside the main enclosure, the spherical enclosure's mesh was created to be extremely fine as flow around the part geometry is captured within this enclosure. *Proximity and curvature* was used as the main size function enable accurate meshing of curvatures. Tetrahedron sizes were generally close to 0.6 m for the inner enclosure.

8. Meshing - Defining sizing and quality of mesh

Size functions of *proximity and curvature* were once again used. *Relevance center* and *Span Angle Center* were selected to be fine. Tetrahedron sizes of approximately 1 m were used for the outer enclosure while the inner enclosures had a maximum tetrahedron size of 0.3-0.6 m. Smoothing of the mesh was always defined to be high.

9. Meshing - Defining the boundary layer

To add an inflation layer to the geometry, the "y+" and first cell height was first determined. The "y+" parameter is a CFD parameter that is essential for a turbulence approach. Turbulence models are often required for aerodynamic analysis. For a turbulent analysis, a y_+ of 30-50 is generally used. However a value of 12 was used for the analysis on the FALCO E-1 to produce a finer boundary layer. The first cell height of the boundary layer was found using LEAP Australia's CFD y_+ calculator [25]. The inflation layer was added to the surface geometry with the first layer thickness as the first cell height. Twenty to thirty layers with a growth rate of 1.1 was used to define the boundary layer.

10. Analysis Setup - Model

A realizable k-epsilon model was selected to simulate turbulent flow conditions. The k-epsilon model utilizes turbulent kinetic energy and energy dissipation, along with mass

continuity and velocity continuities to simulate fluid flow.

11. Analysis Setup - Materials

Different air properties such as density and dynamic viscosity were selected for different analysis depending on the analysis conditions.

12. Analysis Setup - User Defining Variable

Different user defined variables were created so that their convergence could be monitored along with the residuals.

13. Analysis Setup - Boundary Conditions

Inlets were defined as a velocity-inlet while outlets were defined as a pressure-outlet with zero gauge pressure. Different parameters were inserted for different analysis.

14. Analysis Setup - Initialization and Run Calculation

Initialization was computed from the velocity inlet. Calculations were then ran.

5.2 FALCO E-1 Clean Configuration Wing CFD Analysis

Several wing configurations at different angles of attack were analyzed. The first analysis was done on the wing using clean configuration at cruise conditions of 8000 feet altitude and a cruise speed of 64 m/s . The mesh of the box enclosure is shown below in Figure 5.1.

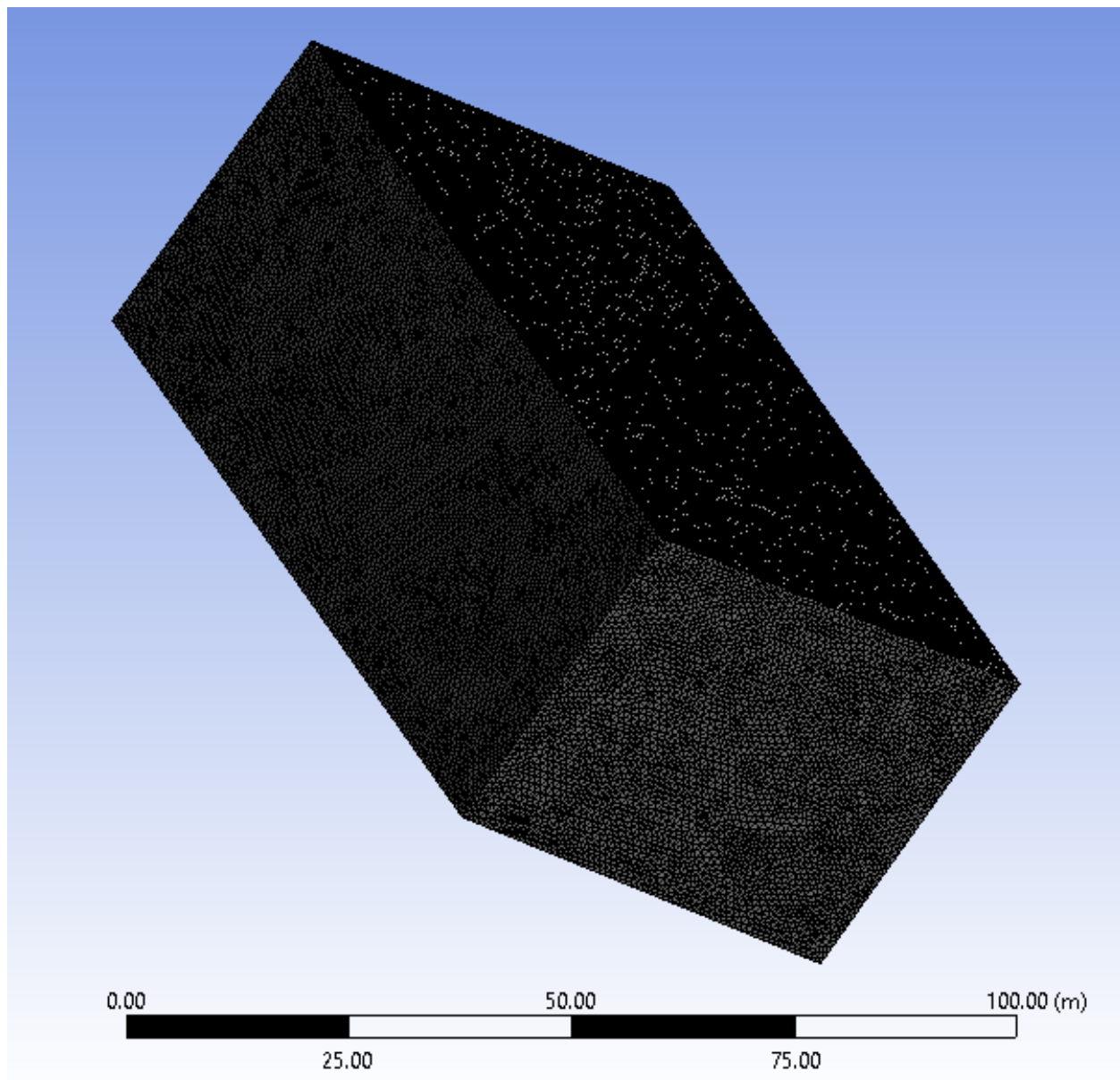


Figure 5.1: Enclosure Mesh of Wing at Cruise Conditions

A cross-section of the mesh is shown below in Figure 5.2. From the figure, the mesh is more dense near the wing, capturing the simulated fluid flow near the wing more accurately.

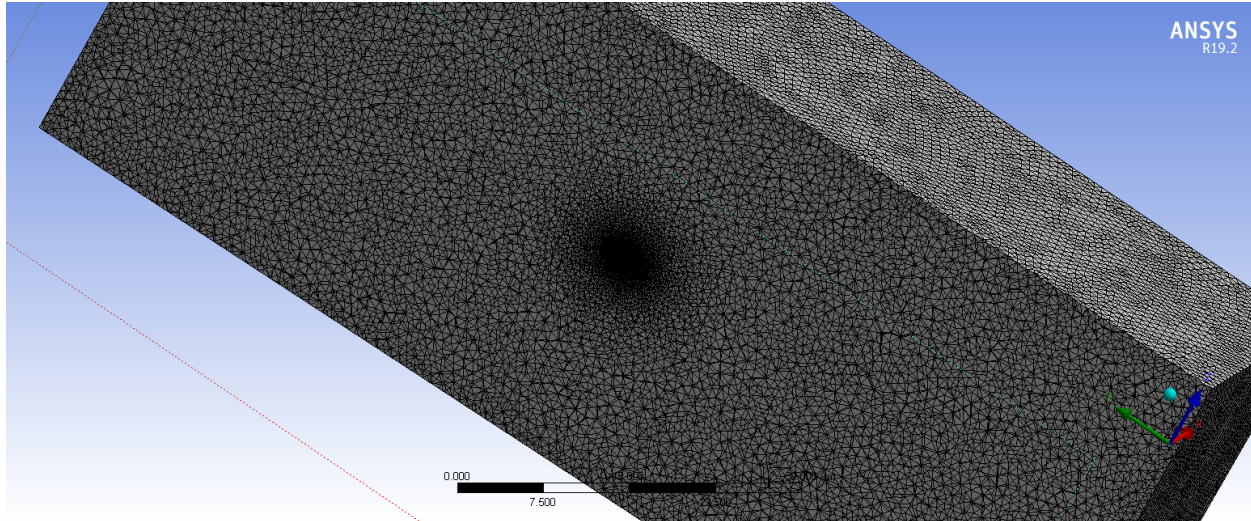


Figure 5.2: Cross Section of Wing Mesh at Cruise Conditions

A close-up of the wing cross-section is shown in Figure 5.3. The wing geometry can be seen in this figure as well as the dense boundary layer outline of the wing.

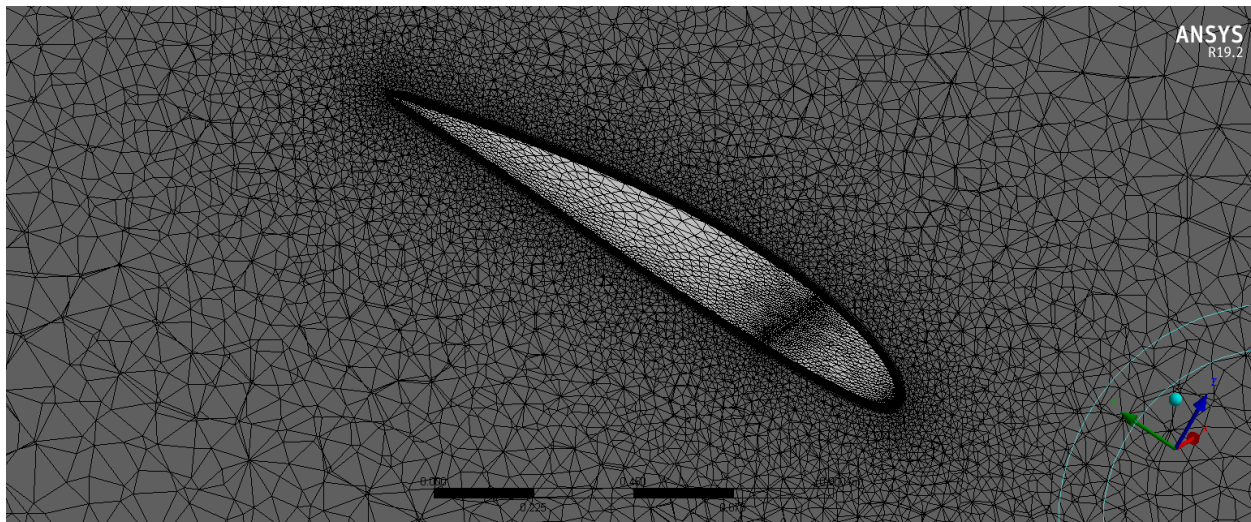


Figure 5.3: Close Up of Wing Mesh Cross-Section

At an even closer view of the wing surface in the mesh, the development of the boundary layer can be seen in Figure 5.4. The $y+$ thickness used was 12; using cruise conditions and the mean chord of the wing, the first cell height generator provided by LEAP Australia calculated the first cell height or first layer thickness of the boundary layer inflation to be 0.185963 mm [25].

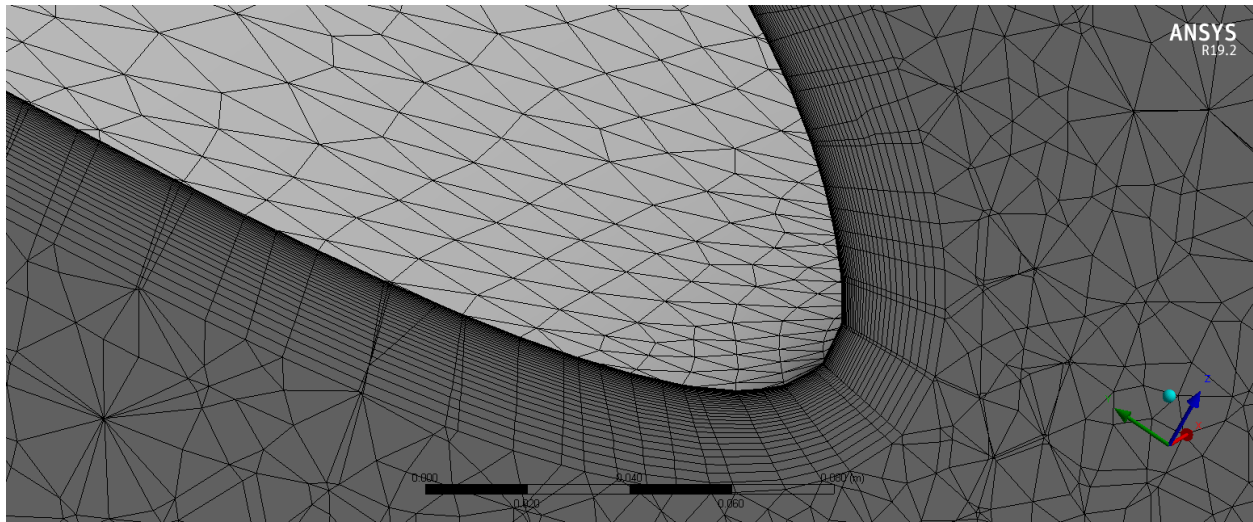


Figure 5.4: Wing Boundary Layer At Cruise Conditions

After over 1000 iterations, the solution was determined to be converged. The residuals per iteration are shown below in Figure 5.5 for the analysis.

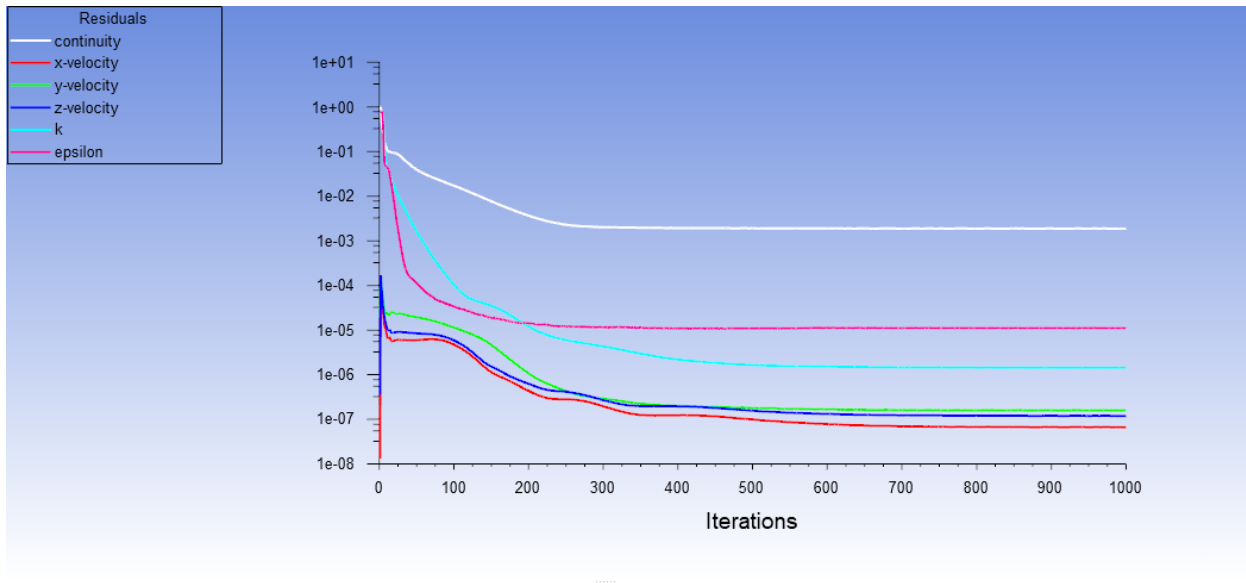


Figure 5.5: Residuals for Cruise Analysis Clean Wing Configuration

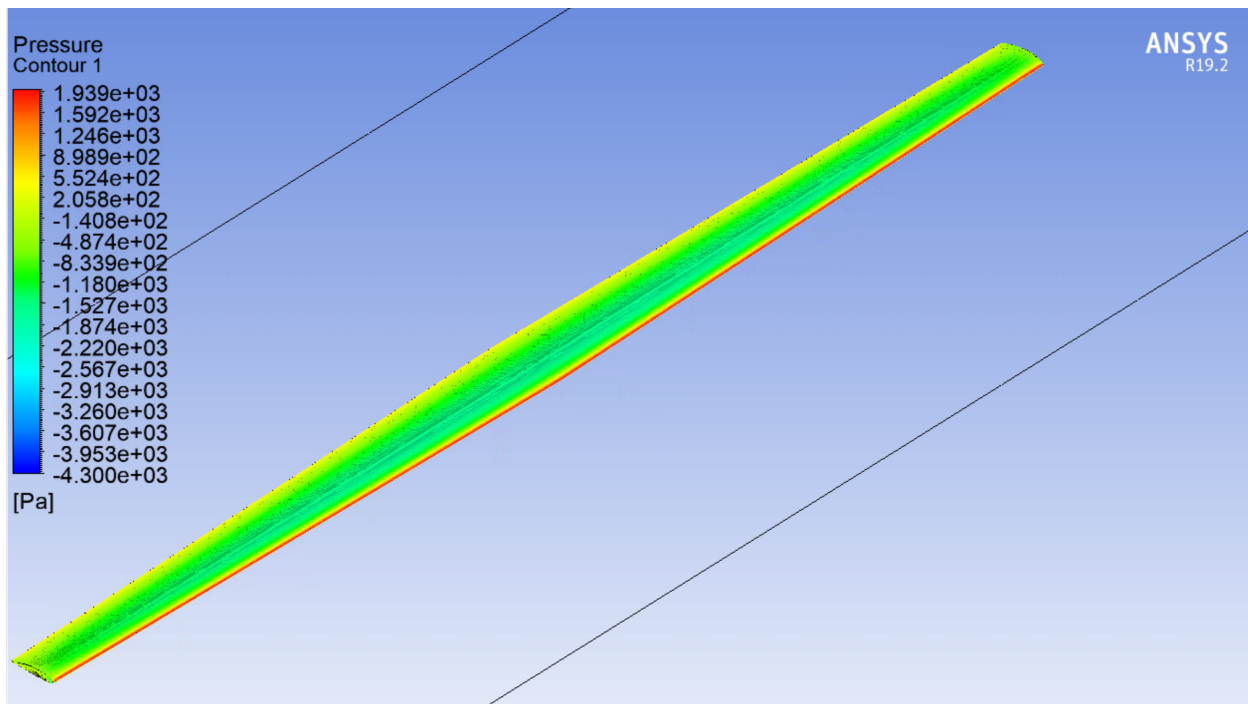


Figure 5.6: Clean Wing Configuration Top Pressure Gradient

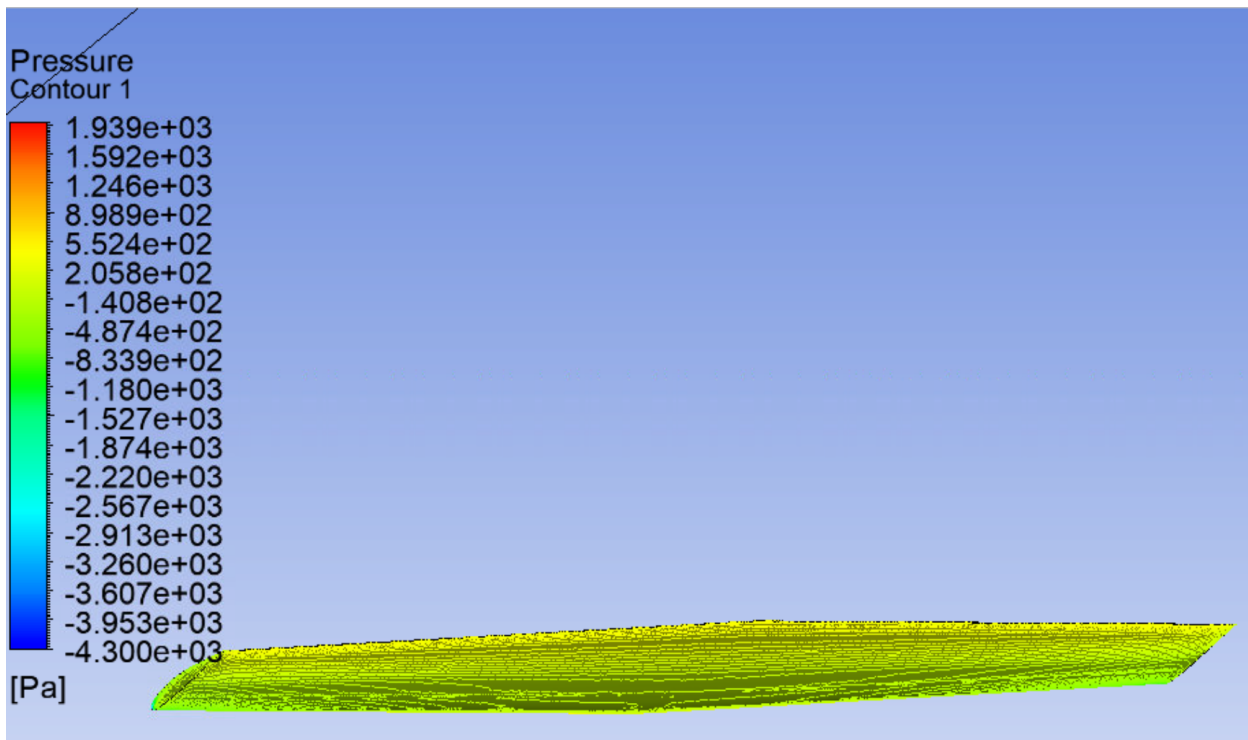


Figure 5.7: Clean Wing Configuration Bottom Pressure Gradient

From the analysis, the lift at 8000 feet at an airspeed of 64m/s is 11975.4 N , while the drag is

424.728 N. A summary of the results ANSYS Fluent provided of the simulation are shown in Table 5.1 below.

Table 5.1: Aerodynamic Characteristics of FALCO E-1 Wing at Required Cruise Conditions

Air Speed [m/s]	64
Air Density [kg/m^3]	0.92687
Wing Area [m^2/s]	13.975
Angle of Attack [°]	0
Flap Deflection [°+down]	0
Lift Force [N]	11975.4
Drag Force [N]	424.728
Lift Coefficient	0.4346
Drag Coefficient	0.0154
Aerodynamic Efficiency	28.19

5.3 FALCO E-1 Wing CFD Analysis at Max Flaps Down Configuration

Like the analysis done for cruise conditions, a CFD analysis was done for maximum flap deflection configuration to determine stalling characteristics and the effectiveness of the flaps. The wing model with flaps at 30 °deg deflection downwards was modelled in CATIA, imported into ANSYS Workbench, and rotated for 12 °deg angle of incidence. The simulation was done using an altitude of 8000 feet and an airspeed of 64 m/s .

Figure 5.8 below details the mesh of the enclosure using a wire-frame view. The inner spherical enclosure is much more element/tetrahedron dense than the outer box enclosure.

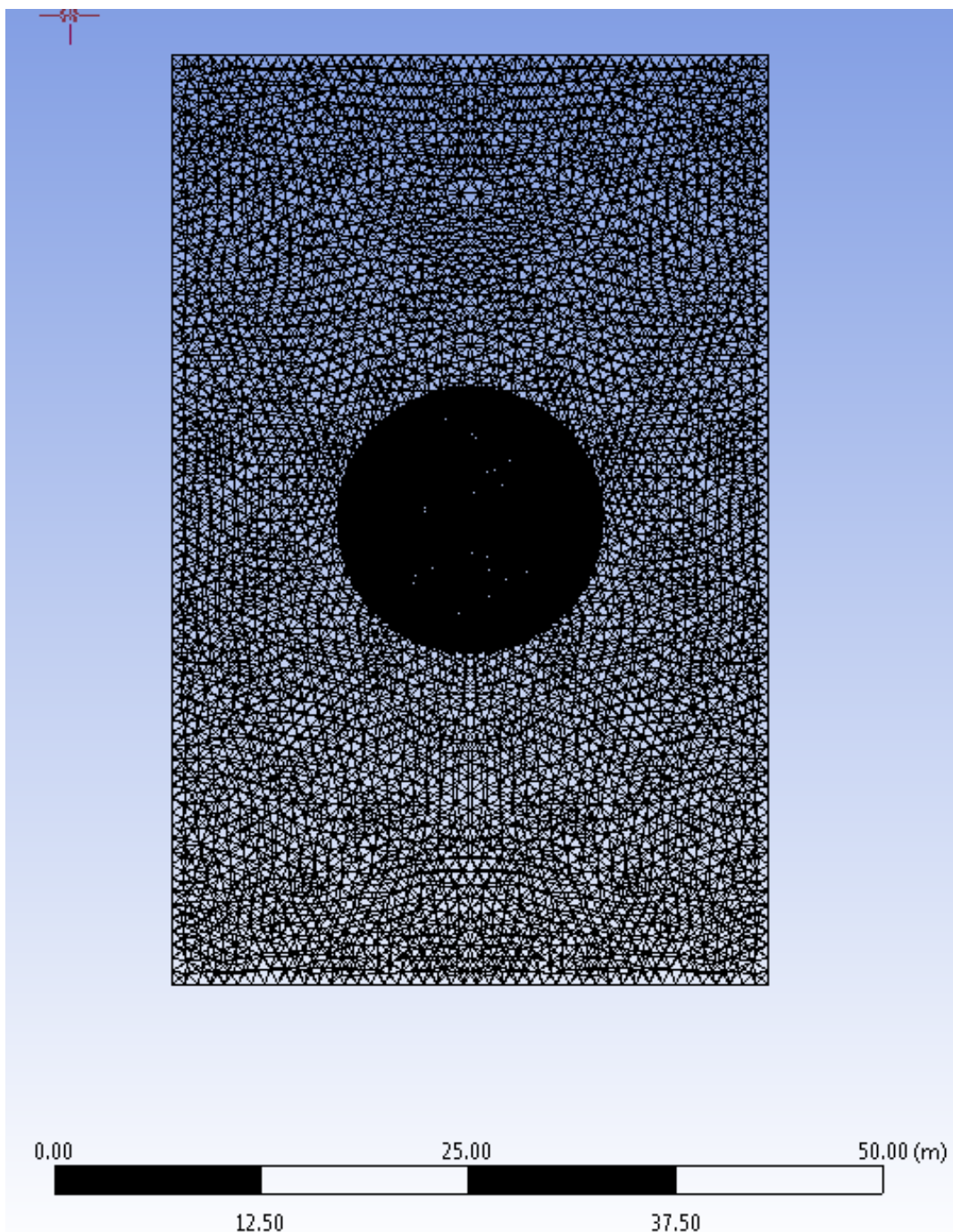


Figure 5.8: Enclosure Mesh at Flaps Down Configuration Wireframe View

A cross-section of the mesh enclosure is shown below in Figure 5.9

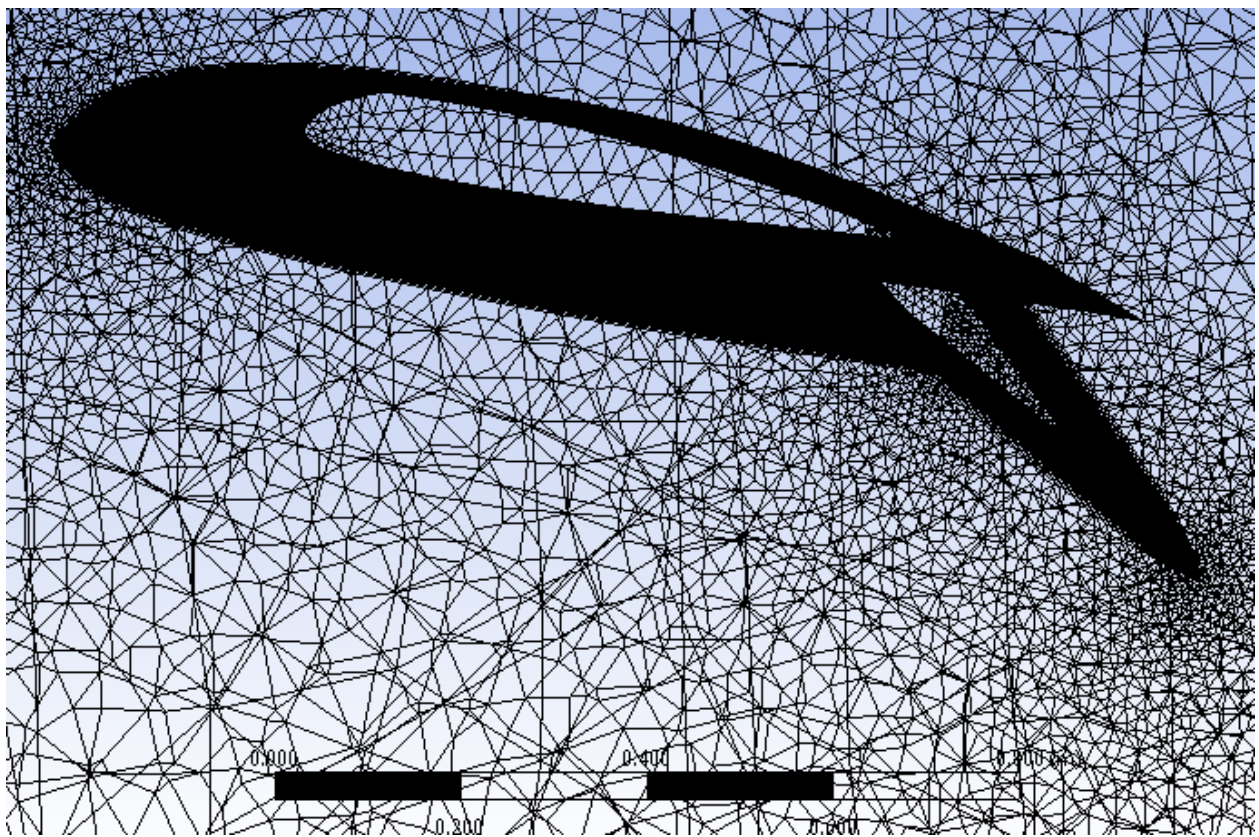


Figure 5.9: Cross Section at Flaps Down Configuration Wireframe View

The boundary layer was defined with the same parameters from Section 5.2 above. The boundary layer is shown in Figure 5.10

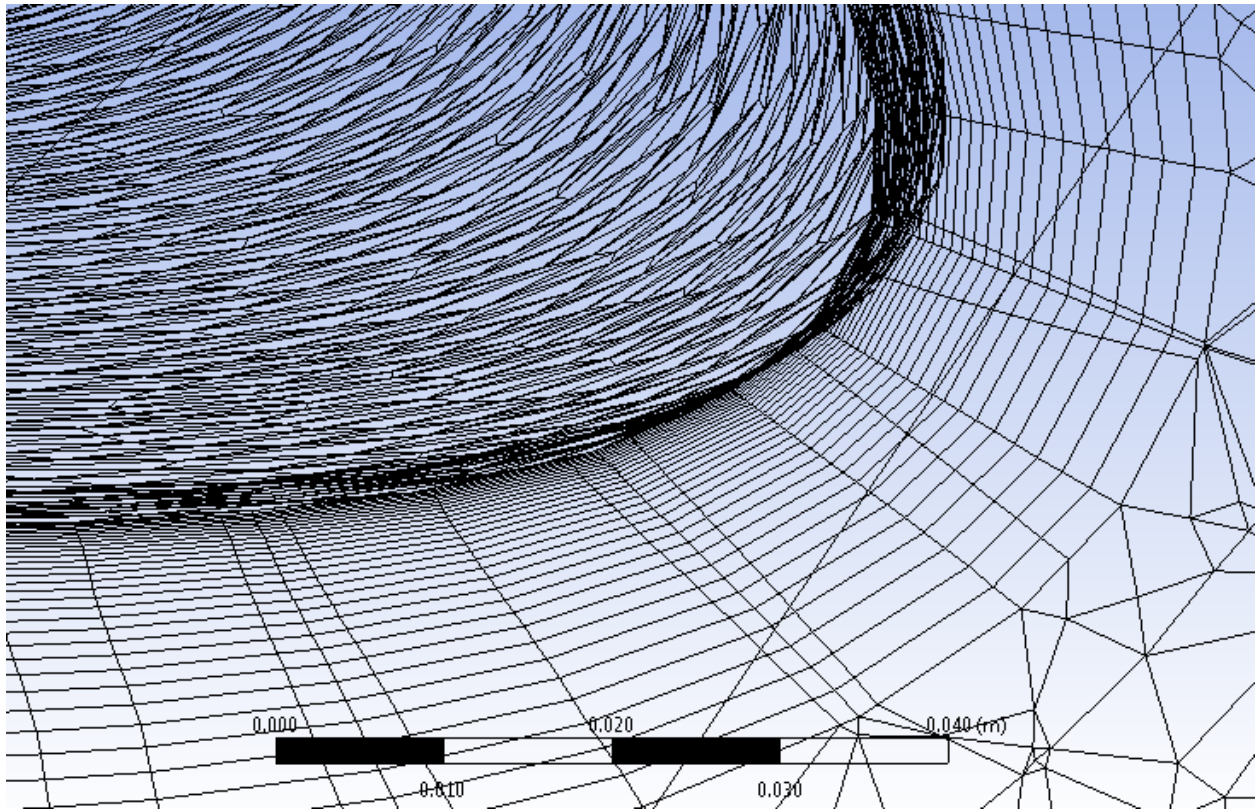


Figure 5.10: Boundary Layer at Flaps Down Configuration Wireframe View

The resulting lift and drag forces are 64607.3 N and 7052.32 N respectively. Table 5.2 list the results of the simulation.

Table 5.2: Aerodynamic Characteristics of FALCO E-1 Wing with Max Flap Deflection at Required Cruise Conditions

Air Speed [m/s]	64
Air Density [kg/m^3]	0.9628
Wing Area [m^2/s]	13.975
Angle of Attack [°]	12
Flap Deflection [°+down]	30
Lift Force [N]	64607.3
Drag Force [N]	7052.32
Lift Coefficient	2.3444
Drag Coefficient	0.2559
Aerodynamic Efficiency	9.1633

5.4 FALCO E-1 Aircraft Analysis

Using an assembled model of the FALCO E-1, the entire plane design was imported into ANSYS Workbench for CFD analysis. The analysis was performed simulating an altitude of 8000 ft at an airspeed of 64 m/s . The FALCO E-1 was configured at 0 °degrees angle of incidence with a clean wing configuration. The plane and enclosure in ANSYS Geometric Design Modeller is shown in Figure 5.11

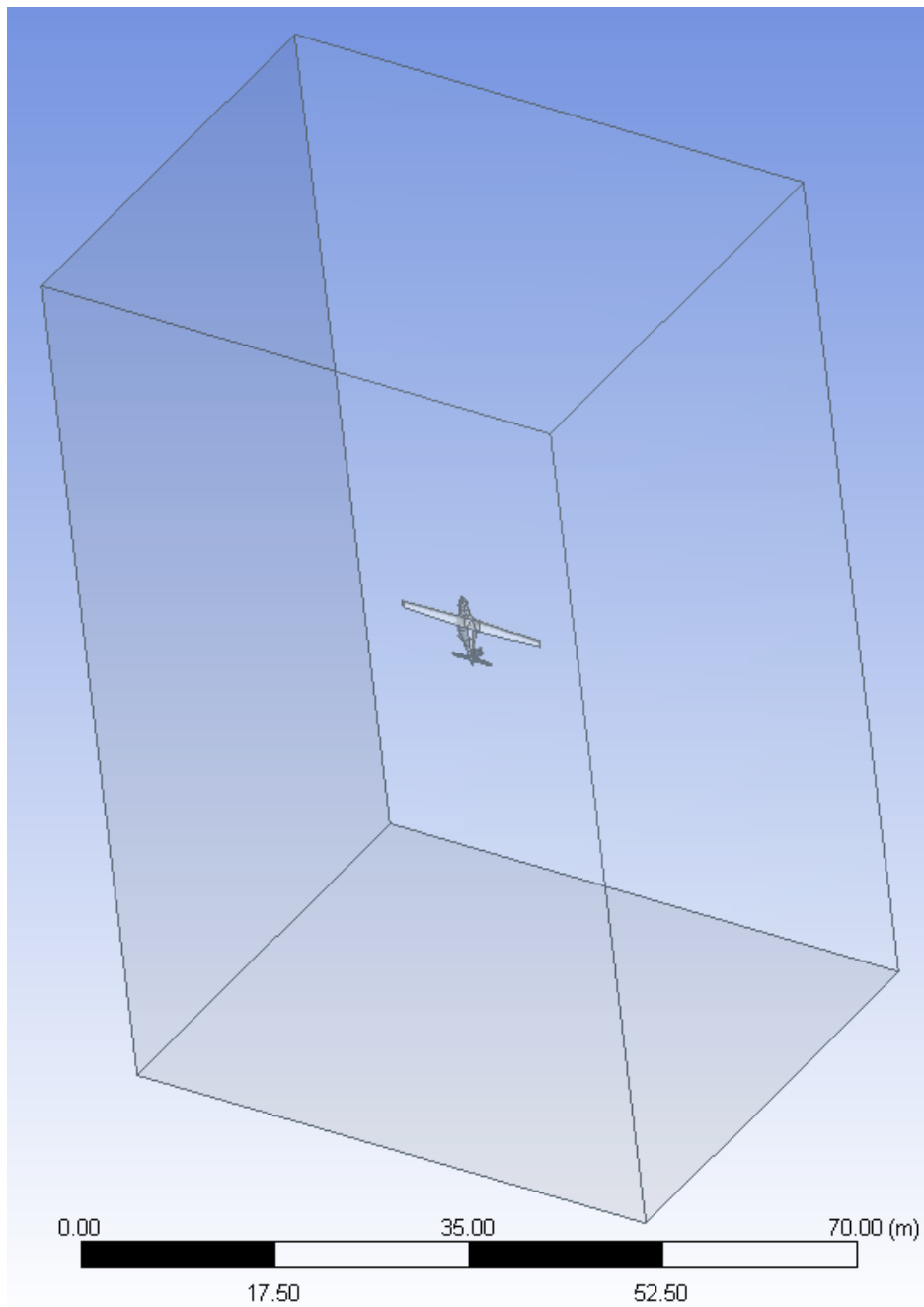


Figure 5.11: FALCO E-1 in Design Modeller

A wire-frame view of the mesh along with a cross-sectional view is provided in Figures 5.12 and 5.13. The inflation boundary layer can also be seen in 5.13.

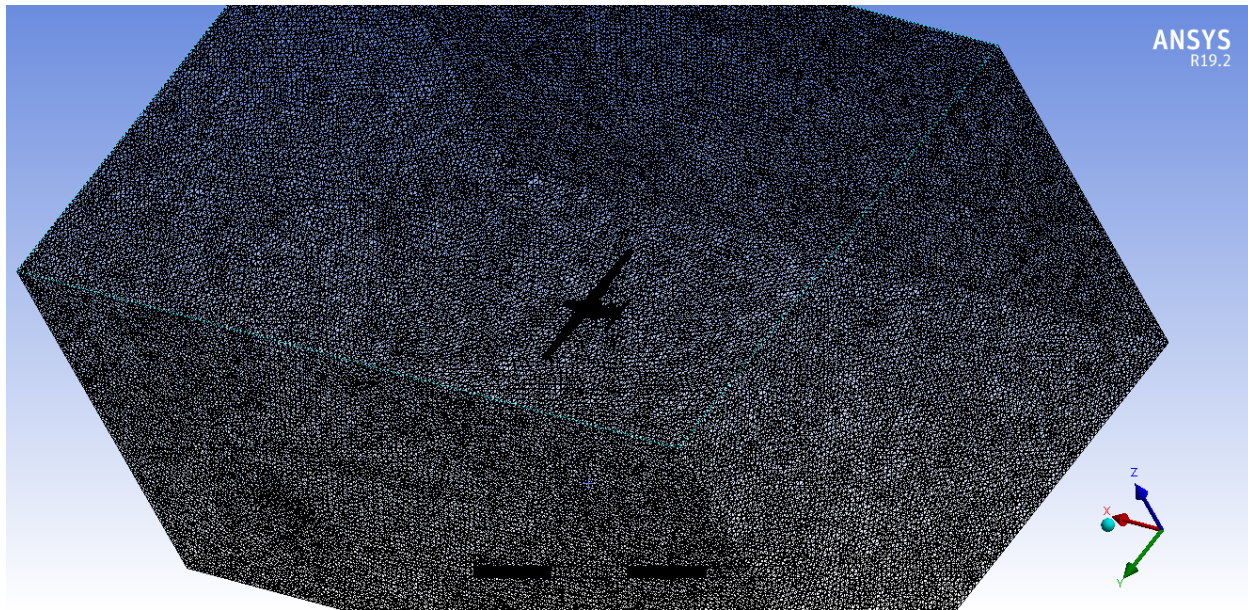


Figure 5.12: FALCO E-1 Mesh Wire-Frame View

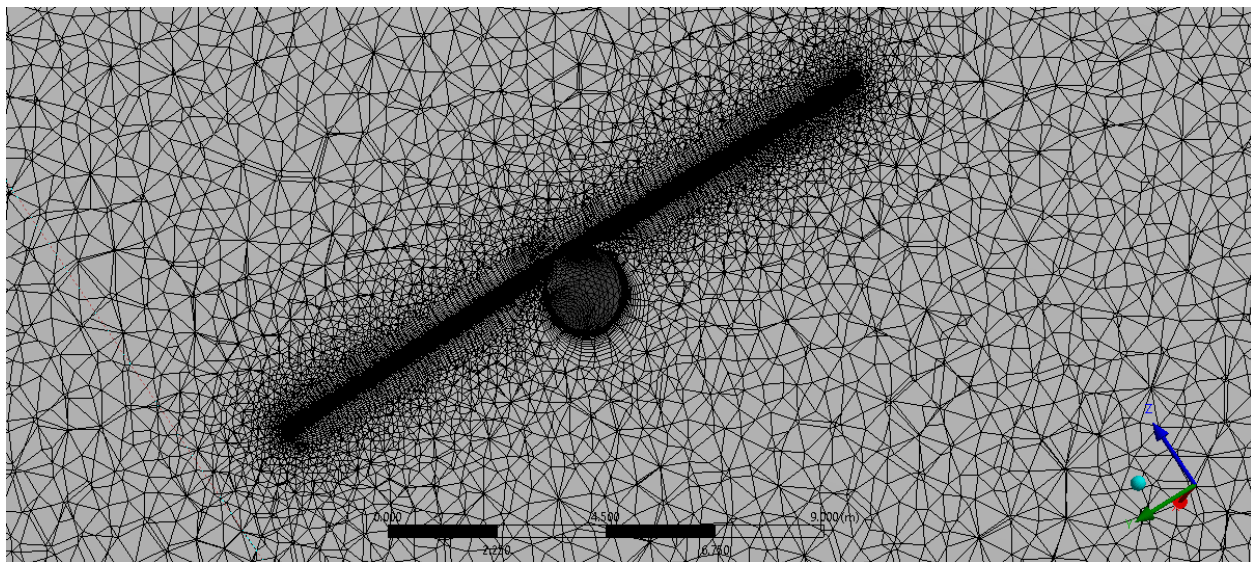


Figure 5.13: FALCO E-1 Mesh Cross Section

Through 500 iterations, the iterations were found to have converged enough for approximate results. From Figure ref below, the k-epsilon turbulence model has not completely converged. Both the turbulent kinetic energy and energy dissipation equation residuals were oscillating with low amplitudes.

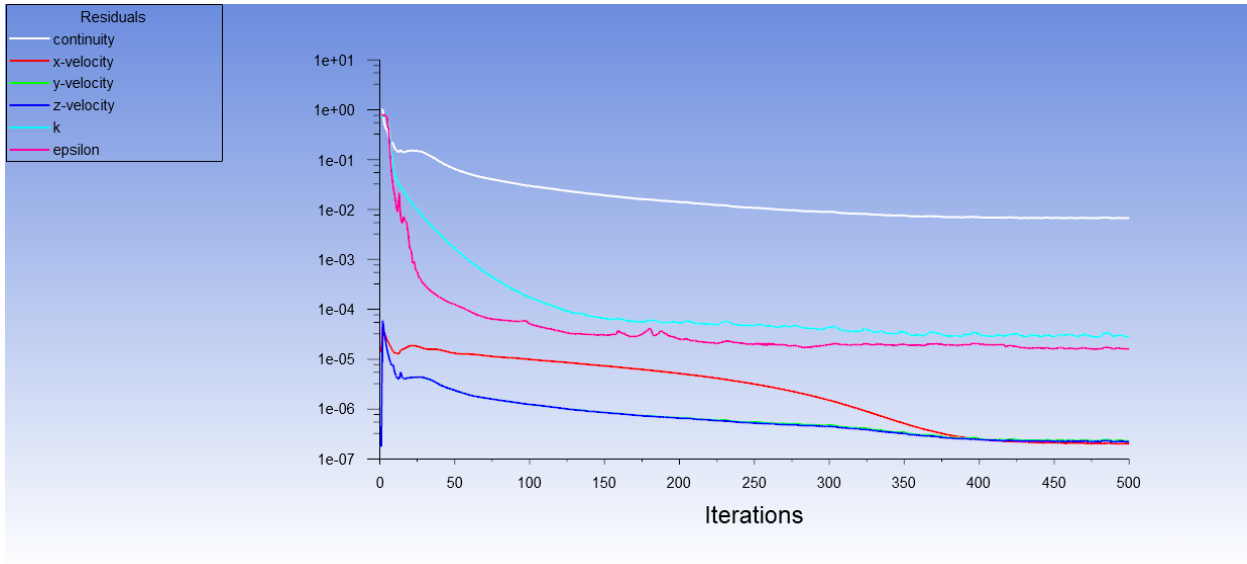


Figure 5.14: FALCO E-1 Mesh Analysis Residuals

The summary table of the analysis on the FALCO E-1 plane is given in Table 5.3. From this table, the FALCO E-1 has a total drag coefficient of 0.0289 at

Table 5.3: FALCO E-1 CFD Crusie Analysis

Air Speed [m/s]	64
Air Density [kg/m^3]	0.9628
Wing Area [m^2/s]	13.975
Angle of Attack [$^\circ$]	0
Flap Deflection [$^\circ$ +down]	0
Lift Force [N]	11276.43
Drag Force [N]	798.087
Lift Coefficient	0.0409
Drag Coefficient	0.0289
Aerodynamic Efficiency	14.16

5.5 XFLR5 Analysis vs ANSYS Fluent Analysis

The simulated results from ANSYS Fluent's turbulence modelling are more accurate than those provided by XFLR5's horseshoe vortex VLM analysis. Comparing the results provided by both, XFLR5 tends to underestimate the total drag produced by the wing and tail models. However, lift estimation using XFLR5 is accurate as the lift predicted by both programs are very similar.

6 Aerodynamics Conclusion

DACION's flagship aircraft, the FALCO E-1, utilizes the DAC-Hybrid airfoil spanning throughout the entirety of the wing. The FALCO E-1 incorporates an unswept compound tapered geometry with a wing twist of 2.5 °degrees. The wing root has a chord length of 1.35 m while the wing tips have a chord length of 0.8, tapering linearly. Along with the tapering, the wing twist improves stalling characteristics by having the wing root stall before the wing tip. Furthermore, this configuration allows for a more elliptical lift distribution, increasing Oswald efficiency and aspect ratio while decreasing induced drag. The compound tapered wing tips decrease the effect of tip vortices, also decreasing induced drag. The wing was designed so that the FALCO E-1 reaches peak aerodynamic efficiency of 15 at a cruise altitude of 80,000 ft with an angle of incidence between 0°- 0.5°degrees.

Part III

Book III: Structural Analysis of FALCO E-1

1 Material Selection

The material selection and properties for the overall fuselage can be seen below.

Table 1.1: Material Selection for Structural Components of the Air-Frame [17]

Component	Material	Density (kg/m3)	Tensile Yield Strength (MPa)	Modulus of Elasticity (GPa)	Shear Strength (MPa)
Skin	AL 6061-T6	2700	276	68.9	207
Stringers	AL 6061-T6	2700	276	68.9	207
Bulkhead	AL 6061-T6	2700	276	68.9	207
Ribs	AL 6061-T6	2700	276	68.9	207
Firewall	Ti - 6Al - 4V	4430	880	113.8	550

Table 1.2: Material Selection for Windscreen and Windows [18]

Component	Material	Density (kg/m3)	Tensile Yield Strength (MPa)	Impact Strength (kJ/m2)	Flexural Strength (MPa)	Compressive Yield Stress (MPa)	Modulus of Elasticity (MPa)
Windscreen	Plexiglas GS 249	1190	110 (-40C) 80 (23C) 40 (70C)	15	115	110	3300
Door Glass	Plexiglas GS 249	1190	110 (-40C) 80 (23C) 40 (70C)	15	115	110	3300

The aluminum alloy selected is widely used in the aviation industry and has been proven to be reliable. The air-frame is made completely out of the alloy. The homogeneous material selection for the structure allows for better predictions in stress analysis. The firewall material was chosen based on FAR 23 requirements for firewalls. The titanium alloy selected is a mid-range alloy in terms of weight and strength. This will allow the addition of a strong firewall without an increase in weight.

2 Fuselage Design

The design of the fuselage was an iterative process, and the process produced 7 iterations. Fuselage structures mainly carry bending moments, shear forces, and torsional loads. Due to the fact that the cabin will not be pressurized, less structural support was needed in the design as the fuselage would not experience hoop stress. The thickness of the skin panels is generally small, so the shear flow is assumed to be uniform through adjacent stringers. Using this assumption, the stringers can be idealized to carry all direct stresses. The reduced structural weight was at an advantage for the team as it allowed for more weight to be allocated for the batteries which would increase our flight time and range.

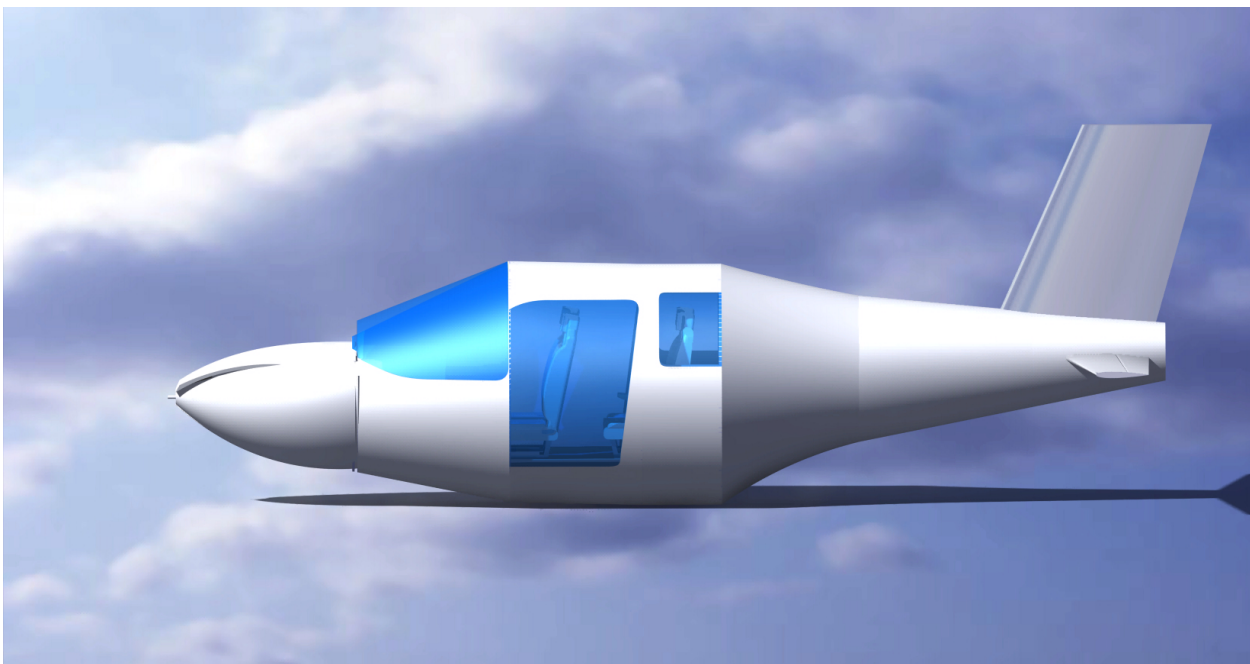


Figure 2.1: Falco E-1 Fuselage

2.1 Stringers and Bulkheads

The original design of the fuselage included square interior and exterior bulkheads. A figure of the partial skin of the first design can be seen below.

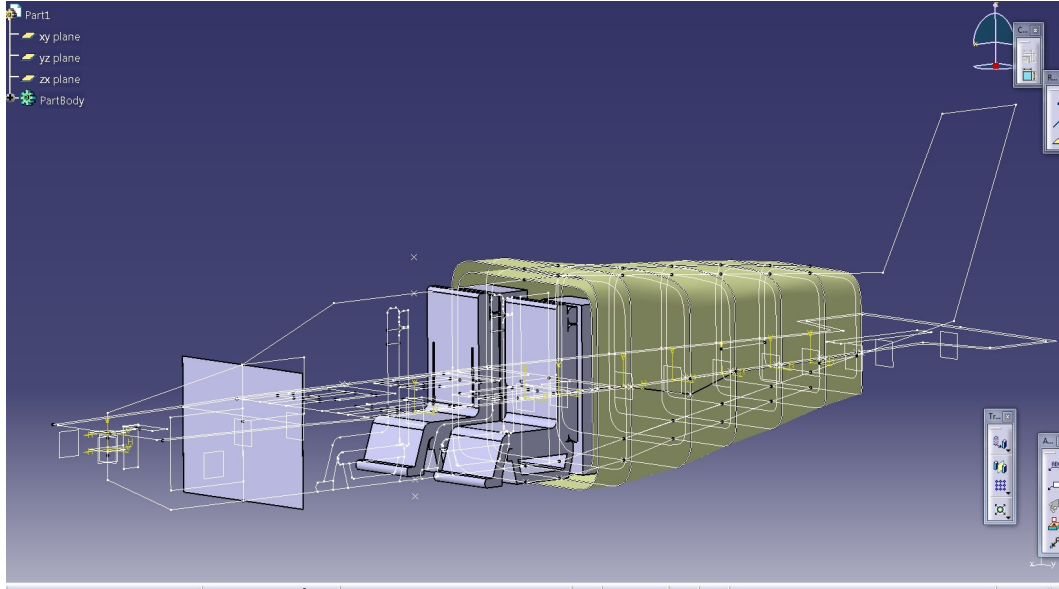


Figure 2.2: Fuselage Structure with Square Bulkheads

The first design faced challenges when it came to streamlining the cabin with the nose as the nose would be of a circular shape and the fuselage was of a square shape. A new circular design was proposed with decreased the area of the bulkheads for weight reduction. The complete fuselage structure, as well as structural dimension, can be seen below.

Table 2.1: Bulkhead Dimension

Number of Bulkheads	3
Thickness (in)	0.25
Exterior Diameter (inch)	66.67
Interior Width (inch)	50
Interior Height (inch)	46
Top Radius (inch)	7.5
Bottom Radius (inch)	1



Figure 2.3: Complete Fuselage Structures

Table 2.2: Stinger Dimensions

Number of Stringer	14
Web Thickness (in)	0.125
Flange Thickness (inch)	0.125
Beam Depth (inch)	1.5
Flange Width (inch)	1
Fillet Radius (inch)	0.1

The new design still maintains a square interior cabin to allow for better comfort of the passengers. A circular interior cabin would be too sharp near the top and would decrease headroom for passengers. Instead of increasing the diameter of a circular interior, it was made square instead. The bulkheads incorporate lightening holes, with 4 on the bottom and 2 smaller ones on the top, to allow for weight reduction. The saved weight was allocated to the battery containment units found in the nose and boom. The stringers have an I-beam shape, and the dimensions can be seen in Figure 5.

2.2 Firewall

Typical recreational aircrafts have one firewall placed between the engine and the cabin. The purpose of the firewall is to protect the passengers from heat and flames in the event of an engine fire or failure. The designed aircraft has batteries stored at the front and back. Both sets of batteries are prone to failure and thus the cabin must be protected from both side. Below, a figure of the front and back firewalls can be seen highlighted in orange.

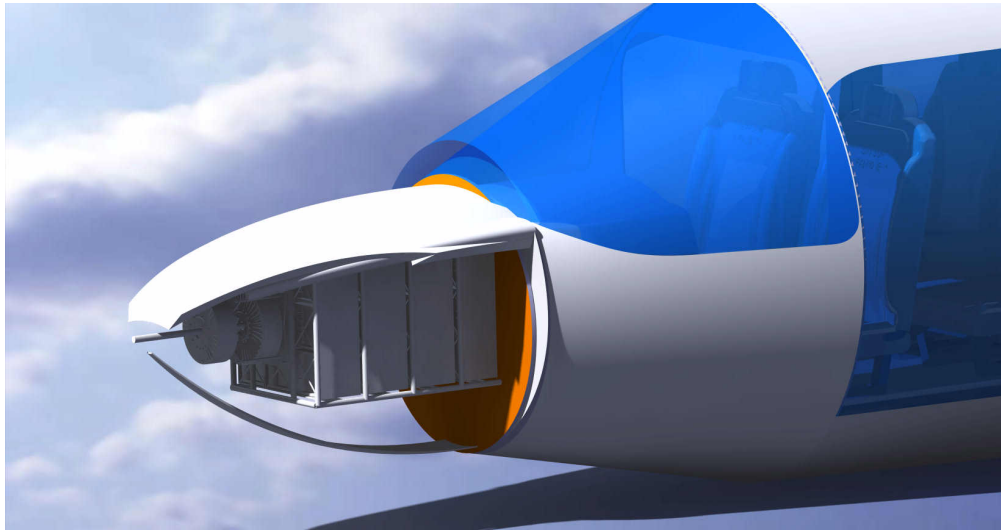


Figure 2.4: Front Firewall

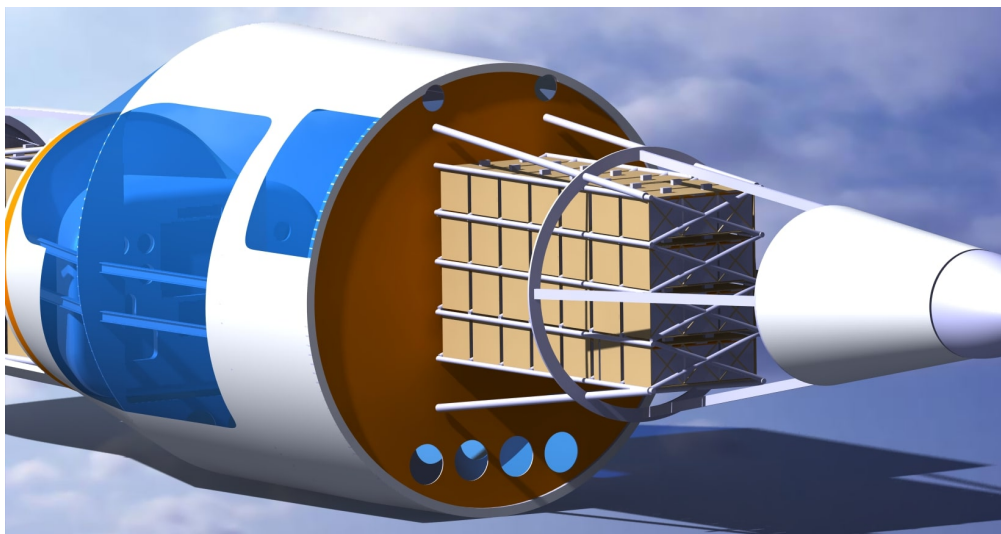


Figure 2.5: Rear Firewall

Both firewalls have the batteries and their encasement, which was designed by Walid, attached to them. The firewall dimensions can be seen below.

Table 2.3: Dimensions of Firewall

Firewall subsubsection	Outer Diameter (inch)	Inner Diameter (inch)	Thickness (in)
Front Firewall	41.9	41.6	0.9
Rear Firewall	66.7	64	0.2

The front firewall was made thicker compared to the back one as the front nose houses the batteries and the motor. The increased number of components requires more protection to failure. Furthermore, if a fire does occur in the nose, the flames and smoke will be pushed back into the cabin due to flight, whereas if a fire occurs at the back the fire and smoke would be pulled back into the free stream air.

FAR 23.1191 sets the regulations for firewall designs. It addresses materials and sheet thicknesses that can be used in firewalls without testing. Due to this, there is not set requirement for sheet thickness, as long as it meets the other requirements such as fireproofing, corrosion resistance, burn temperature and time, and sealing. Therefore, the designed thickness does meet FAR 23 requirements with additional testing.

2.3 Windscreens and Doors

The door to the cabin was first designed to be fully glass with a small black bezel. The door would open up and provide comfortable access to the cabin. The door would resemble that of the Pipistrel Virus aircraft seen below.



Figure 2.6: Pipistrel Virus Aircraft [5]

The windscreen was designed to allow for maximum visibility for the pilot, as the aircraft would also be used as a trainer aircraft, and the increased visibility would benefit new pilots. Due to the

extended windscreen and nose, the placement of the Pipistrel door did not allow access to the cabin. The designed windscreens and door can be seen below.

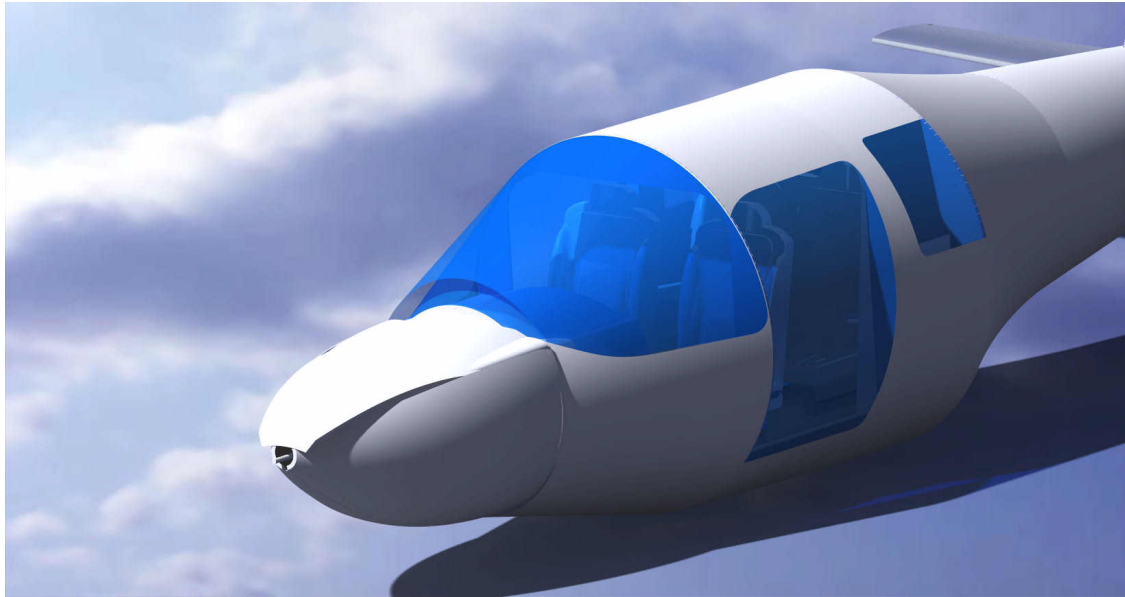


Figure 2.7: Merged Windscreen and Door

The door to the cabin will have a very thin bezel to allow for a seamless 360 view of the surroundings during flight. The overall dimensions of the windscreens and door can be seen in the table below.

Table 2.4: Dimensions of Windscreens and Door

Component	Surface Area (m ²)	Thickness (inch)
Windscreen	1.657	0.75
Door	1.458	0.25

The front windscreens were designed to be thicker compared to the door, as it faces more loading, and protects the passengers in the event of engine or propeller failure.

2.4 Skin Panels

As mentioned above, the panels of the fuselage will be made of AL 6061-T6. The panels will sustain a lower load than compared to that of aircrafts with a pressurized cabin. The thickness of the skin panels is generally small, so the shear flow is assumed to be uniform through adjacent stringers. Using this assumption, the stringers can be idealized to carry all direct stresses. The basic geometry of the skin panels can be seen in the table below.

Table 2.5: Dimensions of Skin Panels

Surface Area (m²)	15.955
Thickness (m)	0.000254
Weight (kg)	10.94

The two figures below show the inner and outer skin of the aircraft. The inner skin only exists in the cabin, as it is not needed in other areas and will only add unwanted weight. The inner skin, as seen as purple in the figure below, is of the same thickness as the outer skin. As it is seen in Figure 1, the skin is used to blend the fuselage into the boom seamlessly. The smooth transition from nose, to windscreens, to cabin, to boom makes the fuselage more streamlined, and will result in lower drag values once CFD analysis is performed on it.

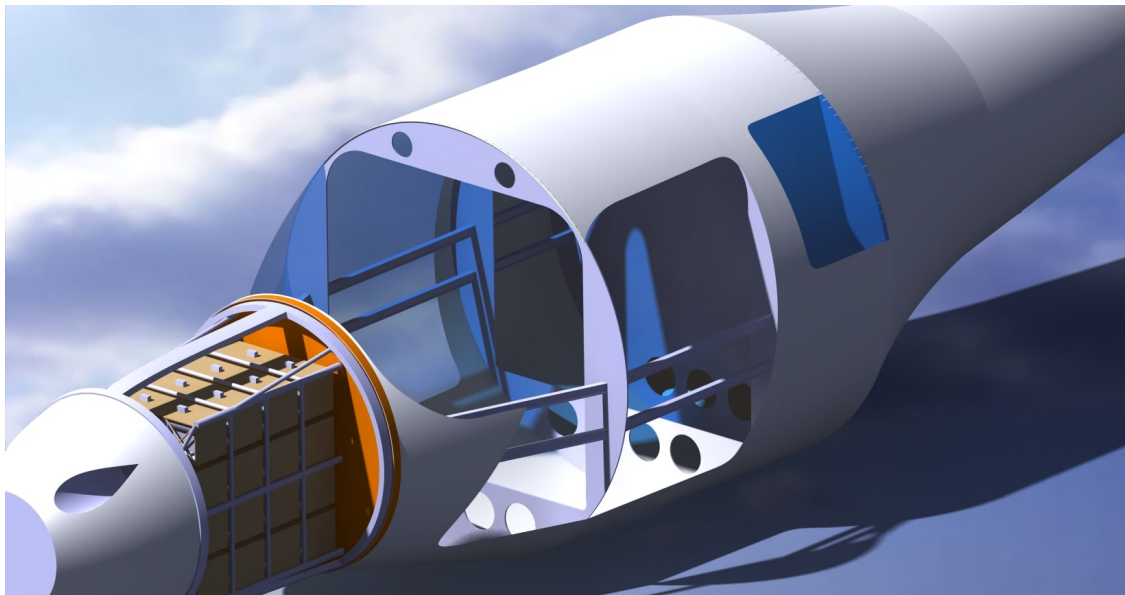


Figure 2.8: Outer Skin



Figure 2.9: Inner and Outer Skin

3 Boom Design

The boom was designed to house the allocated additional batteries for flight. A boom idealization calculation was performed by Ahmed on the stability team, which lead to a boom that was twice as long, but also half the width of the current one. The result he obtained was more geared towards the booms found in gliders, and thus was rejected. Below the structures of the boom can be seen.



Figure 3.1: Boom Structures With Batteries

Table 3.1: Boom Rib Dimensions

Number of Component	3
Outer Diameter (inch)	40.4
Inner Diameter (inch)	36.4
Thickness (in)	0.394

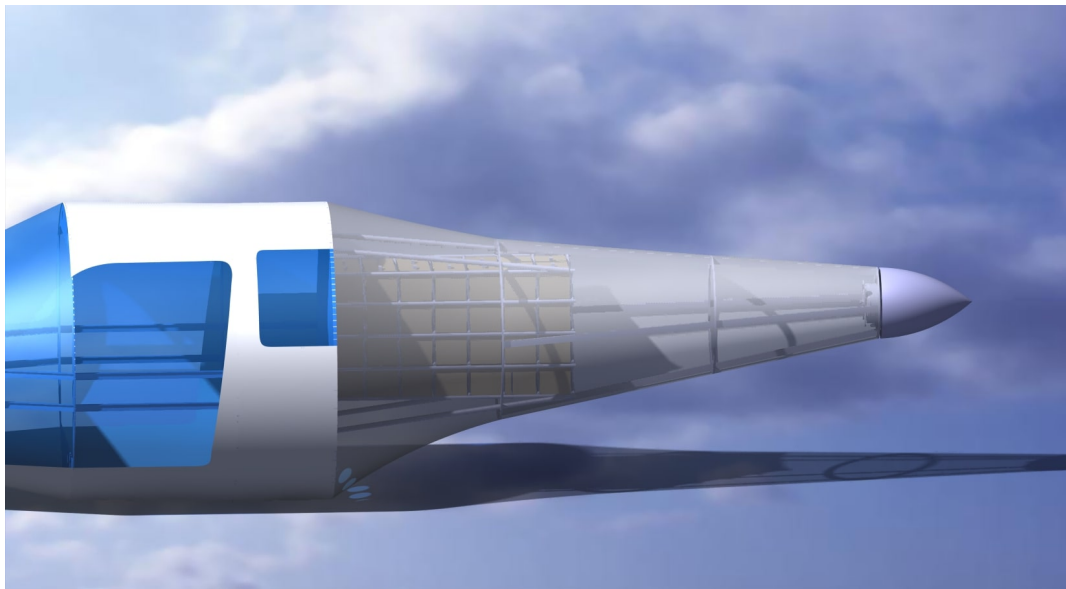


Figure 3.2: Boom Structure With Skin and Batteries (transparent to allow visibility of batteries in figure)

As mentioned above the boom houses up to 28 additional battery packs. The above boom was designed for the maximum allowance of batteries, and allows for battery configuration for different flight conditions. Less weight allocated to passengers and baggage, such as in a 2 passenger flight compared to 4, will allow for more weight to be allocated to the batteries. This will allow for a longer range and flight time. The boom was designed to withstand the tail load, while being as light as possible by reducing the number of structural bulkheads to 3 from 8. Below are the dimensions of the boom.

Table 3.2: Boom Stinger Dimensions

Number of Stringer	16
Web Thickness (in)	0.125
Flange Thickness (inch)	0.125
Beam Depth (inch)	1.5
Flange Width (inch)	1
Filet Radius (inch)	0.1

4 Structural Analysis

Structural analysis of the designed fuselage structures was performed in ANSYS Workbench. Through the analysis, more supports were added in areas that experienced high stress.

4.1 First Iteration

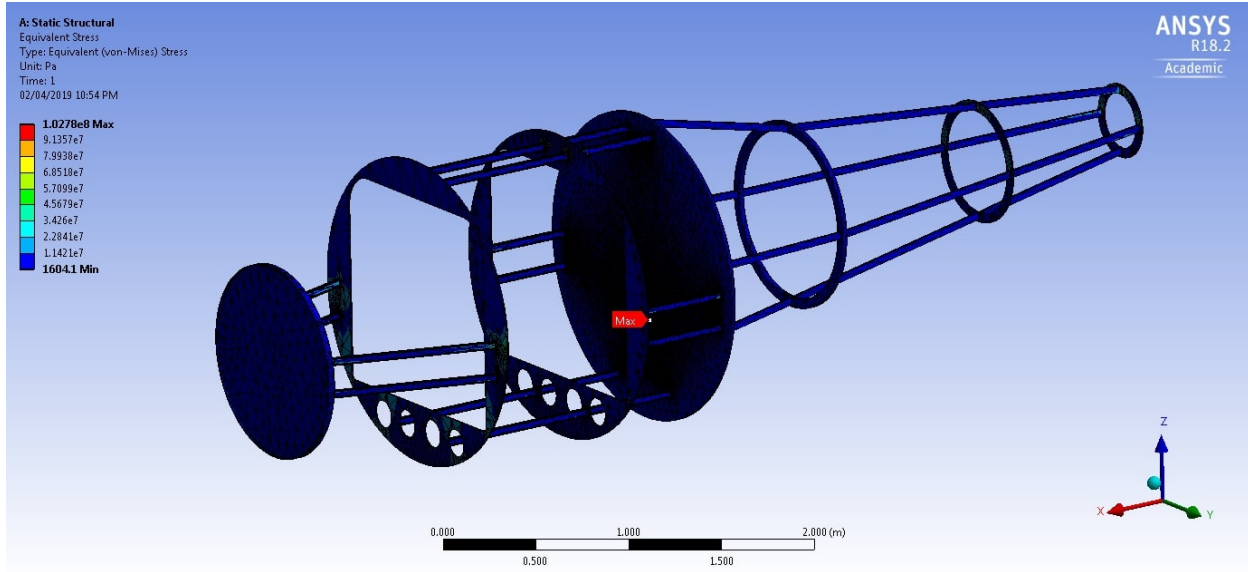


Figure 4.1: First Iteration - Stress

The above analysis was conducted under the assumption of 4 passengers and the lower battery mass of 80 Kg in the front at 120 Kg in the rear. The equivalent von-Mises Stress and deformation

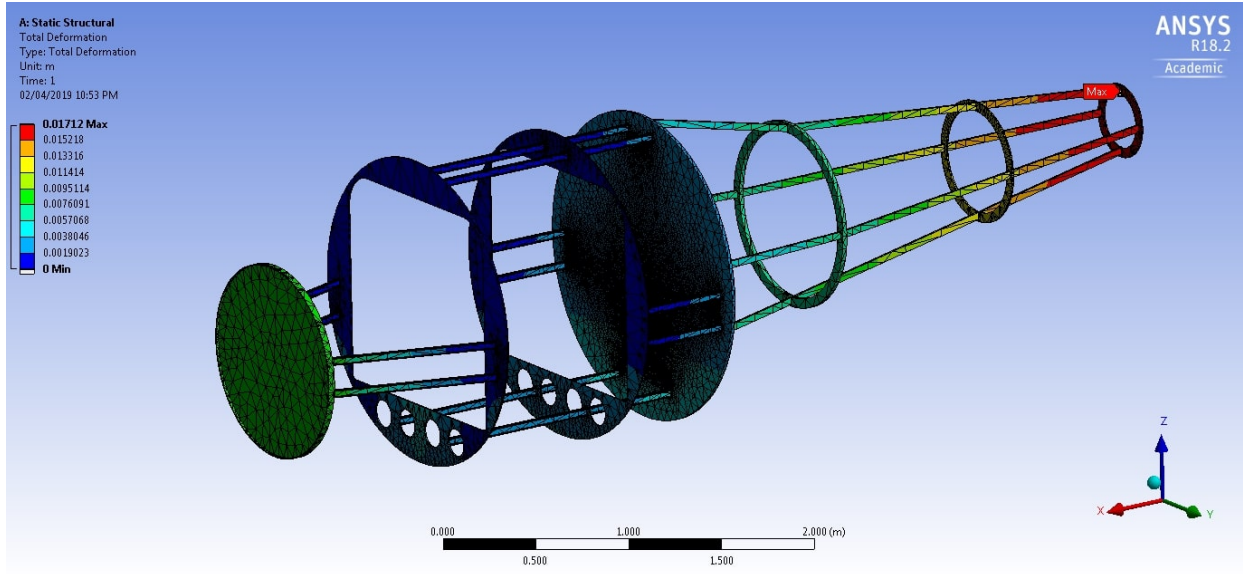


Figure 4.2: First Iteration - Deformation

of the first iteration can be seen. The design has a maximum stress of 103 MPa, at the location indicated by MAX on the figure, and a maximum deformation of 0.017 m occurring at the end of the boom. The yield strength of the aluminum alloy used is 240 MPa. Factoring in a factor of safety of 1.5, the maximum allowable stress is 160 MPa. The stress in this iteration is too high, as it does not allow for high loading factors such as in turning conditions.

4.2 Final Design

The loading for the final design can be seen in the figure below. A summary of the loading as well their magnitudes can be seen in the table below.

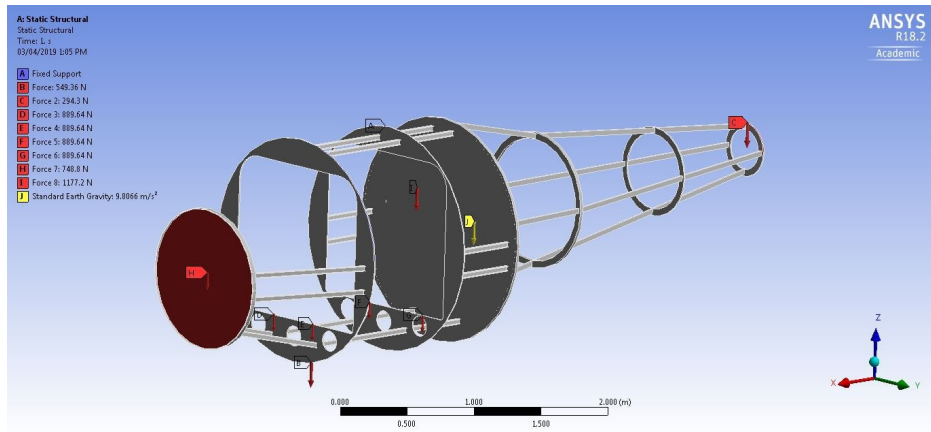


Figure 4.3: Loading for Final Design

The wing is deemed a fixed support, as in flight the wing weight is counterbalanced by the lift

Table 4.1: Fuselage Loading

Force	Type of Load	Contribution	Magnitude
A	Fixed Support	Wing Placement	N/a
B	Force	Landing Gear	549.36 N
C	Force	Tail Weight	294.3 N
D	Force	4 Passengers and Baggage	3558.56 N
E	Force	Front Batteries	748.8 N
F	Force	Rear Batteries	1177.2 N
G	Earth Gravity	Weight of Structure	9.8066 m/s ²

is produced. The fuselage must also be able to support its own weight, thus the addition of the body force for the whole structure is applied. The new design incorporates two more stingers linking the firewall to the bottom of the first bulkhead. This will ultimately reduce the stress on the first bulkhead. The addition of the stingers did not impact the overall weight of the fuselage, as it only added 2 Kgs.

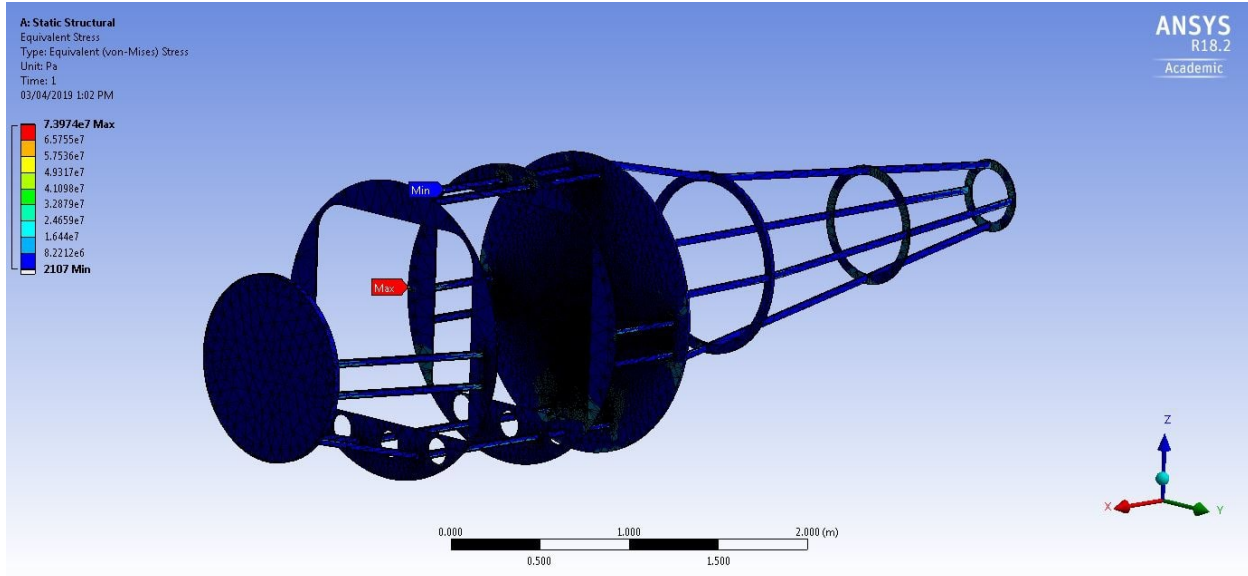


Figure 4.4: Final Design - Stress

The above analysis is conducted with the same assumptions as the first iteration. Adding the two additional stringers has drastically reduced the maximum stress to 73.9 MPa. The maximum deformation has also decreased to 0.012 m. Taking into account the safety factor, the new stress is roughly half the yield strength of aluminum.

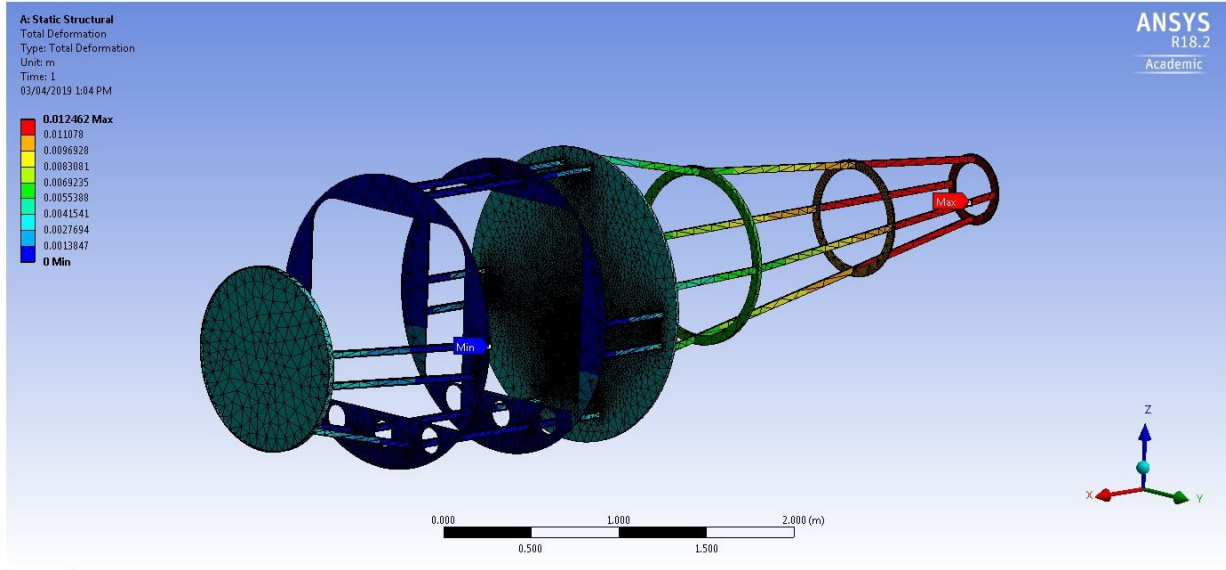


Figure 4.5: Final Design - Deformation

4.3 Maneuvering Loads

Under FAR requirements, aircrafts must be able to withstand a maneuvering load factor of 3.8. The new loading can be seen in the figure and tables below.

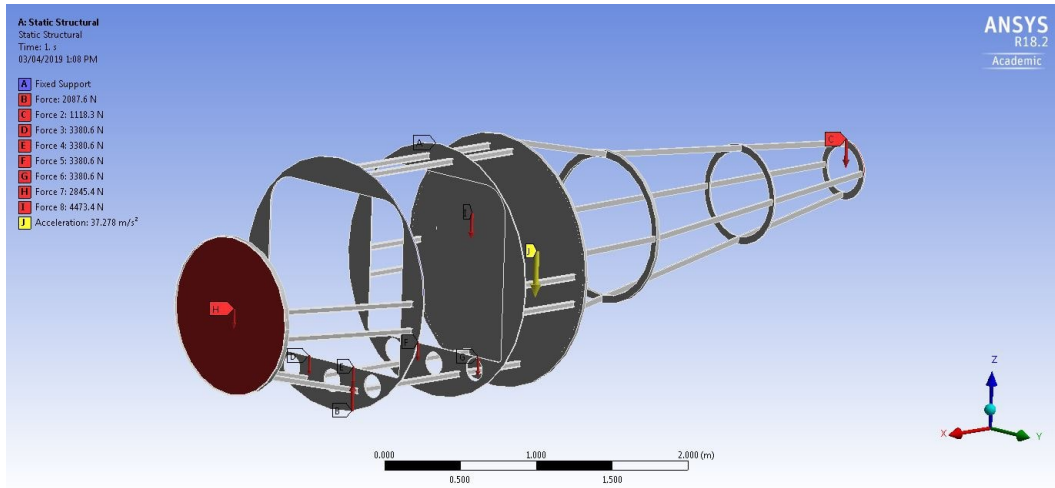


Figure 4.6: Maneuvering Loading Final Design

Referring to the figures above, the maximum stress experienced by the aircraft is 133.9 MPa, and the maximum deformation is 0.018 m occurring at the end of the boom. The increases in stress and deformation were expected. The design was able to withstand the 3.8 loading factor, while keeping the stress under the allowable 160 MPa.

Table 4.2: Fuselage Maneuvering Loading

Force	Type of Load	Contribution	Magnitude
A	Fixed Support	Wing Placement	N/a
B	Force	Landing Gear	2087.6 N
C	Force	Tail Weight	1118.3 N
D	Force	4 Passengers and Baggage	13522.5 N
E	Force	Front Batteries	2982.2 N
F	Force	Rear Batteries	4473.4 N
G	Earth Gravity	Weight of Structure	37.278 m/s ²

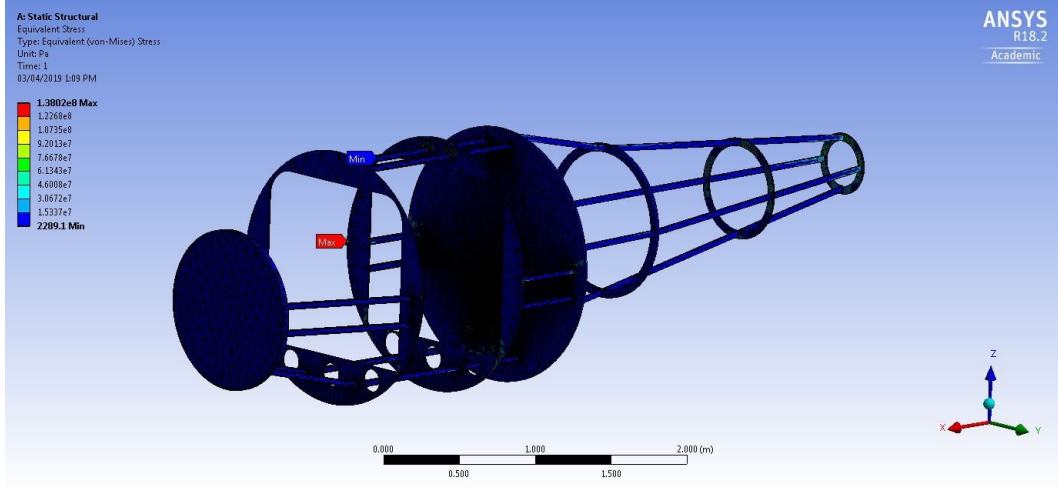


Figure 4.7: Final Design - Maneuvering Stress

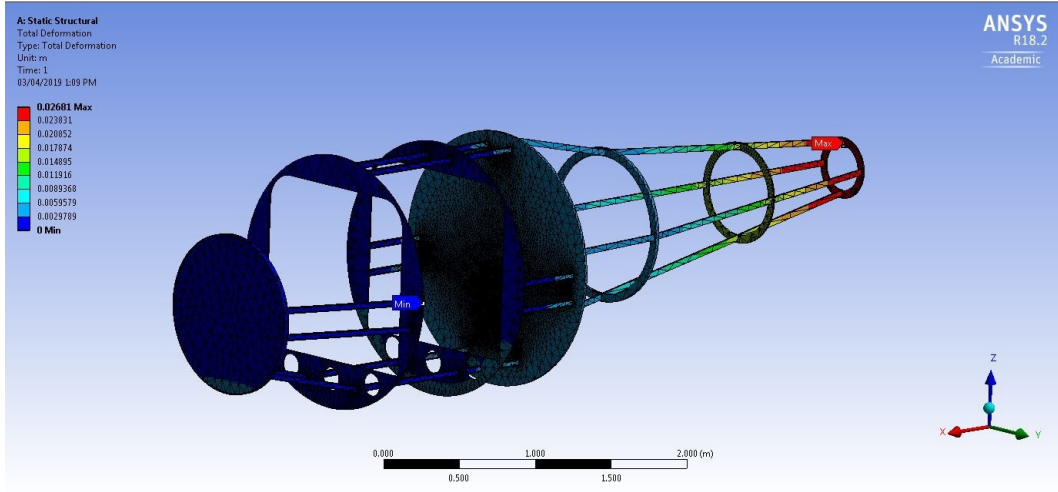


Figure 4.8: Final Design - Maneuvering Deformation

The design was successful in withstanding the loading of the passengers, baggage, tail weight, landing gear, and batteries. The overall stress experienced by the fuselage was well under the allowable for the material to yield. The high margin of safety is ideal for new pilots, as it provides

more allowable error in flight training. The design also met FAR requirements for maneuvering loads, with a slight margin as well. The structure is able to withstand sharper turns than those deemed "regulation". This also allows for more allowable error in flight training.

5 Landing Gear

5.1 Landing Gear Introduction

The Landing Gear supports the weight of an aircraft during take-off, landing and ground operations. This is one of the most critical subsystems of an aircraft and it is attached to the aircraft frame structure. Since the landing gear can have serious influence on the aircraft structure, the design of the landing gear is started in the early stage along with the aircraft design.

This report presents the design methodology and the results of the landing gear analysis and the cabin design for the Falco E-1. The landing gear and cabin are designed to meet the operation and safety requirement provided by the Canadian Aviation Regulation (CAR) and Federal Aviation Administration (FAR). A tricycle fixed landing gear configuration was selected for the aircraft with two main wheels aft of the c.g. and an auxiliary wheel forward of the c.g. . This type is the most commonly used configuration for light general aviation aircraft.

The shock absorbers types were selected for the landing gear with an oleo-pneumatic shock absorber on the nose gear and a leaf spring shock absorber on the main gear. The materials chosen for all the components of both main and nose landing gear is Titanium Ti-10V-2Fe-3Al, Aluminum A356.0-T6, Aluminum 7075-T6 and 4340 Alloy Steel. In addition, the geometric layout, tire selection, shock absorber sizing, ground loads, stress analysis and cabin design are discussed in the subsequent sections.

5.2 Design Requirement

The following table outlines the design requirement and objectives given by the MR&O for landing gear design. The design has to follow the safety requirements presented in Canadian Aviation Regulation and Federal Aviation Administration.

Table 5.1: Given Design Requirement

Category	MR&O Attribute	Requirement
Weights & Payload	Maximum Take-off Weight (MTOW)	2550 lbs = 1156.661 kg
	Maximum Landing Weight (MLW)	100% MTOW

5.3 Landing Gear Geometry Layout

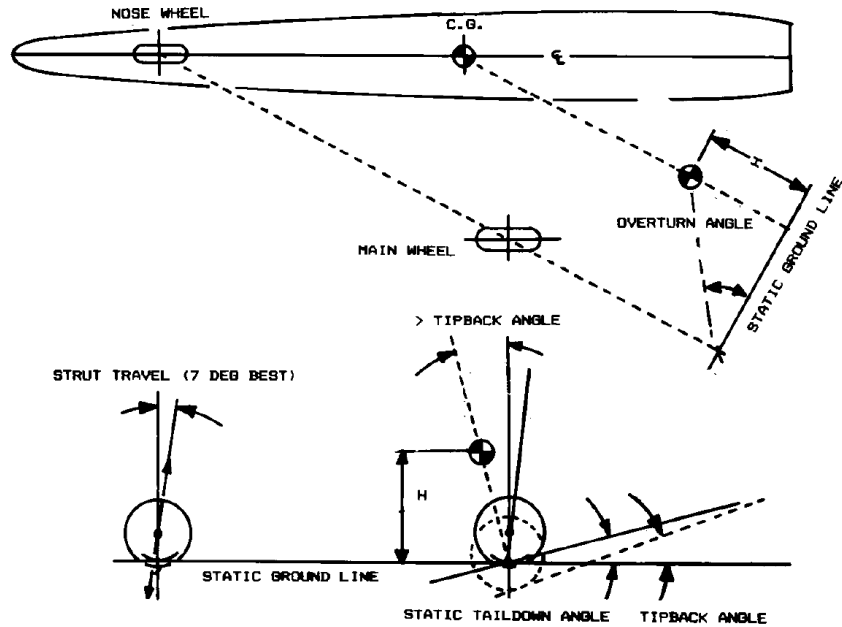


Figure 5.1: Landing Gear Layout [6]

The nose landing gear must be able to withhold a certain percentage of the weight of the aircraft. The optimum nose landing gear loading range is 10-15%. If the nose wheel carrying less than 5% of the maximum weight, it will not have enough traction to steer the aircraft. Also, if the nose wheel is carrying over 20% of the aircraft weight, the main landing will be too far away from the aft c.g. According to Daniel P. Raymer, the desired strut-travel is 7° and it allows the tire to move up and down and smooth out the ride when a larger bump is encountered. [26]

When the strut is fully extended and the tail touching, the tip back angle is at maximum attitude. In order to prevent the aircraft tipping back on the tail, the angle of the vertical from the main wheel to the c.g. has to be greater or equal to the tipback angle of 15°. [26]

The overturn angle is the angle from the c.g. to the main wheel and it is a measure of the aircraft tendency to overturn a sharp angle on the ground. The overturn angle is required to be in the range of 25 to 63°. For a paved runway, the overturn angle is typically less than 60° and less than 50° for unprepared field. [26]

Table 5.2: Aircraft's Weight On Gear and Geometry Layout

Component	Parameter
Percentage of Aircraft's Weight on Nose Gear	15%
Percentage of Aircraft's Weight on Main Gear	85%
Tipback Angle	15 deg
Overtake Angle	40 deg
CG Height	1.1745m
Wheel Base	2.35 m
Wheel Track	2.3608 m
Aircraft Nose to Nose Gear	1.05 m
Aircraft Nose to Main Gear	3.4 m

The table above outlines the aircraft's weight distribution on the wheel and the geometry layout of the landing gear. The wheel base was determined by the stability team, the wheel base ensures the landing gear can support the maximum load and the aircraft will not tip. In addition, the CG height was determined from the landing gear length and the height of the fuselage.

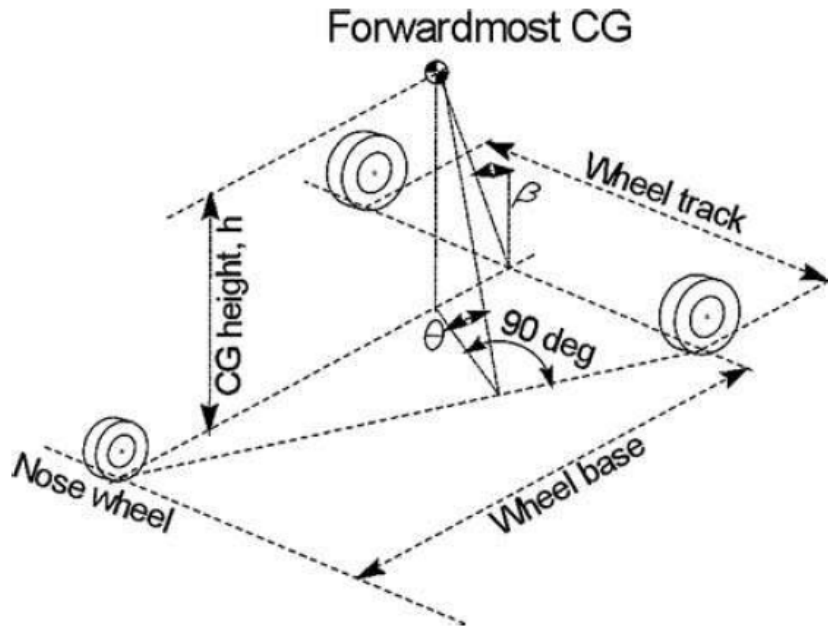


Figure 5.2: Landing Gear Geometry Location [6]

5.4 Static loads and Tire Selection

5.5 Tire Selection

The equation below used to calculate the minimum and maximum static load on nose wheel and main wheel. According to FAR 25.733, the static load has to be multiplied by a factor of 1.07 for safety concerns.

$$\text{Static Load} = MTOW * (\text{Percent of Aircraft's Weight}) * 1.07 \quad (5.1)$$

The following table indicates the maximum and minimum static load on each wheel. The results were used to determine the tire sizing for the nose and main landing gear.

Table 5.3: Maximum and Minimum Gear Load

	Static Load per Tire
Max. Nose Gear Load	409.2750 lbs = 185.64 kg
Min. Nose Gear Load	272.85 lbs = 123.76 kg
Max. Main Gear Load	1227.8 lbs = 556.93 kg
Min. Main Gear Load	1159.6 lbs = 525.99 kg

The nose landing gear has a dynamic load which is added to the static load to determine the nose tire sizing. The 10ft/s is the sink speed provided by CAR.

$$\text{NLG Dynamic Load} = \frac{10HW}{gB} = 179.6128kg \quad (5.2)$$

Table 5.4: Static Load Per Tire

Landing Gear	Load per Tire
Nose	805.24 lbs = 365.25 kg
Main	1227.8 lbs = 556.93 kg

The tire sizing for the nose wheel and main wheel were selected based on the load per tire obtain from the *Goodyear Aircraft Data Book*. [7]

Table 5.5: Tire Selection

	Nose Landing Gear	Main Landing Gear
Tire Name	Type III	Type III
Tire Size	5.00-5	6.00-6
Ply Rating	6	6
Rated Load	1285 lbs	1750 lbs
Nominal Diameter	14.2 in	17.5 in
Nominal Section Width	4.95 in	6.3 in
Rim Diameter	5 in	6 in

5.6 Growth and Minimum Clearance Allowance

The following figure represents the minimum clearance required for an unloaded free-spinning grown tire or a loaded grown tire above the axle center line [7]. After calculating the minimum clearance required, the nose landing gear fork layout can be designed¹.

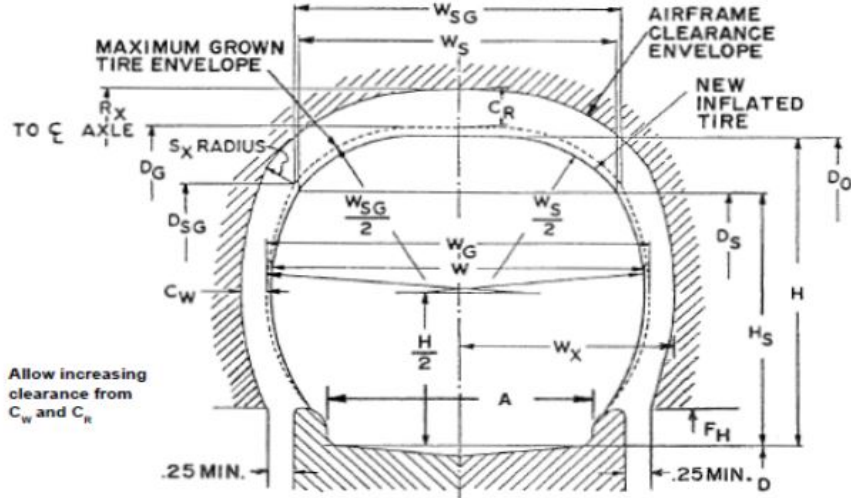


Figure 5.3: Growth and Minimum Clearance Allowance [7]

1. D = Specified Rim Diameter
2. D_{SG} = Maximum Grown Shoulder Diameter
3. D_o = Maximum Outside Diameter
4. D_G = Maximum Grown Outside Diameter
5. H = Maximum Section Height
6. W_{SG} = Maximum Grown Shoulder Width

¹All the dimensions of the tire are given in the Goodyear aircraft data book.

7. W = Maximum Cross Section Width
8. C_R = Radial Clearance
9. D_s = Maximum Shoulder Diameter
10. C_W = Lateral Clearance
11. H_s = Maximum Shoulder Height
12. R_x = Radial Distance from Axle
13. A = Width Between Flanges
14. W_x = Lateral Distance from Centerline
15. W_s = Maximum Shoulder Width
16. W_G = Maximum Grown Section Width

The following equations are used to calculate the growth and minimum clearance².

Section width growth factor $G_W = 1.04$

$$W_G = G_W * W \quad (5.3)$$

$$D_G = D + 2G_H \cdot H \quad (5.4)$$

$$W_{SG} = G_W * W_s \quad (5.5)$$

$$D_{SG} = D + 2 * G_H * H_s \quad (5.6)$$

$$H = \frac{D_o - D}{2} \quad (5.7)$$

$$H_s = (D_s - D)/2 \quad (5.8)$$

$$C_R = \frac{17.02 + 2.61 \cdot Speed/100)^{3.348}}{1000} \cdot W_G + 0.4 \quad (5.9)$$

$$C_W = 0.019 \cdot W_G + 0.23 \quad (5.10)$$

The following table presents the tire deflection of the main landing gear and nose landing gear. Moreover, the minimum clearance between the nose wheel and the nose fork is also presented.

Table 5.6: Minimum Clearance and Tire Deflection Data

Component	Parameter
C_R for Nose	0.49
C_W for Nose	0.3278
Nose tire Deflection	3.4226
Main tire Deflection	4.445

²Refer to Appendix C for calculations regarding tires

5.7 Material Selection

Aluminum Alloy 7075-T6:

Aluminum alloy 7075-T6 is a lightweight material with very high tensile strength of 572 MPa. Al 7075-T6 is a major alloy in 7000 series and contains 5.1%-6.1% zinc by weight. It possesses high static strength and is generally used to manufacture airframe structures and highly concentrated stressed parts. [27][28]

Steel Alloy AISI 4340:

AISI 4340 is mainly composed of 1.8(%) Ni, 0.8(%) Chromium and 0.25 (%) molybdenum. Due to its high tensile strength, high fatigue strength, high melting point and corrosion resistance steel alloy AISI 4340 is a favorable material for manufacturing various components of landing gear. Although, having high strength AISI 4340 has a relatively low strength to weight ratio due to its high density. Therefore, AISI 4340 is limited to manufacturing highly stressed components of a landing gear.[27][29]

Titanium - Ti-10V-2Fe-3Al:

Titanium is one of the most commonly used metal in aerospace industry due to its high strength to weight ratio, excellent fatigue strength, better heat resistance, resistance to embrittlement at low temperature, high corrosion resistance and low-thermal expansion. Ti-10V-2Fe-3Al is a beta titanium alloy, combining both strength and toughness and thus is superior to other commercial titanium alloy. Due to its high strength titanium supports greater loads with little deformation and was thus considered to manufacture a light-weight high performance landing gear.[27][30]

Table 5.7: Data of Selected Materials

Materials	Density (kg/m ³)	Tensile Yield Strength (MPa)	Ultimate Tensile Strength (MPa)	Fracture Toughness	Strength to Weight Ratio
Steel 4340	7850	470	745	101.2	0.0904
Al 7075-T6	2810	503	572	159	0.1790
Ti-10V-2Fe-3Al	4650	1170	1260	490	0.2516

5.8 Nose Landing Gear

The oleo-pneumatic shock absorber is implemented in the nose landing gear design. The diameter of strut, stroke calculation, single-acting shock absorber calculation and CAD model will be presented below.

5.9 Stroke Calculation

Stroke is the length of required deflection to fully absorb the landing energy. It depends on sink speed or landing velocity at touchdown, shock absorption mechanism and residual lift on wing after touchdown. The sink speed is 3.05m/s or 10 ft/s, and if the sink speed is 4-5 ft/s is considered bad landing. In addition, by following the MR&O requirement, the maximum landing weight 100% of the maximum take-off weight. Therefore, leveling landing conditions is set to lift equal maximum aircraft weight. The equation below is used to determine the stroke:

$$Stroke(S) = \frac{V_v^2}{2 * g * \eta * N} - \frac{\eta T}{\eta} * S_T \quad (5.11)$$

$$Strut = 3 * Stroke \quad (5.12)$$

$$W_{NLG} = (1156.661 * 9.81 * 1.5 * 0.15) / \cos(7) = 2572.2 \quad (5.13)$$

Where S is the gear stroke, Vv is the sink speed, St is the tire deflection, N is the Gear load factor and nS and nT is the efficiency coefficients for the shock absorber and the tire. The gear load factor N depends on the type aircraft, for general aviation is set to be 3. The weight of the NLG is multiplied with 1.5 safety factor. According to Daniel P. Raymer, the total length of the oleo shock absorber will be multiplied by a factor of approximately 2.5 or greater. For safety concerns, 3cm is added to the stroke and strut length for additional space [26].

Table 5.8: Stroke Calculation Data

Component	Parameter	Component	Parameter
W_{NLG}	2572.2 N	nt	0.47 m/s ²
S_T	0.03m	V_v	3.05 m/s
n	0.8	2/3 of Stroke	13.9953 cm
Stroke	20.9931 cm	Strut	62.9782 cm

5.10 Strut Diameter and Piston Diameter

According to Raymer, the external diameter is typically 30% greater than the piston diameter. [26] Therefore, the diameter of the piston can be determined by dividing the strut diameter by 1.3 . The following equations are used to calculate the diameter of the strut and the diameter of the piston.

$$P_m = \frac{W_L}{\eta_s} \quad (5.14)$$

$$d_s = 0.041 + 0.0025\sqrt{P_m} \quad (5.15)$$

$$\text{Piston Diameter} = \text{Strut Diameter}/1.3 \quad (5.16)$$

Table 5.9: Diameter of the strut and Piston

ns	1
Pm	$1.8613 \cdot 10^4$ lbs
Strut Diameter (ds)	0.3821 ft = 11.6457 cm
Piston Diameter	8.9583 cm

5.11 Performance Characteristics of the Shock Absorber

The performance characteristics of the oleo-pneumatic shock strut can be calculated by internal pressures and the internal volumes obtained during the landing simulations. Single acting shock absorber is used in the nose gear [6].

Table 5.10: Two Compression Ratio

Total Stroke (m)	0.209931
Static to extended	2.1:1
Compressed to Static	1.9:1

The static to extended, compressed to static pressure ratios and static pressure, P2, were given by Norman S. Currey. The piston area A was determined from the CAD model [6].

Table 5.11: Calculated Loads at Different Position

	kg	lb	Stroke (m)
Max NLG Load (15%) in kg	173.4694	382.500027	
Load Extended in kg	82.60447619	182.14287	0
Load static in kg	173.4694	382.500027	0.139954
Load Compressed in kg	329.59186	726.7500513	0.209931

$$V_3 = 0.1 * (\text{Stroke} * \text{PistonArea}) \quad (5.17)$$

$$\text{Displacement} = \text{Stroke} * \text{PistonArea} \quad (5.18)$$

$$\text{Max Strut Pressure } P_3 = 1.9 * 10342.14 \text{ kpa} = 19650.066 \text{ kpa}$$

$$\text{Fully Extended Volume } V_1 = V_3 + D \quad (5.19)$$

$$P_1 * V_1 = P_3 * V_3 \quad (5.20)$$

$$P_1 = \frac{P_3 V_3}{V_1} \quad (5.21)$$

$$\text{Static Volume} = \frac{P_1 V_1}{P_2} = V_2 \quad (5.22)$$

$$S_s = TotalStroke - (V_2 - V_3) / A \quad (5.23)$$

$$P_x = \frac{P_1 V_1}{V_X} \quad (5.24)$$

The equations above were used to calculate volume, pressure and load inside the oleo strut. The results are shown in the table below, and a load-stroke curve was then plotted.

Table 5.12: Calculation of Isothermal Compression

Stroke m	V, m^3	P, kpa	Load (A*Px)
0	0.016551072	4924.828571	290.9637968
0.01049655	0.015930925	5116.538472	302.2902094
0.0209931	0.015310778	5323.77838	314.5341505
0.03148965	0.014690632	5548.515036	327.8118168
0.0419862	0.014070485	5793.06191	342.2598907
0.05248275	0.013450338	6060.159136	358.0402619
0.0629793	0.012830192	6353.076625	375.3461201
0.07347585	0.012210045	6675.748599	394.409903
0.0839724	0.011589898	7032.951324	415.5137972
0.09446895	0.010969752	7430.541123	439.0038001
0.1049655	0.010349605	7875.777956	465.3088374
0.11546205	0.009729458	8377.772756	494.9671922
0.1259586	0.009109312	8948.117486	528.6637292
0.13645515	0.008489165	9601.791351	567.2834348
0.1469517	0.007869018	10358.49552	611.9902738
0.15744825	0.007248872	11244.67296	664.3465232
0.1679448	0.006628725	12296.66208	726.4990922
0.17844135	0.006008578	13565.80324	801.4812215
0.1889379	0.005388432	15127.07159	893.7225168
0.19943445	0.004768285	17094.44628	1009.956981
0.209931	0.004148138	19650.066	1160.945549

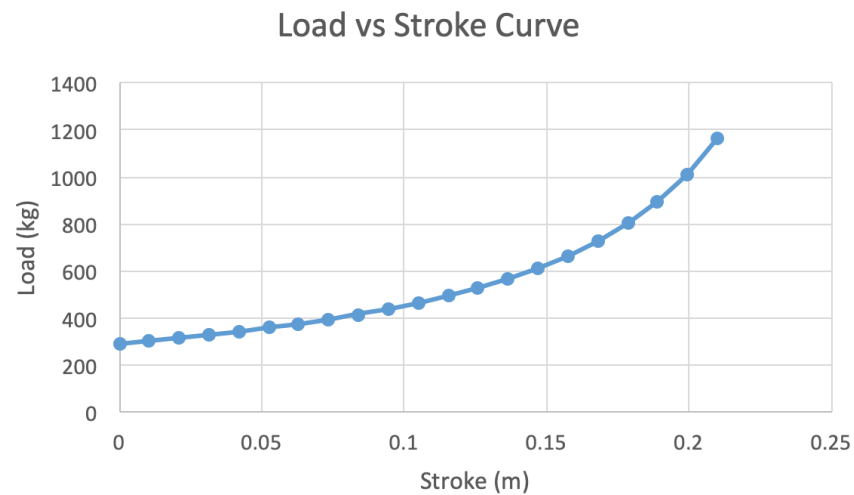


Figure 5.4: Load vs Stroke Curve

5.12 CAD Model

The table below is the materials that will be used on the nose landing gear. The oleo strut and the axle were tested in ANSYS and it is shown in the stress analysis and ground load section.

When designing the nose landing gear, the torque link angle is ensured that it has no more than 135° when it is fully extended. For nose wheel steering, a steering rod is attached on each side of the nose landing gear and it is controlled by the rudder pedal. When the rudder pedal is depressed, a spring-loaded steering bungee will turn the nose wheel through an arc about 10° each side of center. Through applying the brake, the angle to turn is increased up to 30° each side of center. Moreover, a shimmy damper is added on the side to ensure that the angle to turn will not exceed 30° . [31] Besides, all the bolt and nut that is used in the nose landing gear will be same as the Cessna 172s.

The wheel for the nose gear is made out of A356.0-T6 and it is manufactured by Grove Aircraft Landing Gear System Inc. Therefore, the axle was designed to fit the sizing of the wheel and brake. The wheel is already FAA TSO-C26d certified and the wheel assembly tests are listed below: [32]

- limit radial static load test at 153% of rated static load
- Ultimate radial static load test at 266% of rated static load
- Overpressure test at 350% of max rated wheel pressure
- Roll test of 1000 miles at full static load and 110% wheel rated pressure

Table 5.13: Selected Material for Each Component on NLG

Component	Material
Oleo Strut	Ti-10V-2Fe-3A
Nose Fork	Ti-10V-2Fe-3A
Upper Mount	Ti-10V-2Fe-3A
Lower Mount	Ti-10V-2Fe-3A
Axle	Steel 4340
Torque Link	Steel 4340
Shimmy Damper	Al 7075-T6
Steering Rod	Al 7075-T6
Wheel	Aluminum A356.0-T6

The nose landing gear will be attached at the front of the bulkhead in front of the avionics system. Two mounts will be holding the landing gear in place and each mount is welded in to the bulkhead.

The following figure is the nose landing gear for the Falco E-1:

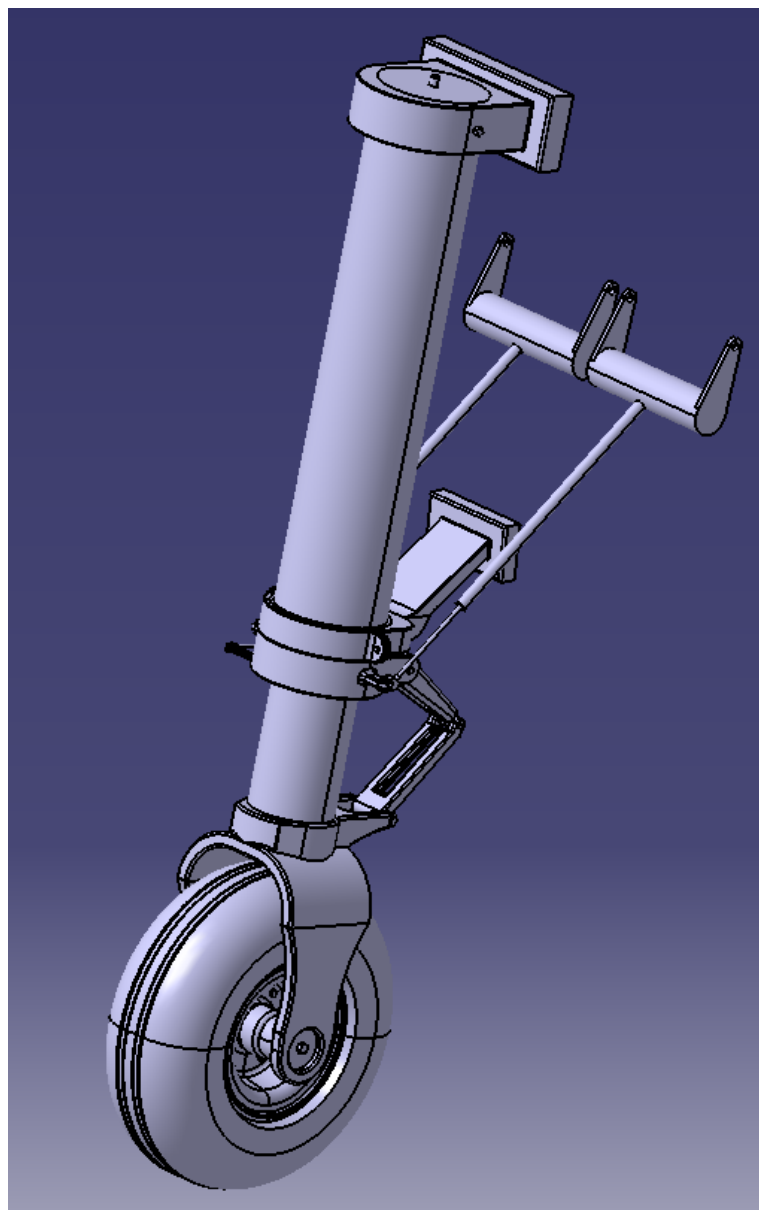


Figure 5.5: Nose Landing Gear CAD Model

5.13 Stress Analysis

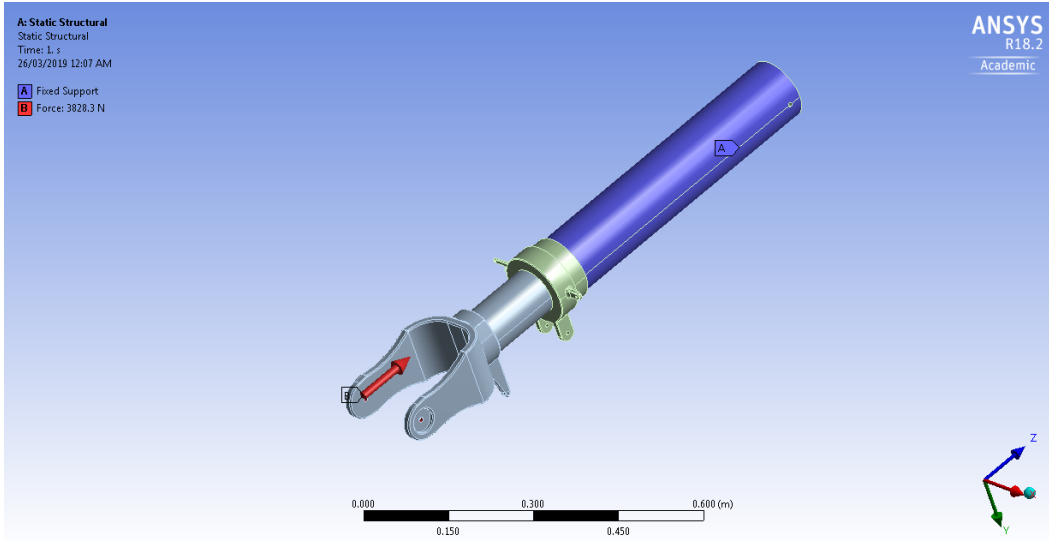


Figure 5.6: Nose Landing Gear

The upper part of the oleo strut was constrained, as it is attached to fuselage. According to CARs part V 523.499, a vertical component factor of 2.25 is the static load on the wheel. Therefore the ground load that will be encountered under the nose fork will be 3828.3N . [33]

$$Force = 2.25 * 1701.48N = 3828.3N$$

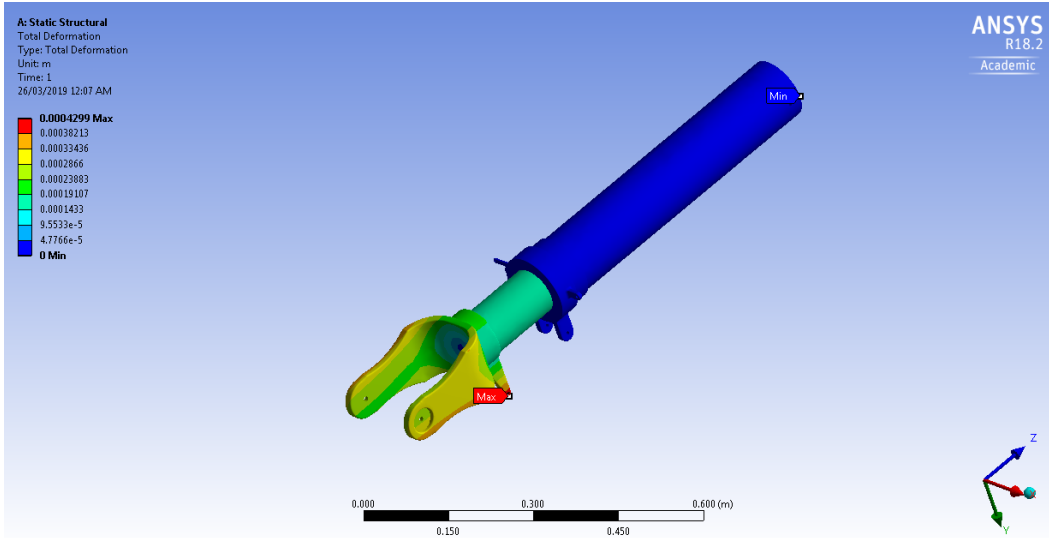


Figure 5.7: Nose Landing Gear Total Deformation

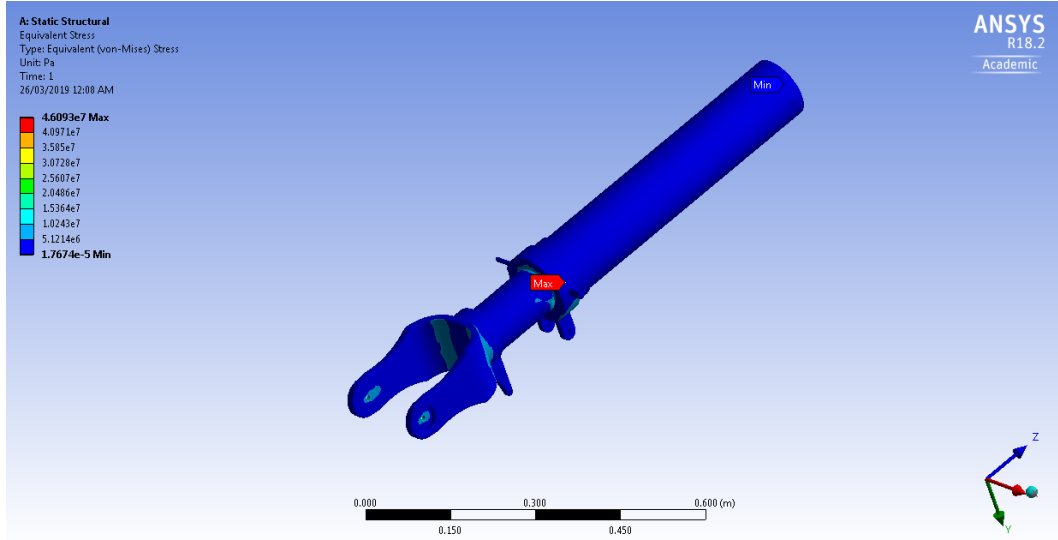


Figure 5.8: Nose Landing Gear Equivalent Stress

Figure 5.7 and Figure 5.8 demonstrated the total deformation and equivalent (von-Mises) stress of the nose landing gear. The total deformation is 0.0004299m and the maximum equivalent stress is $4.6093 \cdot 10^7 \text{Pa}$.

6 Main Landing Gear

A leaf spring shock absorber design was used in the main landing gear. This type of shock absorber is the most commonly used for light aircraft. An initial layout of the leaf spring shock absorber was first obtained and the CAD model was produced to be used in ANSYS.

6.1 Stroke Calculation

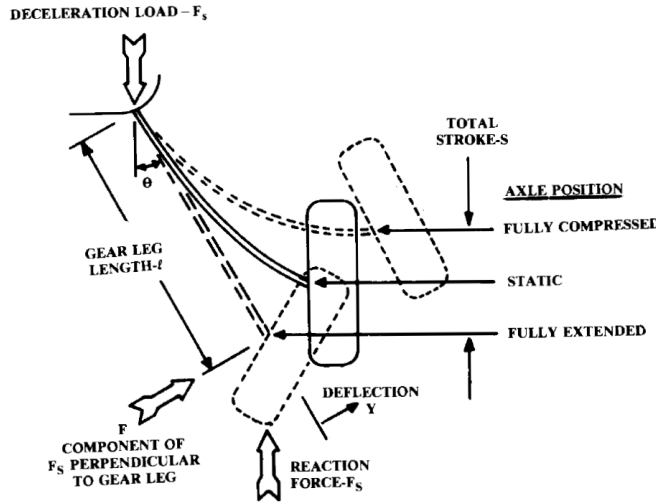


Figure 6.1: leaf spring gear [6]

$$S = \frac{\frac{V_z^2}{2gN} - \eta_t S_t}{\eta_S} + 0.03 = 0.3038m \quad (6.1)$$

- Leaf Spring efficiency $\eta_S = 0.5$
- Main tire Deflection $S_t = 0.045$

Table 6.1: Leaf Spring Calculation Data

Component	Part
Modulus of Elasticity (Ti-10V-2Fe-3Al)	107 GPA
Gear Leg Length	0.8397 m
Weight on MLG (W)	14467 N
Reaction Force (F _s)	21701 N
Force (F)	13949N
Deflection (y)	0.4726 m
Total Stroke	0.3038 m

The leaf spring sizing was determined by calculating the beam width and the variables: W_R & W_B can be obtained from Figure 6.3.

The equation below is in inches, therefore the gear leg length is multiplied by 39.37 . W denotes the maximum weight of the aircraft.

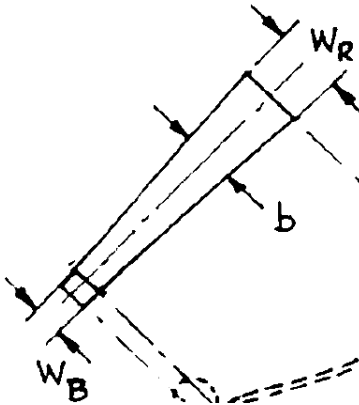


Figure 6.2: leaf spring gear beam width [6]

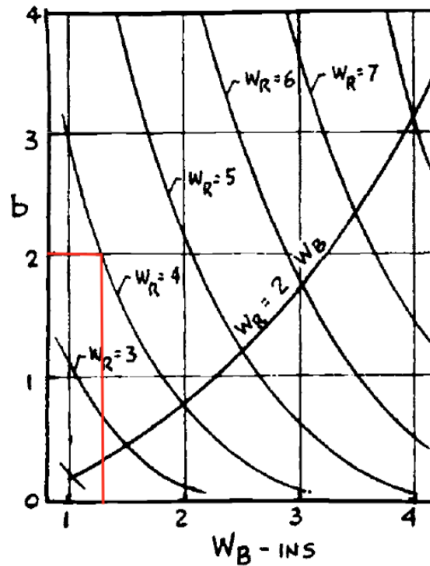


Figure 6.3: leaf spring sizing [6]

$$b = \frac{0.0067 * W * (W/A)^{0.5}}{\text{Gear Leg Length} * 39.37} \quad (6.2)$$

Using Figure 6.3, $b = 2.1053$ and find that $W_R = 4$ in and $W_B = 1.35$ in. However, this value is the minimum sizing of the leaf spring. Since the brake and wheel was already selected for the design, thus W_B was set to 1.7131 inch and $W_R = 4.5$ inch to ensure there is enough space to install the axle and the brake.

- $W_R = 4.5/39.37 = 0.1143$ m
- $W_B = 1.7131/39.37 = 0.0435$ m
- The minimum thickness of the leaf spring (t) = $W_R/8 = 0.0143$ m

The initial leaf spring was tested in ANSYS, and the equivalent stress and total deformation did not meet the safety factor. Therefore, a c beam is added on leaf spring and increased the outer thickness to 0.0404 m.

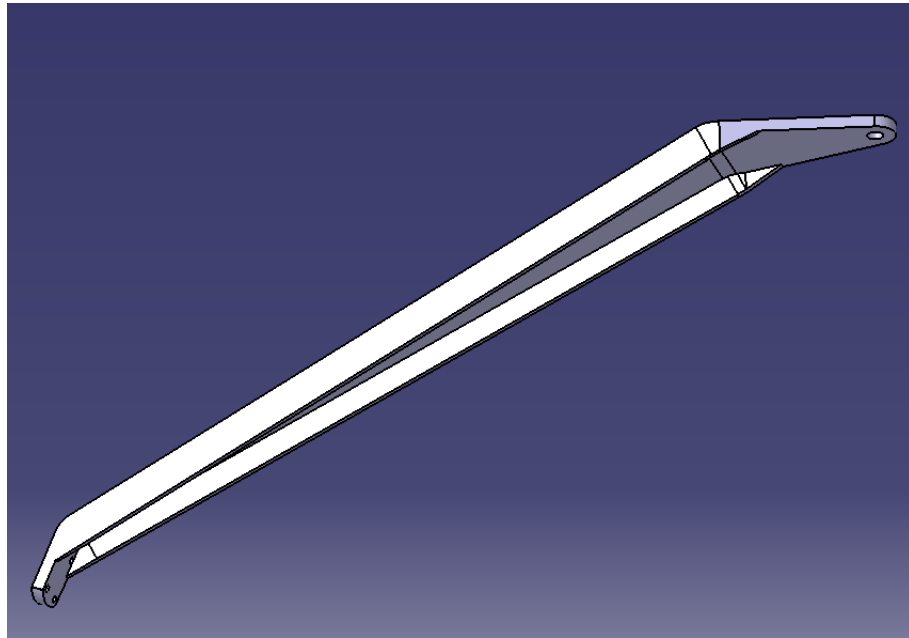


Figure 6.4: Finalized leaf spring

6.2 Breaking Energy

Area = 13.975, cl max = 1.740, Density = 1.225

$$V_{stall} = \sqrt{(2 * Wl_{max}) / (density * Area * cl_{max})} \quad (6.3)$$

$$\text{KE Breaking} = 0.5 * (Wl_{max} / g) * V_{stall}^2 \quad (6.4)$$

$$\text{KE Breaking on Each Wheel} = KE_{Breaking} / 2 \quad (6.5)$$

Kinetic breaking on each wheel is $1.132 * 10^4$

6.3 CAD Model

Both wheel and brake are manufactured by the Grove Aircraft Landing Gear System Inc. and they are FAA TSO-C26d certified. The brake caliper was tested in 100 stop design-landing test kinetic energy, structural torque test of 150% max actual torque, overpressure test at twice max rated pressure and caliper endurance test of 100000 cycles at design rated landing pressure and 500 cycles at brake rated max pressure. [34]

The main landing gear is placed 3.4m away from the nose and it is attached to two mounting plates. Each mounting plate is welded to the bulkhead. All of the bolts and nuts that were used in the main landing gear will be same as the Cessna 172s. The following figure shows how the main landing gear is mounted to the fuselage.

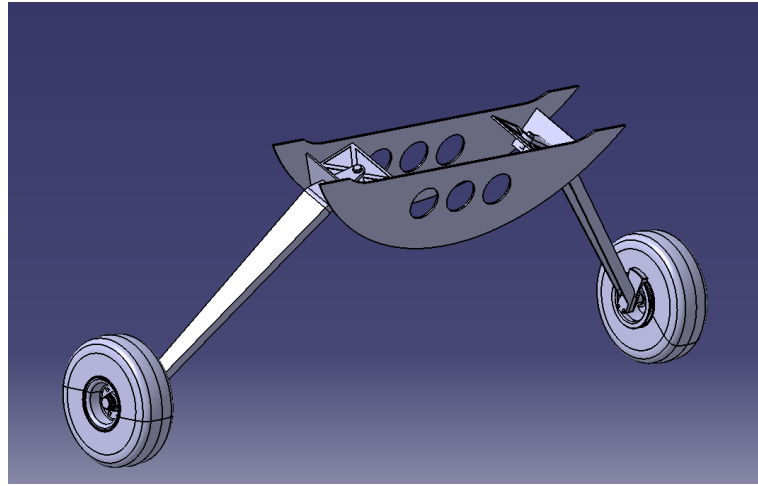


Figure 6.5: Main Landing Gear Assembly View

Table 6.2: Selected Material for Each Component on MLG

Component	Material
Leaf Spring	Ti-10V-2Fe-3Al
Axle	Steel 4340
Wheel	Aluminum A356.0-T6
Brake	Aluminum A356.0-T6

The figures below is the front and rear view of the main landing gear model.

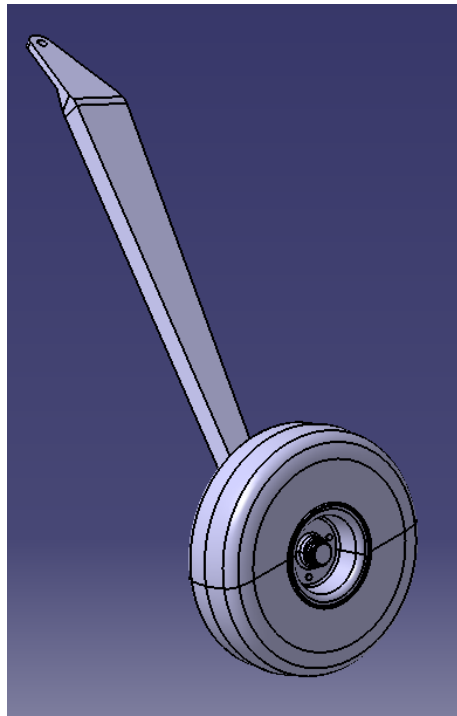


Figure 6.6: Main Landing Gear CAD Model Front View

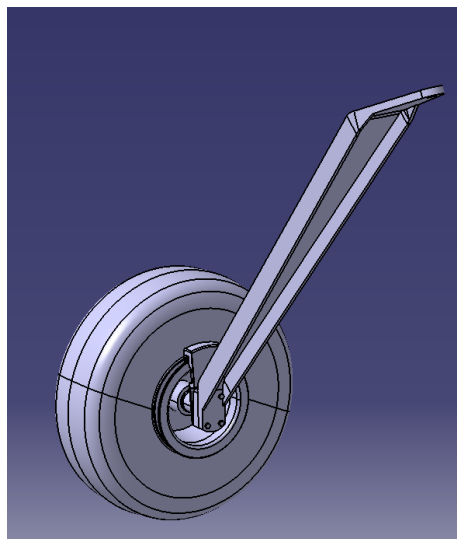


Figure 6.7: Main Landing Gear CAD Model Rear View

6.4 Stress Analysis

The ground load adding on the main landing gear is 9641.7 N and 4820.9 N on each main landing gear. The leaf spring and the axle was tested with 4820.9 N. The fixed support was constrained at the top of the leaf spring and the force was applied on the bottom of the axle. In addition, The

total deformation has to be lower than 0.3038m and the equivalent stress has to be lower than 780 MPa for safety factor.

The following figures are the stress analysis with 4820.9 N. The maximum total deformation is 0.075835 m and the maximum equivalent stress is 621.88 MPa. Therefore, the main landing gear can withstand the impact force from landing.

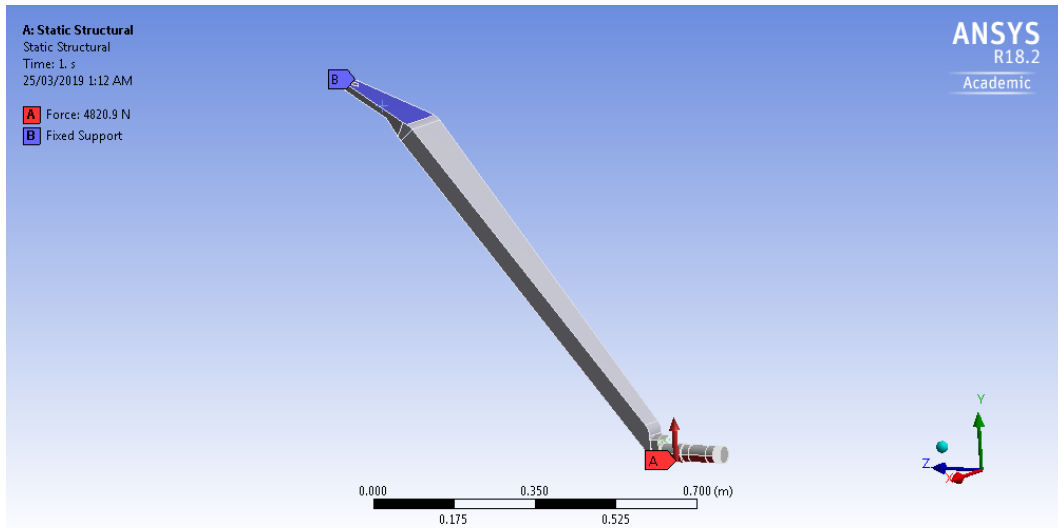


Figure 6.8: Main Landing Gear Load Layout

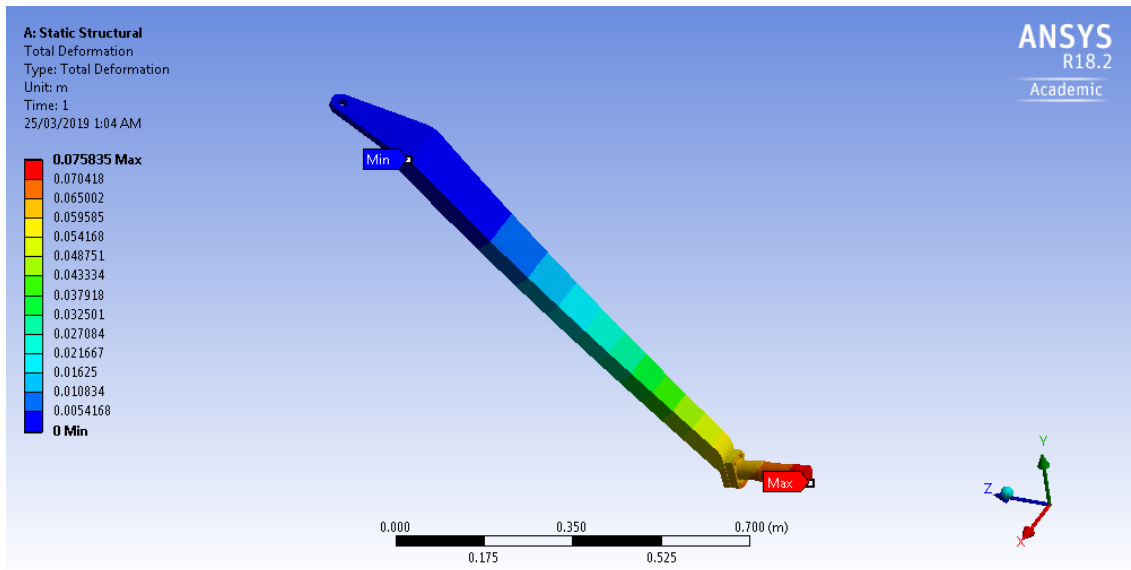


Figure 6.9: Main Landing Gear Total Deformation

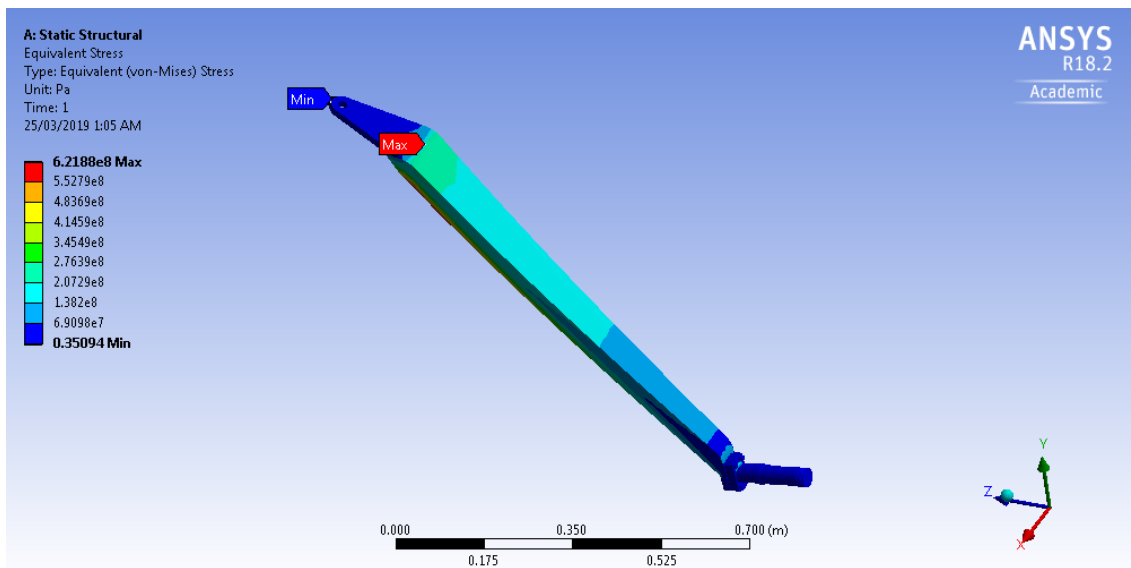


Figure 6.10: Main Landing Gear Equivalent Stress

7 Cabin Interior Design

The cabin design is clearly laid out in the MR&O. In the table below, the requirements, objectives, and the designed values are compared.

Table 7.1: MR&O Requirements Compared to Designed Values [1]

MR&O Attribute	Requirement (R)	Objective (O)	Actual	Cessna 172
Minimum Cabin Width (inside)	48 inch	52 inch	50 in	39 inch
Minimum Cabin Height (inside centerline)	46 inch	52 inch	46 inch	48 inch
Cabin Seating Length	34 in-seat pitch	36 in-seat pitch	34 inch	40 inch
Cabin Length	N/a	N/a	96.5 inch	141.7 inch
Baggage Area Length	N/a	N/a	17.19 inch	N/a

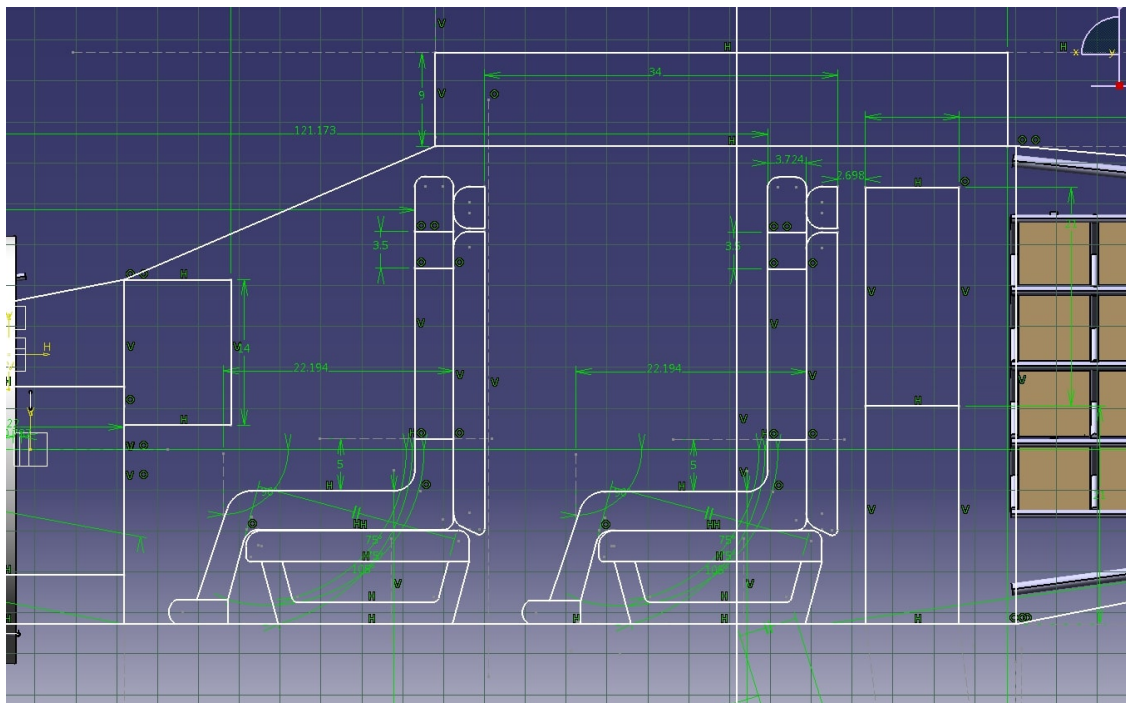


Figure 7.1: Cabin Layout (Side View)

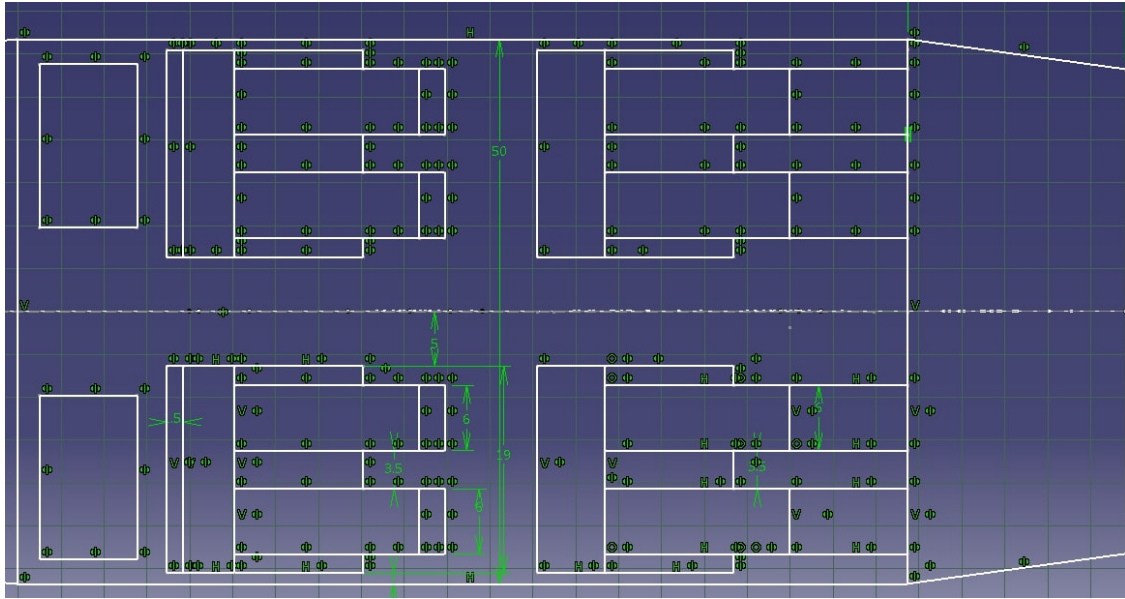


Figure 7.2: Cabin Layout (Top View) - Tentative

The cabin layout incorporates 4 passengers, as well as an area for baggage. The area allocated for the baggage was based off of the smallest class of Heys luggage which is a 21" carry on. The dimensions of the luggage can be seen in the table below. It was assumed that the luggage would be stacked on top of each other, two behind each seat. The total height of the combined baggage is a minimum of 42 inches. The cabin height was designed to be 46 inches tall based on the MR&O, and therefore the assumption is valid. The above layout was modified by the interiors team to have a combined back seat. This design change resulted in the loss of the middle opening, which was designed wide enough to be able to slide a luggage throw it and into the baggage area. To combat this lose of access, the new seats will fold down to allow access to the baggage area. This would imply that the passengers would not have access to the baggage during flight. As stated in the MR&O, “Access to the baggage is not a requirement, but access to baggage is seen as a positive sales feature.”, therefore we are still meeting the requirement for baggage access.[1]

Table 7.2: Baggage Dimensions [19]

Height (inch)	21
Length (inch)	15
Depth (inch)	9
Weight (kg)	2.8

7.1 Cabin Front and Rear Seat

An outline of a general American male was used as a reference to design the seat layout. The cabin layout incorporates 4 passengers, one for crew (single pilot operation) and three for passengers (includes fwd RH seat). The seat is designed to give the passenger and pilot a comfortable ride, keeping their posture correct and reducing the pressure on their spine and lower back.

The following figures are the new front and rear seat design.



Figure 7.3: Rear Seat



Figure 7.4: Front seat

The following figures showcase the function of the rear seat. There is a folding armrest on each side and a center folding armrest with cup holder for the passenger. The cup holder is made of plastic and it is attached to the center folding armrest by two fasteners rivet clips. By using the clips, the cup holder can be easily detached from the armrest for cleaning. Each seat has a headrest which allows the passenger to adjust the angle to their own comfort. A USB and USB-C port is added to the center front of the seat, which allow the passenger easier to use it. The rear seat can be folded forward, allowing the pilot or passenger easy access to the baggage area.



Figure 7.5: Rear Seat with Cup holder and Armrest



Figure 7.6: USB Port on the Rear Seat

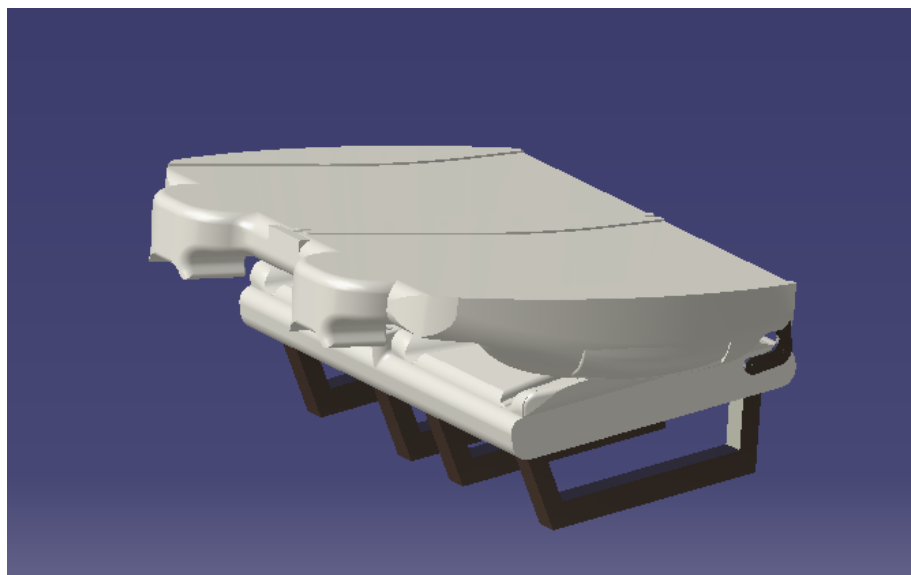


Figure 7.7: Foldable Rear Seat

In addition, the seat belt will be attached to the side of the seat. Each seat will have one inertial reel equipped shoulder harness and one lap belt with buckle and end fittings. The restraint mounts attach to the outboard sides near the door post and window.



Figure 7.8: Cabin Seat Assembly View



Figure 7.9: Cabin Seat Front View

The figures above showcase the seat layout inside the cabin. Passengers and pilot can enter the aircraft through the door beside the rear seat. The pilot's position can be reached by going in between the two front seats. If there is not enough space to access to the seat, the front seat can be folded down or it can slide back and forth.

7.2 Cabin Interior Materials

The aircraft seat is made out of aviation Leather Upholstery - Whithorn. The leather is manufactured by Gilbreath Upholstery Supply and it is FAA approved. For the seat foam, it is made by Confor Foam. The foam has the capability of absorbing impact shock and it is flame resistant. The faom has 3 layer of CF42/CF45/CF47 laminate. Confor Foam meets FAR 25.853, FAR 25.855, and CAL 117 burn specifications. [35]

The carpet is made out of aviation Carpet Upholstery - AC 7315 - Gargoyle. The carpet is manufacture by Gilbreath Upholstery Supply and it is FAA approved.

Before installing any application to the cabin interior, a soundproofing and heat barrier adhesive need to be installed to the aircraft first. By applying this materials on the aircraft interior, the

cabin will be more quiet and improve the quality of flight. Soundex basic aircraft soundproofing and materials are selected for the cabin interior. The materials are manufactured by Soundex and it meet the requirements for FAR 23.856 and FAR 25.856 Part II.

8 Wing Structures

The purpose of a wing box is to withstand the loads acting on the wing. These loads come in the form of moments, shear forces, compressive/tensile forces and torsion. These forces are caused by the lift created by the wing. All these loads should be withstood by the wing box during all phases of flight, mainly at the top corners of the V-n diagram.

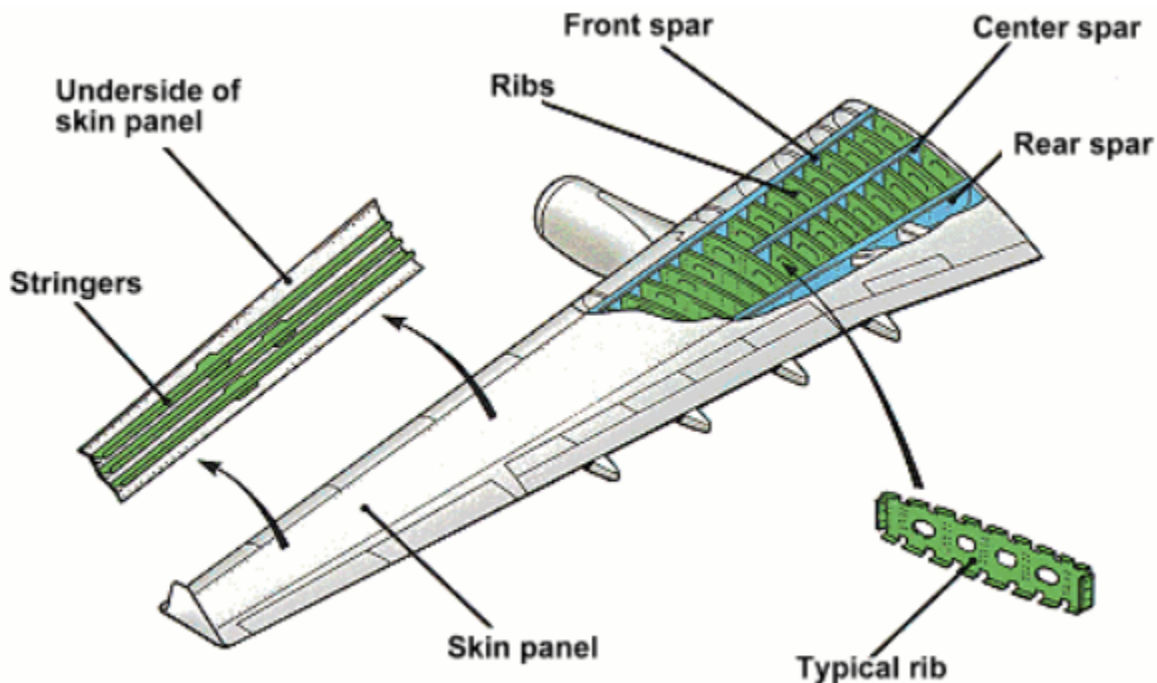


Figure 8.1: Wingbox Structural Components

8.1 Wing Spars

The wing spars run along the length of the wing starting at the root and ending at the tip. The spars are responsible for supporting the weight of the wing while grounded and support the weight of the loads when in flight. This project consisted of a two spar design. These two spars were the front spar and the rear spar. The top/bottom of the spar are referred to as spar caps. In flight, the top spar cap is under compression and the bottom spar caps are under tension, due to the net force distribution on the wing acting upwards.

8.2 Wing Ribs

The wing ribs are mainly there to provide structural shape as well as rigidity for the wing. They also help transfer loads to the main spars

8.3 Wing Stiffeners

Stiffeners help stiffen the skin which helps to prevent buckling of skin panels.

9 Load Analysis

9.1 V-n Diagram/Flight Envelope

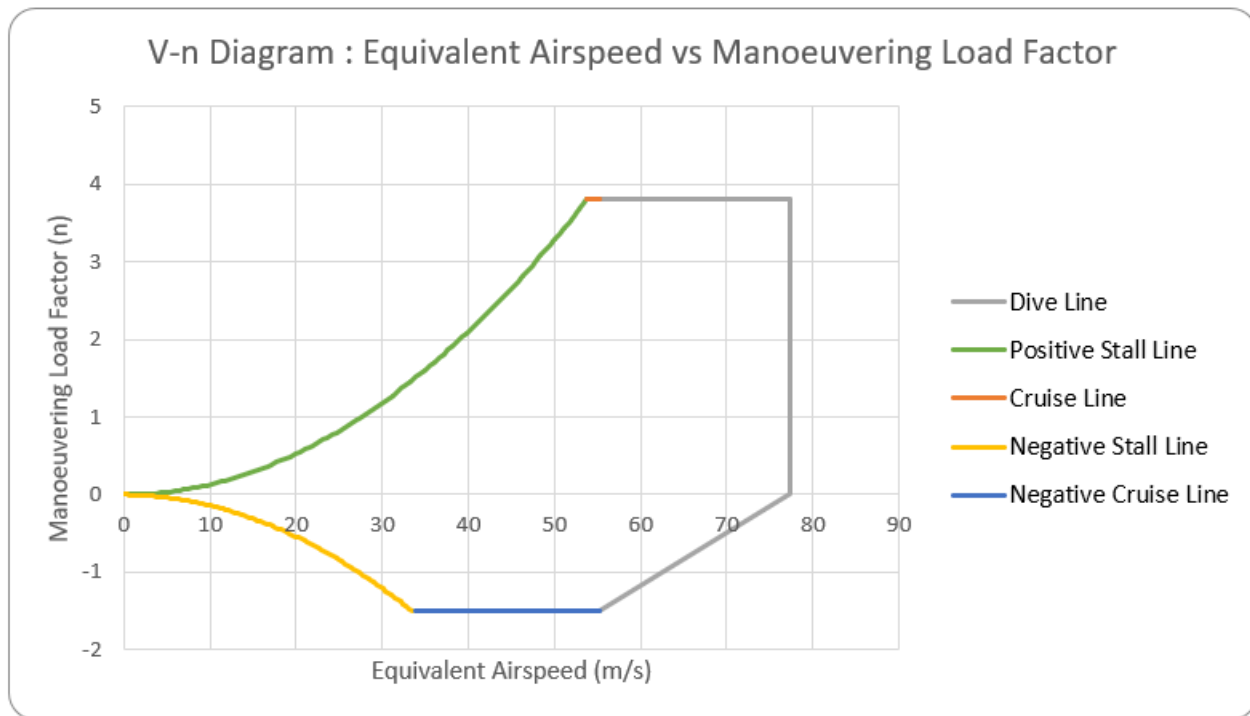


Figure 9.1: V-n Diagram at equivalent speeds

The V-n diagram 9.1 plots the range of speeds vs load factor. At 8000ft, the range of airspeeds were calculated for different load factors on the airplane. The maximum load factor that an airplane weighing less than 19000 lb, according to FAR 23 and CAR523, would be calculated using the following formula,

$$\text{Load Factor} = 2.1 + \frac{24000}{W + 10000} \quad (9.1)$$

The aircraft weight of 2550 lb was used for W. The positive limit maneuvering load factor n was then determined to be 4.01g. According to CAR Chapter 523.337, this limit need not be more than 3.8g, therefore, the positive limit maneuvering load factor was chosen to be 3.8g, as seen in the diagram. The negative load factor was assumed to be -1.58g as set by the CAR 523 rules.

The top left corner is the PHAA (Positive High Angle of Attack) and the top left corner is the PLAA (Positive Low Angle of Attack). These points are also called VA and VD, respectively. VA is the end of the stall curve and its velocity was found to be 53.8 m/s and was calculated using with an n=3.8,

$$L = nW = \frac{1}{2} \rho V^2 S C_{L,max} \quad (9.2)$$

According to CAR 523.335, the dive speed was calculated for 1.4 VC. VC was given from the MR&O, which was the High-Speed Cruise of 125 ktas or 64.3 m/s. Therefore, VD was calculated to be 77.4 m/s. The speeds mentioned above are equivalent airspeeds and were found using the following equation,

$$V_{eq} = \sqrt{\frac{\rho}{\rho_{SL}} V_{actual}} \quad (9.3)$$

V _A (m/s)	V _{Aeq} (m/s)	M _c	V _c (m/s)	V _{Ceq} (m/s)	M _D	V _D (m/s)	V _{Deq} (m/s)	V _F (m/s)	V _{Feq} (m/s)
62.60	53.81	0.20	64.31	55.27	0.27	90.03	77.38	39.33	33.80

Table 9.1: V-n Diagram Speeds and Mach Numbers

The above table summarizes the speeds and Mach numbers at 8000ft as well as their equivalent speeds. These were then used to construct the V-n diagram, with a positive maneuvering load factor of 3.8g and a negative load factor of 1.58g.

9.2 Load Analysis for Lift

Using Schrenk's approximation for the lift distribution on the wing, the following equation was used:

$$w_y = \frac{4L}{\pi b} \sqrt{1 - \left(\frac{2y}{b}\right)^2} \quad (9.4)$$

The above equation is for an elliptical wing with a lift distribution that is also elliptical. However, since the wing is tapered, the following equation is used for an ideal tapered lift distribution:

$$w_y = \frac{2L}{(1+\lambda)b} \left(1 + \frac{2y}{b} (\lambda - 1)\right) \quad (9.5)$$

Once the value has been calculated the average between the values of the two equations had to be calculated for a more exact value. The following graphs show the lift distribution for both PHAA and PLAA flight design points. The lift distribution is the same for both since there is no fuel on board the aircraft, therefore, making it a constant lift distribution at both design points.

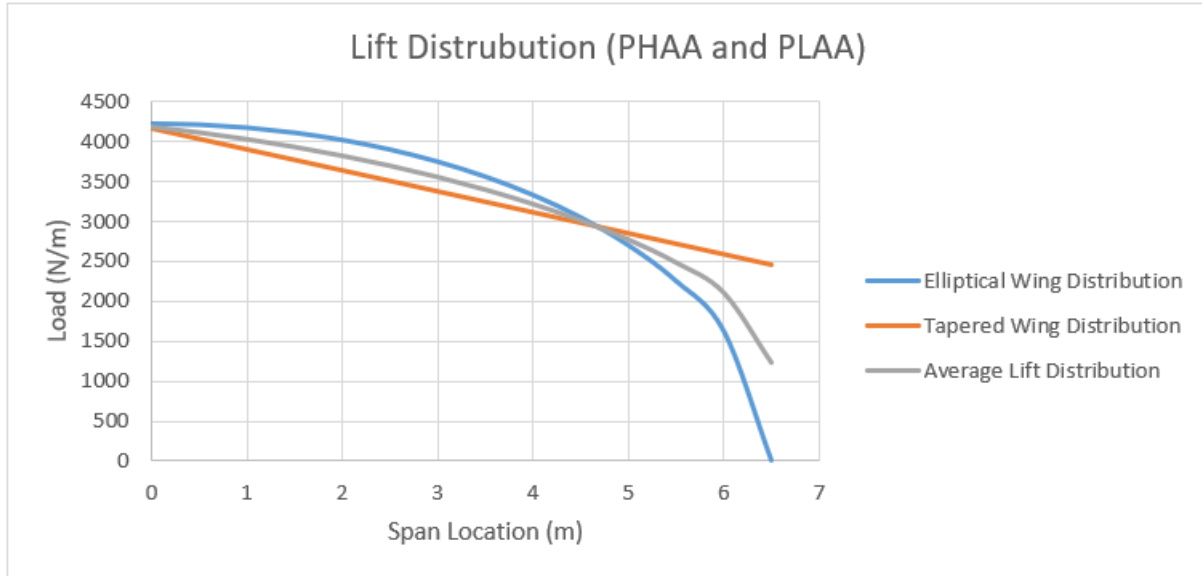


Figure 9.2: Lift Distribution

9.3 Structural load

The Cessna 172B's wing weight was used as a starting point to approximate the wing weight for the DACION Falco E-1. The C172B has a total wing weight of 236 lb. The plane is designed for an MTOW of 2250 lb, having a strut-based wing design, as well as having a shorter wing span than the Falco E-1. The fuel is also stored in the wings, which help to reduce the stresses experienced on the wing.

The DACION has an MTOW of 2550 lb, a strut less wing design, a much longer wingspan of 6.5 m and no fuel in the wings. This should theoretically increase the wing weight of the Falco E-1 by a sizeable amount. However, modern materials such as Aluminum 7175 Alloy have a high strength-to-weight ratio compared to the metals used to design the C172 in the 1960s. Combining these factors and through the iterations, a final wing weight of the Falco E-1 was found to be 125 kg (265 lb) for the first few iterations. The final iteration had a wing weight of 172kg. This weight was then divided by two to get the weight of each wing. This point load would then be converted to a distributed load varying linearly from the root to tip. The following graph shows the wing structural weight distribution along the wing half span:

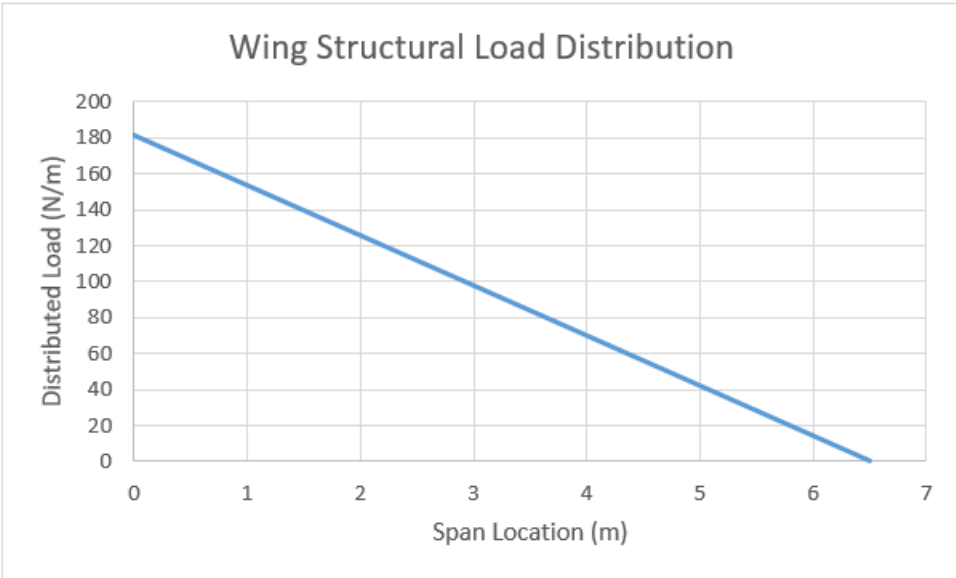


Figure 9.3: Wing Structural Load Distribution

9.4 Resultant Load Distribution

The resultant load distribution that the wing experiences is the structural load subtracted from the lift distribution. The resultant force distribution over the wing at PHAA and PLAA, since the high and low angle of attacks (AoAs) of the wing as well as the wing twist, affects the vertical components. The following graphs show the final distribution:

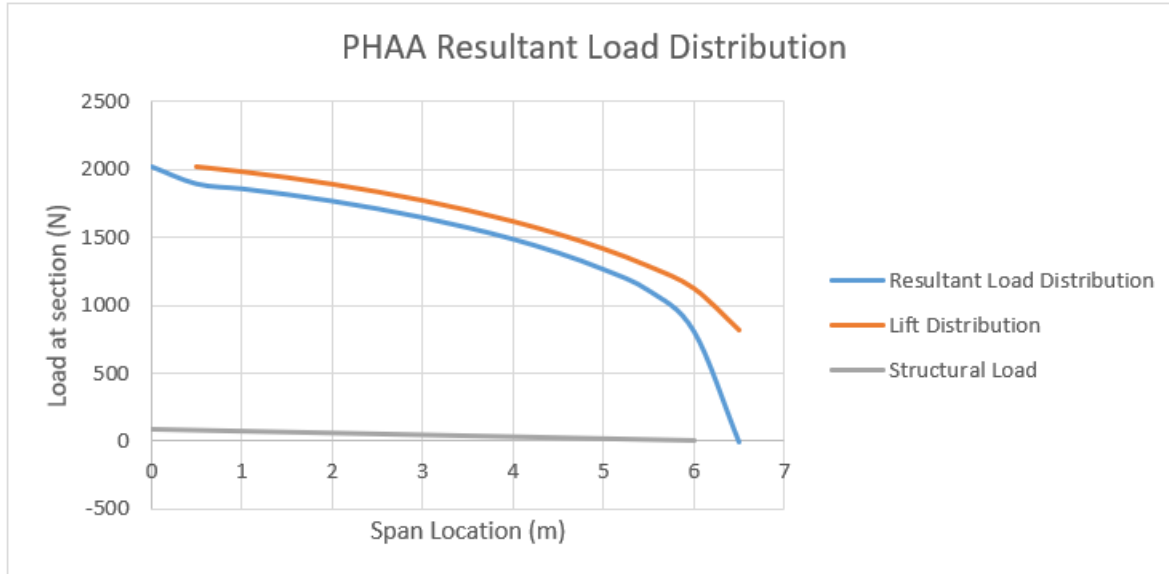


Figure 9.4: PHAA Resultant Load Distribution

The wing was divided into 0.5 m sections from 0m to 6.5 m. At each section the following calculations were done in excel to get the resultant load distribution. The first step is to find the



Figure 9.5: PLAA Resultant Load Distribution

lift, ΔL , produced at each wing section. The following equation was used:

$$\Delta L_i = \left(\frac{w_i + w_{i+1}}{2} \right) (y_{i+1} - y_i) \quad (9.6)$$

The Drag load for each wing section was also calculated by first finding the surface area for each 0.5 m section. Then using the following drag equation at a PHAA speed of 53.8 m/s and a PLAA speed of 77.4 m/s for 3.8 g. The C_d was obtained from the aerodynamics team, which was 0.0106 at 0.5 degrees. The density used was 0.962 kg/m³ at 8000 ft.

$$\Delta D_i = \frac{1}{2} \rho V^2 S_i C_{d,i} \quad (9.7)$$

The Lift and the Drag at each section was then used to find the γ , which is angle of the resultant vector of the two forces. This angle was then added to the local angle of attack due to the wing twist, which varies linearly from 2.5° at the root to 0° at the tip. The shear force normal to the wing chord, V_Z and parallel to the wing chord, V_X is then calculated. The V_Z cause a moment about the x-axis called M_X and the V_X causes a moment about the z-axis, called M_Z . The structural weight of the wing, N_{si} was also subtracted from the V_{zi} vertical load. The following equations were used:

$$\gamma = \text{TAN}^{-1} \left(\frac{\Delta L}{\Delta D} \right) \quad (9.8)$$

$$\beta = \gamma + \alpha \quad (9.9)$$

$$R = \sqrt{(\Delta L^2 + \Delta D^2)} \quad (9.10)$$

$$N = R \sin \beta \quad (9.11)$$

$$P = R \cos \beta \quad (9.12)$$

$$V_{zi} = V_{zi+1} + N_i - N_{si} \quad (9.13)$$

$$M_{xi} = M_{xi+1} + \frac{N_i(y_{i+1} - y_i)}{2} + V_{zi+1}(y_{i+1} - y_i) \quad (9.14)$$

$$V_{xi} = V_{xi+1} + P_i - P_{si} \quad (9.15)$$

$$M_{zi} = M_{zi+1} + \frac{P_i(y_{i+1} - y_i)}{2} + V_{xi+1}(y_{i+1} - y_i) \quad (9.16)$$

These distributions, as well as the drag force experienced at cruise at 3.8g, were then used to calculate the shear and moment experienced at the root for both PHAA and PLAA. Assuming that the origin of axis on the center of the aircraft, the z-axis is positive vertically upward, the x-axis is positive towards the tail of the aircraft and the y-axis is positive outwards along the span of the wing. The following table compiles these numbers:

	PHAA	PLAA
Vz (N)	20392	20853
Mx (Nm)	58493	59505
Vx (N)	4678	219
Mz (Nm)	12918	173

Table 9.2: PHAA and PLAA Shear Loads and Moments

10 Wingbox Design

10.1 Structural Idealization

To design the wingbox, a series of designs were created iteratively to determine an optimal wingbox design. A visual representation can be seen in the figure below which shows the custom airfoil obtained from the aerodynamics team, the wingbox and the stringer locations. The front spar is located at 25% of the chord length and the rear spar is located at 65% of the chord length. The height of the wingbox was then set by the bounds of the upper and lower camber of the airfoil which gives a slightly tapered shape. Due to the taper of the wing, the wing box will also have a taper in the vertical direction, z-axis as well as the x-axis. The dimensions of the wingbox at the root of the wing and the tip of the wing are listed in the table below. The wingbox will be designed to handle loads placed at the root as this is the location of max shear and moment. Designing for this will automatically be able to handle loads at farther locations as they are lower. The final iteration used a 7175-T7351 Aluminum. Wingbox stresses for latter sections were only done at 2m and 3.8m. The flap ends at 3.8m and was used as a suitable analysis section.

Note: All the following calculations were done using a general code in MATLAB for each of the iterations per material, which provided all the required values. Please refer to the Appendix 9.5 and 9.6 for the MATLAB code named General_Code.m.



Figure 10.1: Spar and stringer locations

Dimension	Root
Wingbox Width (m)	0.56
Wingbox Height (m)	0.18
Number of Stringers	6

Table 10.1: Root Dimensions

The above graph shows the locations for a normalized 1m chord airfoil. The actual locations can be found by multiplying them by the chord length at the section being analyzed. The number of stringers were initially guessed based on the number of stringers for the Cessna 172, which was 3 stringers top and bottom. This was found to be suitable even for the larger wing for the FALCO E-1. The following table summarizes the root dimensions, where the heights would be used to determine the spar web's height.

The wingbox can now be idealized using the following boom areas. The boom areas were initially guessed. Later during each iteration, the boom areas were modified in an attempt to keep the stresses at each stringer at a minimum. A final panel thickness of 1.1mm, from 0 – 2m wing half span and 0.8mm for the rest of the wing. Both spar web thicknesses were found to be 3mm. Booms B1 and B10 were assigned the highest areas as this location was expected to have the highest stresses and the locations of the front spar caps are expected to be farthest from the neutral axis of the wing box. Booms B5 and B6 were assigned the second highest stresses, due to this being the location of the rear spar caps as well. The stringers on top are named B2- B4, while the stringers at bottom are named B7-B9. The booms are assumed to handle all direct stresses while the skin and spar webs are effective only in shear. The boom idealization was then used to include the contribution of the skin panels and spar webs, which would change the boom areas accordingly. The idealized boom areas were calculated by using the following, where t_D is the skin/spar web thickness and b is the distance between adjacent stringers at each wing station:

$$B_i = B_i + \Sigma \left(\frac{t_D b}{6} \left(2 + \frac{\sigma_2}{\sigma_1} \right) \right) \quad (10.1)$$

The next step is to calculate the \bar{x} and \bar{y} locations of the wingbox which is more commonly known as the centroid. These datum points for the x locations are from the front spar and the y locations are from the horizontal axis as seen on Figure 7. After this is done the moment of

Wing Box Properties	Values
\bar{x}	196.7618 mm
\bar{y}	46.6192 mm
I_{xx}	1.78E+07 mm ⁴
I_{zz}	4.62E+07 mm ⁴
I_{xz}	5.04E+06 mm ⁴

Table 10.2: Wing box Properties

inertias for the wingbox can be calculated, which are I_{xx} , I_{yy} , and I_{xz} . The \bar{x} 's datum point and the \bar{y} 's datum is the same as the x and y locations. The following equations were used:

$$\bar{x} = \frac{\Sigma \text{Moments of areas in } x \text{ direction}}{\Sigma A} \quad (10.2)$$

$$\bar{y} = \frac{\Sigma \text{Moments of areas in } y \text{ direction}}{\Sigma A} \quad (10.3)$$

$$I_{xx} = \Sigma B_r y_r \quad (10.4)$$

$$I_{yy} = \Sigma B_r x_r \quad (10.5)$$

$$I_{xy} = \int xy \, dA \quad (10.6)$$

The following table summarizes the wing box properties at the root.

The direct stresses through the booms caused by bending can now be calculated using the stress equation below that uses the moments M_X and M_Z found from section 2.2.

$$\sigma_z = (M_z I_{xx} - M_x I_{xz}) / (I_{xz} I_{zz} - I_{xz}^2) x + (M_x I_{zz} - M_z I_{xz}) / (I_{xx} I_{zz} - I_{xz}^2) y \quad (10.7)$$

In addition to this, the 7175-Aluminum used has a Yield Strength of 435 MPa. Applying a factor of safety of 1.5, results in a max allowable stress of 290 MPa.

The stresses were optimized by manipulating the areas in such a way that the centroid is brought closer to booms with higher stresses and farther from the booms with lower areas, as the distance of the boom from the neutral axis is a significant factor. This also helps in reaching a more optimal weight for the wing as there are more booms being utilized to their maximum potential, which is close to 290 MPa. The following table summarizes the idealized boom areas and its direct stresses,

Boom Name	Starting Boom Area (mm ²)	Idealized Boom Area (mm ²)	Stress (σ_z) (MPa)
B1 (Upper Front Spar Cap)	340	577	-289
B2 (Stringer)	40	229	-256
B3 (Stringer)	40	229	-223
B4 (Stringer)	40	229	-191
B5 (Upper Rear Spar Cap)	100	307	-158
B6 (Lower Rear Spar Cap)	130	33	247
B7 (Stringer)	60	249	258
B8 (Stringer)	60	249	269
B9 (Stringer)	60	249	280
B10 (Lower Front Spar Cap)	560	550	290

Table 10.3: Final Boom Areas and Direct Stresses

10.2 Shear Flow Calculations and Analysis

Shear flow analysis was also conducted via the use of the closed section shear flow distribution, q_s . The following formula was used:

$$q_s = -((S_x I_{xx} - S_z I_{xz}) / (I_{xx} I_{zz} - I_{xz}^2))(\Sigma B_r x_r) - ((S_z I_{zz} - S_x I_{xz}) / (I_{xx} I_{zz} - I_{xz}^2))(\Sigma B_r y_r) + q_{s,0} \quad (10.8)$$

Where the Shear loads S_x (Drag load) and S_z (Lift load) were taken from Section 2.2. These loads were then converted $S_{x,w}$ and $S_{z,w}$ to take into account the taper. However, this taper only affects the calculations at the other analyzed sections and doesn't affect the root shear flow analysis. The correction factor $q_{s,0}$ was calculated using the following equation:

$$S_x \eta_0 - S_z \xi_0 = \oint p q_b ds + 2A q_{s,0} - \Sigma P_{x,r} \eta_r + \Sigma P_{z,r} \xi_r \quad (10.9)$$

For simplicity, the location of the shear center was assumed to be at the same location of the centroid. The drag load S_x was also assumed to act through the shear center, thus eliminating the term $S_x \eta_0$. The $\Sigma P_{x,r} \eta_r$ and $\Sigma P_{z,r} \xi_r$ are correction terms to consider the force components of all the booms as a result of the wingbox taper. p is the distance of the boom from the \bar{y} and ds is the length of the panel between booms. A is the area of the wingbox, which is a trapezoid. From this the $q_{s,0}$ was calculated, which is also the shear flow value at the point where the cut was made in order to calculate the q_b , which was at the front spar web (i.e B10-B1). The shear stress in the panels are then found by dividing the q_s by the thickness of the panel, which is 1.1mm/0.8mm (0m-2m/2m-6.5m) for a skin panel and 3mm for the spar webs.

An additional component of shear flow is also contributed by the wing torque, $M_{y,i}$ generated due to the lift force being a distance away from the shear center. In our case, the lift was assumed

to act at the $\frac{1}{4}$ chord point which is also the same location as the front spar. As stated above, the shear center was assumed to be at the same location as the centroid of the wingbox for simplicity. The shear stress on the panels are then calculated using the following formula,

$$\tau_{torque} = M_{yi}/2At \quad (10.10)$$

Where A is the area of the wingbox and t is the local panel thickness. Both the shear stresses are combined for the total shear stress experienced by each panel.

Finally, the equivalent Von Mises stress was calculated using the following formula,

$$\sigma_{eq} = \sqrt{3(\tau_{shear\ flow}^2 + \tau_{torque}^2)} \quad (10.11)$$

The reason there is no σ_z term in Von Mises equation is because the panels only handle shear stresses and no direct stresses. This shear stress was then compared to the critical stress for buckling of each skin panel via the use of the following formula,

$$\sigma_{cr} = \left(\frac{K_c \pi^2 E}{12(1-\nu^2)} \right) \left(\frac{t}{b} \right)^2 \quad (10.12)$$

Where K_c is the stress concentration factor which is 11, E is the materials elastic modulus which is 72 GPa, ν is the Poisson's ratio of 0.33, t is the panel thickness which is 1.1mm/0.8mm for a skin panel and 3mm for the spar webs and b is the length of panel being analyzed.

The Von Mises was then compared to the critical stress to ensure that it was lower by a factor of safety of 1.5 at all wing sections. The factor of safety was calculated for each panel by dividing the critical stress by the Von Mises Stress. For the root, the lowest factor of safety of 1.63 was found at the B9-B10 panel. The following table highlights the main results at the root section for shear calculations,

The shear flow analysis and direct stresses were also calculated at wing sections at 2 m and 3.8 m. 3.8 m is where the flap section ends. The tables are shown in the appendix for these sections.

Panel Name	Shear Flow (N/mm)	Shear Stress due to Shear flow (N/mm ²)	Shear Stress due to wing torque (N/mm ²)	Von Mises equivalent Stress (N/mm ²)	Critical Stress due to Buckling (N/mm ²)	Calculated Factor of safety for shear stress
B10-B1 (Front Spar Web)	49.18	16.39	8.34	31.86	214.76	13.10
B1-B2	0.71	0.65	22.74	39.40	74.45	114.94
B2-B3	-17.20	-15.64	22.74	47.80	74.45	4.76
B3-B4	-33.42	-30.38	22.74	65.72	74.45	2.45
B4-B5	-47.94	-43.58	22.74	85.13	74.45	1.71
B5-B6 (Rear Spar Web)	-25.07	-8.36	8.34	20.45	441.63	52.84
B6-B7	-22.45	-20.41	22.74	52.92	74.45	3.65
B7-B8	-0.15	-0.14	22.74	39.38	74.45	547.97
B8-B9	24.03	21.85	22.74	54.61	74.45	3.41
B9-B10	50.09	45.54	22.74	88.16	74.45	1.63

Table 10.4: Shear stress distribution

11 Material Selection

Material Selection was done in tandem with the calculations mentioned in Section 3.0 above. Initially, there were 3 main classes of materials considered: Aluminum, Steel and Carbon Fiber Composites. The Carbon Fiber Composite would give the highest strength-to-weight was rejected as it was found that it was much more expensive, takes more time to design a proper laminate (considering the number of plies and its orientation) as well as the complexity in manufacturing which would ultimately increase manufacturing and labour costs for the airplane.

The above chart compares each material based on their most important properties. These properties are given a rating out of 10. If a material is superior in one criterion it is given 10 points multiplied by the weighting factor for that criterion. For example, the yield strength is given a relative score of 9/10 when compared to other criteria. Carbon Fiber is the best in this area, when compared to other materials, and gets 10 points. Therefore, the final score for Carbon Fiber for Yield Strength would be 9 times 10 which is 90. From the above comparison chart, it can be seen that Aluminum 7175-T7351 had the best overall score of 490, making it a desirable material of choice for all wing components, mainly due to its high strength-to-weight ratio combined with the fact that it is a common and easily obtainable material.

The properties of Aluminum 7175-T7351 are listed below,

Criteria	Weighting Factor out of 10	Aluminum 7175-T7351	Aluminum 7075	Steel 4140	Carbon Fiber Composite
Strength-to-Weight Ratio	10	90	90	80	100
Yield Strength	9	81	72	63	90
Density	7	63	56	35	70
Shear Strength	8	64	64	72	80
Elastic Modulus	7	56	56	63	70
Cost	7	56	56	63	7
Manufacturing and Maintainability/Ramp Appeal	8	80	80	24	0
Total	-	490	474	400	417

Table 11.1: Material Selection chart

Properties	Aluminum 7175-T7351
Strength-to-Weight Ratio (kN-m/kg)	180
Yield Strength (Mpa)	435
Density (Kg/m ³)	2800
Shear Strength (MPa)	300
Elastic Modulus (GPa)	72
Cost (\$/Ton for metal sheets)	1000-2000
Ultimate Tensile Strength (MPa)	505

Table 11.2: 7175 Aluminum Material Properties

12 Discussion and Conclusion

12.1 Stringer Design and Rib Spacing

There was a variety of shapes of stringers to choose from, mainly y-shape, t-shape, J-shape, top hat, and z-shaped stringers. The z-shaped stringers were chosen due to its popularity in usage for many wings. Also the z-shape allows for the stringer to be riveted easily to the skin panel due to it having a relatively longer end cap, thus reducing stress concentrations around the riveted area. The J-shape and top hat are also easily riveted but they are a more complex shape to extrude and thus would increase manufacturing costs. Thus, the z-shape was chosen based on the above considerations and was geometrically shaped to match the area determined in Section 3.2. The area was chosen to be constant along the wing span as this would also reduce manufacturing costs as it would not have a complex taper in its area. The thickness of the stringer was chosen to be 3mm. Choosing a small thickness in general allows for easier manufacturability as sheet metal is easier to bend into desired shapes.

The Rib spacing was determined by finding the shear buckling coefficient, K when calculating the critical stress for buckling. It can be seen that the skin panels are riveted to the stringers. This setup is a doubly clamped edge which gives a shear buckling coefficient, k of 10 from the below chart. The equation used to solve for the rib spacing is,

$$\sigma_{cr} = \frac{k\pi^2 E}{12(1-\nu^2)} \left(\frac{t}{b}\right)^2 \quad (12.1)$$

Substituting, a shear strength value of 300 MPa divided by a factor of safety of 1.5, posson's ratio of 0.33, elastic modulus of 72 GPa, and a skin panel thickness of 1.4 mm, gives a b value of 8 cm. From the below chart it can be seen that k reaches a constant value at an a/b ratio of approx. 3-5. Multiply the b value by 4, gives a rib spacing a of 32 cm.

12.2 Wingbox Design

The wingbox was designed with 2 spars and 6 stringers. The material chosen was 7175 Aluminum Alloy with a yield strength of 435 MPa. The direct stresses were calculated using boom structural idealization and a factor of safety of 1.5 was applied in order to make sure the stresses were below 290 MPa. The shear flow was also calculated at the root with a factor of safety of 1.5 as well. The wing weight was determined by uploading the CAD CATIA model into ANSYS. The total wing weight was determined to be 172 kg which is a sensible number given the larger size of the wing in comparison to the Cessna 172. Skin panel thickness is 1.1mm from 0m to 2m half span, followed by 0.8mm for the rest of the wing.

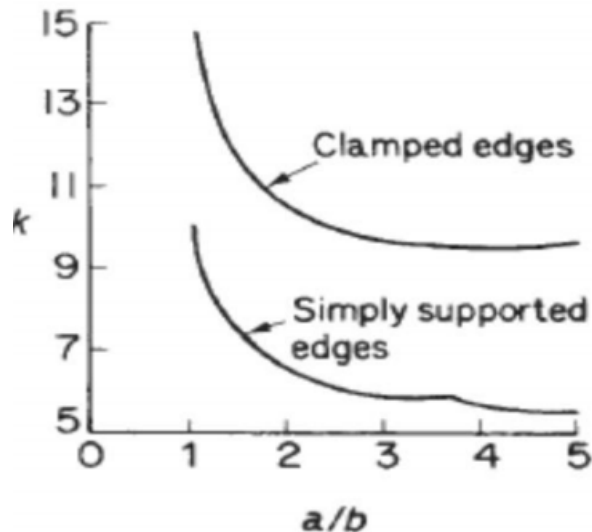


Figure 12.1: Shear Buckling coefficient

13 Appendix

13.1 Wing Load distribution

y	lambda (Taper Ratio)	b (Wingspan)	Total Angle (PHAA)	Beta (PHAA)	Total Angle (PLAA)	Beta (PLAA)	L (Lift PHAA)	D (Drag PHAA)
0	0.59	13.00	17.00	103.56	3.00	91.59	43117.87	124.88
0.5	0.59	13.00	16.81	103.37	2.81	91.40	43117.87	120.91
1	0.59	13.00	16.62	103.18	2.62	91.20	43117.87	116.93
1.5	0.59	13.00	16.42	102.99	2.42	91.01	43117.87	112.96
2	0.59	13.00	16.23	102.79	2.23	90.82	43117.87	108.98
2.5	0.59	13.00	16.04	102.60	2.04	90.63	43117.87	105.00
3	0.59	13.00	15.85	102.41	1.85	90.43	43117.87	101.03
3.5	0.59	13.00	15.65	102.22	1.65	90.24	43117.87	97.05
4	0.59	13.00	15.46	102.02	1.46	90.05	43117.87	93.08
4.5	0.59	13.00	15.27	101.83	1.27	89.86	43117.87	89.10
5	0.59	13.00	15.08	101.64	1.08	89.67	43117.87	85.12
5.5	0.59	13.00	14.88	101.45	0.88	89.47	43117.87	81.15
6	0.59	13.00	14.69	101.26	0.69	89.28	43117.87	77.17
6.5	0.59	13.00	14.50	101.06	0.50	89.09	43117.87	0.00
				Gamma 86.56289	Gamma 88.588267			

Table 13.1: Wing Load Distribution Part 1

wy (Elliptical PHAA)	wy (Taper PHAA)	wy Average PHAA	L (Lift PLAA)	D (Drag PLAA)	wy (Elliptical PLAA)	wy (Taper PLAA)	wy Average PLAA
4223.03	4165.69	4194.36	43118.01	51.17	4223.04	4165.70	4194.37
4210.52	4035.09	4122.80	43118.01	49.54	4210.53	4035.10	4122.81
4172.75	3904.48	4038.62	43118.01	47.91	4172.77	3904.49	4038.63
4109.04	3773.88	3941.46	43118.01	46.29	4109.06	3773.89	3941.47
4018.15	3643.27	3830.71	43118.01	44.66	4018.17	3643.28	3830.72
3898.18	3512.67	3705.42	43118.01	43.03	3898.19	3512.68	3705.44
3746.33	3382.06	3564.20	43118.01	41.40	3746.35	3382.07	3564.21
3558.54	3251.46	3405.00	43118.01	39.77	3558.55	3251.47	3405.01
3328.71	3120.85	3224.78	43118.01	38.14	3328.72	3120.86	3224.79
3047.35	2990.25	3018.80	43118.01	36.51	3047.36	2990.26	3018.81
2698.39	2859.64	2779.02	43118.01	34.88	2698.40	2859.65	2779.03
2250.62	2729.04	2489.83	43118.01	33.25	2250.62	2729.05	2489.83
1624.24	2598.43	2111.34	43118.01	31.62	1624.25	2598.44	2111.34
0.00	2467.83	1233.91	43118.01	0.00	0.00	2467.83	1233.92

Table 13.2: Wing Load Distribution Part 2

PHAA		
Wing Section Span location	wi	wi+1
0	4194.36008	4122.801237
0.5	4122.801237	4038.617128
1.0	4038.617128	3941.459692
1.5	3941.459692	3830.711928
2.0	3830.711928	3705.423446
2.5	3705.423446	3564.197818
3.0	3564.197818	3404.996048
3.5	3404.996048	3224.778387
4.0	3224.778387	3018.797185
4.5	3018.797185	2779.017394
5.0	2779.017394	2489.826059
5.5	2489.826059	2111.336735
6.0	2111.336735	1233.913329
6.5	1233.913329	0

Table 13.3: Wing Load Distribution Part 3

yi	yi+1	delta L	Structure load/m	structureR delta	N
0	0.5	2079.290329	188.6538	0	2083.04 2024.947777
0.5	1	2040.354591	174.1419	790.6989	2043.93 1988.532452
1	1.5	1995.019205	159.6301	483.443	1998.44 1945.814873
1.5	2	1943.042905	145.1183	176.1871	1946.32 1896.546396
2	2.5	1884.033844	130.6064	868.9312	1887.18 1840.331627
2.5	3	1817.405316	116.0946	561.6753	1820.44 1776.584781
3	3.5	1742.298467	101.5828	254.4194	1745.23 1704.453742
3.5	4	1657.443609	87.07099	47.1635	1660.28 1622.684029
4	4.5	1560.893893	72.55916	39.9075	1563.67 1529.357828
4.5	5	1449.453645	58.04733	32.6516	1452.19 1421.334302
5	5.5	1317.210863	43.5355	25.3957	1319.96 1292.813929
5.5	6	1150.290698	29.02367	18.1398	1153.15 1130.209758
6	6.5	836.3125159	14.51184	10.8839	839.865 823.7128387
6.5	7	0	1E-05	3.62796	0 0

Table 13.4: Wing Load Distribution Part 4

Span Location	net load	Shear force(z)	Bending moment(about x-axis)
6.5	- 3.512403334	0	0
6	813.1848443	813.18484	203.29621
5.5	1112.678645	1925.8635	888.05829
5.0	1268.292405	3194.1559	2168.0631
4.5	1389.835315	4583.9912	4112.5999
4.0	1490.894559	6074.8858	6777.3192
3.5	1575.520577	7650.4063	10208.642
3.0	1650.034374	9300.4407	14446.354
2.5	1714.909498	11015.35	19525.302
2.0	1771.400429	12786.751	25475.827
1.5	1820.359284	14607.11	32324.292
1.0	1862.371845	16469.482	40093.44
0.5	1897.83351	18367.315	48802.639
0.0	2024.947777	20392.263	58492.534

Table 13.5: Wing Distribution Part 5

Span Location	net load	Shear force(z)	Bending moment(about x-axis)	P
6.5	0	0	0	- 488.499
6	- 163.924	-163.924	-40.9811	- 472.657
5.5	- 228.866	-392.79	-180.16	- 455.609
5.0	- 266.313	-659.103	-443.133	- 437.363
4.5	- 297.764	-956.867	-847.126	- 417.899
4.0	- 325.757	-1282.62	-1407	- 397.158
3.5	- 351.333	-1633.96	-2136.14	- 375.031
3.0	- 375.031	-2008.99	-3046.88	- 351.333
2.5	- 397.158	-2406.15	-4150.66	- 325.757
2.0	- 417.899	-2824.04	-5458.21	- 297.764
1.5	- 437.363	-3261.41	-6979.57	- 266.313
1.0	- 455.609	-3717.02	-8724.18	- 228.866
0.5	- 472.657	-4189.67	-10700.9	- 163.924
0.0	- 488.499	-4678.17	-12917.8	0

Table 13.6: Wing Distribution Part 6

PLAA					
Wing Section Span location	wi	wi+1	yi	yi+1	
0	4194.373771	4122.814694	0	0.5	
0.5	4122.814694	4038.63031	0.5	1	
1.0	4038.63031	3941.472558	1	1.5	
1.5	3941.472558	3830.724432	1.5	2	
2.0	3830.724432	3705.435541	2	2.5	
2.5	3705.435541	3564.209452	2.5	3	
3.0	3564.209452	3405.007163	3	3.5	
3.5	3405.007163	3224.788913	3.5	4	
4.0	3224.788913	3018.807039	4	4.5	
4.5	3018.807039	2779.026465	4.5	5	
5.0	2779.026465	2489.834186	5	5.5	
5.5	2489.834186	2111.343626	5.5	6	
6.0	2111.343626	1233.917357	6	6.5	
6.5	1233.917357		0	6.5	

Table 13.7: Wing Distribution Part 7

delta L	Structures load/m	structure delta	R	Span Location	net load	N
2076.447512	188.6538	0	2077.08	6.5	- 3.6279625	
2037.91194	174.14197	90.6989	2038.51	6	825.9020082	2076.28
1992.947605	159.63014	83.443	1993.52	5.5	1132.449415	2037.91
1941.311934	145.11831	76.1871	1941.86	5.0	1292.026118	1993.08
1882.612187	130.60648	68.9312	1883.14	4.5	1416.906495	1941.56
1816.261144	116.09465	61.6753	1816.77	4.0	1520.949079	1882.95
1741.399782	101.58282	54.4194	1741.89	3.5	1610.057551	1816.66
1656.75858	87.07099	47.1635	1657.24	3.0	1687.422334	1741.84
1560.391184	72.55916	39.9075	1560.86	2.5	1754.986745	1657.22
1449.10275	58.04733	32.6516	1449.56	2.0	1814.018135	1560.86
1316.982494	43.5355	25.3957	1317.44	1.5	1865.374007	1449.56
1150.157354	29.02367	18.1398	1150.64	1.0	1909.640592	1317.42
836.2541955	14.51184	10.8839	836.852	0.5	1947.210122	1150.59
0	1E-05	3.62796	0	0.0	2076.279987	836.786

Table 13.8: Wing Distribution Part 8

Shear force(z)	Bending moment(about x-axis)	P
825.902010	- 57.5703	
1958.3514696.06336	- 49.6616	
3250.37751998.2456	- 41.8762	
4667.2843977.661	- 34.2746	
6188.23316691.5403	- 26.9184	
7798.290710188.171	- 19.8723	
9485.71314509.172	- 13.207	
11240.719690.775	- 7.00293	
13054.71825764.63	- 1.35682	
14920.09232758.332	3.605241	
16829.73240695.788	7.698479	
18776.94349597.457	10.58564	
20853.22359504.998	10.50751	

Table 13.9: Wing Distribution Part 9

Span Locations	net load	Shear force(z)	Bending moment(about x-axis)
6.5	0		
6	10.50751	10.50751	0
5.5	10.58564	21.09315	7.900167
5.0	7.698479	28.79163	20.37136
4.5	3.605241	32.39687	35.66849
4.0	- 1.35682	31.04006	51.52772
3.5	- 7.00293	24.03713	65.29702
3.0	- 13.207	10.83009	74.01383
2.5	- 19.8723	- 9.04223	74.46079
2.0	- 26.9184	- 35.9606	63.21008
1.5	- 34.2746	- 70.2352	36.66112
1.0	- 41.8762	- 112.111	-8.92555
0.5	- 49.6616	- 161.773	-77.3967
0.0	- 57.5703	- 219.343	-172.676

Table 13.10: Wing Distribution Part 10

Span Location	cr	ct	h	Delta Area
0	0.55	0.507692	0.5	0.664423
0.5	0.507692	0.465385	0.5	0.643269
1	0.465385	0.423077	0.5	0.622115
1.5	0.423077	0.380769	0.5	0.600962
2	0.380769	0.338462	0.5	0.579808
2.5	0.338462	0.296154	0.5	0.558654
3	0.296154	0.253846	0.5	0.5375
3.5	0.253846	0.211538	0.5	0.516346
4	0.211538	0.169231	0.5	0.495192
4.5	0.169231	0.126923	0.5	0.474038
5	0.126923	0.084615	0.5	0.452885
5.5	0.084615	0.042308	0.5	0.431731
6	0.042308	0	0.5	0.410577
6.5	0	0	0.5	0
Total				6.9875

Table 13.11: Wing Distribution Part 11

13.2 7.2 Shear Flow Calculations

Root Chord							
	Sigmay (N/mm ²)	Boom Area	Sx (N)	Sz (N)	Ixx (mm ⁴)	Izz (mm ⁴)	Ixz (mm ⁴)
Fspar Cap Upper	-289	566	4678.171	20392.26	1.78E+07	4.62E+07	5.04E+06
	-256	229	4678.171	20392.26	1.78E+07	4.62E+07	5.04E+06
	-223	229	4678.171	20392.26	1.78E+07	4.62E+07	5.04E+06
	-191	229	4678.171	20392.26	1.78E+07	4.62E+07	5.04E+06
Rspar Cap Upper	-158	307	4678.171	20392.26	1.78E+07	4.62E+07	5.04E+06
Rspar Cap Lower	247	32	4678.171	20392.26	1.78E+07	4.62E+07	5.04E+06
	258	249	4678.171	20392.26	1.78E+07	4.62E+07	5.04E+06
	269	249	4678.171	20392.26	1.78E+07	4.62E+07	5.04E+06
	280	249	4678.171	20392.26	1.78E+07	4.62E+07	5.04E+06
Fspar Cap Lower	290	559	4678.171	20392.26	1.78E+07	4.62E+07	5.04E+06

Table 13.12: Shear FLow Calculations Part 1

Boom	Py,r (N)	Pr (Lbf)	Sx,w (N)	Sz,w (lbf)	Panel name	qs,b (N/mm)	p
1	- 163574	163574	4678.171	20392.26306	/10-1	0	
2	-58624	58624	4678.171	20392.26306	/1-2	- 4.85E+01	75.8123
3	-51067	51067	4678.171	20392.26306	/2-3	- 6.64E+01	69.2513
4	-43739	43739	4678.171	20392.26306	/3-4	- 8.26E+01	62.6903
5	-48506	48506	4678.171	20392.26306	/4-5	- 9.71E+01	56.1293
6	7904	7904	4678.171	20392.26306	/5-6	- 7.43E+01	65.9242
7	64242	64242	4678.171	20392.26306	/6-7	- 7.16E+01	72.6067
8	66981	66981	4678.171	20392.26306	/7-8	- 4.93E+01	79.2892
9	69720	69720	4678.171	20392.26306	/8-9	- 2.52E+01	85.9717
10	162110	162110	4678.171	20392.26306	/9-10	9.09E-01	92.6542

Table 13.13: Shear FLow Calculations Part 2

ds	q _{sb} *p*ds	q _{s,0} (lbf/in)	q	Panel thickness	Shear stress	Ty shear stress
			49.18	3	16.39	8.34
109	-400521.642	49.1810152	0.71	1.1	0.65	22.74
109	- 501073.3908	49.1810152	- 17.20	1.1	-15.64	22.74
109	-564407.538	49.1810152	- 33.42	1.1	-30.38	22.74
109	- 594165.1369	49.1810152	- 47.94	1.1	-43.58	22.74
122.0535	-597480.433	49.1810152	- 25.07	3	-8.36	8.34
109	- 566897.7798	49.1810152	- 22.45	1.1	-20.41	22.74
109	- 426339.6409	49.1810152	-0.15	1.1	-0.14	22.74
109	- 235681.6584	49.1810152	24.03	1.1	21.85	22.74
109	9183.206108	49.1810152	50.09	1.1	45.54	22.74
Total	- 3877384.014					

Table 13.14: Shear FLow Calculations Part 3

Von Mises	Sigma,cr	Shear FoS					dist from ybar	dist from xbar
31.86	214.76	13.10	y top and bot	b top and bot	xbar	196.7618	82.3733	196.7618
39.40	74.45	114.94	128.9925	0	ybar	46.6192	75.8123	61.7618
47.80	74.45	-4.76	122.4315	135	Ixx	1.78E+07	69.2513	73.2382
65.72	74.45	-2.45	115.8705	270	Izz	4.62E+07	62.6903	208.2382
85.13	74.45	-1.71	109.3095	405	Ixz	5.04E+06	56.1293	343.2382
20.45	441.63	-52.84	102.7485	540	Area		- 65.9242	343.2382
52.92	74.45	-3.65	- 19.305	540	80211.87		- 72.6067	208.2382
39.38	74.45	-547.97	- 25.9875	405			- 79.2892	73.2382
54.61	74.45	3.41	-32.67	270			- 85.9717	61.7618
88.16	74.45	1.63	- 39.3525	135			- 92.6542	196.7618
			- 46.035	0				

Table 13.15: Shear FFlow Calculations Part 4

2m Chord								
	Sigmay (N/mm ²)	Boom Area	Sx (N)	Sz (N)	Ixx (mm ⁴)	Izz (mm ⁴)	Ixz (mm ⁴)	
Fspar Cap Upper	-164	426	-2824	12786	1.17E+07	3.05E+07	2.88E+06	
	-148	229	-2824	12786	1.17E+07	3.05E+07	2.88E+06	
	-133	229	-2824	12786	1.17E+07	3.05E+07	2.88E+06	
	-117	229	-2824	12786	1.17E+07	3.05E+07	2.88E+06	
Rspar Cap Upper	-101	236	-2824	12786	1.17E+07	3.05E+07	2.88E+06	
Rspar Cap Lower	130	30	-2824	12786	1.17E+07	3.05E+07	2.88E+06	
	140	249	-2824	12786	1.17E+07	3.05E+07	2.88E+06	
	149	249	-2824	12786	1.17E+07	3.05E+07	2.88E+06	
	159	249	-2824	12786	1.17E+07	3.05E+07	2.88E+06	
Fspar Cap Lower	168	414	-2824	12786	1.17E+07	3.05E+07	2.88E+06	

Table 13.16: Shear FFlow Calculations Part 5

Boom	Py,r (N)	dxr/dy	dzr/dy	Px,r	Pz,r (N)	Pr (N)	Sx,w (N)
1	-69864	0	0.008496250		-593.58201	69866.5216	-2824
2	-33892	0	0.007715750		-261.502199	33893.0088	-2824
3	-30457	0	0.007435250		-226.4554093	30457.8419	-2824
4	-26793	0	0.007154750		-191.6972168	26793.6858	-2824
5	-23836	0	0.006874250		-163.854623	23836.5632	-2824
6	3900	0	-0.0011525	0	-4.49475	3900.00259	-2824
7	34860	0	-0.00199375	0	-69.502125	34860.0693	-2824
8	37101	0	-0.002335	0	-86.630835	37101.1011	-2824
9	39591	0	-0.00267625	0	-105.9554138	39591.1418	-2824
10	69552	0	-0.0030175	0	-209.87316	69552.3166	-2824
					-1913.547742		

Table 13.17: Shear Flow Calculations Part 6

Sz,w (lbf)	Panel name	qs,b (N/mm)	p	ds	qs _b *p*ds	qs,0 (lbf/in)	q
10872.4522610-1	0	0	0	0		33.0047046	
10872.4522611-2	- 2.43E+01	67.4952	84.4	- 138493.8661	33.0047048.69301159		
10872.4522612-3	- 3.65E+01	61.4952	84.4	- 189334.6108	34.8589176		
10872.4522613-4	- 4.76E+01	55.4952	84.4	- 222785.8319	35.0369754		
10872.4522614-5	- 5.76E+01	49.4952	84.4	- 240490.7584	33.1827625		
10872.4522615-6	- 6.68E+01	56.5048	106	- 399889.3801	31.3285496		
10872.4522616-7	- 6.54E+01	61.5048	94.4	- 379893.0679	31.3285496		
10872.4522617-8	- 5.34E+01	67.5048	94.4	- 340126.3588	33.1827625		
10872.4522618-9	- 4.01E+01	73.5048	94.4	- 278541.7307	35.0369754		
10872.4522619-10	- 2.57E+01	79.5048	94.4	- 193140.7421	34.8589170.12484317		
				- 2382696.347			

Table 13.18: Shear FLow Calculations Part 7

Panel thickness	Shear stress	Ty shear stress	Von Mises	Sigma,cr	Shear FoS
3	11.0015682	25.436276722	21.25	284.755795	525.8832004
0.8	10.8662645	20.38603771	40.01	65.6768505	56.04410564
0.8	- 2.02546232	20.38603771	35.48	65.6768505	- 32.4256096
0.8	- 15.6603319	20.38603771	44.53	65.6768505	- 4.19383516
0.8	- 30.4834888	20.38603771	63.52	65.6768505	- 2.1545057
3	- 11.8121404	5.436276722	22.52	585.52847	- 49.5700567
0.8	- 42.6274616	20.38603771	81.84	52.4992649	- 1.23158319
0.8	- 25.2396444	20.38603771	56.20	52.4992649	- 2.08003188
0.8	- 6.38169302	20.38603771	37.00	52.4992649	- 8.22654188
0.8	11.406054	20.38603771	40.46	52.4992649	4.60275439

Table 13.19: Shear FLow Calculations Part 8

				dist from ybar	dist from xbar
y top and bot	b top and bot	xbar	182.6657	72.4952	182.6657
112	0	ybar	39.5048	67.4952	64.6657
107	118	Ixx	1.17E+07	61.4952	53.3343
101	236	Izz	3.05E+07	55.4952	171.3343
95	354	Ixz	2.88E+06	49.4952	289.3343
89	472	Area 60888		-56.5048	289.3343
-17	472			-61.5048	171.3343
-22	354			-67.5048	53.3343
-28	236			-73.5048	64.6657
-34	118			-79.5048	182.6657
-40	0				

Table 13.20: Shear FLow Calculations Part 9

3.8m Chord							
	Sigmay (N/mm ²)	Boom Area	Sx (N)	Sz (N)	Ixx (mm ⁴)	Izz (mm ⁴)	Ixz (mm ⁴)
Fspar Cap Upper	-54.5	304	-1407	6777	7.66E+06	1.94E+07	1.28E+06
	-51.6	229	-1407	6777	7.66E+06	1.94E+07	1.28E+06
	-48.65	229	-1407	6777	7.66E+06	1.94E+07	1.28E+06
	-45.69	229	-1407	6777	7.66E+06	1.94E+07	1.28E+06
Rspar Cap Upper	-42.73	173	-1407	6777	7.66E+06	1.94E+07	1.28E+06
Rspar Cap Lower	39.26	30	-1407	6777	7.66E+06	1.94E+07	1.28E+06
	45.2	249	-1407	6777	7.66E+06	1.94E+07	1.28E+06
	51.14	249	-1407	6777	7.66E+06	1.94E+07	1.28E+06
	57.079	249	-1407	6777	7.66E+06	1.94E+07	1.28E+06
Fspar Cap Lower	63.0165	285	-1407	6777	7.66E+06	1.94E+07	1.28E+06

Table 13.21: Shear Flow Calculations Part 10

Boom	Py,r (N)	dxr/dy	dzr/dy	Px,r (Lbf)	Pz,r (Lbf)	Pr (Lbf)	Sx,w (lbf)
1	-16568	0	0.0077777778	- 128.8622222	16568.5011	-1407	
2	- 11816.4	0	0.0077777778	- 91.90533333	11816.7574	-1407	
3	- 11140.9	0	0.0072222220	- 80.46169444	11141.1406	-1407	
4	-10463	0	0.0066666660	-69.7534	10463.2425	-1407	
5	- 7392.29	0	0.0061111110	- 45.17510556	7392.42803	-1407	
6	1177.8	0	- 0.0016666667	0	-1.963	1177.80164	-1407
7	11254.8	0	- 0.0016666667	0	-18.758	11254.8156	-1407
8	12733.86	0	- 0.002222222	0	- 28.29746667	12733.8914	-1407
9	14212.67	0	- 0.002777778	0	- 39.47964167	14212.7258	-1407
10	17959.7	0	- 0.002777778	0	- 49.8880625	17959.7718	-1407
					- 554.5439264		

Table 13.22: Shear Flow Calculations Part 11

Sz,w (lbf)	Panel name	qs,b (N/mm)	p	ds	qs*b*p*ds	qs,0 (lbf/in)	q
6222.4560	7410-1	0					52.300456
6222.4560	741-2	- 1.38E+01	59.3388 81.6		- 66874.00469	52.300456 638.4893514	
6222.4560	742-3	- 2.34E+01	54.3388 81.6		- 103784.8371	52.91661529.5102653	
6222.4560	743-4	- 3.22E+01	49.3388 81.6		- 129610.8354	53.10159620.908514	
6222.4560	744-5	- 4.02E+01	44.3388 81.6		- 145341.6205	52.48543712.3141353	
6222.4560	745-6	- 4.56E+01	- 47.6612	92	199894.40481.8692776.28156067		
6222.4560	746-7	- 4.46E+01	- 52.6612	81.6	191558.84031.8692771.29120428		
6222.4560	747-8	- 3.53E+01	- 57.6612	81.6	166180.88232.48543717.1665324		
6222.4560	748-9	- 2.52E+01	- 62.6612	81.6	128752.33633.10159627.9209866		
6222.4560	749-10	- 1.42E+01	- 68.6612	81.6	79352.866782.91661598.7534262		
					320128.033		

Table 13.23: Shear Flow Calculations Part 12

Panel thickness	Shear stress	Ty shear stress	Von Mises	Sigma,cr	Shear FoS
3	17.43348533.802860889	30.91		371.92593621.3339977	
0.8	48.111689314.26072834	86.92		70.26141531.46038138	
0.8	36.887831614.26072834	68.50		70.26141531.90473151	
0.8	26.135642514.26072834	51.57		70.26141532.68833703	
0.8	15.392669214.26072834	36.34		70.26141534.56460245	
3	2.093853563.802860889	7.52		777.29181371.225489	
0.8	9.1140053514.26072834	29.31		70.26141537.70916985	
0.8	21.458165414.26072834	44.63		70.26141533.274344	
0.8	34.901233314.26072834	65.30		70.26141532.01314993	
0.8	48.441782714.26072834	87.46		70.26141531.45043001	

Table 13.24: Shear Flow Calculations Part 13

				dist from ybar	dist from xbar
y top and bot	b top and bot	xbar	169.6311	64.3388	169.6311
98	0	ybar	33.6612	59.3388	66.8311
93	102.8	Ixx	7.66E+06	54.3388	35.9689
88	205.6	Izz	1.94E+07	49.3388	138.7689
83	308.4	Ixz	1.28E+06	44.3388	241.5689
78	411.2	Area 46260		-47.6612	241.5689
-14	411.2			-52.6612	138.7689
-19	308.4			-57.6612	35.9689
-24	205.6			-62.6612	66.8311
-29	102.8			-68.6612	169.6311
-35	0				

Table 13.25: Shear FLow Calculations Part 14

Part IV

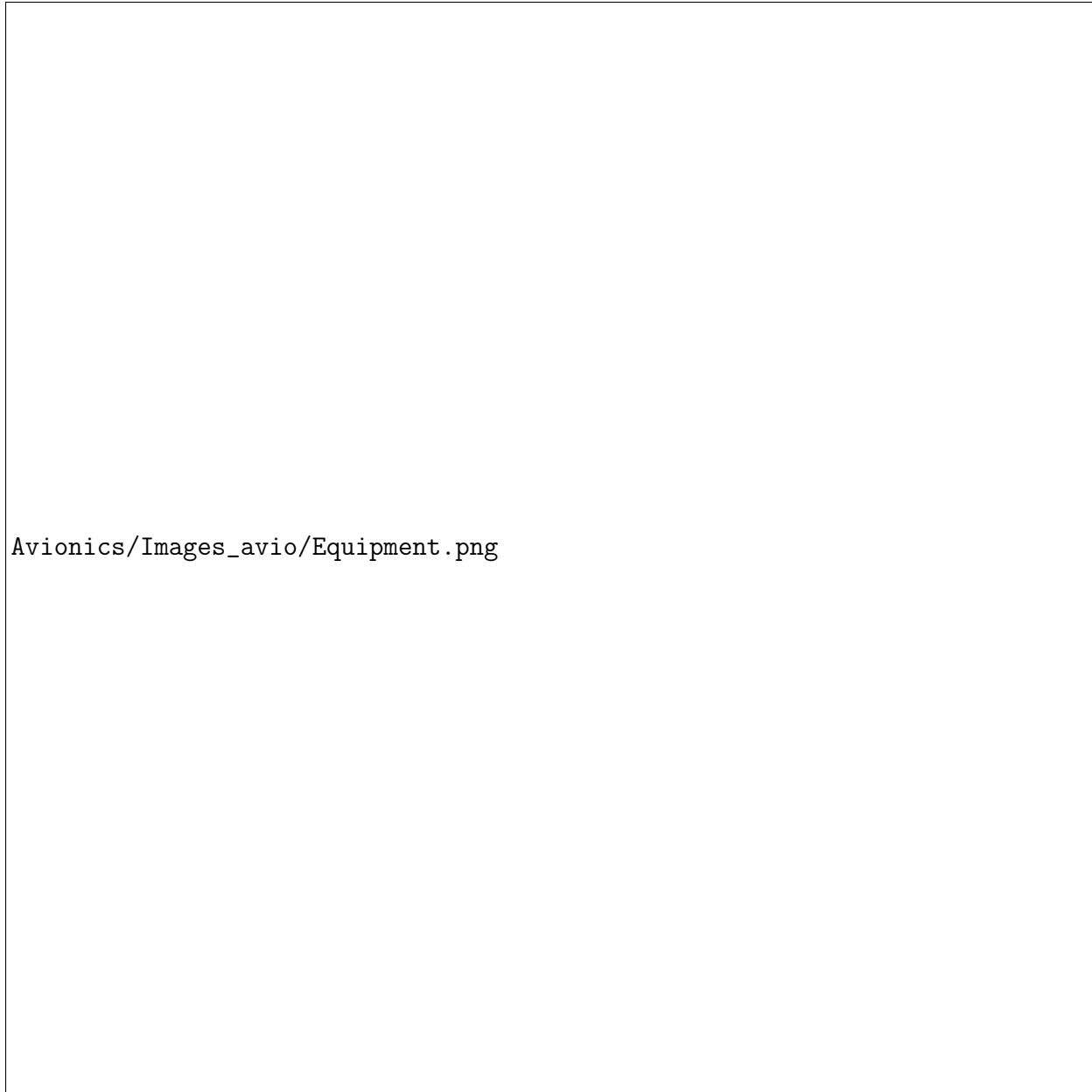
Book IV: Avionics Systems for FALCO E-1

1 Introduction

2 Instruments Panel Design

2.1 Design Parameters

The design parameters were based on the Cessna 172 instrument panel in terms of dimensions and what specific instruments were required. Seen below, a diagram was found labeling the instruments on the panel and a checklist of all the items was created.



Avionics/Images_avio/Equipment.png

Figure 2.1: Cessna 172 Instrument Panel Diagram[8]

Table 2.1: Instrument Panel Checklist

Class	Instrument	Class	Instrument
Required	Vacuum gauge and ammeter		Elevator trim control
	Digital clock		Trim position indicator
	O.A.T. indicator		Glare shield and pedestal dimming
	Turn indicator		Radio and panel dimming control
	Airspeed indicator		Avionics master switch
	Directional gyro		Parking brake pull knob
	Attitude indicator		Circuit breakers and switch breakers
	Yoke (attitude)		Equipment switches
	Annunciator panel		Master switch
	Altimeter		Avionics circuit breakers
	Vertical speed indicator		Ignition switch
	Course deviation and glide		Angle of attack indicator
	Course indicator head		Audio Panel Interface
	Engine data monitor system		Map
	Audio selector panel		Air Data
	GPS		Glideslope indicator
	Emergency GPS		Rate of Climb
	NAV/COM radio 1		Air Traffic Overlay
	NAV/COM radio 2		AOA indicator
	Stormscope		Cabin pressure
	Portable ipad mini mount		Pedals
	Dual usb power outlet	Gas Specific	Mixture control
	Hour meter		Fuel shut off valve control
	ELT		Fuel selector
	Glove box	Unnecessary	Edm-900 remote annunciate light
	Cabin Heater		Alternate static air control
	Avionics air control	Additional	Motor Temp.
	Flap switch		Battery Temp.
	Flap position indicator		Motor RPM
	Transponder		Power output in KW
	Single axis autopilot		Controller temp.
	Handheld microphone		Battery voltage
	Throttle control		Battery current
	Pedestal light		Remaining battery %

All the none highlighted components are one's that are required, gas specific ones highlighted blue mean that they are not necessary for the FALCO E-1 since it is a fully electric plane. The purple highlighted ones are those that are just unnecessary and the green highlighted ones are components that are not on the original 172 diagram and are specifically required for a fully electric plane. The following diagram shows the dimensions of the instrument panel dimensions.

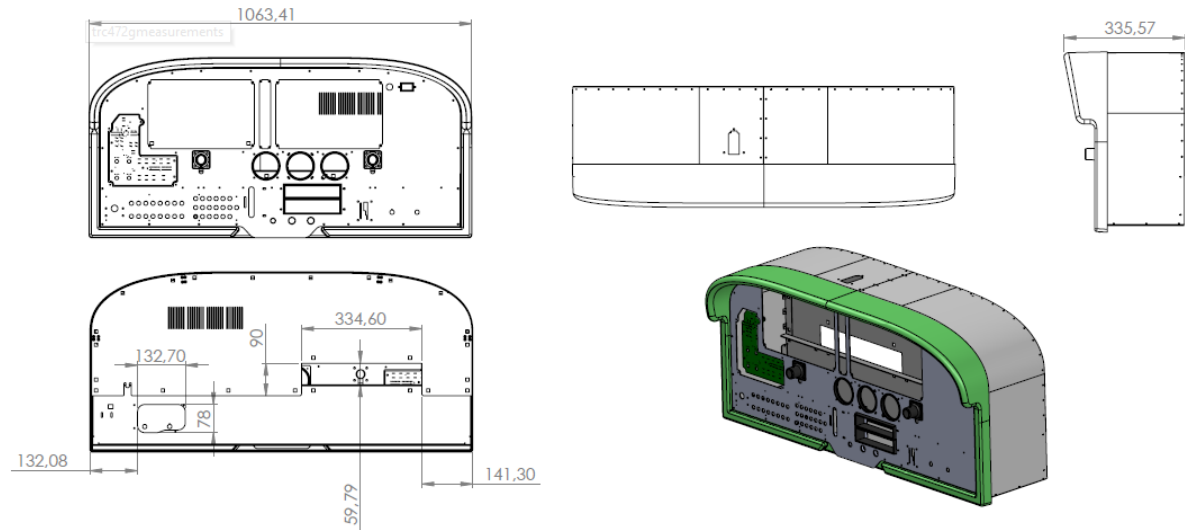


Figure 2.2: Instrument Panel Dimensions[9]

2.2 Final Instrument List

After research was done to match all the required instruments along with all the new instruments needed, a list was created showcasing all components with their description with pictures of each component in the appendix.

Table 2.2: Final Equipment List

Component	Description
Glass cockpit	Glass cockpit replaces 6 pack system with Advanced Technology
Autopilot	Roll and Pitch autopilot designed to integrate with the glass cockpit.
Yoke (Steering Wheel)	Steering Wheel
Standard Switch Panel	Switch panel
Trim Switch	Switch to control the trim angle
Speed Brake	Switch to control the flaps
Master Switch	Master switch control inboard electronics and passenger outlet power
Micro Relay	Used to control windshield heating
Ignition Switch	Switch to turn on the powerplant
Rocker Switches Mount	Switches to control the backup battery
Throttle	Used to accelerate the plane
Flap Switch	Switch to control the flap angle
Panel Dimming Rheostat	Used to dim the lights of instruments
Knob	Placed on top of the rheostat
Cabin Heater	Heater used to warm the airplane in colder conditions
Cabin Heater Rheostat	Rheostat to control the cabin heater
Cabin Temperature Screen	Indicates the temperature within the cabin
LXNAV FES Unit	Powerplant monitoring system : rpm, power, battery
Chronometer (Clock)	Digital clock to tell the time
Prog. Annunciator	System that signals any problems, or emergencies within the aircraft
Hour Meter	Indicates the total operating time
Transponder	Receives and transmits radio signals
Flap Angle Indicator	Indicates the angle of the flaps
Cabin Pressure Indicator	Indicates the internal cabin pressure
Rudder pedals, 2 place	Rudder pedals
Parking Brake, pull	Parking brake
NAVCOM	Navigation and Communication systems
iPad mount	Mount for iPads
ELT	Emergency Locator Transmitter
Wing tip light	Lights to indicate the edges of the wings
Tail and Nose Lights	Lights to indicate the ends of front (nose) and backend (tail)
Cabin Lights (with dimmer)	Lights to illuminate the interior of the cabin
Flight Management System	Helps the pilots navigate while flying with traffic updates
Custom Instrument Panel	Custom panel to fit all the instruments within the cockpit
Brake Valve	Valve connecting from the rudder pedals to the brakes
Lining (Cost per foot)	Lining to encase the hydraulic fluid for the braking system
ORION 2	Orion is a battery charger and a management system for Falco E1
Motor Controller	Works by diverting battery power based on pilot requirement

2.3 Instrument Panel Design

In any aircraft Instruments and Crew Plane interface plays a vital role when it comes to flying. The Falco E-1 comes in with built-in custom panels from AeroTeknic inc. Below is a picture of Falco E-1 Preliminary design.

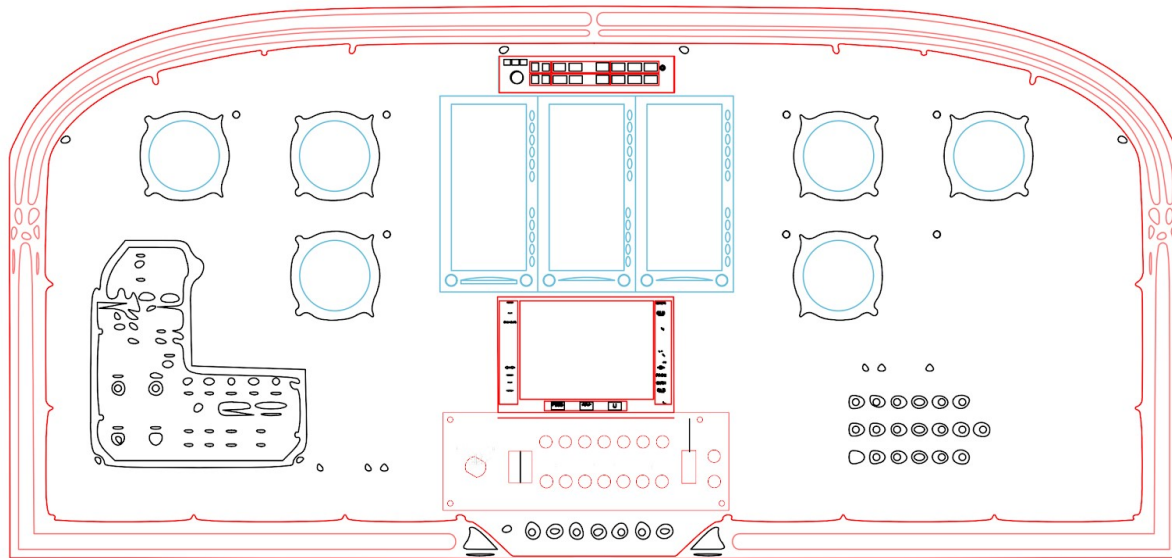


Figure 2.3: Instrument Panel Initial Design CAD

The panels come in finished with fine-textured powder coated which gives the panels a scratch-resistant and glare-free finish that will last as long as the aircraft itself. The powder paint is electrostatically applied as a preventive maintenance technique.

DACION was offered a price of CAD 3500 for the panel based on the drawing given to them by the avionics experts of Falco E-1.

The picture below shows the final design of Falco E-1 instrument panel which consists of all systems needed based on CAR compliance and the main 6 analog flight instruments with an integrated Glass cockpit

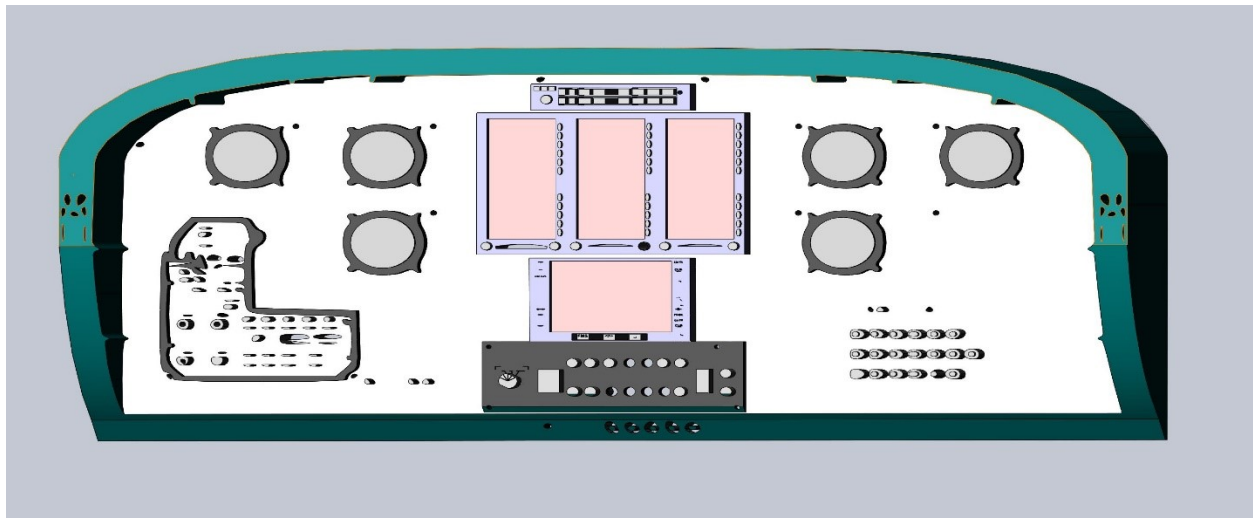


Figure 2.4: Final Design of the Instrument Panel

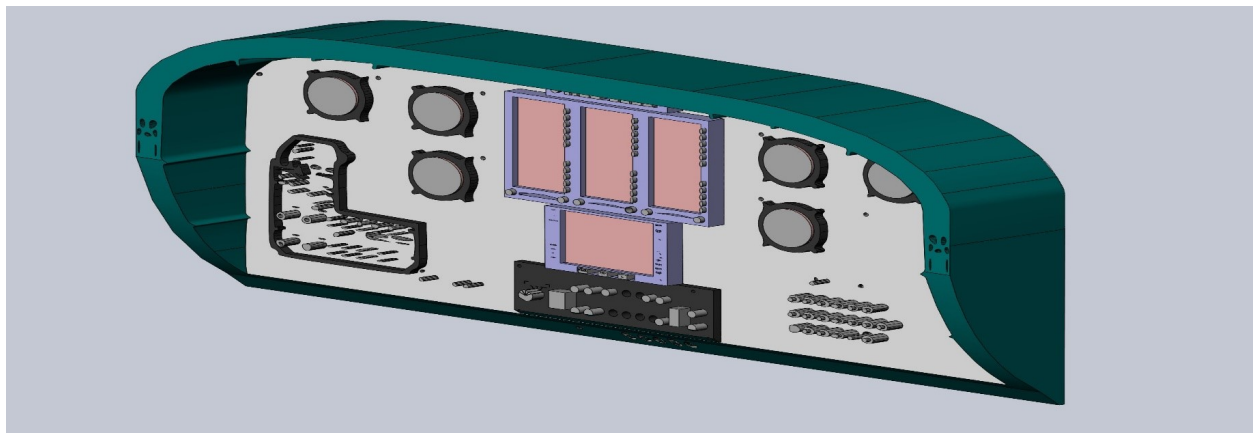


Figure 2.5: Final Design Instrument Panel II

3 Instruments and Crew-Plane Interface

3.1 Glass Cockpit

Aspen Avionics was used for glass cockpit deployment of Falco E-1. Aspen was chosen over Garmin and Avidyne instruments as Aspen came in with more redundancies compared to Garmin.



Figure 3.1: Aspen Avionics Evolution 1000 Pro MAX[10]

The 1000 Pro offers multiple redundancies when it comes to 6 pack flight instrument replacement. The 3 screens of 6.00" can be merged to work as one display or split in between 1 Pilot and a Co-pilot. All 3 displays are wired separately, thus if one system goes down the other 2 screens will work without shutting down. The screens are also equipped with built-in with backup batteries which can last minimum of 4 hours during a power failure as a redundancy.

* Refer to Appendix for Garmin vs Aspen comparison.

3.2 Six Pack Instruments

As per FAR and CAR certification requirement a redundancy of six pack instruments were also put into the instrument panel of Falco E-1. The Instruments were purchased from AircraftSpruce.com which offered FAA approved instruments for a reasonable price with 3-year limited warranty on the instruments. The placement of the 6 pack can be seen in the figure below as the instruments split in 3's to offer visibility for both pilots. This design is to ensure the Co-Pilot can takeover the aircraft as well.



Figure 3.2: 6-Pack Arrangement

3.3 Autopilot

Genesys System was used for Falco E-1. Genesys Autopilot integration was fully compatible with Aspen Systems. The digital autopilot is an integrated solution that is intuitive and easy to use. When used with Aspen's Pro PFD the Genesys System 55X autopilot enhances and expands the basic 55X autopilot function and streamlines the controls, reducing workload.



Figure 3.3: Genesys System 55X Digital Autopilot[11]

The Genesys System 55X is a fully IFR-capable autopilot with nav and glide slope intercepts that makes it ideal for approaches. With its GPS roll steering feature, it provides extremely accurate navigation which helps when it comes to training new students during training exercises. The main key features of Genesys Autopilot system are as follow

- Ability to set desired vertical speed and altitude capture on the PFD.
- All autopilot annunciations are displayed in the pilot's line of sight, reducing pilot scan.
- Adds flight director capability for coupled autopilot operations as well as hand flying for smoother control.
- Autopilot vertical speed command reduces when approaching set altitude for smooth transitions during altitude capture.
- High Performance: Fully IFR-capable, with nav and glide slope intercepts that make it ideal for approaches.
- GPS Roll Steering: Extremely accurate, hands-off GPS navigation.
- Control Wheel Steering: Hand-fly aircraft and then let the autopilot take over to hold the existing turn rate and vertical speed.

3.4 Flight management system

Falco E-1 is quipped with IFD 550 from Avidyne for Flight management system. The system combines the latest in touchscreen, WAAS/SBAS GPS/VHF navigation and communication along with stunning 3D synthetic vision technology to deliver the most powerful and capable touchscreen, panel-mounted navigator. IFD550 – Key Features are as follows

- Geo Fill automatic way-point nomination, and easy Airway flight planning.
- 3D Terrain & FLTA - Terrain Awareness (SVS-TA) is provided via hashed coloration of terrain. Textual and aural alerts provided for terrain hazards.
- Forward Looking Terrain Alerting (FLTA) provides an extra measure of safety by displaying a solid yellow or red impact point based on projected flight path in the event that a collision with terrain is projected.



Figure 3.4: Avidyne IFD550[12]

3.5 Audio Panel

AMX240 is a audio panel with 6-place VOX intercom and added capabilities to monitor standby frequencies when paired with an IFD (FMS). Supporting three transmitter inputs, nine receiver inputs, plus two inputs for stereo music and five switched inputs, the AMX240 also features a six-place high-fidelity stereo intercom, public address (PA) function, plus Bluetooth® music and full-duplex cell phone interfaces.



Figure 3.5: AMX240 Audio Panel

Pilot, crew, and passenger isolation settings are easily selectable with a single dedicated button and are graphically displayed for clear mode annunciation. Dedicated knobs for Pilot, Copilot and Passenger intercom volumes allow for full customization for personal preferences without relying on headset volume controls. Pilot Isolated selected. Specification :

Dimensions W: 6.30" H: 1.3" D: 7.12"

Weight 1.40 lbs (0.63 kg)

Certification TSO C50c, C35d Class A

Compliance RTCA DO-178B , DO-254, DO-160D, DO-214

Power 11 – 33 V 2.5 A

Environmental -20 to +55 C, 35,000ft. No external cooling fan required

Marker Beacon 75 MHz , 1000 mV low sensitivity, 200 mVolt High sensitivity

3.6 Switches

The Composite Design Standard Power Panel was used for master controls. This panel was fully customizable thus giving us full opportunity to change it as per our needs



Figure 3.6: Rocker Panel[13]

Dimensions: 2.25”H x 13.00”W x 7.75”D

Weight: approx. 2.75 pounds

Capacity: 17.5 V max. at 80A (Main Buss)

Radio Buss: 25A cont.

Essential Buss: 10A cont.

4 Avionics System Design and Framework

Falco E-1 is equipped with Astronics AB2000 I/O system. The AB2000 Series is a small form factor system that delivers outstanding performance on the ground and in the air. The System is conduction-cooled. AB2000 Series supports multiple Bus Protocols, for Civilian Aircraft purposes DACION chose to go with ARINC429 coding for better control and compatibility. The bus offers powerful application solutions.

- Data and Protocol Converter
- Network Server
- Monitor Local/distributed control
- Electronic Flight Bag (EFB) integration
- Maintenance Gateway
- Data Recorder
- Ethernet Switch



Figure 4.1: Ballard :AB2000

5 Avionics Engine Control System

5.1 Speed Controller

The speed controller used for Falco E-1 is manufactured by MGM COMPORO. At the moment the manufacturer is in the process of getting the speed controller certified within 2 years. The controller is capable of managing up to 400V, 400A 150KW. The controller comes in with built-in 32-bit ARM Cortex processors used for control. These speed controllers also offer a range of innovative functions, control and configuration options and PC communication capabilities. Real-time monitoring and logging of operating data are given.

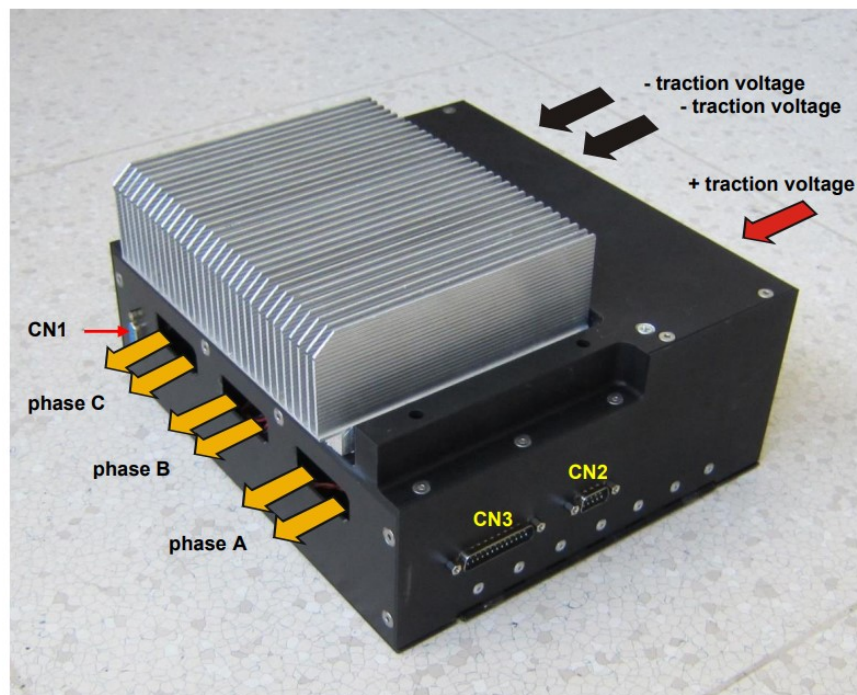


Figure 5.1: Motor Controller[14]

Active safety components, expanded to include the Emergency Stop function, make operation even safer. This is a completely unique feature and particularly invaluable for electric Aircraft (EV). Each cell monitoring: all controllers have the option to measure each battery cell.

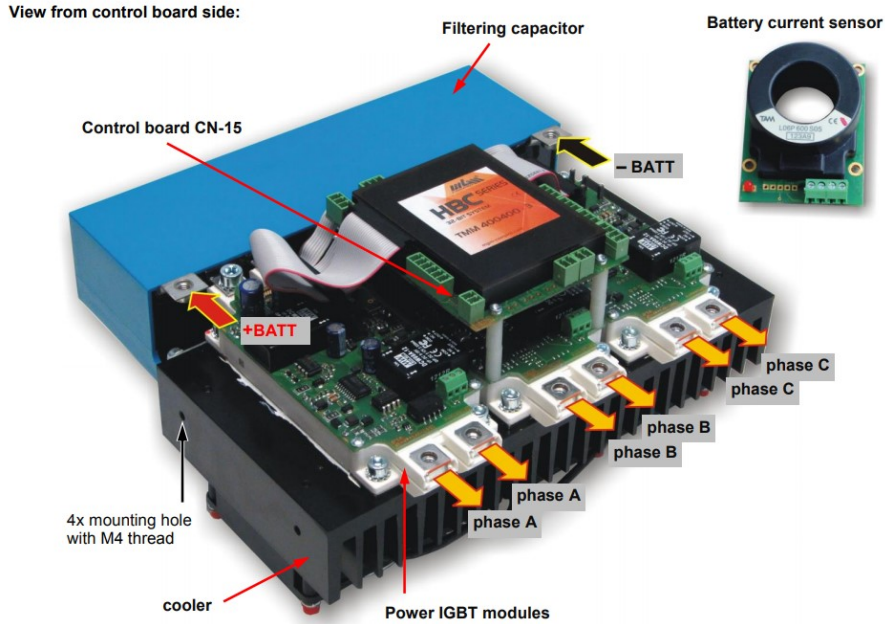


Figure 5.2: Motor Controller PCB[14]

5.2 Battery Management System

Falco E-1 comes equipped with Orion 2 Battery Management System. The Orion BMS is designed at its core to operate in environments with harsh electrical noise and under constant vibration.



Figure 5.3: Cell Balancer

The centralized design allows the Orion BMS 2 to withstand very significant EMI interference. Orion BMS also provides the pilot with the overall health of the battery pack cell by cell. The system monitors the internal resistance of each cell and tracks the capacity of the weakest cell. It uses this information to calculate a cell health percentage value from 0 to 100. The BMS then compares the calculated cell health information against pre-programmed thresholds and if any cells (or the entire pack) fall short of the threshold

Intelligent Cell Balancing

The BMS uses an intelligent approach to balancing that seeks to maintain and improve balance

from cycle to cycle. Unlike lead-acid batteries, lithium ion batteries tend to stay in balance once initially balanced, as long as an intelligent approach is used to maintain the balance.

Specification Item	Min	Typ	Max	Units
Input Supply Voltage	8		30	Vdc
Supply Current—Active (at 25 degrees Celsius)		< 2		Watts
Supply Current—Sleep (at 25 degrees Celsius, 12vDC)		450		µA
Operating Temperature	-40		80	C
Sampling Rate for Current Sensor		8		mS
Sampling Rate for Cell Voltages		25	40	mS
Isolation Between Cell Tap #1 and Chassis / Input Supply	1.5			kVrms
Isolation Between Cell Taps #2+ and Chassis / Input Supply	2.5			kVrms
Isolation Between Cell Tap Connectors	2.5			kVrms
Digital Output Switching Voltage (Open Drain)			30	V
Digital Output Sink Continuous Current (Some outputs can pulse up to 4A for contactors —see wiring manual for details)			175	mA
Cell Voltage Measurement Range	0.5		5	V
Cell Voltage Measurement Error (over 1-5v range)			0.25	%
Cell Balancing Current			200	mA
Cell Current (Operating)		0.5		mA
Cell Current (Low Power Sleep)		50		µA
Thermistor Accuracy		1		C
Cell Voltage Reporting Resolution		0.1		mV

5.3 Battery Charging Station

The chosen battery charger can charge the aircraft fully in 8 hours. In order to save time 2 chargers can be used to charge the batteries at the same time. The charger uses fast charge technology to charge individual cells. The Charging station can be stationed at local airports & pilot schools to maximize the use of aircraft.



Figure 5.4: Charging Station

Charger Features	
Environmental – Non-Operating	
Altitude	0 to 40,000 feet
Ambient Temperature	-40°F to 159°F
Environmental – Operating	
Altitude	0 to 8,000 feet
Ambient Temperature	32°F to 104°F
Charger Function	
Constant Current Mode	Programmable for any value between 0 and 65 Amps
Battery Voltages – Constant Current Charge	1.25, 2, 6, 12, 24, 28, 36
Constant Potential Mode	Programmable for any value between 0 and 40 Volts
Battery Voltages – Constant Potential Charge	1.25, 2, 6, 12, 24, 28, 36
Number of Profile Steps	1 to 10
Charge to Voltage, Current, Time, Negative Slope Sensing, Temperature Compensation, Delta Thermal Protection	
Other Functions	
Capacity Test, Voltage / Current Monitoring, Serial Data Collection Compatible (RS-232), Data Collection Software Included, Pause / Resume Function, Viewable Profile History Summary, Audio / Visual Indicators, Can Store Up to 80 Different Battery Profiles	
Available Accessories	
Generic Battery Cable Included, Optional Battery Cables Available on Request	

Figure 5.5: Charging Station Specifications

5.4 Portable Battery Charger

The portable battery charger can charge the aircraft fully in 12-16 hours. This is only a redundant or as an emergency use. The portable charging station will always be inside the aircraft. This is manufactured by MGM COMPRO and they specialize in all electric propulsion.



Figure 5.6: Charging Station Portable

Charger Features

Environmental – Non-Operating	
Altitude	0 to 40,000 feet
Ambient Temperature	-40°F to 159°F
Environmental – Operating	
Altitude	0 to 8,000 feet
Ambient Temperature	32°F to 104°F
Charger Function	
Constant Current Mode	Programmable for any value between 0 and 25 Amps
Battery Voltages – Constant Current Charge	1.25, 2, 6, 12, 24, 28, 36
Constant Potential Mode	Programmable for any value between 0 and 48 Volts
Battery Voltages – Constant Potential Charge	1.25, 2, 6, 12, 24, 28, 36
Number of Profile Steps	1 to 10
Charge to Voltage, Current, Time, Negative Slope Sensing, Temperature Compensation, Delta Thermal Protection	
Other Functions	
Capacity Test, Voltage / Current Monitoring, Serial Data Collection Compatible (RS-232), Data Collection Software Included, Pause / Resume Function, Viewable Profile History Summary, Audio / Visual Indicators, Can Store Up to 80 Different Battery Profiles	
Available Accessories	
Generic Battery Cable Included, Optional Battery Cables Available on Request	

Figure 5.7: Portable charger functions

6 Environmental Control

The Enviornmnetal Control of the Aircraft was divided into 4 subsections. TALK ABT ENV LMAO

6.1 Aircraft Cooling

The Aircraft Environmental Control System was monitored thru the CANBUS system and Pneumatic valves were used to open and close small hatches to regulate temperature throughout the aircraft. The tubes will be monitored by the CANBUS system which will supply power to control the valves. This system is only for cooling and balancing humidity for the aircraft.



Figure 6.1: Pneumatic Valves

The air distributer on the picture below is supplied by Astronics, as part of the environmental control system of an airplane, the diffuser is the interface between the HVAC system and the passenger environment. Harnessing air from the central air supply, the environmental control system produces laminar airflow and uniformly distributes air throughout the cabin.



(a) Air Distributer by Astronics



(b) HVAC Controller

The controller on the picture to the right is provided by Aircraft Spruce, The controller keeps the ambient temperature of the aircraft on pilot's preference . This acts as a system between the valves and the computer as user can input their desired temperature and flow speed of air.

6.2 Aircraft Heating

For Falco E-1 heating needs DC thermal heater built in USA was used. The product is approved by FAA for Civilian Aircraft use, The heaters are made out of vinyl clad aircraft aluminum which is riveted together.

- Heater Dimensions: 6"x 5" X 4"
- Brushless 50,000 Hour Ball Bearing Fan
- 10,000 Hour DC Thermal ©RuCar Vacuum Sealed Elements.
- Case Construction: Riveted T5052 Aircraft Aluminum.
- Wired Entirely with GXL Wire
- Thermally Protected

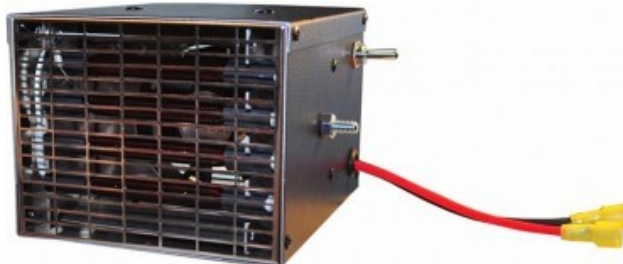


Figure 6.3: DC heater by Aircraft Spruce[15]

7 Flight Control System

The flight control system will be a pulley and cable method as it is easy to map through the plane, light weight, and reliable. A small plane like the FALCO E-1 does not require a complex, fly-by-wire system since its purpose is to be a trainer/leisure aircraft. The mapping of the pulleys and cables will be similar to the ones presented below, the mapping of the Cessna 172 flight control system.

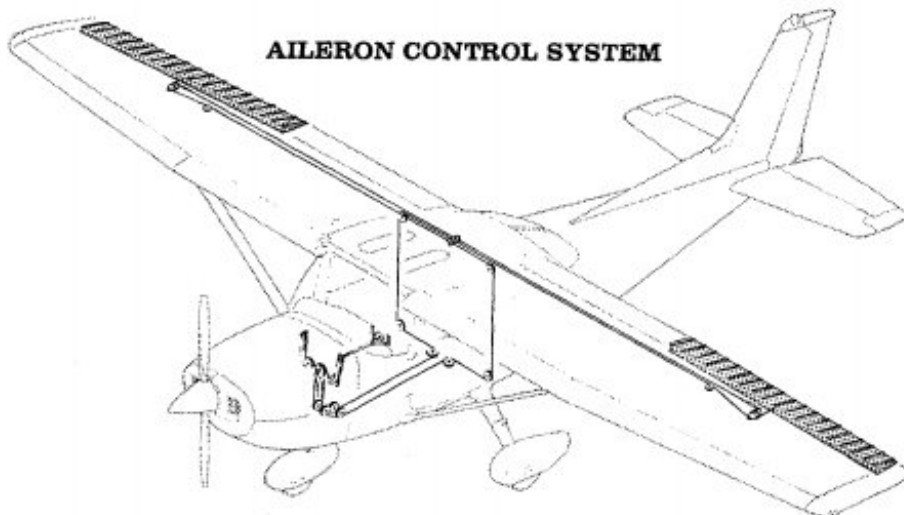


Figure 7.1: Cessna 172 Aileron Control Mapping[9]

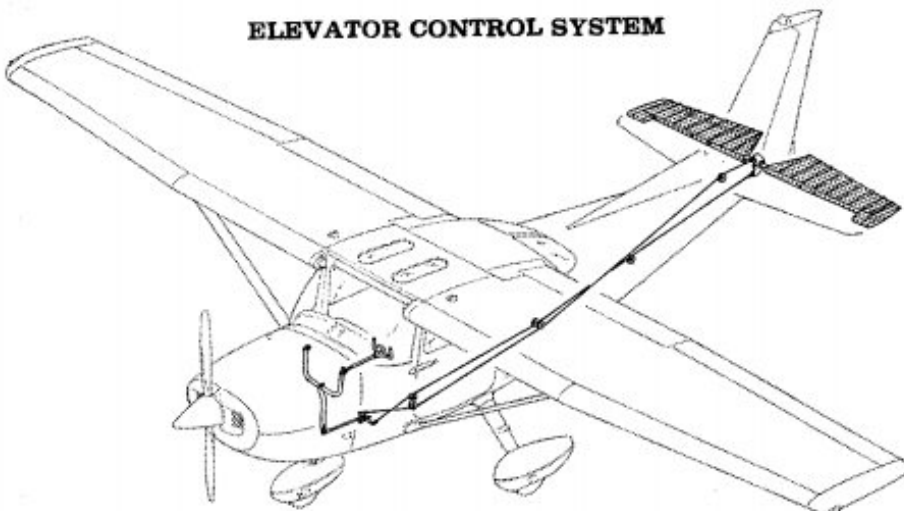


Figure 7.2: Cessna 172 Elevator Control Mapping[9]

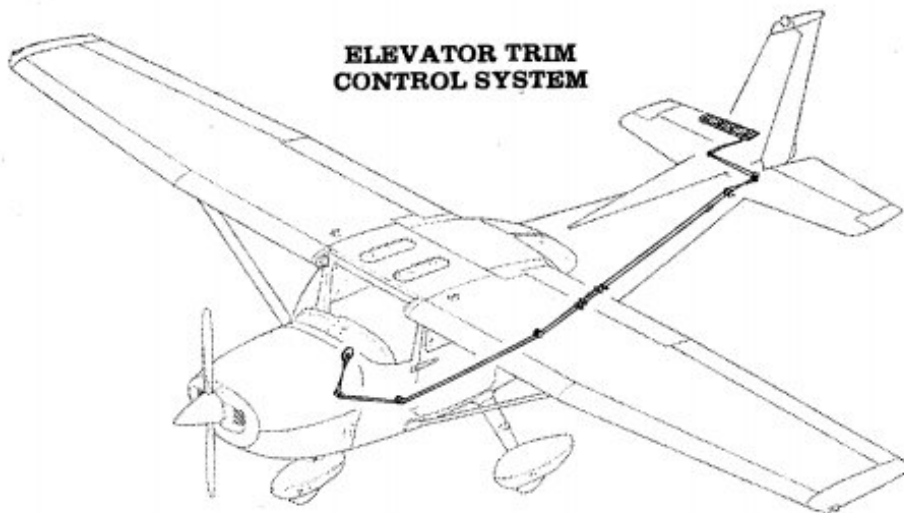


Figure 7.3: Cessna 172 Elevator Trim Control Mapping[9]

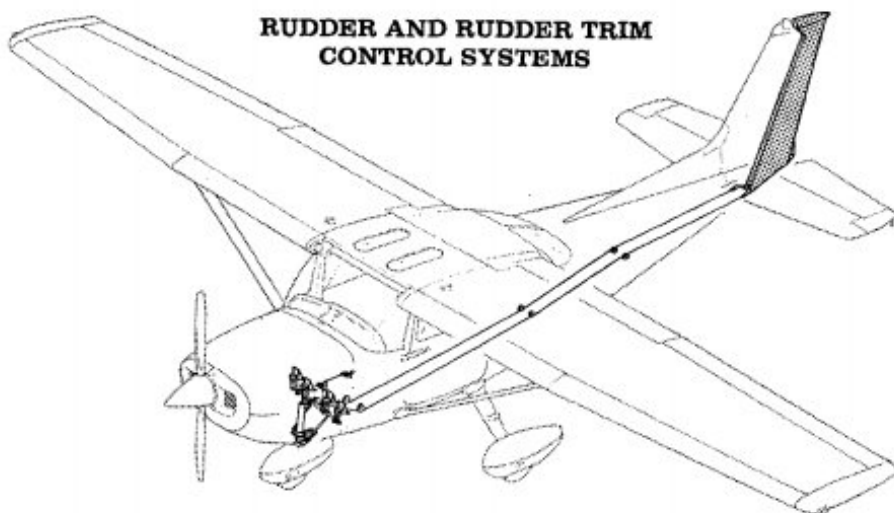


Figure 7.4: Cessna 172 Rudder Control[9]

8 Hydraulics

The hydraulics system within the FALCO E-1 will consist of only the braking system. The braking system includes five parts: the rudder pedals, the brake valve, the brakes, the lining, and the hydraulics fluid. The whole system starts from the pedals which connect to the valve through the lining and from that valve, the lining continues until the brakes. The hydraulic fluid being used is the trusty MIL-H-5606 hydraulic fluid.

9 Exterior Lighting

As per FAR23 and CAR523 regulations, the plane is mounted with one light at each wing tip, and one on the tail, and it was decided to place one on the nose as well for extra safety precautions. As for the interior lights, they provide sufficient lighting for operators to pilot the plane during the night and/or less visible lighting conditions.

9.1 Strobe Lights & Anti-Collision Lights

The strobe lights on the Falco E-1 are located on the trailing edge of the wing tops. They flash at a high intensity at programmed intervals. They can also be used to provide additional lighting when crossing an active runway during ground maneuvering. The anti-collision light system consists of two beacon/strobe light units. The Anti-collision lights are developed to accurately match the size and shape of Falco E-1. The package includes upper and lower fuselage, tail and wing strobe lights that are resistant to the toughest environmental conditions such as high temperature, electro-magnetic interference, vibration and shock.



Figure 9.1: Strobe and Anti-Collision lights

9.2 Taxi Lights

Parmetheus PAR36 LED lights were fitted for Falco E-1 as taxi lights. The lights are PMA Approved, lightweight, low-current and moisture resistant, they provide stable light output for thousands of operating hours. These LED lights are 40% brighter output than most of the lights on the market.

- 10,000-hour operating life.
- Power wiring attaches to brass terminals
- Poly-carbonate, replaceable, hard-coated outer lens.
- Metal, heat dissipating coated housing.
- Whelen TIR™ strobe in intensity and effectiveness.



Figure 9.2: Taxi Lights

9.3 Wing Inspection Lights

The LED is mounted on the side fuselage under the wing. When the maintenance crew needs to inspect the aircraft for icing and maintenance purposes this light is used. The LED eliminates the need for thousands of hours of operation.

- Fully FAA/TSO-C96a & TSO-C30c Approved
- FAR SPEC Certified STC SA800EA
- Aerodynamic design without sacrificing light output
- FAA minimum intensity requirements for maximum visibility and increased safety of flight
- Environmentally tested and certified to RTCA/D0-160G standards



Figure 9.3: Taxi Lights

9.4 Landing Lights

This model is a self-contained all LED Landing Light Assembly. The design is intended to provide a solution to the needs for a Taxi & Landing Light on a wide variety of aircraft. All current source and electronic circuitry is contained within the housing. Unit is available in several mounting configurations to retrofit existing typical PAR-36 lighting. Outer lens allows for mounting externally on aircraft, option of diffusion lens available upon request.



Figure 9.4: Landing Lights

Part V

Book V: Propulsion

1 Propulsion Design Parameters & Initial Considerations

2 Flight Performance & Range

2.1 Mission Profile & Power Requirements

For performance calculations the flight mission was divided into 4 categories: cruise, takeoff, climb and landing. Rough power required estimates were calculated for each and energy consumption was determined based on those numbers. The energy available (Wh) divided by the energy consumption (W) yielded flight time

The MATLAB code for flight time relied on an average consumption rate divided by a flight time variable in hours. The flight time estimation begins at an arbitrary time and reduces itself until the average power matches the power requirements at cruise *and* takeoff. The original model did not account for takeoff leading to a situation where the plane seemingly flies for a long time but does not meet the power outputs at takeoff. Splitting the velocity into X and Y components allowed the horizontal distance travelled to be calculated i.e. the range.

2.1.1 Cruise

The cruise portion of flight was the easiest to calculate. The power required was roughly calculated using the equation in the figure below from the MIT propulsion lectures [36]. Equation 2.1 relates shaft power to velocity, thrust and propeller efficiency.

$$P_{shaft} \approx TV \frac{1}{\eta_v} \quad (W) \quad (2.1)$$

Thrust was calculated for steady level flight at cruise altitude, meaning a perfect counter to the drag force. Initially, the total drag of the aircraft was not calculated yet so wing drag was taken and multiplied by a factor to get total drag. Velocity was given by the MR&O specifications and propeller efficiency was initially set at 80%. This yielded power usage in Watts for the cruise stage.

2.1.2 Takeoff

The power required was roughly calculated using the equation in the figure below from the MIT propulsion lectures [36]. Equation 2.2 relates shaft power to thrust, propeller radius and propeller efficiency. The propeller efficiency was again set at 80% for our estimate and the radius was determined from the propeller team as 0.96 meters.

$$P_{shaf t} \approx \frac{T^{3/2}}{(2\pi\rho)^{1/2}} \frac{1}{R} \frac{1}{\eta_v} \quad (W) \quad (2.2)$$

Thrust was calculated from 3 sources of resistant forces the acceleration to takeoff velocity, the air resistance and the ground roll resistance. The equation below demonstrates the factors considered. The dynamic friction coefficient (μ) was determined from NASA aviation tire research [37]. The μ calculated was 0.2 at 50knots. The air resistance was conservatively calculated as drag at takeoff speed even though it only reaches that magnitude near the end of the roll. The acceleration was calculated using equation 2.4.

$$F_{TOThrust} = ma + F_N\mu + F_D \quad (N) \quad (2.3)$$

$$a_{TO} = \frac{V_{TO} - 0}{TakeoffTime} \quad (m/s^2) \quad (2.4)$$

By increasing takeoff time, the acceleration was lowered and the power demand as well. However, too low an acceleration meant incurring the risk of exceeding field length. Using the position derivatives. The code integrated the acceleration and used the takeoff speed to calculate field length. If field length is more than the MR &O allows, a warning appeared to warn the user to increase reduce the takeoff time. The full code is in the appendix.

$$a_{TO} = \frac{dv}{dt} = \frac{d^2y}{dt} \quad (2.5)$$

The takeoff time was set to 34 seconds, yielding an acceleration of 0.82 m/s^2 . Based on this acceleration, takeoff speed is reached as the aircraft covers 471.75 meters of ground roll. This is below the maximum of 518.16 m (1700 ft) as per the requirement target of the MR&O.

The aerodynamic drag was calculated using Equation 2.6, the velocity chosen was takeoff velocity for a conservative estimate and a simplified calculation. The S and C_D were taken from the wing only. To account for the whole body drag a correction factor of 1.8 was selected. After completion of the fuselage, tail and landing gears, the actual factor was closer to 3 and actual cruise drag force was determined from CFD.

$$F_{drag} = \frac{1}{2}\rho * V^2 * S * C_D * CorrectionFactor \quad (N) \quad (2.6)$$

With all parameters set, the takeoff thrust required was calculated to be approximately 3.41 kN. Based on this thrust, Equation 2.2 was used to determine the shaft power, 94.08 kW, required from our motor. This is lower than the maximum continuous power output by the EMRAX 268, 100 kW which meant the aircraft was capable of taking off.

$$P_{shaft} \approx \frac{3413.33^{3/2}}{(2\pi * 1.225)^{1/2}} \frac{1}{0.96} \frac{1}{0.80} \approx 94.08 \text{ kW}$$

2.1.3 Climb

The climb portion used takeoff velocity to determine drag and did a thrust balance to determine climb angle using the climb angle equation [36]. Assuming takeoff thrust is used continuously until cruise altitude and speed is reached, the velocity component in the X and Y axes give the travel distance and the rate of climb. Rate of climb and cruise altitude are then used to determine the time to reach cruise. This time and the power consumed during provide the takeoff and climb energy consumption.

$$\sin\gamma = \frac{T - D}{W} \quad (2.7)$$

The drag component of the equation was calculated using C_d value at the takeoff angle of attack(AoA) at the MR &O best-angle-of-climb speed and at sea level air density. This meant a pessimistic approximation of drag as the reduction in AoA and air density would, in the real case, result in less drag. This reduced drag translates to less thrust required and as a result less energy consumed. When inputting the flight data into the equation, the angle outputted was 13.02 degrees which is slightly to those seen in jetliners as shown in Figure 2.1 when fully loaded [38].

2.1.4 Landing

The landing approximation was also done in order to calculate the final portion of flight range. For simplicity in calculations, the landing segment began from the cruise altitude and ended at sea level. The approach angle was chosen based on typical approach behaviour for general aviation aircraft of degrees downward. The engine power was set to 25% of max power available and the climb equation from the previous sub-section but with a slight modification. Due to thrust adding to gravity, the Drag and Thrust terms are reversed.

$$\sin\gamma = \frac{D - T}{W} \quad (2.8)$$

With the thrust, the angle and weight set, the drag was isolated. With the drag isolated and C_D set, the descent speed was calculated as 22.07 m/s. From the descent speed and, the sink rate and ground speed were found to be -6.35 m/s and 21.14 m/s respectively. The sink rate gave us the cruise to land time which contributes to flight time.

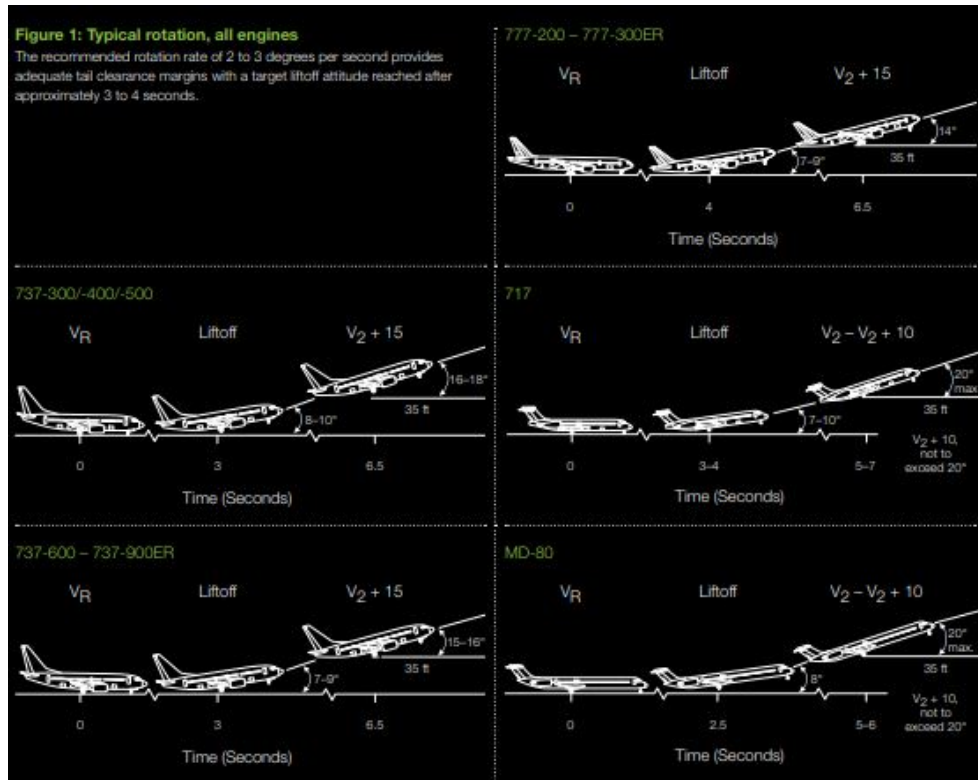


Figure 2.1: Common Takeoff Angles

$$V_{Descent}^2 = \frac{2 * Drag}{\rho * C_D * S} \quad (2.9)$$

2.1.5 Power Requirements & Range Calculation

The thrust required at each stage of flight was calculated in the flight mission profile just covered and then converted to power required using either Equation 2.2 for takeoff and climb or Equation 2.1 for cruise and descent.

The power usage calculations were done based on Watt-hours available and Watt-hours used. The Watt-hours available were calculated using the Equation 3.1 with battery mass in kilograms and battery capacity in Wh/kg. The battery packing efficiency accounts for the weight of a battery pack that is purely battery (excludes BMS,Casing,Wires,etc). The manufacturer touted a pack efficiency of 80% for their new batteries [39].

$$Energy\ Available = m_{battery} * battery\ capacity * pack\ efficiency \quad (Wh) \quad (2.10)$$

The flight time was calculated using Equation 2.11, where power output is expressed in Watts. The average power output was initially set at 70% of maximum power continuous power available in order to ball park the battery mass required for our range target. Once battery mass was fixed, the average power output was more exactly calculated. It was calculated using the weighted average shown in Equation 2.12.

$$Flighttime = \frac{Energy Available}{P_{average}} \quad (hours) \quad (2.11)$$

$$P_{avg} = \frac{(P_{to,climb} * t_{to,climb}) + (P_{cruise} * (t_{total} - (t_{to,climb} + t_{descent}))) + (P_{descent} * t_{descent})}{t_{total}} \quad (W) \quad (2.12)$$

The takeoff to cruise time and cruise to landing time were constrained by climb rates which meant the cruise portion was the time segment that changed. This led to a refinement in which the takeoff and descent energy consumed were subtracted from the energy available and the code solved for the cruise power. Once cruise energy is found, the cruise time is proportional to it and cruise power output as shown in Equation 2.14.

$$Energy_{av,cruise} = Energy_{av} - (P_{toff} * t_{toff-to-cruise}) - (P_{descent} * t_{cruise-to-land}) \quad (Wh) \quad (2.13)$$

$$P_{cruise} = \frac{Energy_{av,cruise}}{t_{cruise}} \quad (W) \quad (2.14)$$

The MATLAB code for range begins at an initial guess of cruise time and calculates the cruise power it yields. If the cruise power calculated is less than the one available, it iterates again but with a time guess 0.01 hrs shorter. This loops until the cruise power is greater than the power required at which point the cruise time is selected. Summing the cruise, takeoff and descent times yields the total flight time of the aircraft. As per FAR 25, half an hour is subtracted from the endurance to account for emergency range available.

The range is also a summation using the 3 phases of flight. The range uses the horizontal velocity segment and time spent for each phase and adds them up. Finally, the sum is converted from meters to nautical miles to compare with the MR&O targets. The range equation is shown below, where velocities are in m/s and time in seconds.

$$Range = (V_{climb,x} * t_{toff-to-cruise}) + (V_{cruise} * t_{cruise}) + (V_{descent,x} * t_{cruise-to-land}) \quad (m) \quad (2.15)$$

3 Battery Selection

3.1 Project Constraints

The MR &O dictates the limitations on battery technology available for consideration. The MR &O limitations prevented this design competition from turning into a battery tech arms race. The battery characteristics were constrained on the following criteria:

1. Li-ion type or equivalent]
2. Maximum capacity of 300 Wh/kg
3. Removable from aircraft for separate charging
4. Battery units change-over time within 20 minutes
5. Certifiable for airworthiness

These constraints guided the selection process and were the main driving force during the design phase.

3.2 Selection Process

The battery cells chosen were the Licerion lithium metal cells developed by Sion Power. Figure 3.1 below shows the base module of the currently available model. The cells used for the Falco E-1 is the next generation of Licerion cells which will be covered in the energy density section. The following section describes the selection process to meet the battery criteria. There is a decision table at the end where all candidate batteries are weighted against each other on these criteria.



Base module
917 Wh (12 V or 24 V)

Figure 3.1: Licerion Battery Module

3.2.1 Specific Capacity

The first criteria chosen for selecting batteries was the energy density per kilogram. The MR &O capped it at a maximum of 300 Wh/kg. This limit matches current high performance which peak at between 250 and 300 Wh/kg such as the Panasonic 18650 and 2170 cells used by the Tesla Model S and Model 3 respectively [40]. The principal limitation in use of electric power over fuel is the energy density of the batteries. Typical gasoline has an energy density of 12,890 Wh/kg for comparison, almost 45 times more. The initial candidate batteries at 300 Wh/kg yielded flight endurance times of under 2 hours at 62% MTOW, which severely limited weight resources for the rest of the aircraft structures and systems. Furthermore, the estimated was below the MR &O requirement. The project scope changed and uncapped the capacity allowing for more energy dense solutions.

With the cap lifted, more powerful batteries were selected as candidates such as the Tadiran TL-5930/S batteries boasting a 710 Wh/kg energy density while already being available on the market for purchase [41]. To determine a minimum capacity limit for the battery candidates, an initial rough estimate of energy requirements for a 2-hour flight at 75% power was performed. The total energy available calculation was simply based on the *battery capacity* and *total battery mass*. The battery mass was set using the initial mass allocation estimate shown in Table 3.1 below. The actual weight of the airframe and systems changed iteratively as the project matured and as a result the battery mass allocation as well but this was the starting point.

ITEM	MASS(lb)
MTOW	2550
PAX + Bags	-800
Motor	-45
Airframe + Systems (Cessna 172)	-816.25
Remainder (Batteries)	838.75

Table 3.1: Initial Mass Allocation Estimate

The estimated energy available based on capacity was defined with the Equation 3.1 below with battery mass in *kg* and capacity in *Wh/kg*. This equation did not take into account different discharge rates (which are described in the Charge & Discharge section) and the effect of environmental conditions on the battery to simplify the initial estimate.

$$E_{available} = BattCapacity * BattMass \quad (Wh) \quad (3.1)$$

The flight estimate is based on the chosen motor, EMRAX 268, running at 75% of its maximum continuous power. The Flight Mission section will go more in detail when it comes to calculations and power requirements but the initial power estimate followed Equation 3.2 with force in *Newtons* and velocity in *m/s*.

$$Power = 0.75 * P_{maxContinuous} \quad (W) \quad (3.2)$$

Using these two equations and isolating for battery capacity yields Equation 3.3. For the target 2 hour flight at 75% max continuous power, Equation 3.4 states a minimum of 432.79 Wh/kg required. This became the Specific Capacity criteria to be followed during battery selection.

$$MinimumCapacity \geq \frac{(Power * FlightTime)}{BatteryMass} \quad (Wh/kg) \quad (3.3)$$

$$\frac{((0.75 * 110kW * 2hrs)}{381.25kg} \leq 432.79 \quad (Wh/kg) \quad (3.4)$$

3.2.2 Life Span

Any battery, even rechargeable, will need to be replaced as its depth of discharge (DOD) shrinks after each charge/discharge cycle. Battery cycle life is commonly measured the amount of charge/discharge cycles until the DOD is 80% of the initial brand-new DOD [42]. Again, to better scope the selection process a lower limit needed to be set. The cycle life required was based on an initial target of at least *1 year* of use for the Falco E-1 before the need to replace the batteries. The scenario chosen to estimate the usage rate of the Falco E-1 was that of a pilot school aircraft. These aircraft are heavily used as they are the schools' main source of revenue. The presumption is that if a battery is capable of satisfying this demanding function it would be more than enough for other tasks expected from a general aviation (GA) aircraft (ex: farming, traffic surveillance, remote air ambulance).

A typical flight school operates during sunlit hours of the day with the option for an hour of night flying provided the conditions are favorable. This will help determine the yearly work demand of pilot school airplane. Sunlit hours depend on time of year and geographic location, for simplicity Toronto was chosen as the setting. Toronto typically receives 2066 hours of sunshine per year plus another 365 hours of night flying totalling 2431 operating hours per year [43]. Factoring for 2-hour preventive maintenance sessions at every 100 hours, like the Cessna 172, cuts the total down to 2383 operating hours per year [44]. The battery cycle was defined as the time from battery insertion into the aircraft to removal after full depletion. This corresponds to a full flight (minimum 2 hours as per initial estimate) and ground activities (20 mins), this is called battery run time. Note this does not include charging time, charge and discharge requirements are explored in the next section. The flight time depends on battery specific capacity as demonstrated in the previous section but the 2 hours is used to provide a lower limit. The cycles per year can be calculated using Equation 3.5 and inputting the numbers from the assumptions yields a minimum of approximately 1023 cycles as our Life Span criteria.

$$Cycles_{yearly} \geq \frac{OperatingHours_{yearly}}{BatteryRuntime} \quad (\# \text{ of cycles}) \quad (3.5)$$

$$\frac{2383}{2.33} = 1022.75 \text{ cycles} \quad (3.6)$$

3.2.3 Charge and Discharge Rates

Charge and discharge rates are big indicators of the versatility of a battery. A fast charge rate means less down time and a high discharge rate means a high current can be supplied by the cell [42]. The project requirements did not specify a maximum recharging time for the battery units, focusing instead on their changeover time. The motor requires 500 amps to run at max power so this discharge rate was the minimum required for the candidate batteries. For charging, time and rate requirements are not as stringent because the MR&O chooses to gloss over it. However, a shorter recharging time will nonetheless give a candidate battery the edge as opposed to a slower one in this category.

3.2.4 Operating Conditions

The battery cells must withstand the conditions during flight and to a lesser extent the storage conditions of the aircraft. The atmospheric temperature at the objective Maximum Operating Altitude (MOA) of 12,000ft is 16.23 °F or -8.76 °C according to ISA litterature [45]. Colder temperatures as low as -18.6 °C are encountered in winter and at high latitudes like the Canadian North and Alaska. On the other hand summertime can bring temperatures as high as 52 °C in some parts of Nevada. The batteries must be able to operate in this wide range of temperatures with little to no inputs from an Environmental Control System (ECS). The lack of reliance on an ECS means reduced systems mass for the aircraft. A wide range of operating temperatures means the Falco E-1 will reach a wider market. Based on this, the criteria set for Operating Conditions was a temperature range of -10 °C to 40 °C at least.

3.2.5 Airworthiness & Market Availability

For the battery to be implemented in the aircraft it must be available for purchase on the market and meet airworthiness demands. The UN/DOT 38.3 certification is a rigorous transport safety standard that many battery manufacturers follow in their design methodology. This certification in addition to statements from the manufacturer was deemed sufficient proof of airworthiness in our battery selection process.



Figure 3.2: UN 38.3 Certification Badge

Market availability was deemed sufficient if the candidate would available in the next 3 years. Again, confirmation from the manufacturer was a requirement to prove this target was met. The earlier the availability of the battery within these 3 years the higher the ranking it would receive in the market availability category. A candidate with both these aspects would be top this category.

3.2.6 In-built Features

This category was to compare the candidate batteries of in-built features. A battery module with certain features will save our aircraft in design complexity and weight. This is because it eliminates the need for external systems to accomplish those tasks. The features can be divided into 2 types: safety and convenience. A list of features considered initially is given below. The candidate battery that included the most of these was selected as the best in the In-Built Features category.

Safety

1. Battery Management
2. Early Warning/Failure Detection
3. Independent Switch-Off/On
4. Overcharge/discharge Protection
5. Overcharge/discharge Protection

Convenience

1. Modular/Interconnectable Packs
2. Small/Lightweight Packs
3. Manufacturer Customizability

3.2.7 Battery Cell Chosen

Based on the criteria outlined in this section, a few candidate batteries were chosen and ranked on a decision matrix. The matrix assigns the ranking of 1 for the best battery in each category and then 2,3,4 and so on for the others. Batteries with the same numbers in a category are ranked the same number. At the end, the battery with the lowest ranking total was selected as the Falco E-1's power source. The manufacturer specs for each battery candidate are contained in the appendix of this report.

BATTERY	SPECIFIC CAPACITY	LIFESPAN	RATES	AIRWORTHY AVAILABLE	IN-BUILT FEATURES	TOTAL
PolyPlus	1	3	3	1	2	10
Apollo	3	4	1	1	2	11
Enevate Energy	4	2	3	2	3	14
Licerion	2	1	2	1	1	7
Oxis Energy	3	5	2	2	4	16

Table 3.2: Candidate Battery Ranking Matrix

The battery chosen was the Licerion High Capacity Cell (shown in Figure 3.3) which is a scale up of their currently available model. The manufacturer confirmed market availability in 2021 and customization options. The current, lower density, module boasts the pack specifications shown in Figure 3.4, these specifications are used for sizing the Layout & Structures section.

3.2.8 Late Battery Change

After CFD was complete and actual drag was much higher than expected, which caused a giant drop in range, even below the requirement. To mitigate, an alternative battery was chosen. The Spanish company Graphenano and Chinese partner "Chint" have successfully developed a Lithium-Graphene battery called Grabat[46]. The batteries have been tested by 2 independent organisms and are safe to use, they are not prone to explosions like Li-ion batteries [46]. Furthermore, Airbus and a few automotive companies have invested 350 million euros into this company [47]. Airbus has also begun the certification process for this power supply [46].

These became the theoretical batteries of the Falco E-1. In terms of sizing and efficiency, the specs of the Licerion packs when it comes to the physical size and modularity. The main difference is the 1 kWh/kg capacity of the Grabat. With this power supply, the objective range was within reach with a calculated range of approximately 276 nm.

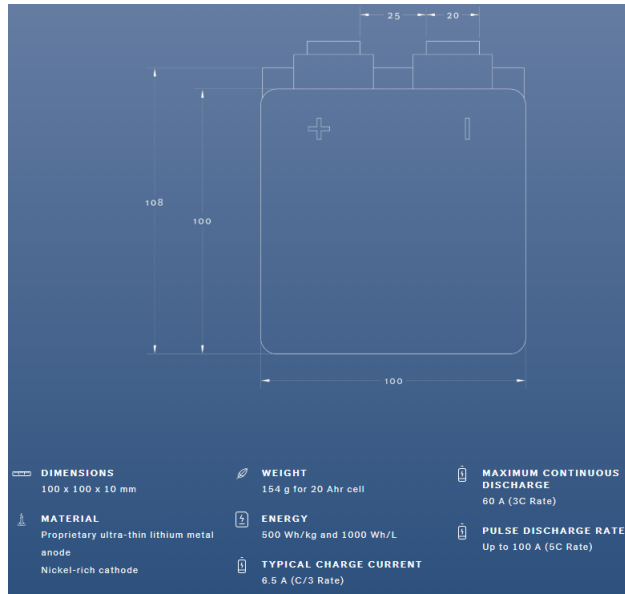


Figure 3.3: Future Licerion High Capacity Cell

Technical Specifications		917 Wh (12 V)
Part Number	BX-354P-12-80	
System Configuration	3Sx4P	
Total Energy	917 Wh	
Pack Capacity	80 Ah	
Nominal Voltage	11.5 V	
Pack Specific Energy	322 Wh/kg	
Pack Energy Density	270 Wh/L	
Continuous Discharge Power (1C)	920 W	
Peak Discharge Power (5s at 5C)	4.58 kW	
Continuous Charge Power (C/4)	230 W	
Pack Mass	2.8 kg	
Pack Volume	3.4 L	
Cycle Life	> 400	
Pack Dimensions (L x W x H)	149 x 149 x 153 mm	
Operating Temperature	-20 to 45 °C	

Figure 3.4: Module Specifications

3.3 Layout and Structural Design

Once the battery was chosen, the containment and integration into the fuselage of the aircraft was the next step. This section explores the design approach to the power supply infrastructure

inside the Falco E-1.

3.3.1 Positioning & Mass Balance

Battery Section Sizing

The batteries hold a high percentage of the aircraft's empty mass. This means the aircraft's center of gravity(CG) is heavily influenced by the battery CG. Another limitation on positioning is the actual volume of the battery packs. To better control the CG position, the batteries were split into a front and rear section. The battery sections were designed symmetrically about the longitudinal axis to match the aircraft center-line laterally. This is shown in the top view provided in 3.6. The section mass depends on the front/rear mass split of the batteries as a percentage of total mass, Equation 3.7 shows this relation. More mass in the front of the aircraft pulls the CG forward and contributes positively to pitch stability. However, the front section size is constrained by the space limitations in the nose meaning the front percentage is always lower than the rear. To satisfy these constraints a 40/60 split was chosen for the front and rear battery sections.

$$m_{section,i} = m_{total} * m_{percent,i} \quad (kg) \quad (3.7)$$

Once the front and rear battery section masses is determined, the number of modules required is calculated by dividing section mass by module mass and rounding up to the nearest whole number. Once the number of modules is determined, sizing is determined based on module dimensions and available space in the fuselage given to batteries by the fuselage team, these zones are shown in Figure 3.5 and Figure 3.6.

$$N_{modules} = \frac{m_{section}}{m_{module}} \quad (3.8)$$

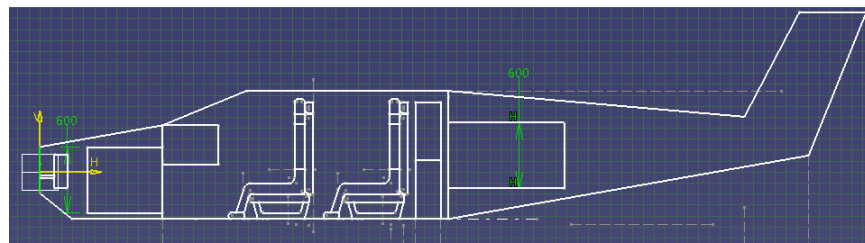


Figure 3.5: Side View of Battery Available Space

The size of the section in any direction is the size of the modules and the spacing between them in that direction. The number of modules in any direction is constrained by the space available in that direction. A MATLAB code was developed to determine the module configuration in each battery section and as a result the size of the actual size of the battery section. The flowchart below shows the algorithm to guide the the MATLAB calculations. The full code is in the appendix of this report. The final outputs were the size of the front and rear battery sections. Their respective CG in the longitudinal axis was their midpoint in the x-axis.

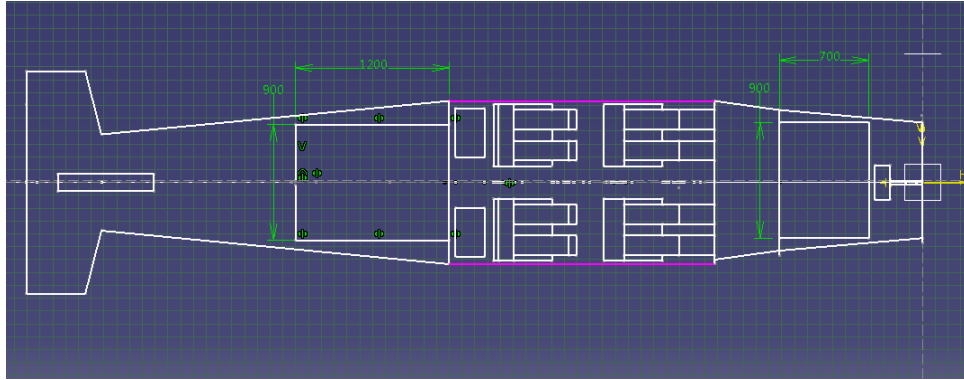


Figure 3.6: Top View of Battery Available Space

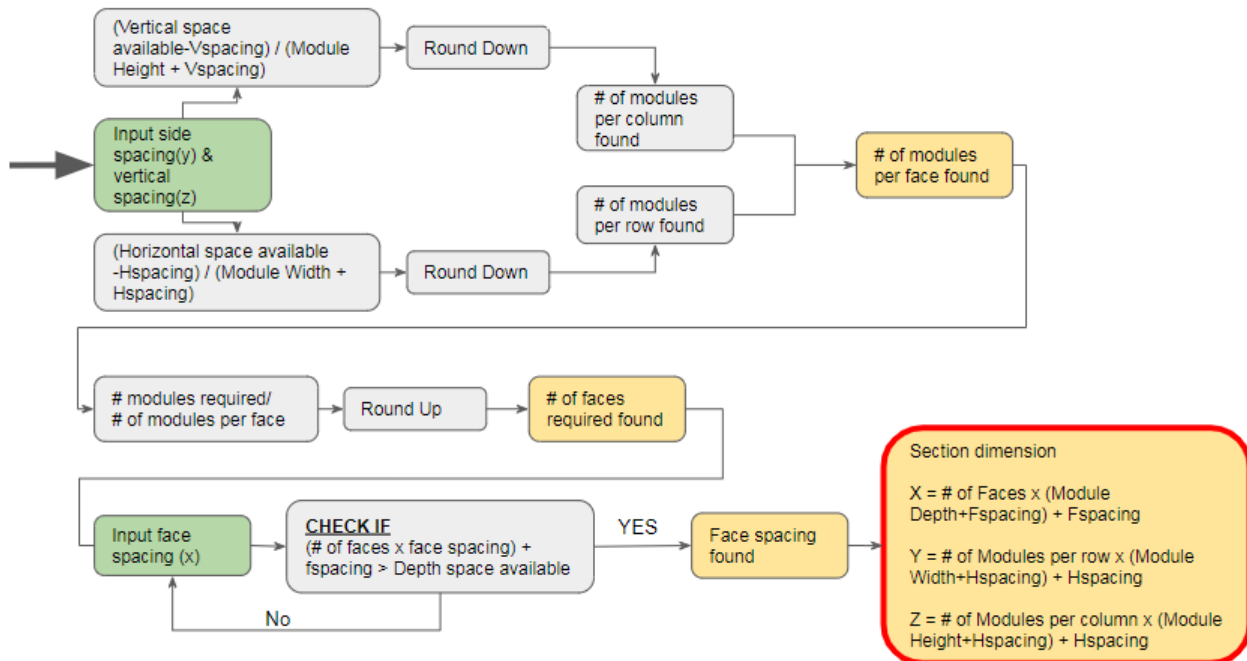


Figure 3.7: Battery Section Sizing Code Algorithm

The sizing (width x height x depth) results in millimeters for the first estimation yielded 465 X 453 X 755 for the front and 465 x 453 x 1057 for the rear. This is within the 900 X 600 X 700 and 900 X 600 X 1200 front/rear limits. This configuration accommodates 97 cells (39 front; 58 rear) at 2.8 kg each [48].

Battery Section Positioning

The battery CG depends on the front and rear section mass and position. The arrow sizes in Figure 3.8 show the difference in mass and the horizontal lines show the distance. The white line is the combined CG position in the longitudinal axis.

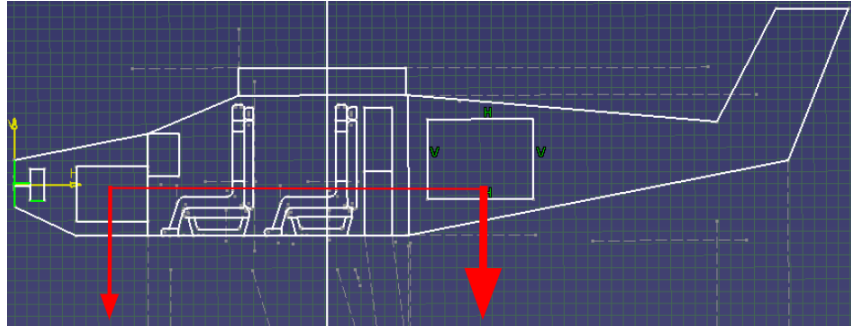


Figure 3.8: Battery CG with Respect to Pack Positioning

The formula to determine the combined battery CG longitudinally is governed by the single-axis CG equation as shown in Equation 3.9. The CG position of each battery section was measured from the nose in meters and defined as the axis of symmetry in the longitudinal direction. The wing team required the CG of the aircraft ahead of the aerodynamic center. A MATLAB code was developed that positions the battery sections to achieve a target x_{cg} .

$$x_{cg} = \frac{\sum(x_{cg,i} * m_{section,i})}{\sum m_{section,i}} \quad (m) \quad (3.9)$$

The front and rear section CGs were originally set at an arbitrary position in front and behind the cabin but within the fuselage limits of the plane. The algorithm moves the sections independently to achieve the target CG location inputted by the user. The flowchart in Figure 3.9 shows the logic the algorithm follows to set the front and rear battery sections' CG positions. The full code is in the appendix of this report. The front and rear sections each have their own front and rear limits. The front battery section must be in front of the cabin (rear limit) but also a minimum distance away from the nose tip (front limit). The rear battery section must be behind the cabin (front limit) but also a minimum distance away from the tail (rear limit).

The original CG positions yielded a combined battery CG of just over 3 meters from the nose. The quarter chord point of the wing location provided by the wing team was 2.6 meters. After setting the target CG at 2 meters (slightly forward of quarter chord), the MATLAB code yielded a front and rear CG location of **1.06 meters** and **2.65 meters** respectively.

3.3.2 Cooling

To ensure proper battery cooling air intakes were designed in different sections of the plane. The front batteries situated near the motor benefited from large intakes right behind the propeller. Putting the intakes right behind the propeller meant the air flow was much faster than the free stream velocity of the plane, especially during takeoff. When cruise altitude is reached, less power is required of the batteries and the ambient temperature is lower. The intakes then close to reduce heat loss and keep the batteries in a favorable environment and at the same time reducing drag to extend range.

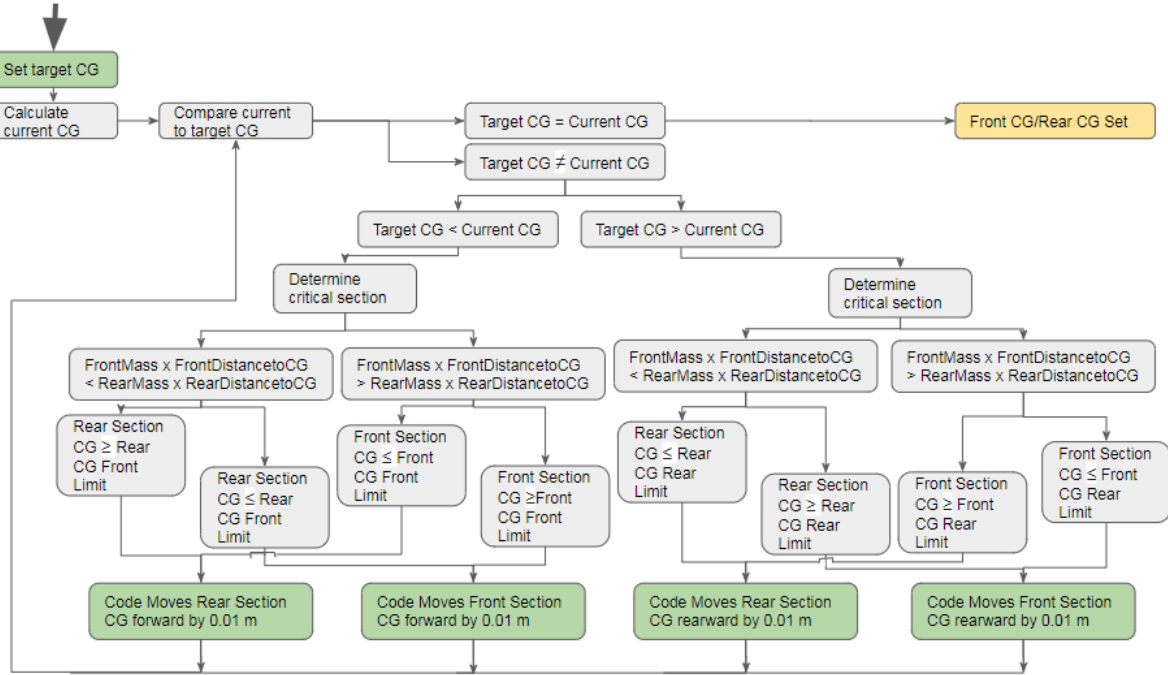


Figure 3.9: Battery CG Controller Code Algorithm

CFD and Thermal analysis has yet to be fully completed to optimize air intake design. However, the initial CAD model features have been completed and are shown below. The nose intakes are shown and the engine bay is opened to show the batteries storage. The geometry will be changed parametrically to improve the environmental and drag consequences. One of the rear intakes on the aft fuselage is also shown in Figure 3.12.



Figure 3.10: Front View of the Nose Intakes

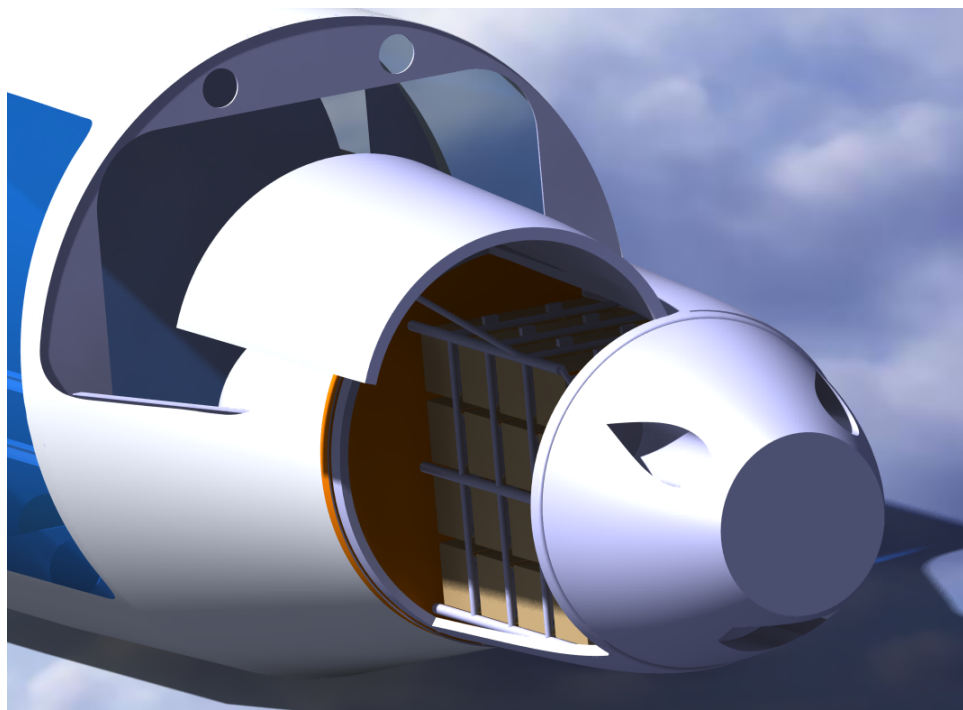


Figure 3.11: Isometric View of the Nose Intakes and Open Engine Bay

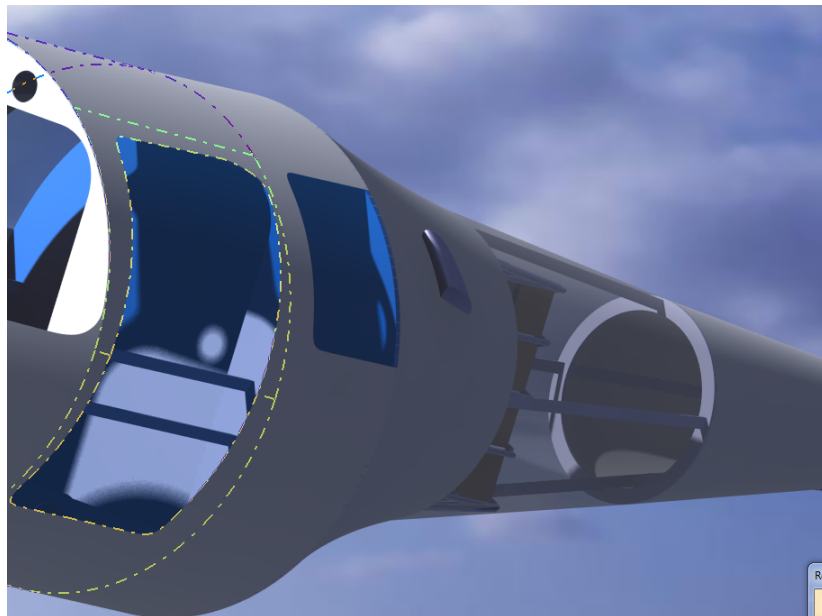


Figure 3.12: Isometric View of Left Rear Intake

3.3.3 Safety Considerations

For safety, there was coordination with the fuselage team to design front and rear firewall to protect passengers from possible battery explosions (Figure 3.13). Furthermore, the front battery section/engine bay was size to allow space for the nose gear to break through during possible

gear failure. The gap shown in 3.14 is for that exact purpose. When the nose gear is fully finalized it is possible the front battery section and engine bay will have to be reconfigured to allow room in those emergency situations.

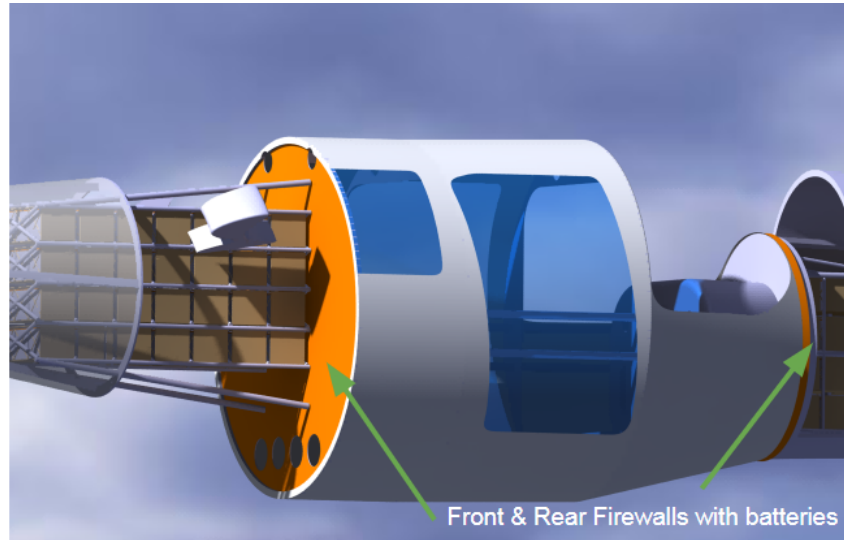


Figure 3.13: Front and Rear Firewalls

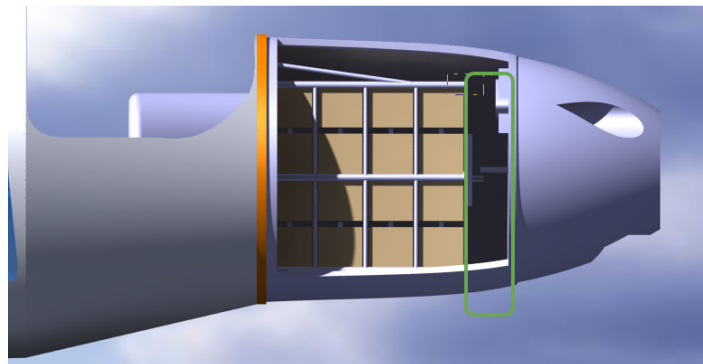


Figure 3.14: Nose Gear Clearance Area

3.3.4 Geometry & Stress Analysis

The preliminary geometry design process for the battery containment trusses simply followed that of current GA planes' engine structures. One such example is shown in Figure 3.15. The rod sizing and configuration followed the same overall look but was modified to properly enclose the batteries, this is presented in the following figures.

For the final report, the truss structures will be analysed under mission loads in ANSYS and the rod cross section will be iteratively optimized to reduce mass. Thermal loads and expansion will also be explored in the optimization process.



Figure 3.15: Cessna 172 Engine Mount and Firewall

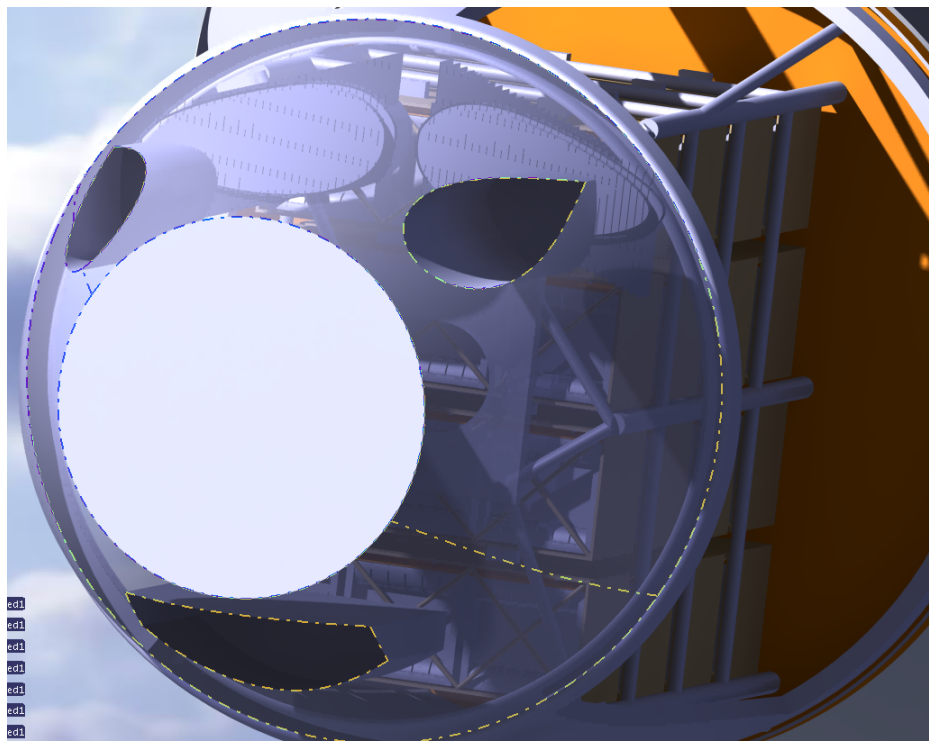


Figure 3.16: Front Battery Section Truss Structure

3.3.5 In-Depth Stress Analysis

Once battery mass and layout was completed for the front and rear battery frames under maneuver loads. The frames were loaded with maximum battery mass (the extra 300 lb configuration) in ANSYS Workbench as shown in the figures below.

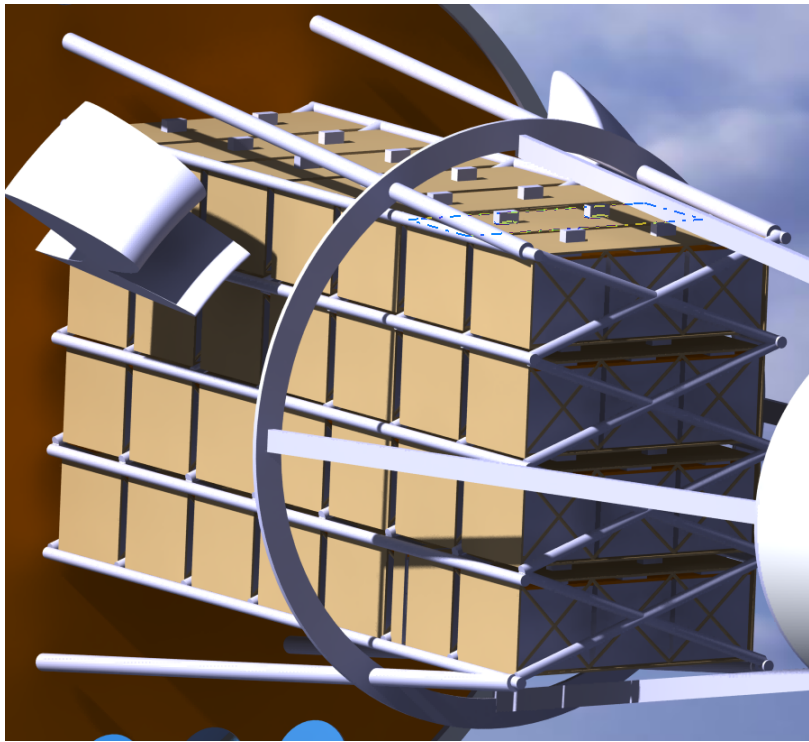


Figure 3.17: Rear Battery Section Truss Structure

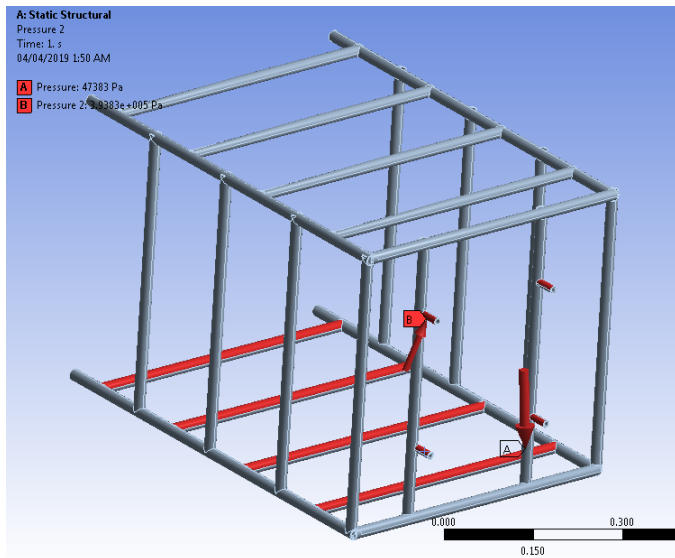


Figure 3.18: Front Battery Section Truss Structure

3.3.6 Jig Assembly & Changeover Time

By taking advantage of the manufacturer's personalizing options, a battery jig was designed for the Falco E-1. The jig is shown Figure 3.20 and contains 3 modules side by side. The spacing helps with cooling the modules and the overall jig size fits perfectly with the remaining space in the front and battery sections. For the 99 modules required as per the requirements set out earlier

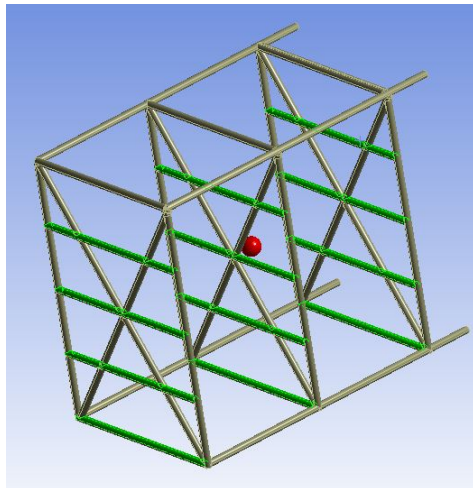


Figure 3.19: Rear Battery Section Truss Structure

in this report, 33 jigs are required. The jig mass is that of 3 modules plus structural weight, the total mass is around 15 kg or 33 lbs. This makes it a *slightly* heavy but still within a comfortable threshold for a typical GA ground staff.

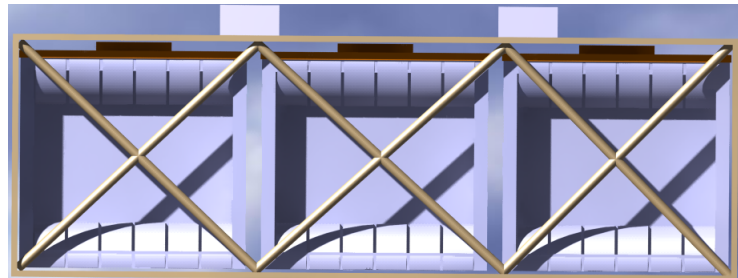


Figure 3.20: Rear Battery Section Truss Structure

The front and rear battery sections have hatch doors significantly bigger than necessary to ease the insertion and removal of the jigs. The estimation of removal and swap time was done by assuming a 10 second cycle time for each jig. The total changeover time for the 99 units was therefore calculated at 990 seconds or 16.5 minutes. This time is less than the 20 minutes, the MR&O requirement.

4 Motor

4.1 Propulsion Overview

This section strictly covers the objectives and requirements that relate to the propulsion team and/or objectives and requirements that are directly motor specific. These objectives and requirements are proposed in the MR&O given by Bombardier. In addition, the overview will

reveal the twin motor setup and demonstrate the basis in which the motors were selected for the FALCO E-1.

Objectives and Requirements

Table 4.1: Table of Objectives and Requirements

Category	MR&O Attribute	Requirement	Objective	Current
Performance	Long Range Cruise Speed (LRC)	110 ktas	120 ktas	120 ktas
	High Speed Cruise Speed (HSC)	125 ktas	135 ktas	135 ktas
Airfield Performance	TOFL @ ISA, MTOW, to 50 ft altitude	1700 ft	1500 ft	1362 ft
	Landing Distance, ISA, MLW, from 50ft	1400 ft	1200 ft	1200 ft
	VR – (take-off speed)	55 KIAS	N/A	55 KIAS

The objectives and requirements dictated the motor choice. The primary motor used is EMRAX 268. The motor when combined with the batteries chosen surpasses all requirements with performance numbers that meet the objectives. Notice, two important requirements not listed above also influenced the motor design and selection. The first being, propulsion installation satisfies the requirement for a quiet cabin. To respect this requirement, EMRAX 268 instead of the more powerful EMRAX 348 was chosen. EMRAX is known for their highly efficient quiet motors. The second is continued safe flight after single failure of any propulsion component. To respect this requirement, a backup engine was proposed. However, the configuration is different than the conventional engine set up. EMRAX 268 is the engine running and in the case of engine failure, an EMRAX 228 will deploy from the tail section. Furthermore, both engines are air cooled and run at low voltage; this set up is explained in detail in the motors section of this report.

4.2 Motor Selection

For a fully electric airplane an electric motor is required. Unlike an internal combustion engine, there is only one moving part and that is the rotor. With only one piece moving, the complexity of the system decreases. Electric motors can demand high torque at low RPM, hence, gearing is no longer required. In addition, the efficiency in electric motors is often much higher than internal combustion engines. EMRAX was selected to provide the electric propulsion for the FALCO E-1. Beforehand, some research was done on the market of electric motors and their type. The market initially has four types of electric motors and they are AC Single Phase, AC Multi Phase, DC Brushed and DC brushless.

Table 4.2 describes two basic kinds of motors, Alternating Current (AC) and Direct Current (DC). Among these two motors are Single-Phase AC motors, which differ from Multi-phase AC motors by the different number of phases associated with the power supply. AC Multi-Phase motors are known to have higher starting torques and have better control of the power than Single-Phase, however, the extra control requires more cost. The DC motor has both brushed and brushless options. Brushed DC motors are simpler to build and do not require a complex control system, however, the brushes wear out over time and can arc. Arcing can lead to an explosion if there are any flammable vapors around and can create interference with electronic components. Without brushes, Brushless DC motors have a longer lifetime. Furthermore, of the

Table 4.2: Pros and Cons of Each Motor

Motor	Pros	Cons
Ac single phase	Good for small HP	Current from batteries is DC, Current does not need to be converted to AC
	AC power easier to change voltage with transformer than DC	Not Generally available for high HP Application
AC Multi Phase	AC power easier to change voltage with transformer than DC	Current from batteries is DC, Current does not need to be converted to AC
	Can get higher HP motors than single phase	Starting current can be high
	More control of power than single phase	Speed control is required AC multi-phase power supply is required
DC Brushed	Current from batteries is DC, Current does not need to be converted to AC	Brushes can wear down and break
	Cheaper and easier to make than brushless	Brushes can arc and cause interference with electronic equipment
	Speed control is simple compared to DC brushless	High maintenance costs DC power more difficult to change voltage than AC
DC Brushless	Current from Batteries is DC, Current does not need to be converted to AC	Costs more than brushed
	No brushes	Requires more complex speed control
	High Efficiency Low Maintenance	DC power more difficult to change voltage than AC

four options both Multi-Phase AC and Brushless DC motors are currently the best options for the automotive industry and the aviation industry. Batteries provide DC therefore to use an AC motor an inverter is required which decreases the efficiency of the overall system. This would suggest that Brushless DC motors might be the better option however the Brushless DC motors require high initial costs and complex control systems.

Table 4.3: Electric Motor Trade Study

Feature	Joby Motor JM Series	Launchpoint Halbach Arrays	Compact Dynamics	EMRAX Electric Motors
Efficiency at 2,800 RPM / %	<90	<90	<90	>95
Technology Readiness Level				
	7	7	8	9
Cost / CAD Dollar	>7000	>7000	>7000	>7000
Maximum Power of Expected Product Line / HP	19	34	65	200
Cooling Options	Air-cooled	Air-cooled	Liquid cooled	Air Cooled/ Liquid Cooled/ Combined Cooling

From table 4.3 , the trade study table and the discussion above, the EMRAX brand was chosen to propel the FALCO E-1. The market seems to favor DC Brushless for their high starting torque and super high efficiency. A high starting torque can be fundamental in ground roll and take off performance parameters. In addition, high efficiency is crucial to conserve battery weight as the team is constricted on the overall payload. Finally, after specifying the type of electric motor and the manufacturer, further selection parameters arise. These parameters include: the size of the engine, the cooling method and the desired voltage regulation method. These parameters are to be discussed in detail after a brief introduction to EMRAX and their motor lines.

About EMRAX

The development of EMRAX electric motors begins in 2005, when Mr. Roman Sušnik made the first electric flight in Slovenia and the third in the world. He developed an electric propulsion system for his glider plane with the most suitable electric motor that was then available on the global market. Still, this motor had many irregularities, which caused a forced landing. This was the reason Mr. Sušnik developed his own electric motor being light weight, powerful, ultimately reliable and having no vibration and no noise. After testing, the results showed that axial flux motors are winners for his application, because of high power and torque at low RPM and light weight. EMRAX now produce the EMRAX motor line, which consists of 5 motor sizes

(diameter 188, 208, 228, 268 and 348 millimeters), and every motor can be made for 3 voltages (high/medium/low) and has a specific cooling option (air/liquid/combined) ("History - EMRAX", 2019). It's important to note, EMRAX is extensively used in electric propulsion vehicles and used commonly in automotive, motorsport, off-road, marine, industrial and aerospace applications. Some Aerospace applications include Alexander Schleicher GmbH glider plane, DG Flugzeugbau GmbH glider plane, Axter Aerospace airplane, Efesto airplane and many more found on their website.

Air Cooled Vs Liquid Cooled Vs Combined Cooling

The cooling method was an important parameter to consider thereafter selecting the engine. One of the most common causes of electric motor failure is a low-resistance insulation failure due to overheating the motor. Overheating the motor can quickly degrade motor life. For example, a common rule of thumb is that for every 10C above the insulation temperature rating motor life is reduced by 50%. Conversely, operating 10C below the insulation temperature rating doubles motor life (Escobar et al, 2017). From the EMRAX data tables in the appendices, the maximum winding and magnet temperature for the EMRAX 228 and 268 is 120C. To properly cool the motor, the EMRAX motors require an airflow of 20 m/s at 25C, or a liquid-coolant flow of 8 L/min at 50C. To ensure that the motor is not over heating, it was chosen that the motor be air cooled. Inlet ducts were designed to ensure that the airspeed inside is much greater than 20m/s and close to the free stream velocity. When the aircraft is on the ground, or at an airspeed significantly less than 20m/s the propeller at idle thrust can generate adequate air inflow for cooling the motor. Three inlets were chosen to both provide the required inflow speed and for ramp appeal purposes shown in Figure 4.1.

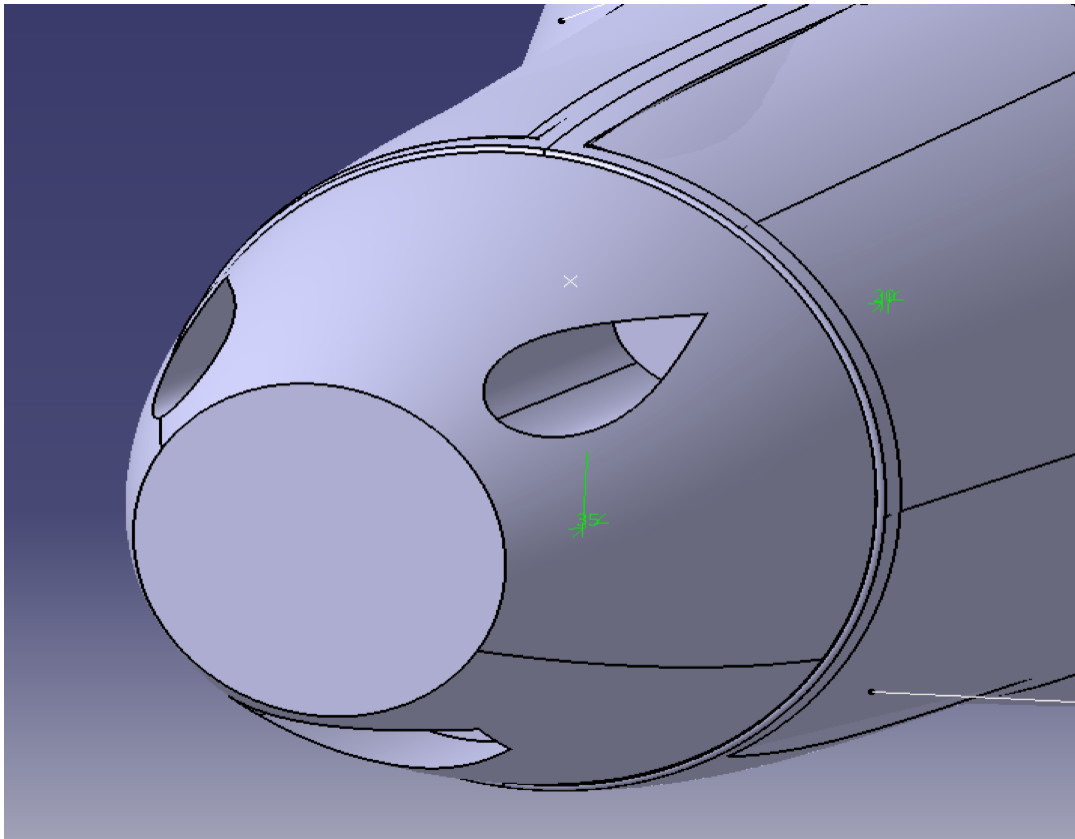


Figure 4.1: Nose Air Intake

Air cooling pros include even temperature distribution, easy maintainability, less design complexity, less operational costs and weight saving when compared to liquid cooling. However, air cooled cons include possibility of shocks at high speeds and the fact that air removes less heat than liquid. Liquid cooling advantages include more even temperature distribution, less hazard of shock when cooling the engine and more efficient in heat absorption than air cooling. On the other hand, liquid cooling disadvantages are added weight, increased operational cost such as flushing and draining fluids,a more complex and high maintainability. Finally, combined cooling facilitates the cooling process even further; combining the advantages and disadvantages of air and liquid cooling techniques.

liquid cooling and or combined cooling maybe the ideal choice. However, owing to high maintainability, high costs and complexity it was chosen that an air-cooled system to be implied. In addition, most single engine propeller set up utilize the air cooling technique, hence, being the more conventional method for engine cooling.

High Vs Medium Vs Low Voltage

Low voltage configuration was chosen because the horsepower required to meet the MR&O is not of large magnitude. Usually a high or medium voltage motor is used when the horsepower required is more than 500 Hp (400 kW). For the case of the FALCO E-1 the chosen motor provides a continues power of 115 kW and a maximum power of 230 kW. Therefore, a low voltage motor is sufficient. It's important to note that the battery set up chosen also effects the choice of

motor voltage. When making the single cell equivalent models and the battery back models, the Thevenin equivalent current will be high. To compensate for a high current drawn from the battery packs, a low voltage motor is selected. Generally, a low voltage motor requires current of at least 4 times higher than the voltage rating. On the other hand, a high voltage rating would require a current at least 4 times less. Therefore, due to the high current delivered from the battery packs and relatively low horsepower rating, a low voltage motor is the ideal choice.

Low Voltage Motor Protection

According to the NEC (National Electrical Code) a motor circuit should follow the schematic in figure 4.2.

1. Motor should employ disconnecting switches to power off supply
2. Short-Circuit protection device to cut the circuit when current regulation is faulty
3. Motor controller
4. motor overload protection

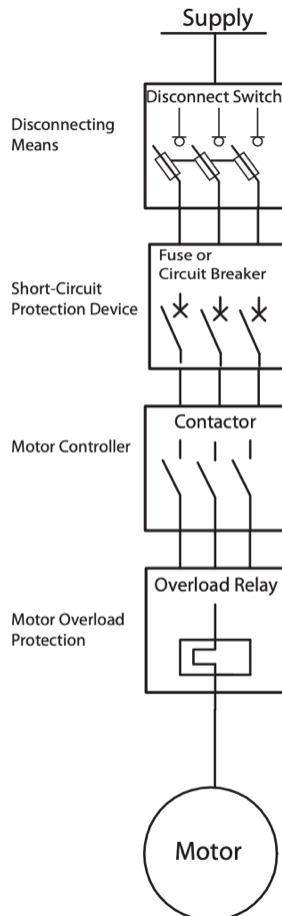


Figure 4.2: NEC Article 430 Motor Branch Circuit Requirements

4.3 Motor Calculation

This section of the report outlines the motors used for the FALCO E-1 and their individual specs. The motors were selected according the specs needs to meet the MR&O and to determine the appropriate specs a MATLAB code was written and provided in the appendices. However, the primary equations are listed below. Since electric airplanes store a specific amount of energy and that energy is based on both power and time, the following can be said.

$$T = \frac{E_T}{P} \quad (4.1)$$

E_T is the total energy stored on board the electric airplane, and P is the power available and V is the velocity where T is the endurance (time).

$$P = DV \quad (4.2)$$

is the basic definition of Power which is defined by the drag (D) of the airplane and the velocity (V). As mentioned above, drag is a function of velocity and can change, just as power can, with different airspeeds. Note, drag values were obtained from the aerodynamics team.

$$D = \frac{1}{2} \rho V^2 S C_D \quad (4.3)$$

$$L = \frac{1}{2} \rho V^2 S C_L \quad (4.4)$$

In cruising level flight, which is the assumption for the derivation of range, the lift (L) can be equated to the weight of the airplane. The range of the electric airplane can now be solved for by rearranging the equations.

$$R_e = \frac{E_T}{\frac{1}{2} \rho V^2 S (C_{DO} + \frac{1}{\pi A e} (\frac{W}{\frac{1}{2} \rho V^2 S})^2)} \quad (4.5)$$

now defines the endurance for an electric airplane. This equation relates the total energy of the airplane to aerodynamic properties and can only be changed based upon the altitude and the velocity. These two variables are the only ones that can be changed in a flight. The other values are all airplane specific and can only be changed if the airplane is changed.

$$R_e = \frac{E_T}{\frac{1}{2} \rho V^3 S (C_{DO} + \frac{1}{\pi A e} (\frac{W}{\frac{1}{2} \rho V^2 S})^2)} \quad (4.6)$$

Using the MATLAB code and the above equations, the EMRAX 268 will generate 2.35 hours of flight time and 276.81 nm at 100% climb and 75% cruise when mounted on the FALCO E-1.

EMRAX268

The motor selected was the best choice to achieve the desired range and endurance. The Emrax 268 has a casing diameter of 268 millimetres, an axial length of 91mm and a dry mass of 19.9 kg.

The front mounting on the motor are 6x M8 threaded holes and the back are 8x M8 threaded holes. The motor can handle up to 130 Vdc. The peak power is at 4500 RPM of 230 kW and continues power of 110 kW. In addition, the motor is run at 98% efficiency which is ideal as battery weight is restricted due to other component weights. The motor provides a peak torque of 500 nm and a continues torque of 250 nm. Finally, figure D.1 in the appendices demonstrates a detailed spec overview of the motor.

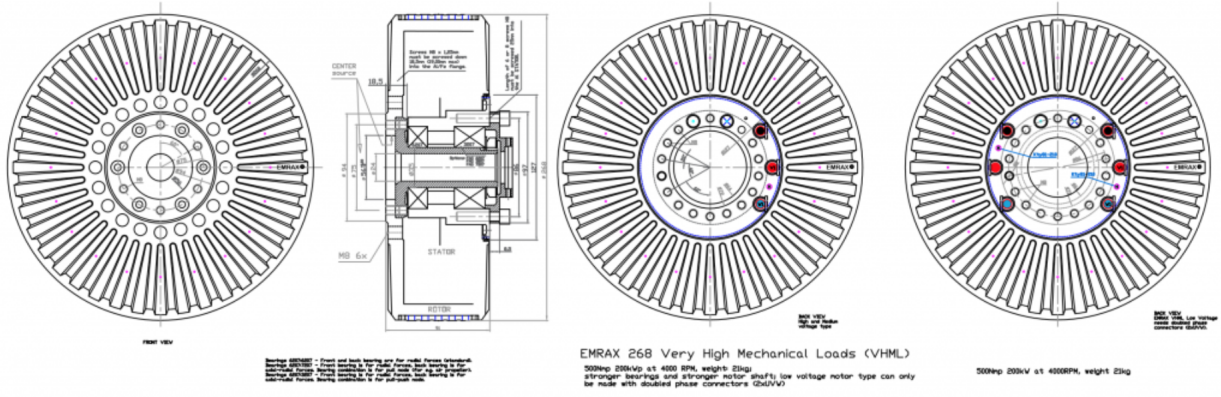


Figure 4.3: EMRAX268 Motor

EMRAX228

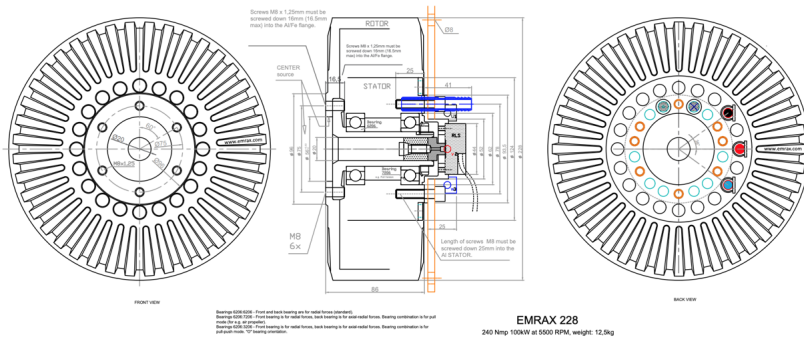


Figure 4.4: EMRAX228 Motor

The 228 was the best choice to achieve and maintain cruise when the primary motor fails. The EMRAX 228 has a casing diameter of 228 millimetres, an axial length of 86 mm and a dry mass of 12.0 kg. The front mounting on the motor are 6x M8 threaded holes and the back are 8x M8 threaded holes. The motor can handle up to 130 Vdc. The peak power is at 5500 RPM of 100 kW and continues power of 55 kW. In addition, the motor is run at 98% efficiency. The motor provides a peak torque of 230 nm and a continues torque of 120 nm. Finally, figure D.2 in the appendices demonstrates a detailed spec overview of the motor.

Motor Layout and Placement

The motor placement for the primary 268 or engine 1 is at the nose as per conventional single

engine aircraft. The motor lays behind the intakes and propeller. The motor is supported on an aluminum plate mounted on the caging structure for the batteries. The aluminum plate facilitates the mounting process to the cage whilst reducing vibration as well; this set up is demonstrated in Figure 4.3.

The 228 or engine 2 is placed in on the same shaft as the main one. This engine does not operate unless in the unlikely event of engine 1 failing and is engaged via switch in the cockpit and a clutch to drive the shaft. The design is as follows:

1. The motor is disengaged during normal flight, the main motor's clutch holds the prop shaft and spins it
2. If the main motor fails, the aircraft system detects main motor failure and disengages the main clutch
3. The power supply goes to the secondary motor and its clutch engages which powers the prop
4. The aircraft remains in powered flight albeit with less power

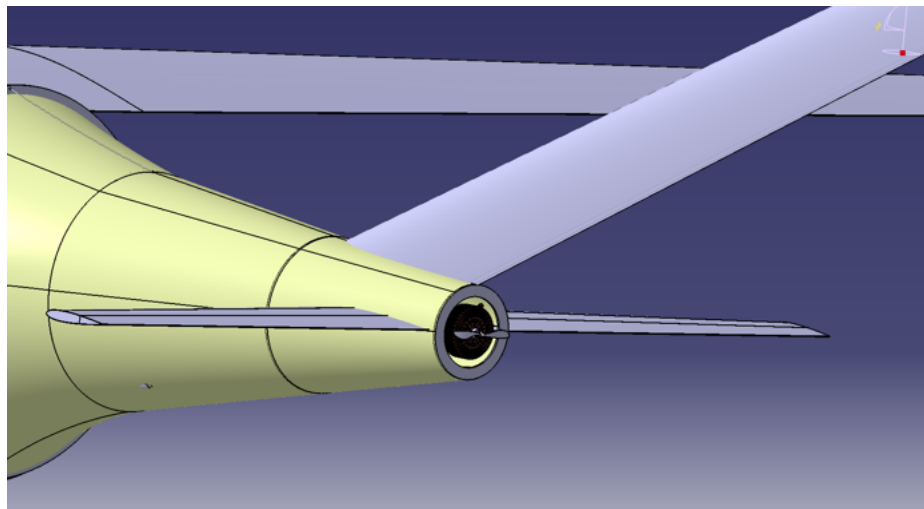


Figure 4.5: EMRAX268 & 228 Motor Placement in Nose

4.4 ENGINE FAILURE PROCEDURE

This section outlines Engine Failure Procedure during different flight conditions

Engine Failure During Take Off Role

1. Idle Engine 1
2. Shut OFF Engine 1
3. Retract Flaps
4. Apply Breaks
5. Master Switch OFF

Engine Failure Immediately After Take OFF

1. Idle Engine 1
2. Shut OFF Engine 1
3. Start Engine 2
4. Thrust 100%

Engine Failure During Flight

1. Idle Engine 1
2. Start Engine 2
3. Thrust 90%
4. Cruise Thrust 75%

5 Propeller Design Criteria and Initial Consideration

For the propeller selection of the FALCO E-1, many possible objectives could have been accounted for due to the variability in propeller design and performance. It was determined that the major decision factors that most accurately aligned with the overall aircraft objectives were: certification, weight, cost, efficiency, and safety to rank these factors, a pairwise comparison matrix was created to determine the respective importance where each factor was considered over the others and rank them by score. The factors with the highest score are considered most important.

From the ranking result above, it is evident that the certification ability for the propellers on the FALCO E-1 is considered as the most important factor on the decision-making process. Weight and efficiency are the second and third important factors because this is a small aircraft with maximum capacity of four passengers, the weight of propeller needs to be minimized. The factor of safety and cost of the propeller would be considered as less important as weight and efficiency.

	Certification	Weight	Cost	Efficiency	Safety
Certification	x	0	0	0	0
Weight	1	x	0	1	0
Cost	1	1	x	1	0
Efficiency	1	0	0	x	1
Noise	1	1	1	0	x
Score	4	2	1	2	1
Weight	40%	20%	10%	20%	10%
Rank	1	2	5	3	4

There are two types of aircraft propeller for option, fixed pitch propeller and constant speed/ variable pitch propeller. A fixed pitch propeller has one single pitch for its blades regardless of operation condition, it is usually designed for best efficiency at either climb or cruise. In general, the constant speed/ variable pitch propeller is the propeller that can change its pitch to a desired RPM at any kind of flight condition to maintain a high efficiency. The following tables which illustrate the advantages and disadvantages for each type of propeller will be analyzed to determine the best option for FALCO E-1.

Table 5.1: Fix Pitch Propeller [20]

Advantages	Disadvantages
Inexpensive	Lack of efficiency outside of its design operation conditions
Light weight	Windmill in the case of engine failure
Simple configuration	
Little maintenance	
Failsafe	

Table 5.2: Variable/Constant Pitch Propeller [20]

Advantages	Disadvantages
High efficiency for all flight condition	Complex configuration
Maintain constant RPM	More cost
	Heavy weight

By comparing table 5.1 and 5.2 above and according to the pairwise comparison table presented earlier, the factors of weight and cost had a higher rank than efficiency. As the result, fixed pitch propeller were the best option for the operational objectives set for FALCO E-1.

5.1 Propeller Material Selection

Wood, aluminum, and composite material are the three types of material generally used in propeller manufacturing today. Propellers made of wood were used on practically all airplanes in the early days of aviation. They were fairly satisfactory in most respects because the airplane

engines were not powerful enough to compare with the modern engines today [21]. As a light weight metal, aluminum has long been the metal of choice for creating airplane propellers. After World War II, by integrating the propeller with new aluminum alloys, aluminum propellers became common enough on aircraft to put into large scale production, led to big changes in overall aircraft efficiency and performance [49]. With the development of composite material industry today, structural composite aircraft propellers have grown popular in aviation. An increasing number of aircraft manufacturers select composite propeller as standard equipment on their airplanes. While the latest composite materials have excellent mechanical properties, wood and metal propellers still continue to be widely designed and produced. Propellers for RC aircraft are often manufactured from wood and composites as with manned aircraft, but also from reinforced plastics due to their low cost and weight and high strength.

The tables below analyzed the advantage and disadvantage properties of each material and the material for FALCO E-1 would be determined according to the decision matrix.

Advantages	Disadvantages
Light weight	Easily nicked and scraped
Low cost	Protective sheathing sometimes comes loose
Very low possibility of failure due to fatigue	Lamination may separate under tropical condition
Easy to manufacture	Decay fast
Damps the engine vibration better than metal propeller	Seldom be repaired satisfactorily when damaged
High strength in compression and tension	Low resistance of wood to splitting due to torsional load

Figure 5.1: Wood Propeller Analysis

Although wood propeller has many advantages as it is light weight and resistance to fatigue is due to its high internal friction, or hysteresis; the blade erosion has been shown to be a major problem on some aircrafts, wood propeller can be broken by rainstorm in minutes [50]. However, the low durability of wood propeller increases the maintenance cost and operational risk, so more metals were used instead of wood propellers operating in severe environment.

Metal (Aluminum) propeller is applied widely in aircraft industry today; it has less minimum thickness than wood propeller which increases the overall propeller efficiency. However, compare to wood and composite material propeller, metal propeller is much heavier and it is more susceptible by fatigue failure.

Composite propellers are typically seen as a recent advancement in aviation. Unlike aluminum

Advantages	Disadvantages
More efficient than a comparable wood propeller due to a thinner airfoil design	Heavier than wood and composite material propeller
A certified propeller shop can change the pitch of a metal propeller	More susceptible by fatigue failure as a result of nicks or cracks in the blade caused by strike damage
Metal propeller can be overhauled if bended	Will be damaged internally by vibration produced by engine
Metal propeller more durable than wood	

Figure 5.2: Aluminum Propeller Analysis

Table 5.3: Composite Propeller Analysis [21]

Advantages	Disadvantages
Light weight	High cost
Easy to repair	Delamination
Eco friendly as reduce noise and vibration	Composite to metal joining
High strength	

blades, which must be filed down to repair nicks and dings, composite propellers can often be repaired and returned to service without adversely affecting the airfoil shape. This repair allowance gives composite propellers a very long blade life, helping owners save money in the long run. The structure of the composite propeller consists of carbon fiber laminates integrated into a co-molded stainless steel shank. The leading edge is protected with a co-molded electroformed nickel-cobalt erosion shield for greater endurance [51]. Composite blades eliminate the shape constraints imposed by wood or metal, resulting in thinner and more efficient propellers and allow greater aerodynamic performance, also it offer unique advantages in terms of reduced weight and vibration, performance, and blade life [50].

According to the propeller selection criteria, composite material and wood propeller have lighter weight than metal propeller. Compare to cost, composite propeller has a high initial cost but very low maintenance cost, metal and wood propellers have low initial cost but relatively high maintenance cost, and low durability. In terms of efficiency and safety, composite material and metal propellers have higher efficiency than wood propeller, also have higher durability than wood propeller under severe flight condition which increase the level of safety. Overall, the composite propeller is the best option here for FALCO E-1.

5.2 Propeller Blade Sizing

The total number of blades is another significant factor to consider in propeller selection. Typically, the propeller with the highest efficiency was the one with simply two blades, because it had less requirement from the motor to overcome the additional drag from the extra blades [20]. In order to generate the same thrust, the propeller with two blades must be substantially larger than the multiple blades propeller. To determine of which propeller to use, a preliminary diameter sizing can be estimated by the following equation to determine if the propeller is a viable option [20].

$$D = K_p * \sqrt[4]{P_{k_w}} \quad (5.1)$$

Where D is the diameter of the propeller in meters, P_{k_w} is the engine shaft power in kilowatts and K_p is obtained from the table below [20]:

Table 5.4: Factor K_p for Typical Propeller Types[20]

Type of Propeller	K_p for P in kw and D in m
Two-bladed	0.56
Three-bladed	0.52
Four or more blades	0.49

The values used for power was the continuous power of 40 kw at 2000 rpm as a minimum, and the peak power of the motor of 220 kw at 4500 rpm as a maximum. The following table listed the diameter ranges from two-bladed propeller to multi-bladed propeller.

Table 5.5: Propeller Initial Sizing

Propeller Types	Minimum Diameter (m)	Maximum Diameter (m)
Two bladed	1.41	2.15
Three bladed	1.31	2.00
Four or more bladed	1.23	1.88

Since the propeller was determined to be made by composite material, more propeller blade could increase the cost of propeller. In addition, the diameter of each type of propeller do not have significant difference, more propeller blades would increase the total weight of the propeller. According to the propeller selection matrix two-bladed propeller was decided with the diameter range between 1.41m to 2.15m, since the design criteria required less weight, lower cost and higher propeller efficiency.

5.3 Contra Rotating Propeller Propulsive System

According to the research by CONTRA ELECTRIC PROPULSION LTD. there were 85% of the world's 410,000 civil fixed wing aircraft are propeller driven, 99.99% of these aircraft are driven by combustion engines and 99.99% of these aircraft have one propeller per engine [16]. By

using contra rotating propeller system, a hugely improved performance can be achieved over a single fixed pitch propeller using the same total power. It was unusual to install a contra rotating propeller in light aircraft due to the high cost and complexity of constructing contra rotating systems using combustion engines. However, using electric motors such as EMRAX 268, enables the use of fixed pitch propellers and the building of a simple, inexpensive contra rotating propulsion systems suitable for general light aircrafts [16].

The advantages of choosing contra rotating propeller were listed as the following [16]:

- Two contra rotating 2-bladed propellers can generate a given thrust by using less power than a single 4-bladed propeller of the same size.
- It could have smaller overall propeller disc diameter than a single 4-bladed propeller of the same power.
- It can generate reverse thrust greatly expanding aircraft operability.
- It can instantly respond with the throttle changing.
- The elimination of propeller torque forces at take-off and during power changes.
- Greater acceleration and shorter take-off distance.
- A 15 to 20 percent increase in propulsive efficiency and higher top speed

The final selected product for the main propeller was the contra rotating propeller from CONTRA ELECTRIC PROPULSION LTD. This is a certified company which professionally design and produce contra rotating propeller for light aircraft. In addition, it was able to use simple and extremely robust fixed pitch propellers with the ability to provide thrust reversal in light aircraft whilst exceeding variable pitch propeller efficiency, and maintain the advantages of low cost and maintenance free operation.



Figure 5.3: Contra Rotating Propeller [16]

The Figure 5.3 was the contra rotating propeller product from CONTRA ELECTRIC PROPULSION LTD. The front propeller is a fixed pitch pull propeller with the diameter of 178 cm, and the rear propeller is a fixed pitch propeller with the diameter of 170 cm [16]. The speed range of

both propeller were 0-2800 rpm. The reason of this design was due to the disadvantage of noise produced by contra rotating propeller in operation, if the rear propeller had fewer blades or a smaller diameter than the front prop, the tip speed and the loading of the blades can be reduced [52].

In terms of aircraft stability, the contra rotating propeller can balance the torque produced by each propeller, so it has no aircraft yaw during power changes, significantly improving safety [16]. The following diagrams were the torque reaction for contra rotating propeller provided by CONTRA ELECTRIC PROPULSION LTD. where the blue points represent the thrust, and the orange points represent the torque. It was obvious that the net torque produced by the contra rotating propeller was zero to the aircraft.

Front Propeller CCW Torque Reaction



Rear propeller CW Torque Reaction



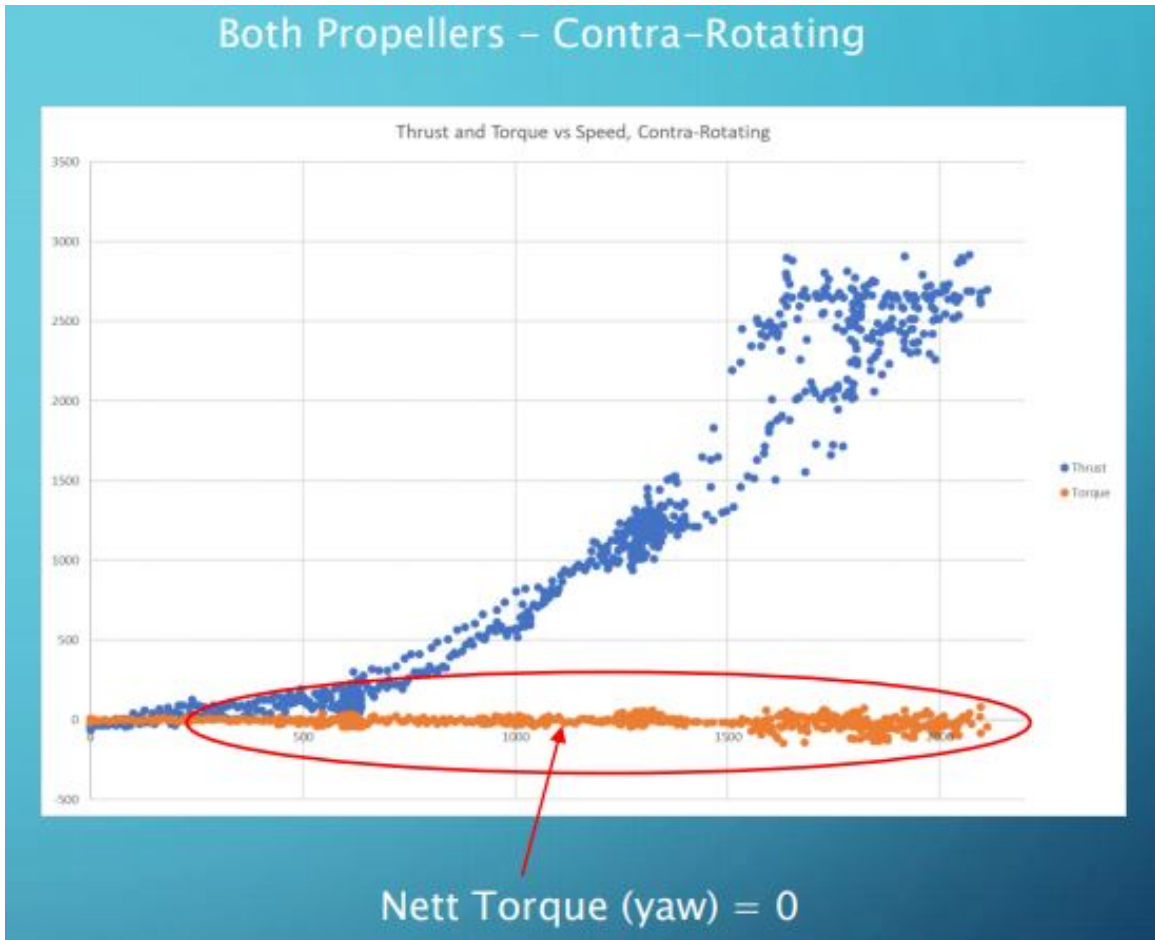


Figure 5.4: Torque, Thrust VS. Speed [16]

CATIA Modelling

The picture shown below was the CATIA model built to illustrate the contra rotating propeller mechanism. The yellow cylinder which connect the two propellers is the contra rotating shaft, it makes the front propeller rotating in opposite direction as the rear propeller roatating. The propeller spinner in front of the front propeller is designed streamlined fitted over the propeller hub to reduce the aerodynamic drag and smooth the airflow so that the air intakes can be flowed more efficiently.

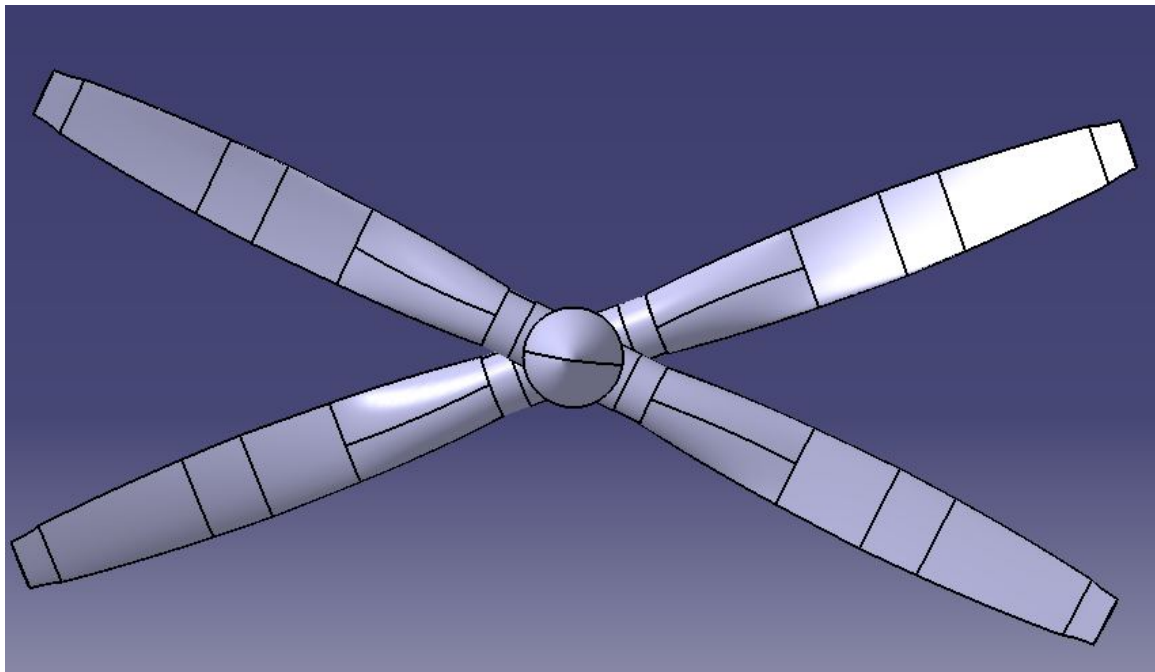


Figure 5.5: Contra Rotating Propeller CAD (Front view)

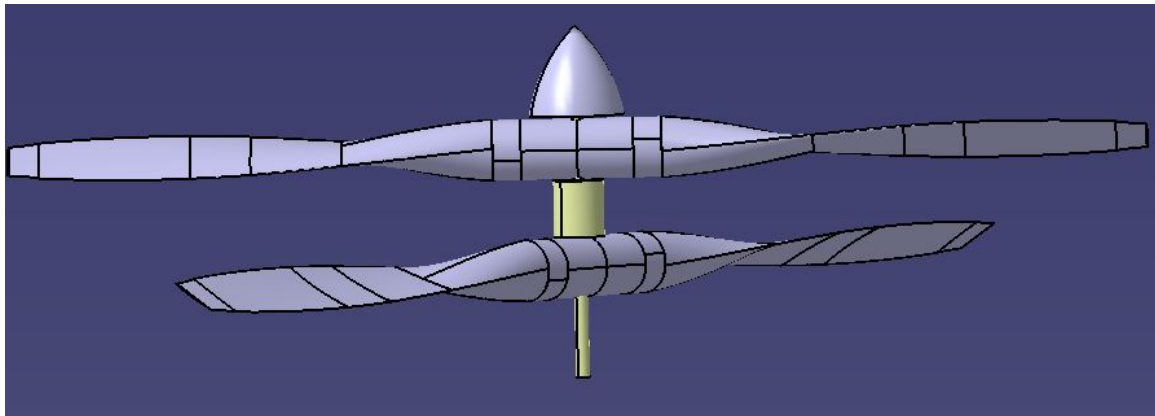


Figure 5.6: Contra Rotating Propeller CAD (Top view)

5.4 Propeller Noise Estimation

Noise associated with the operation of aircraft remains a topic of hotly contested debate in society. In recent years, with the new regulatory policies and increased research effort came out, the noise pollution produced by aircraft propeller had been reduced. It is best to work with a propeller manufacturer and use their expertise to design and select propellers that are both quiet and efficient.

The tip mach number at takeoff was the time that the propeller will be spinning fastest and loudest. This quantifies the public interest factor for each propeller. The following equation was

used [20]

$$M_t = \frac{RPM * D * \pi}{60 * a} \quad (5.2)$$

Where ' M_t ' denotes tip mach number, 'RPM' is maximum revolutions per minute and 'a' is the speed of sound at sea level.

The front propeller on the contra rotating propeller had a diameter of 1.78 meters and was expected to reach $M=0.7586$, also the rear propeller which had a diameter of 1.7 meters was expected to reach $M=0.7245$, if both propellers rotating at its max power of 2800 rpm.

Part VI

Book VI: Stability & Control Analysis

1 Theory

1.1 Center of Gravity

The static center of gravity and dynamic center of gravity varied due to the the loading conditions and different weight configurations. The neutral point(NP) is where the coefficient of moment about the aerodynamic center is equal to 0. The static margin is the difference between the center of gravity position and neutral point can be calculated using:

$$K_n = h_n - h \quad (1.1)$$

where the CG must be forward of the neutral point and the greater the static margin the more stable the aircraft becomes.[53]

1.2 Static Stability

To have static longitudinal stability

$$C_{m\alpha} = \frac{\delta C_m}{\delta \alpha} = \frac{\delta C_m}{\delta C_l} \frac{\delta C_l}{\delta \alpha} < 0 \quad (1.2)$$

For a wing design to be statically stable, the aerodynamic center must be behind the center of gravity in order to make the previous statement true. For longitudinal equilibrium, the coefficient of moment, alpha must be less than 0 and have a positive trim angle. An increase in the banking angle will demonstrate a positive yawing torque creating ore static stability as well. In general, the best way to increase static stability is to add a dihedral, a high wing configuration and/or swept wing.[53]

1.3 Wing Contribution

The center of gravity is typically located aft. of the aerodynamic center therefore the wing must have a positive camber. With a negative camber flight is only possible at $\alpha > 0$ and $C_l > 0$ With a zero camber, the flight possible only at $\alpha = 0$ and $C_l = 0$. Therefore our aircraft was design with a positive camber of 3.5 at 43.41% of chord. With the positive cambered wing, the tail was designed with a negative coefficient of lift.[53]

1.4 Tail Contribution

The tail is usually placed behind the wing and is normally a symmetric airfoil with a negative coefficient of lift with a positive camber. The tail itself produces a lift and drag of its own and must be taken into consideration when calculating the aerodynamics of the entire aircraft. To calculate the lift and coefficient of lift on the tail:

$$L_t = \frac{C_{Lt} q_t S_t}{qS} \quad (1.3)$$

$$C_L = \frac{S_t}{S} \eta C_{Lt} \quad (1.4)$$

The moment of the tail about the mean aerodynamic center of the wing-body.

$$C_{mt} = -V_H C_{Lt} t \quad (1.5)$$

and the moment about the CG is

$$C_{mt} = -V_H \eta C_{Lt} = -V_H \eta C_{Lt} + \frac{S_t}{S} (h - h_{nwb} \eta C_{Lt}) \quad (1.6)$$

1.5 Steps for designing the horizontal tail

The first step in designing the tail geometry is to pick an optimized boom length (the distance between the wing aerodynamic center and the tail aerodynamic center). A boom length that was going to be used for the design project was used as an initial value. An optimum boom length of approximately 7.8 meters (m) was calculated (but that was deemed to be too long), using the equation:

$$l = K_c \sqrt{\frac{4\bar{C}SV_H}{\pi D_f}} \quad (1.7)$$

K_c is the correction factor for the type of aircraft that is being designed, \bar{C} is the mean aerodynamic chord (MAC), S is the wing area and D_f is the max fuselage diameter.

The correction factor varies between 1 and 1.4 depending on the aircraft configuration. $K_c = 1$ when the aft portion of the fuselage has a conical shape, as the shape of the aft portion of the fuselage goes further away from a conical shape, the correction factor is increased up to 1.4. Typically, a single seat single engine prop driven GA aircraft has a correction factor of 1.1, but for a transport aircraft K_c will be 1.4. For the design aircraft, a correction factor of 1.4 was used.

Using a max fuselage diameter of 1.7 m, the optimum fuselage diameter was found too long for our aircraft. Instead of starting with an optimum boom length, a boom length of 4.2875 m was used. Using this boom length.

The practical design steps taken was:

1. Selected the tail configuration
2. Selected the tail location
3. Selected the initial horizontal tail volume coefficient
4. Instead of calculating an optimum tail arm, a specific tail arm was given
5. Calculated the horizontal tail planform area
6. Calculated the wing-fuselage aerodynamic pitching moment coefficient
7. Calculated the cruise lift coefficient
8. Calculated the horizontal tail desired lift coefficient at cruise from trim equation
9. Selected the horizontal tail airfoil
10. Selected the horizontal tail sweep angle and dihedral
11. Selected the horizontal tail aspect ratio and taper ratio
12. Determined the horizontal tail lift curve slope
13. Calculated the horizontal tail angle of attack at cruise
14. Determined the downwash angle at the tail
15. Calculated the horizontal tail incidence angle
16. Calculated the tail span, tail root chord, tail tip chord and tail mean aerodynamic chord simultaneously
17. Calculated the horizontal tail generated lift coefficient at cruise using the given lifting line theory code
18. Iterated the tail incidence to make the tail generated lift coefficient equal to the required lift coefficient
19. Checked the tail incidence angle to make sure the tail does not meet stall
20. Calculated the horizontal tail contribution to the static longitudinal stability derivative ($C_{m\alpha}$)

The tail configuration was decided to be a conventional aft tail. Conventional being horizontal stabilizer fixed on the aft of the aircraft and the vertical fin to be fixed on the middle, aft of the aircraft. Initially, a horizontal tail volume coefficient of 0.3 (the lowest in the range of acceptable volume coefficient) was used, but that resulted in a slightly unreasonable horizontal tail. It resulted in a higher $C_{m\alpha}$ values (closer to 0), thus making the aircraft less statically longitudinally stable, with a horizontal tail span of 2.9 m (typical small for the design aircraft size). The volume ratio was iterated and it was decided a higher range of acceptable volume coefficient of 0.6 would be applicable. This added weight, but it also increased the longitudinal stability of the aircraft. For added trim and a decrease to the pilot's fatigue, a single tab is installed on the right horizontal tail if the propeller is rotating clockwise from the pilot's view. This counteracts the yaw and roll created by the propeller during takeoff and climb (increasing propeller power).

The tail moment arm was no optimzied, but a specific length of 4.2875m was given. An increase in length results in a decrease in total tail area. The length is inversely proportional to the tail area. This makes sense since a longer moment arm resulted in a lower force needed to create a required moment. All calculations where made using MATLAB.

Using the volume coefficient equation, the tail planform area was found:

$$S_h = \frac{\bar{C}SV_H}{l} \quad (1.8)$$

The aircraft cruise lift coefficient was found using:

$$C_L = \frac{2W}{\rho V_c^2 c S} \quad (1.9)$$

Where:

W is the average weight of the aircraft, ρ is the air density at cruise and V_c is the cruise velocity.

$$C_{mowf} = C_{maf} \frac{AR \cos^2(\Lambda)}{AR + 2\cos(\Lambda)} + 0.01\alpha_t \quad (1.10)$$

Where:

C_{maf} is the moment lift curve slope of the fuselage, AR is the aspect ratio of the wing, α_t is the angle of attack of the horizontal tail and Λ is the tail sweep angle.

Fuselage length was also decided based on cabin and power supply size. A length of 4m was given.

X_{cg} was found using the equation:

$$X_{cg} = 0.25MAC - h_o \quad (1.11)$$

Where MAC is the mean aerodynamic chord, $h(o)$ is the cg location X meters ahead of wing aerodynamic center.

$$h = \frac{X_{cg}}{MAC} \quad (1.12)$$

Using the h and cg locations, The horizontal tail required lift coefficient at cruise by using the trim equation was found:

$$C_{Lh} = \frac{C_{mowf} + C_L(h - h_o)}{\bar{V}_H} \quad (1.13)$$

Using a standard NACA 0009 airfoil, the airfoil's aerodynamic characteristics was found. Both the NACA 0009 and the NACA 0012 airfoil where used, both airfoils gave similar results but the NACA 0009 had lower drag coefficient.

An initial tail aspect ratio of 66% of the wing aspect ratio was used to act as a starting point. The Cessna has a horizontal tail of 53% of wing aspect ratio.

$$AR_h = \frac{2}{3} AR_w \quad (1.14)$$

Typically, the horizontal tail taper ratio of a low speed subsonic aircraft is equal to the wing's taper ratio. The horizontal tail has no sweep nor dihedral angle, it is a linearly tapered tail.

For the next step, the tail incidence angle needed to produce the same calculated tail lift coefficient, C_{Lh} . Tail downwash is also needed to calculate the tail incidence angle, but the tail lift curve slope was needed:

$$C_{L\alpha} = \frac{C_{La}h}{1 + \frac{C_{La}h}{\pi AR_h}} 3.9$$

The initial tail angle of attack using the equation below was found, but it was not the final angle because an iteration using the lifting line theory code given by literature (Code in Appendix A) to find the correct angle of attack was needed.

$$\alpha_{Lah} = \frac{C_{Lh}}{C_{L\alpha}h} \quad (1.15)$$

Considering downwash:

$$E_o = \frac{2C_{Lw}}{\pi AR} \quad (1.16)$$

$$\frac{\partial E}{\partial \alpha} = E_\alpha = \frac{2C_{La}w}{\pi AR} \quad (1.17)$$

Then:

$$E = E_o + E_\alpha \alpha_w \quad (1.18)$$

Using the above equations, The tail setting angle was found:

$$i_h = \alpha_h - \alpha_f + E \quad (1.19)$$

Solving the following four equations simultaneously produced the 4 major tail geometries: span, root chord, mean aerodynamic chord and tip chord, b_h , C_{hroot} , \bar{C}_h , C_{htip} respectively.

$$AR_h = \frac{b_h}{\bar{C}_h} \quad (1.20)$$

$$\lambda_h = \frac{C_{htip}}{C_{hroot}} \quad (1.21)$$

$$\bar{C}_h = \frac{2}{3} C_{hroot} \left(\frac{1 + \lambda_h + \lambda_h^2}{1 + \lambda_h} \right) \quad (1.22)$$

$$S_h = b_h \bar{C}_h \quad (1.23)$$

Finally, The geometry of the tail was verified using the static longitudinal equation. The design project has a fixed tail, so the longitudinal stability derivative equation used is:

$$C_{m\alpha} = C_{La}w f(h - h_o) - C_{La}h \eta_h \frac{S_h}{S} \left(\frac{l}{\bar{C}} - h \right) (1 - E_\alpha) \quad (1.24)$$

When the result of the derivative equation is negative, that means the aircraft is statically longitudinally stable.

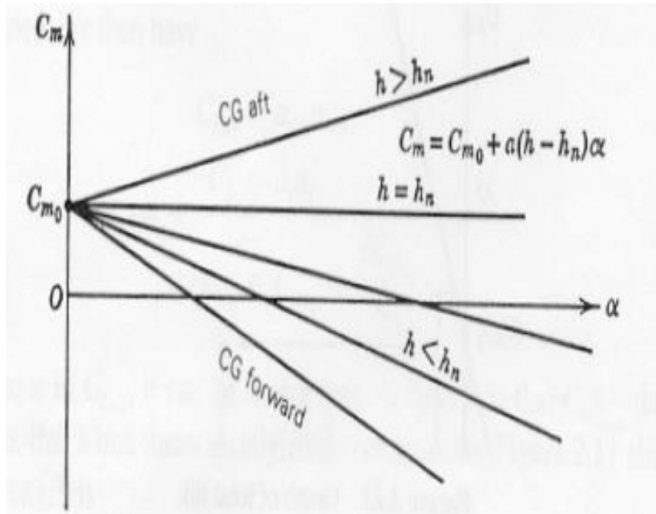


Figure 1.1: $C_m \alpha$ Graph

Stability heavily relies on the CG location of an aircraft. Based on Figure 7, moving the CG forward, also results in a negative $C_m \alpha$ value, thus giving us a more stable aircraft.

1.6 Steps for designing the vertical tail

The main role of the vertical tail is to promote yaw damping which is the tendency of yaw oscillations of aircraft. If the yaw dampening is sufficient then the yaw stability is usually acceptable. The vertical tail volume range was determined to be 0.02-0.05[54]. If the coefficient is too small the aircraft will tend to oscillate and falter as the pilot inputs rudder and aileron control. The oscillation is called Dutch Roll and makes directional control difficult, given the poor rudder roll authority. The acceptable sizing of the tail was determined in a iterative process where the wing area was fixed and an acceptable range was given to compare the area. The final vertical tail volume was determined to be 0.035. This was deemed as plausible as it is in the accepted range and the Cessna's tail volume is 0.0411[55].The wing-tail area ratio was determined to be 0.09096 and this falls within the set range that was determined in the preliminary stage of 0.08-0.107.

The vertical tail is almost designed independently from the horizontal tail, except the spin recovery due to vertical tail location relative to the horizontal tail. The horizontal tail produces a wake region that affects the vertical tail effectiveness thus it is imperative to check the wake region of the horizontal tail.

1. First step in vertical tail design is selecting vertical tail configuration
2. Selecting the initial vertical tail Volume coefficient based on the acceptable range that is in literature.
3. Initially assumed the vertical tail moment arm is equal to the horizontal tail moment arm
4. Calculating the vertical tail planform area using the volume coefficient equation

5. Selecting the airfoil section, but for our project a standard NACA 0009 or 0012 is appropriate
6. Assumed the initial aspect ratio to be initially 20% of the wing aspect ratio
7. Assumed the initial taper ratio to be 1 (no taper)
8. Determining the vertical tail incidence angle
9. Determining the vertical tail sweep angle
10. Determining the vertical tail dihedral angle
11. Finally, for the vertical tail geometry, determine the 4 major geometrical values, span, root chord, tip chord and mean aerodynamic chord.
12. Adjust the location of the vertical tail relative to the horizontal tail by changing the l_v to avoid the horizontal tail wake region and increase the vertical tail effectiveness for spin recovery
13. Calculated the directional stability derivative and made sure its positive for a stable aircraft

For the design project, a configuration of one aft vertical tail was used, which makes the total tail configuration a conventional configuration. A vertical tail volume coefficient of 0.03 (lowest range of acceptable volume coefficient based on literature) was initially used. In the iteration section in results, I will be increasing the volume coefficient.

The vertical tail was assumed to be located at the same location as the horizontal tail, l_h . The vertical tail location was not shifted because the vertical tail is larger than the horizontal tail chordwise, hence, it is not completely submerged in the wake region.

The vertical planform area is calculated based on the volume coefficient equation:

$$S_v = \frac{\bar{C}SV}{l_v} \quad (1.25)$$

The NACA 0012 for the vertical tail was initially chosen but due to the slight difference between the NACA 0009 and NACA 0012, The NACA 0009 was used instead due its lower drag production.

An aspect ratio was chosen to be approximately 20% of the wing aspect ratio, The initial aspect ratio was 20% because the Cessna 172 has a vertical tail aspect ratio of 18.9%. An initial taper ratio of 1 (no taper), an initial sweep of 20 degrees, an initial dihedral of 0 degrees (because our tail is not a V tail) and an incidence angle of 1.5 degrees counter-clockwise (viewing the aircraft from the top where the nose is pointing up) were used. The incidence angle is needed to counter act the yawing moment created by the single propeller engine (during takeoff and climb), if the propeller is rotating clockwise from the pilot's view.

Finally, the 4 major geometries, span, root chord, tip chord and mean aerodynamic chord were found by solving the 4 equations simultaneously.

$$AR_v = \frac{b_v}{\bar{C}_v} \quad (1.26)$$

$$\lambda_v = \frac{C_{vtip}}{C_{vroot}} \quad (1.27)$$

$$\bar{C}_v = \frac{2}{3} C_{vroot} \left(\frac{1 + \lambda_v + \lambda_v^2}{1 + \lambda_v} \right) \quad (1.28)$$

$$S_v = b_v \bar{C}_v \quad (1.29)$$

For calculating the directional stability derivative, the following equation was used. The result needs to be a positive number for a directionally stable aircraft.

$$C_{n\beta} = K_{fl} C_{L\alpha v} \left(1 - \frac{\delta\sigma}{\delta\beta} \right) \eta_v V_V \quad (1.30)$$

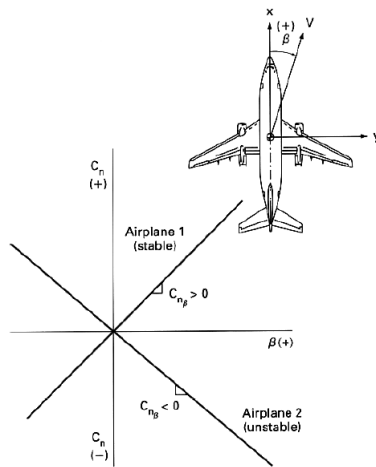


Figure 1.2: $Cn\beta$ stability graph showing a positive value as stable

1.7 Other Considerations

Through more research, the following characteristics were determined for the sweep, taper and composure of the tails.

Table 1.1: Ranges of Lateral Stability for Tails

Tail Characteristic	Range for Subsonic Aircraft
Aspect Ratio for Horizontal Tail	3-5
Taper Ratio for Horizontal Tail	0.3-0.5
Sweep for Horizontal Tail	<10 degrees
Aspect Ratio for Vertical Tail	1-2
Taper Ratio for Vertical Tail	0.6-1
Sweep for Vertical Tail	<20 degrees

1.8 Dynamic Stability

Dynamic stability is used to find natural frequency, damping frequency, and damping ratio. There are two modes that must be analyzed for the entire aircraft: phugoid and short period. To determine these modes, the stability derivative, forces, moments and coefficients must be calculated. Due to the limits of the project, the derivatives must be taken from external programs such as AVL and XFLR, where parameters such as velocity, angles etc can be inputted to determine such values. The following formulas are what the programs used to simulate and calculate the derivatives, forces and moments:

$$X_u = \frac{QSC_{x_u}}{mu_o} \quad (1.31)$$

$$X_w = \frac{-(C_{D\alpha} - C_{L_0})QS}{mu_o} \quad (1.32)$$

$$Z_u = \frac{-(C_{L_u} + 2C_{L_0})QS}{mu_o} \quad (1.33)$$

$$Z_w = \frac{C_{z_\alpha} QS}{mu_o} \quad (1.34)$$

$$Z_{\dot{w}} = \frac{C_{z_\alpha} \bar{c} QS}{2mu_o^2} \quad (1.35)$$

$$Z_\alpha = u_o Z_w \quad (1.36)$$

$$Z_{\dot{\alpha}} = u_o Z_{\dot{w}} \quad (1.37)$$

$$Z_q = \frac{C_{z_q} \bar{c} QS}{2mu_o} \quad (1.38)$$

$$Z_{\delta_e} = \frac{C_{z_{\delta_e}} QS}{m} \quad (1.39)$$

$$M_u = \frac{C_{m_u} QS \bar{c}}{u_o I_y} \quad (1.40)$$

$$M_w = \frac{C_{m_\alpha} QS \bar{c}}{u_o I_y} \quad (1.41)$$

$$M_{\dot{w}} = \frac{C_{m_\alpha} QS \bar{c}^2}{2u_o^2 I_y} \quad (1.42)$$

$$M_\alpha = u_o M_w \quad (1.43)$$

$$M_{\dot{\alpha}} = u_o M_{\dot{w}} \quad (1.44)$$

$$M_q = \frac{C_{m_q} QS \bar{c}^2}{2u_o I_y} \quad (1.45)$$

$$M_{\delta_e} = \frac{C_{m_{\delta_e}} QS \bar{c}}{I_y} \quad (1.46)$$

2 Results and Discussion

2.1 Center of Gravity

Using the equation and theory in the previous sections, the following weight and balance scenarios were conducted. Based on the criticism from the preliminary presentation, the aircraft was analyzed on more than one passenger configuration. In the preliminary analysis, four passengers with baggage and a full configuration of batteries was done. However, we were told to analyze different configurations such as one person (pilot), two people, three people and four people. As per the MR&O, the maximum empty weight depends on the payload to be carried, with the maximum of 1750 without 4 passengers. The empty weight increases to 2050 with a reduced payload of 500 lbs. therefore leaving more weight allocation for batteries.

Working with my battery/ propulsion colleague, the weight balance was conducted again and the tables below show the 6 scenarios for weight balance. Configuration 1 shows one passenger (the pilot) with the extra battery allocation. Configuration 2 shows two passengers in the front seat with the extra battery allocation. Configuration 3 shows three passengers (one pilot in the front and two in the back seats) with the original battery allocation plan. Configuration 4 shows four passengers with the original battery allocation. Configuration 5 shows the aircraft's static stability during charging, where the batteries are taken from the back and configuration 6 showcases the stability with the batteries are taken from the front. All of the scenarios show that the aircraft is statically stable, meaning there is no tipping, and the landing gears are able to withstand the weight shifts. Using the weight balance calculation, the center of gravity was found for each scenario and was applied in the other sectors of this project. This includes the landing gear, wing and tail positioning as well as the maximum batteries that could be available for the propulsion team table.

Table 2.1: Configuration 1

Main Landing Gear Position	3.40 meters
Nose Landing Gear Position	1.05 meters
Wing Position	1.64 meters
Neutral Point Position	0.5176
Center of Gravity Position	0.3240
Static Margin	0.1936
Battery Configuration	60 % Nose 40% Fuse

Table 2.2: Configuration 2

Main Landing Gear Position	3.40 meters
Nose Landing Gear Position	1.05 meters
Wing Position	1.64 meters
Neutral Point Position	0.5176
Center of Gravity Position	0.3880
Static Margin	0.1295
Battery Configuration	60 % Nose 40% Fuse

Table 2.3: Configuration 3

Main Landing Gear Position	3.40 meters
Nose Landing Gear Position	1.05 meters
Wing Position	1.64 meters
Neutral Point Position	0.5176
Center of Gravity Position	0.2051
Static Margin	0.3124
Battery Configuration	55 % Nose 45% Fuse

Table 2.4: Configuration 4

Main Landing Gear Position	3.40 meters
Nose Landing Gear Position	1.05 meters
Wing Position	1.64 meters
Neutral Point Position	0.5176
Center of Gravity Position	0.2051
Static Margin	0.3124
Battery Configuration	55 % Nose 45% Fuse

Table 2.5: Configuration 5: Nose Batteries out

Aircraft Component	Mass (kg)	Arm to CG (m)	Moment(Nm)
Wing	125	2.505	-825.76
Motor	20.3	0.186	-595.92
Battery Nose	0	0.708	0
Battery Fuse	228.6	4.106	2080.24
Tails	25	6	692
Systems	40.05	1.5	-659.43
Nose Landing Gear	26.96	1.1	-549.73
Fuse Landing Gear	26.8	3.7	137.13
Front Passengers	0	2.189	0
Rear Passengers	0	3.059	0
Emergency Motor	12.3	7.18	482.84
Mechanism	20	6.95	739.99
Total Moment			-1088.20

Table 2.6: Configuration 6: Fuselage Batteries out

Aircraft Component	Mass (kg)	Arm to CG (m)	Moment (Nm)
Wing	125	2.505	56.67
Motor	20.3	0.186	-452.61
Battery Nose	95.25	0.708	-1635.94
Battery Fuse	0	4.106	0
Tails	25	6	868.48
Systems	40.05	1.5	-376.70
Nose Landing Gear	26.96	1.1	-359.4
Fuse Landing Gear	26.8	3.7	326.32
Front Passengers	0	2.189	0
Rear Passengers	0	3.059	0
Emergency Motor	12.3	7.18	569.68
Mechanism	20	6.95	881.18
Total Moment			4864.80

As seen in Table 2.5 and 2.6, the moment about the center of gravity was calculated. In the scenario that the fuselage batteries are emptied out for charging, the aircraft demonstrates a positive moment meaning it will be statically stable about the center of gravity. However when the nose batteries are taken out for charging, it demonstrates a negative moment meaning the aircraft could tip backwards on its hinge point. To alleviate the overall moments when batteries are taken out the nose and fuselage, the landing gear was used as a variable in the MATLAB code found in the Appendix. This code essentially moved the landing gear in order to alleviate the tipping moment demonstrated in all six scenarios. In each case, the center of gravity shifted causing the overall moment to change, therefore the landing gears were placed strategically to accommodate the forward and aft center of gravity.

2.2 Aircraft Weight Optimization

One of the most important tasks for the stability and control team, was balancing the aircraft every time the structures and propulsion team changed something. To control the weight variation, each team estimated how much weight needed to be allocated and a temporary center of gravity position was calculated based on the positioning of each component. As the design was iterated, the weight became more solidified and eventually, a firm weight was allocated to each component. To maintain control over the center of gravity, the team was asked to stay within 10-15 kilograms of the original weight allocated to minimize the number of times the stability had to be recalculated. This also minimized the amount of times major design changes needed to be made, and it was only changed drastically if the overall design objective was being compromised. Therefore, the MTOW requirement has been met by continued organization and communication to the stability team.

Table 2.7: Aircraft Weight Optimization

Aircraft Component	Weight Allocation
MTOW	1156 kg
PAX + baggage	362 kg
Primary Motor	20 kg
Air frame	234 kg
Systems	40.05 kg
Batteries Nose	106.8 kg
Batteries Fuse	160.2 kg
Wing	125 kg
Tails	25 kg
Emergency Motor	12.3 kg
Emergency Motor Mechanism	20 kg
Landing Gear	50.6 kg

2.3 AVL Stability Analysis

Below showcases the various run cases for the wing geometry using AVL, a program designed by MIT. The program was used to do fast and efficient static stability checks for the wing geometry proposed by the aerodynamics team.

```
-----  
Geometry-axis derivatives...  
-----  
| axial vel. u | sideslip vel. v | normal vel. w |  
-----  
x force CX | CXu = 0.069242 | CXv = -0.000000 | CXw = 2.507634  
y force CY | CYu = -0.000000 | CYv = -0.010076 | CYw = -0.000000  
z force CZ | CZu = -2.913560 | CZv = 0.000000 | CZw = -4.736841  
x mom. Cl | Clu = -0.000000 | Clv = -0.125138 | Clw = -0.000000  
y mom. Cm | Cmu = -0.671663 | Cmv = -0.000000 | Cmw = -0.351732  
z mom. Cn | Cnu = 0.000000 | Cnv = 0.001258 | Cnw = -0.000000  
-----  
| roll rate p | pitch rate q | yaw rate r |  
-----  
x force CX | CXp = 0.000000 | CXq = 1.310600 | CXr = -0.000000  
y force CY | CYP = 0.266416 | CYq = 0.000000 | CYr = -0.003375  
z force CZ | CZp = -0.000000 | CZq = -5.494821 | CZr = 0.000000  
x mom. Cl | Clp = -0.554398 | Clq = -0.000000 | Clr = 0.392706  
y mom. Cm | Cmp = -0.000000 | Cmq = -1.148077 | Cmr = 0.000000  
z mom. Cn | Cnp = -0.290139 | Cnq = -0.000000 | Cnr = 0.000902
```

Figure 2.1: Wing Geometry using AVL

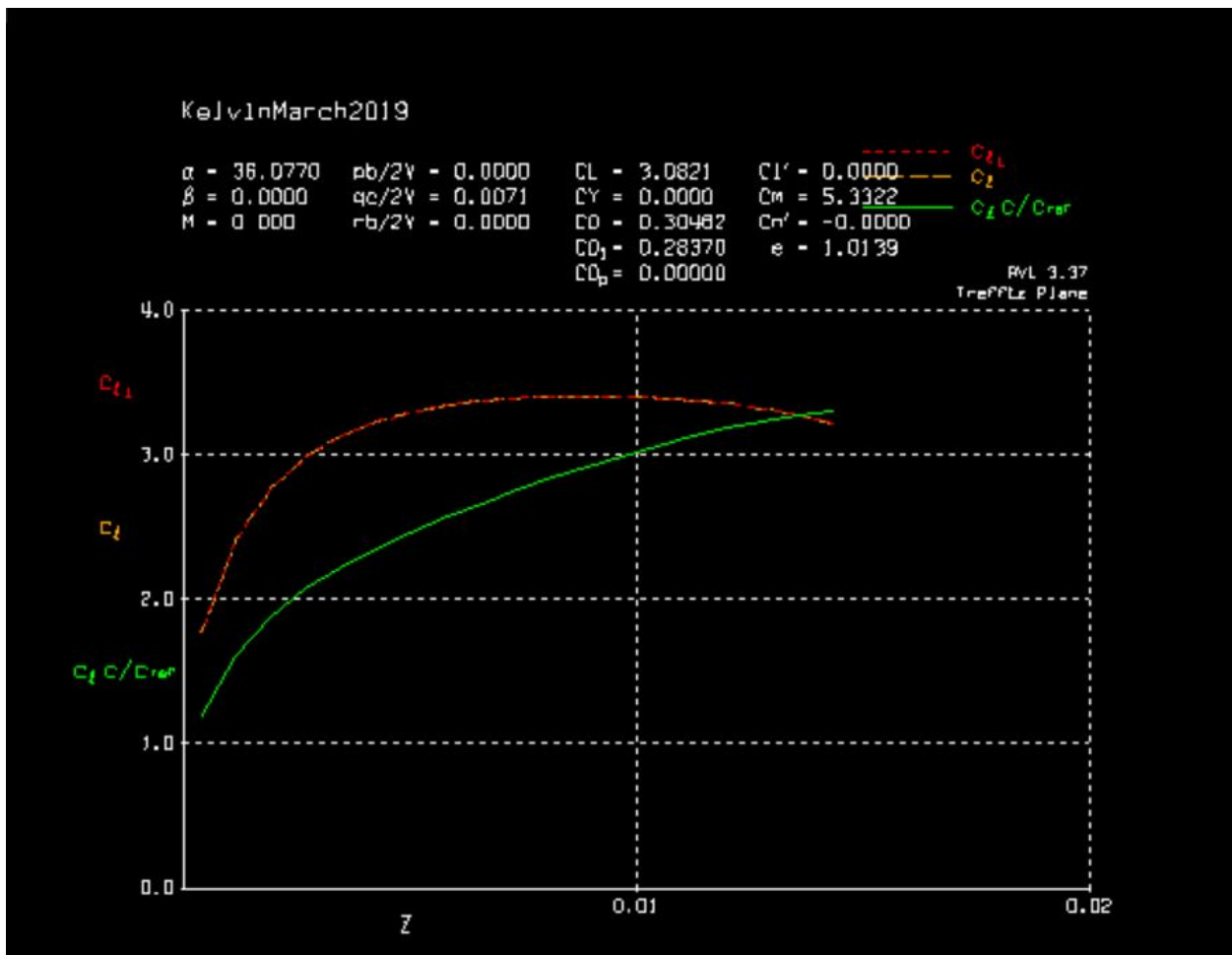


Figure 2.2: Downwash Angle using AVL

Shown below in Figure 2.2, shows the down wash angle in comparison to the coefficient of lift generated by AVL. This graph shows that with the inputted pitch rate and angle of attack, the maximum downwash angle is 0.0148. The graph demonstrates that the pressure differences and local induced angle has a minimum effect on the trimmed aircraft.

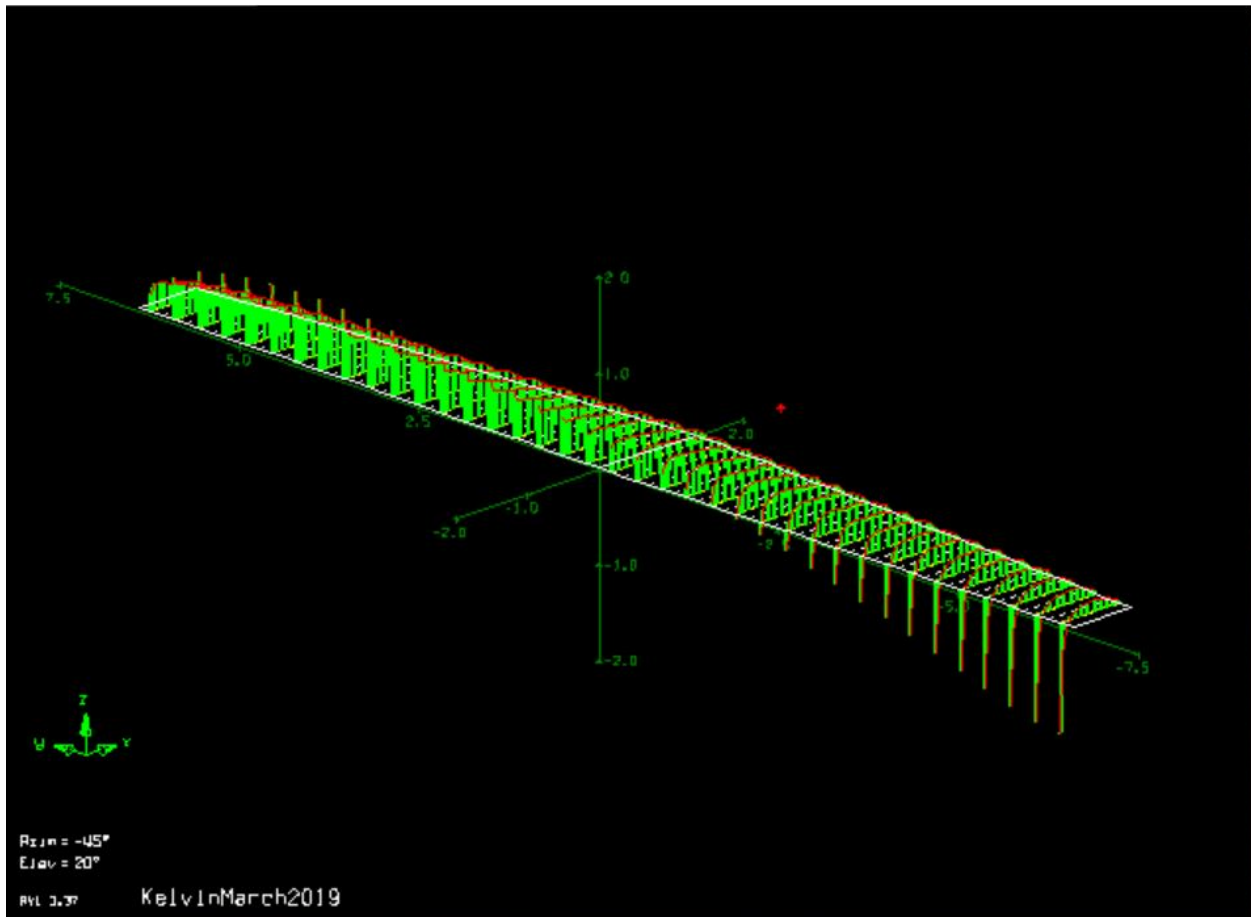


Figure 2.3: Wing Loading Forces using AVL

Figure 2.3 shows the dynamic wing loading and bending forces, where the maximum occurs at the tip and trailing edges of the airfoil during cruise. Below in Figure 2.4, the wing loading forces and moments with the given cruise speed was analyzed.

```
Vortex Lattice Output -- Total Forces

Configuration: KelvinMarch2019
    # Surfaces =    2
    # Strips   =  38
    # Vortices = 494

Sref =  13.975      Cref =  1.0984      Bref =  13.000
Xref =  2.5389      Yref =  0.0000      Zref =  0.0000

Standard axis orientation, X fwd, Z down

Run case: -unnamed-

Alpha =  36.07700      pb/2V = -0.00000      p'b/2V = -0.00000
Beta  =  0.00000      qc/2V =  0.00713      r'b/2V = -0.00000
Mach  =     0.000      rb/2V = -0.00000      r'b/2V = -0.00000

CXtot =  1.56859      Cltot =  0.00000      Cl'tot =  0.00000
CYtot =  0.00000      Cmtot =  5.33224
CZtot = -2.67052      Cntot = -0.00000      Cn'tot = -0.00000

CLtot =  3.08209
CDtot =  0.30482
CDvis =  0.00000      CDind = 0.3048183
CLff  =  3.30564      CDff  = 0.2836951      | Trefftz
CYff  = -0.00000      e =     1.0139      | Plane
```

Figure 2.4: Forces in Run Case using AVL

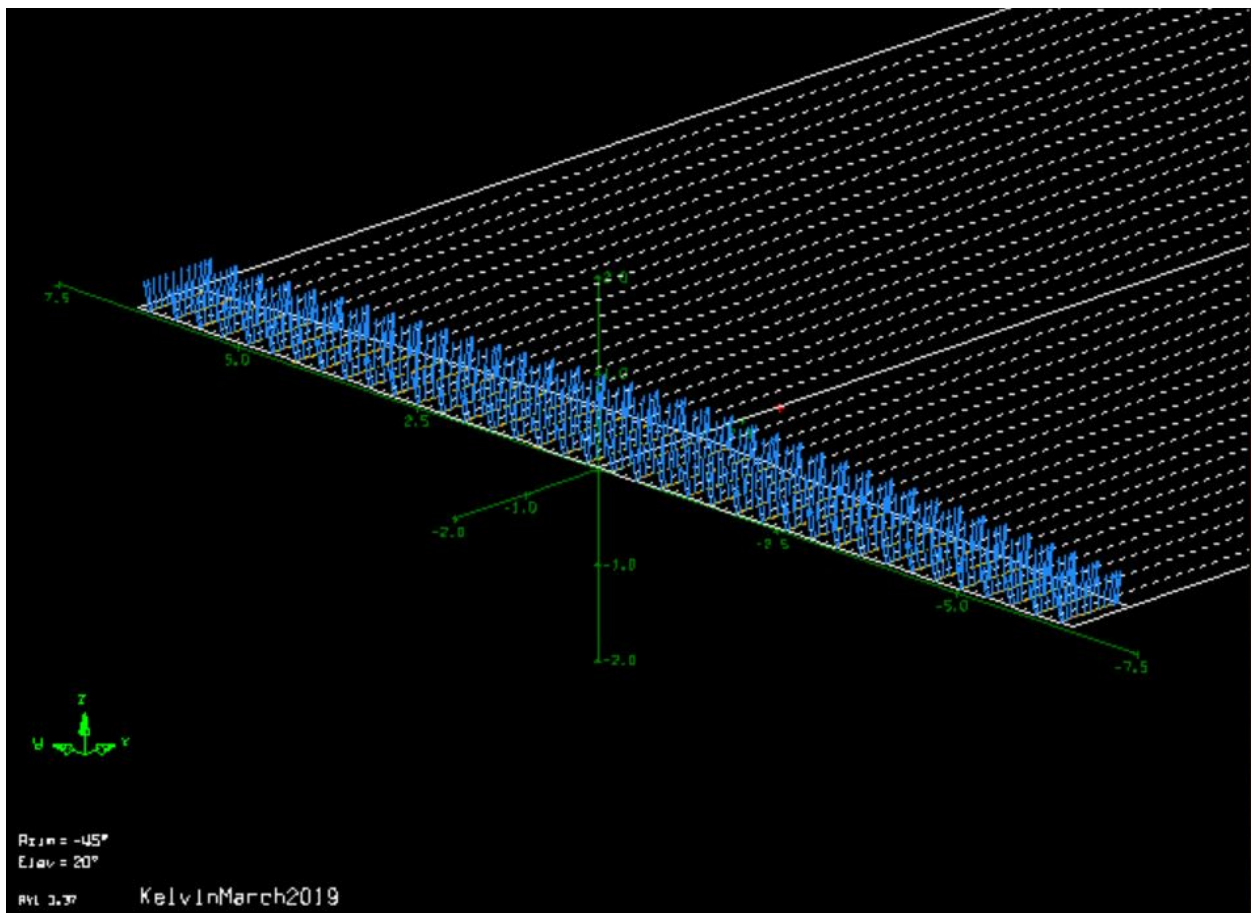


Figure 2.5: Trailing Edges and Normal Vector using AVL

Figure 2.5 shows the dynamic trailing edges and normal vector forces acting on the wing during cruise. As seen in the figure, the trailing edge lines remain stable and show minimum flutter around the wing.

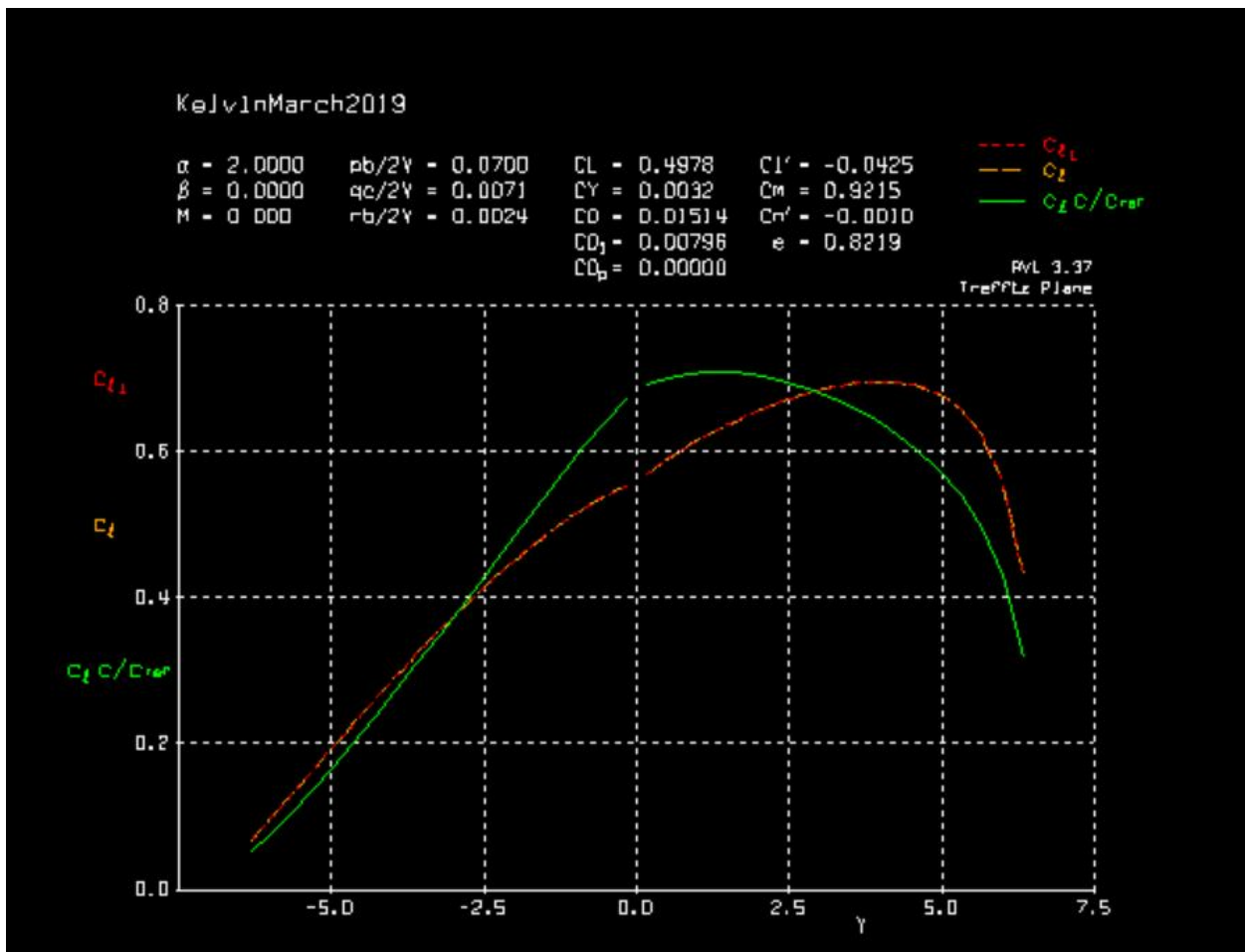


Figure 2.6: Coefficient of Lift vs Angle of Attack

Figure 2.6 show the coefficient of lift as it changes with the angle of attack. This graph was generated by inputting the maximum bank angle of 50 degrees and watching the stability behaviour of the wing as it performed 1) a banked turn 2)constant roll rate of 36 degrees per second and 3)constant pitch of 0.06 rad per second.

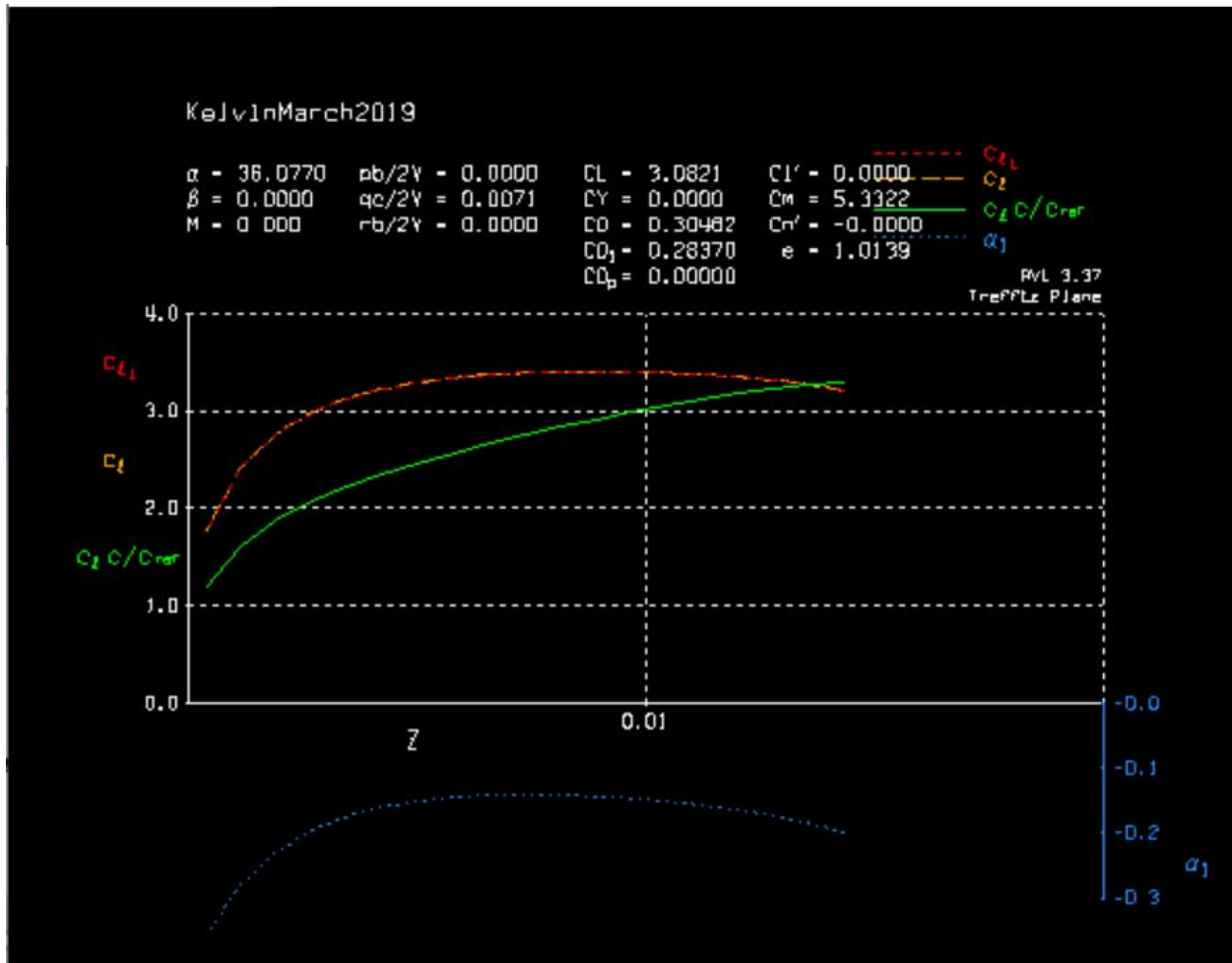


Figure 2.7: Yaw Moment Analysis

Figure 2.7 shows the z-xis, or the yaw behaviour, of the aircraft at the various coefficient of lift and the down wash angle associated with the moment. The tail must overcome the downward deflection of the airflow caused by wing. Therefore, as the angle of attack changed, the circulation around the wing alters the tail downwash. This occurs in a lag and must be further calculated in the future with the pitching moment and change in lift[53].

2.4 Roll Control

With a rudder and elevator the rudder generates a slip angle B , which combines with the dihedral to generate roll moment and provides roll control. Therefore the criteria for adequate roll authority is the product of vertical tail volume and Blaine Rawdon's spiral parameter, B , and was determined to be in the range of 0.1-0.2, where 0.1 is marginal roll control and 0.2 is effective control[54].

2.5 Spiral Stability

The dihedral angle of the wing provides natural spiral stability. A spirally-unstable aircraft tends to constantly increase the bank angle at a constant rate and will require constant attention and correction by the pilot. A spirally-stable aircraft will tend to roll upright with no control input making the aircraft easier to fly. The spiral stability can be determined by Blaine Rawdon, B , which is determined to be spirally stable if $B>5$. This parameter is highly dependant on the dihedral angle γ [54].

```

LU solving for RHS - lateral
Calculating forces and derivatives - lateral
Calculating the control derivatives

Longitudinal derivatives
Xu=      -4.2352      Cxu=     -0.027253
Xw=       58.774      Cxa=      0.3782
Zu=      -158.74      Czu=    -0.0051629
Zw=      -888.51      CLa=      5.7174
Zq=      -1200.7      CLq=      14.068
Mu=      -0.33847     Cmu=    -0.0019828
Mw=      -586.71      Cma=      -3.437
Mq=      -2350.2      Cmq=     -25.067
Neutral Point position=   0.66034 m

Lateral derivatives
Yv=      -68.764      CYb=     -0.44248
Yp=      -9.0997     CYp=    -0.0090084
Yr=      351.42       CYr=      0.34789
Lv=      -61.963      Clb=     -0.030671
Lp=      -8018.1      Clp=     -0.61059
Lr=      2085.5       Clr=      0.15882
Nv=      330.2        Cnb=      0.16345
Np=      -997.51      Cnp=     -0.075962
Nr=      -1659.5      Cnr=     -0.12637

Control derivatives
Xde=      -364.05     CXde=     -0.12903
Yde=     -1.0707e-11   CYde=    -3.7947e-15
Zde=      -13989       CZde=     -4.9583
Lde=     -3.3167e-9    CLde=    -9.0426e-14
Mde=      -1982.8      CMde=     -0.63978
Nde=     -3.6062e-5    CNde=    -9.832e-10

```

Figure 2.8: First Iteration of XFLR Stability Calculation

Figure 2.8 showcases the first attempt to trim the aircraft in XFLR with the wing and tail configuration together. My part was more focused on the lateral stability of the aircraft so the mass, inertia and center of gravity on the x-axis was inputted into the Stability Plan to generate this run case. The derivatives seem implausible based on the variables seen in the Stability and Control course, therefore, a second run case was initiated in order to find more variations of the derivatives.

```

Longitudinal derivatives
Xu=      -5.511          Cxu=     -0.026839
Xw=       76.667          Cxa=      0.37338
Zu=      -209.75          Czu=    -0.0051629
Zw=      -1174             CLa=      5.7174
Zq=      -1586.5           CLq=      14.068
Mu=      -0.44884          Cmu=     -0.00199
Mw=      -775.22           Cma=      -3.437
Mq=      -3105.2            Cmq=     -25.066
Neutral Point position=   0.66034 m

Lateral derivatives
Yv=      -90.857          CYb=     -0.44248
Yp=      -12.023          CYp=     -0.0090084
Yr=       464.32           CYr=      0.34789
Lv=      -81.872           Clb=     -0.030671
Lp=      -10594            Clp=     -0.61059
Lr=       2755.6            Clr=      0.15882
Nv=       436.31            Cnb=      0.16345
Np=      -1324.7            Cnp=     -0.076346
Nr=      -2193.7            Cnr=     -0.12644

Control derivatives
Xde=     -661.48           CXde=    -0.13429
Yde=    -1.428e-11          CYde=   -2.8991e-15
Zde=     -24423             CZde=    -4.9583
Lde=    -6.8808e-9           CLde=   -1.0746e-13
Mde=     -3462.2             CMde=   -0.63989
Nde=     0.00071923          CNde=   1.1232e-8

```

Figure 2.9: Second Iteration of XFLR Stability Calculation

Figure 2.9 showcases the second attempt to trim the aircraft in XFLR with the wing and tail configuration together. The criteria for lateral stability of the aircraft was outlined in the Chapter 2 Theory and based on that the data was deemed more plausible. The main criteria is the coefficient of lift based on sideslip angle is less than 0. As seen in Figure 2.9, the derivative is -0.030671. This run case was executed by inputting a new mass, inertia and center of gravity on the x-axis. Secondly, the control derivatives must also be less than 0 for Roll Control of the ailerons and as seen in the table, all the derivatives were less than 0.

2.6 Tail Sizing and Airfoil Selection

2.6.1 Initial design considerations

The aircraft being a fully electric vehicle added a layer of difficulty due to how uncommon literature covers electric aircrafts. Electric aircrafts are not in demand like single-aisle fuel efficient aircrafts are. The major difference between electric aircrafts and fuel driven aircrafts is the power supply. This shows that the aerodynamics and the design of the aircraft are the same for both electric driven and fuel driven aircrafts.

A general tail configuration for the aircraft was chosen. The configuration of an aft horizontal tail with a single aft vertical tail was chosen for the design. This seems to be a logical choice due to how similar the designed aircraft resembled the Cessna 172. This configuration is simple and effective for a general aviation low speed propeller driven aircraft.

2.6.2 Horizontal and vertical tail initial s

To start the design process, I had to choose an initial volume coefficient for both the vertical and horizontal tail. Based on literature , the typical values for \bar{V}_H and \bar{V}_V for a general aviation single prop-driven engine are 0.3 to 0.7 and 0.03 to 0.05 respectively. I have iterated outside this range but within this range the size of the tail seemed appropriate. Further analysis of the typical values would be done through AVL (Athena Vortex lattice).

Table 2.8: Typical values for horizontal and vertical tail volume coefficients

Aircraft	Horizontal tail volume coefficient (\bar{V}_H)	Vertical tail volume coefficient (\bar{V}_V)
Glider and motor glider	0.6	0.03
Home built	0.5	0.04
GA single prop driven engine	0.7	0.04
GA twin prop driven engine	0.8	0.07
GA with canard	0.6	0.05
Agricultural	0.5	0.04
Twin turboprop	0.9	0.08
Jet trainer	0.7	0.06
Fighter aircraft	0.4	0.07
Fighter (with canard)	0.1	0.06
Bomber/military transport	1	0.08
Jet transport	1.1	0.09

Other than the volume coefficient of the tail, the cg (Center of gravity) limit of the aircraft also affects the tail design because this affects the length of the boom, l_h . The length of the boom decides how big the tail is required to be for producing enough moment to rotate the aircraft pitch up and down. The shorter the boom length the bigger the tail size needs to be because a large lifting surface is needed to produce the required moment to pitch the aircraft. The longer the boom length the smaller lifting surface is needed to produce the required moment to pitch the aircraft.

An aircraft's tail also has control surfaces such as the elevator, rudder and tab. The elevator is used to pitch the aircraft nose up and down, while the rudder is used to yaw the aircraft to the right and left. Tabs are used to relieve the pilot from constantly trimming the aircraft, this reduces the pilot's fatigue and increases the aircraft stability.



Figure 2.10: Saab 37 Viggen, aft horizontal tail, canard configuration



Figure 2.11: B2 spirit bomber Tailless aircraft

Iterations of several variables such as the V_v , V_h , ARh, ARv, and different passenger configurations were made.

Showing the worst-case scenarios gives an idea of the worst condition our aircraft will be operating in. Although having all passengers onboard gives us a -4.1 degree incidence angle is almost half the stall of the horizontal tail, the aircraft is still stable. Having the worst-case scenario of only fuse batteries plus pilot and two rear passengers resulted in a -5.15 degree angle but also stable.

#Passengers + pilot	description	Tail incidence angle needed for trim (degrees)	Description	Cmalpha (negative = stable)	Cnbeta (positive = stable)
no passengers, only pilot and only rear batteries	Starting with the scenario of only fuse batteries and pilot, Cg of 0.286 of MAC	-4.9	Stable but half way to stall where stall of the horizontal tail is ± 10	-3.9748	29.4453
Fuse batteries plus pilot plus 2 rear passengers	Next case is fuse batteries, pilot and 2 rear passengers	-5.15	Stable but still half way to stall	-4.0093	29.445
Both batteries, pilot and all passengers	All seats taken with both batteries available	-4.1	Stable and best angle that we got	-3.8653	29.4453

Figure 2.12: Different Cases for Tail Designs

Increasing V_h from the minimum range of 0.3 to 0.6 increases the horizontal tail geometry, thus increasing longitudinal stability due to the decreasing C_m alpha value. Increasing V_v from the minimum range of 0.02 to 0.055 increases the vertical tail geometry, thus increasing the directional stability due to the increasing C_n β value. Increasing the aspect ratios of both vertical and horizontal tail results in an increase of both geometries, but it does not change the longitudinal and the directional stability derivatives. This occurs because the stability derivative equations do not include aspect ratio and the code optimizes the geometry to keep the stability derivative.

For the design, the values of the horizontal and vertical tail geometries closest to the Cessna 172 were chosen due to it being one of the most stable 4-seater, low speed aircrafts in the industry while reducing as much mass as we can from the tail structure. Using the Cessna as a reference, the following tail geometry was obtained:

Table 2.9: Chosen tail geometry with stability values

V _h	AR _h (in percentage of wing AR)	V _v	AR _v (in percentage of wing AR)	Horizontal Geometry (m)				Vertical Geometry (m)				Cm alpha	Cn beta
				b	Croot	Cbar	Ctip	b	Croot	Cbar	Ctip		
0.6	0.66	0.035	0.115	4.17	0.635	0.517	0.38	1.44	1.14	1.03	0.91	-3.83	29.4

2.7 Dynamic Longitudinal Analysis

Analysing the dynamic stability is an important aspect of aircraft design. Insuring the aircraft is stable during takeoff, cruise and landing is essential to the passenger's well being. When

Vh	ARh (in percentage of wing AR)	Vv	Arv (in percentage of wing AR)	Horizontal Geometry (m)				Vertical Geometry (m)				Cmalpha	Cnbeta
				b	Croot	Cbar	Ctip	b	Croot	Cbar	Ctip		
0.3	0.66	0.035	0.115	2.95	0.449	0.266	0.3654	1.44	1.143	0.91	1.0	-1.975	29.4
0.35	-	-	-	3.2	0.49	0.39	0.29	1.44	1.14	1.0	0.9	-2.3	29.4
0.4	-	-	-	3.4	0.52	0.42	0.31	1.44	1.14	1.0	0.9	-2.6	29.4
0.45	-	-	-	3.6	0.55	0.45	0.326	1.44	1.14	1.0	0.9	-2.9	29.4
0.5	-	-	-	3.8	0.58	0.47	0.34	1.44	1.14	1.0	0.9	-3.23	29.4
0.55	-	-	-	3.99	0.61	0.49	0.36	1.44	1.14	1.0	0.9	-3.55	29.4
0.6	-	-	-	4.16	0.63	0.52	0.38	1.44	1.14	1.0	0.9	-3.86	29.4
-	-	0.02	-	4.16	0.63	0.52	0.38	1.1	0.86	0.78	0.69	-3.86	16.8
-	-	0.025	-	4.16	0.63	0.52	0.38	1.2	0.97	0.87	0.77	-3.86	21.0
-	-	0.03	-	4.16	0.63	0.52	0.38	1.33	1.06	0.96	0.85	-3.86	25.2
-	-	0.035	-	4.16	0.63	0.52	0.38	1.44	1.14	1.03	0.92	-3.86	29.4
-	-	0.04	-	4.16	0.63	0.52	0.38	1.53	1.22	1.1	0.98	-3.86	33.6
-	-	0.045	-	4.16	0.63	0.52	0.38	1.63	1.3	1.17	1.04	-3.86	37.8
-	-	0.05	-	4.16	0.63	0.52	0.38	1.72	1.4	1.24	1.1	-3.86	42
-	-	0.055	-	4.16	0.63	0.52	0.38	1.8	1.43	1.3	1.15	-3.86	46.3
-	0.1	0.035	-	1.6	1.6	1.3	0.97	1.44	1.14	1.03	0.92	-3.86	29.4
-	0.2	-	-	2.3	1.16	0.94	0.69	1.44	1.14	1.03	0.92	-3.86	29.4
-	0.3	-	-	2.8	0.95	0.77	0.56	1.44	1.14	1.03	0.92	-3.86	29.4
-	0.4	-	-	3.2	0.82	0.67	0.49	1.44	1.14	1.03	0.92	-3.86	29.4
-	0.5	-	-	3.6	0.73	0.6	0.43	1.44	1.14	1.03	0.92	-3.86	29.4
-	0.6	-	-	3.95	0.67	0.54	0.4	1.44	1.14	1.03	0.92	-3.86	29.4
-	0.7	-	-	4.3	0.62	0.5	0.37	1.44	1.14	1.03	0.92	-3.86	29.4
-	0.66	-	0.01	4.16	0.63	0.52	0.38	0.42	3.9	3.5	3.1	-3.86	29.4
-	-	-	0.05	4.16	0.63	0.52	0.38	0.95	1.7	1.6	1.4	-3.86	29.4
-	-	-	0.07	4.16	0.63	0.52	0.38	1.1	1.5	1.3	1.2	-3.86	29.4
-	-	-	0.09	4.16	0.63	0.52	0.38	1.27	1.29	1.17	1.03	-3.86	29.4

Figure 2.13: Different initial Geometry Configurations

an aircraft is stable along its flight envelope, it will stay steady and avoid any kind of stressful maneuvers that may damage the aircraft itself and avoid meeting stalling conditions.

Both AVL and xflr5 were used to analyse our aircraft's longitudinal stability. By using both of these programs, we can observe and confirm our aircraft's stability.

2.7.1 Xflr5 short period longitudinal stability analysis

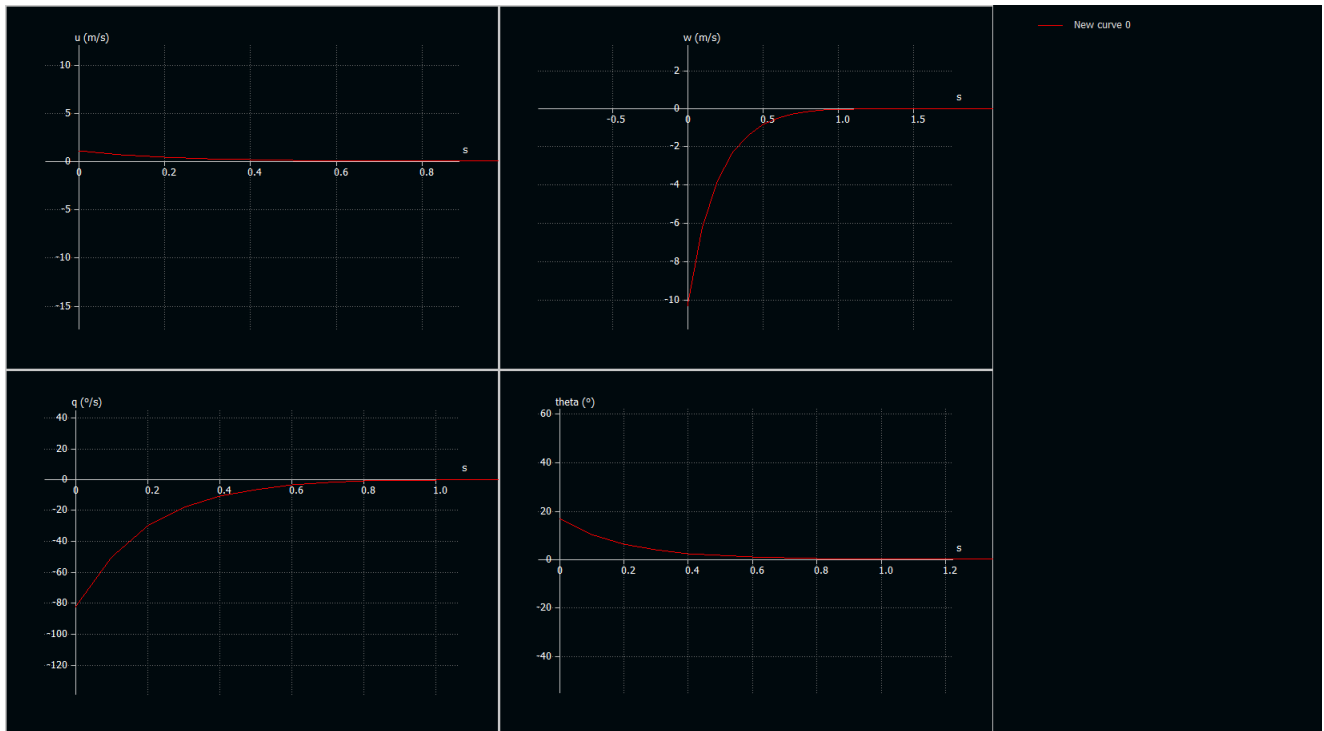


Figure 2.14: Short Period Cruise at 0 degrees

2.14 shows the short period motion of the aircraft. Our short period motion reaches steady state in approximately 1.3 seconds. The initial perturbation used to destabilize the aircraft are a vertical velocity of -10 m/s, a horizontal velocity of 1 m/s. This resulted in an initial angle of attack of 17 degrees, returning to steady state (0 degrees) in approximately 1.3 seconds.

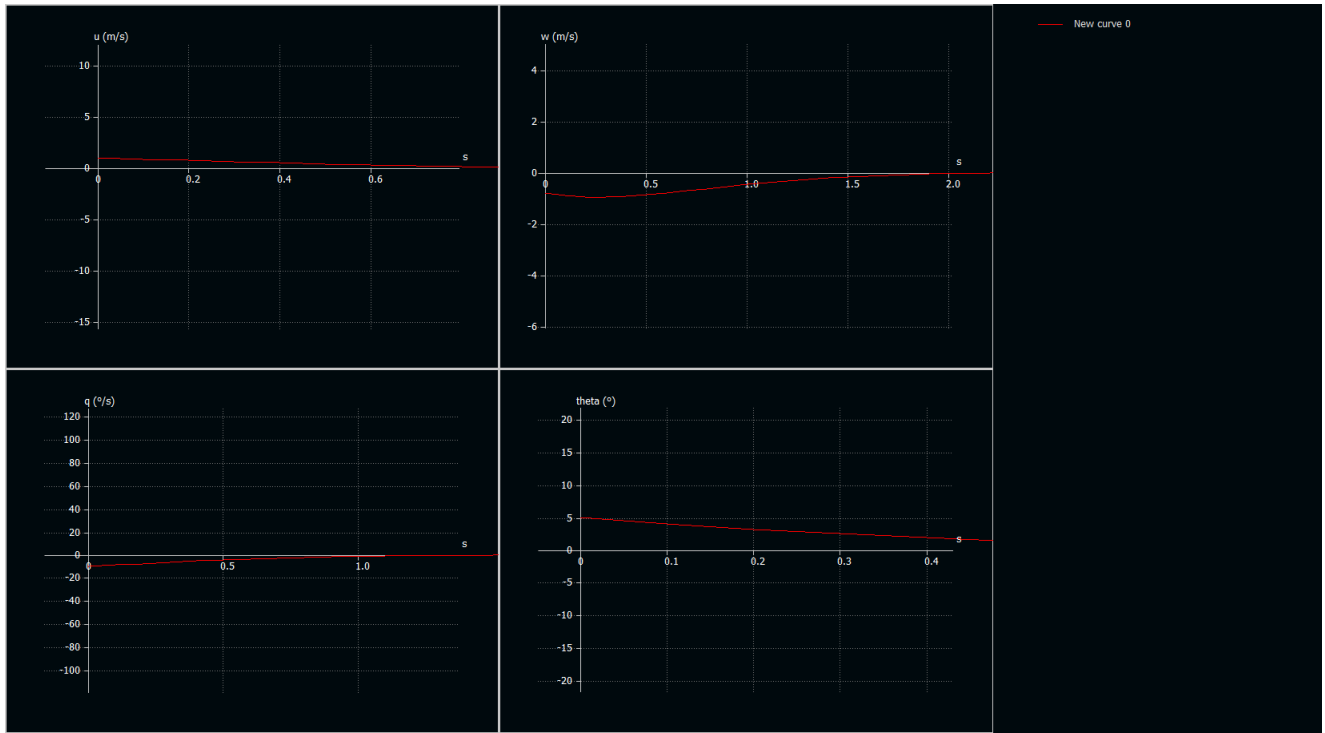


Figure 2.15: Short period motion at climb of 7 degrees AoA

In the case of climb (2.15), a climb angle of 7 degrees was used as the steady state during climb. The short period motion time is approximately 1.5 seconds, which is approximately 0.2 seconds greater than our cruise (0 degrees). At a climb of 7 degrees, the aircraft is stable in terms of short period motion.

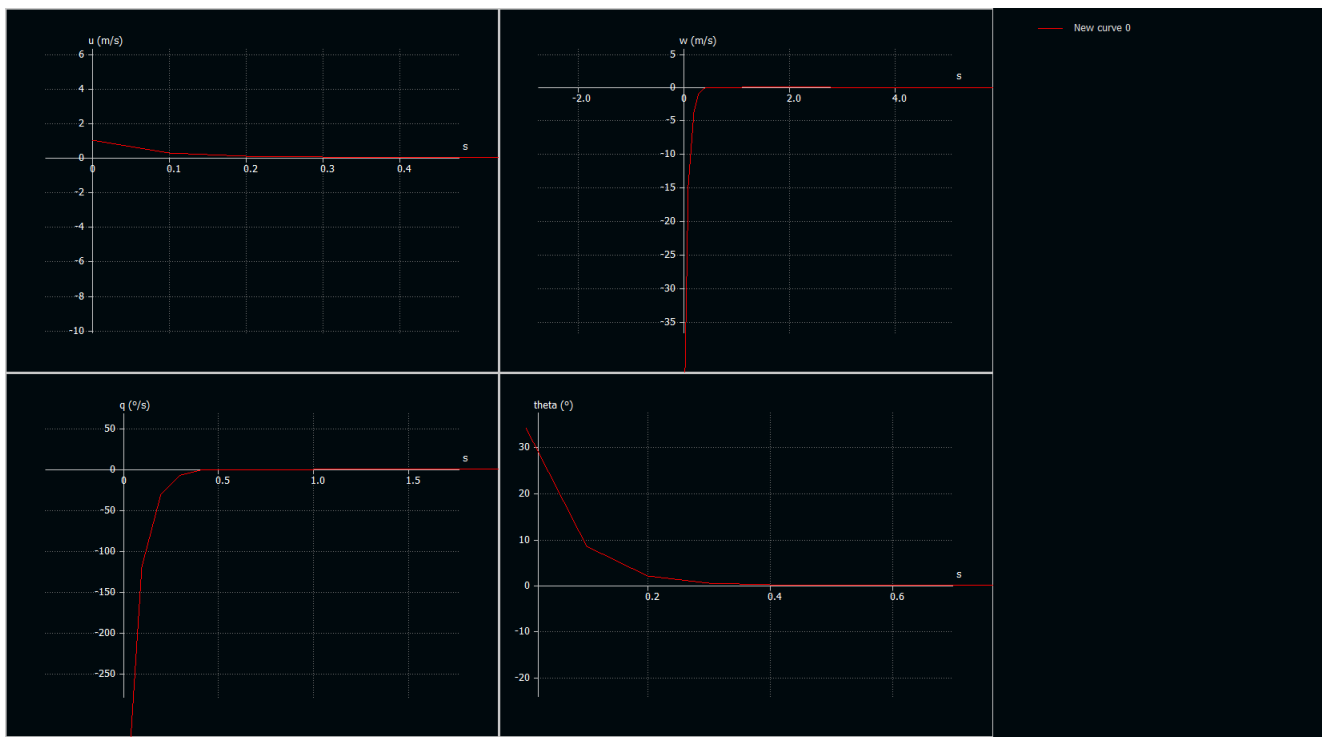


Figure 2.16: Short period motion for descent of -0.5 degrees

In the case of descent (2.16), a descent angle of -0.5 degrees is used as the steady state during descent. The short period motion time is approximately 0.5 seconds, which is approximately 0.8 seconds lower than the cruise (0 degrees). At a descent of -0.5 degrees, the aircraft is stable in terms of short period motion.

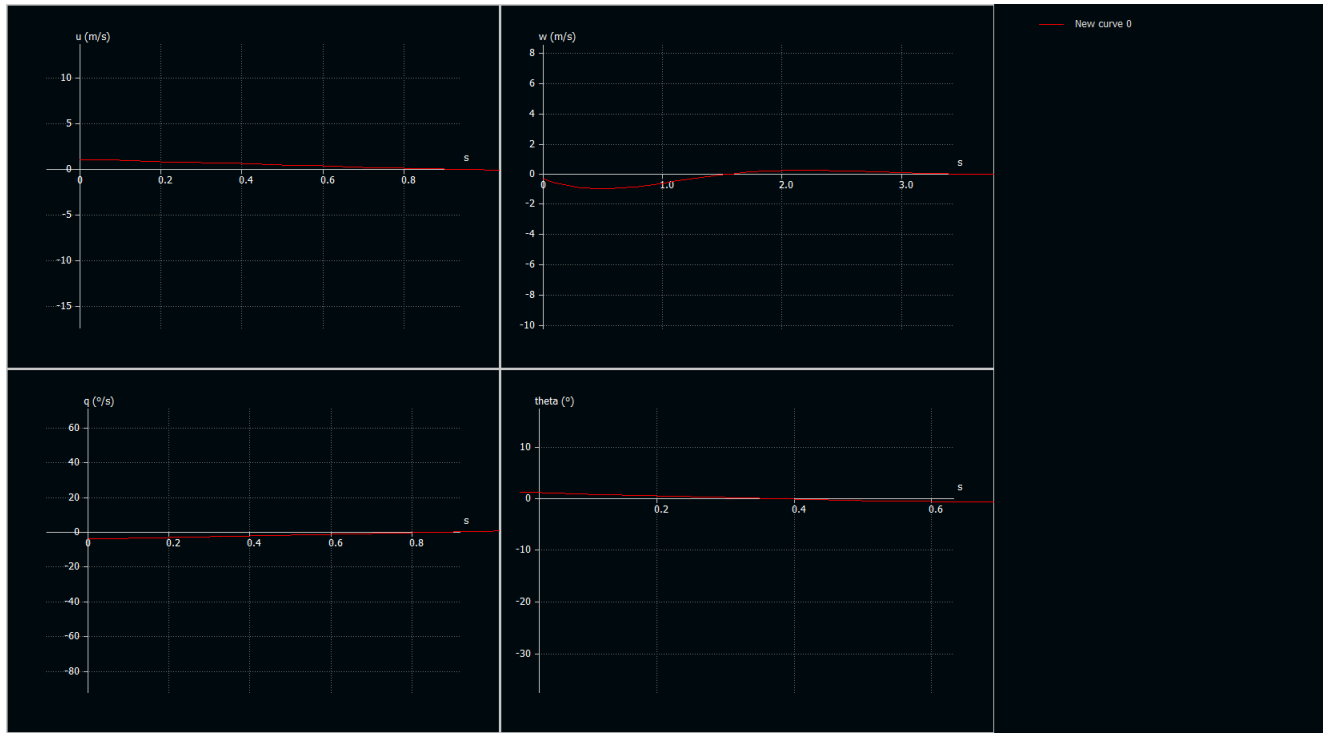


Figure 2.17: Short period motion at max AoA 14 degrees

In the case of maximum angle of attack at an angle of 14 degrees, the short period motion time is approximately 3.1 seconds, which is approximately 1.8 seconds greater than the cruise (0 degrees). At the maximum angle of attack, the aircraft is stable in terms of short period motion.

2.7.2 Xflr5 long period motion longitudinal stability analysis

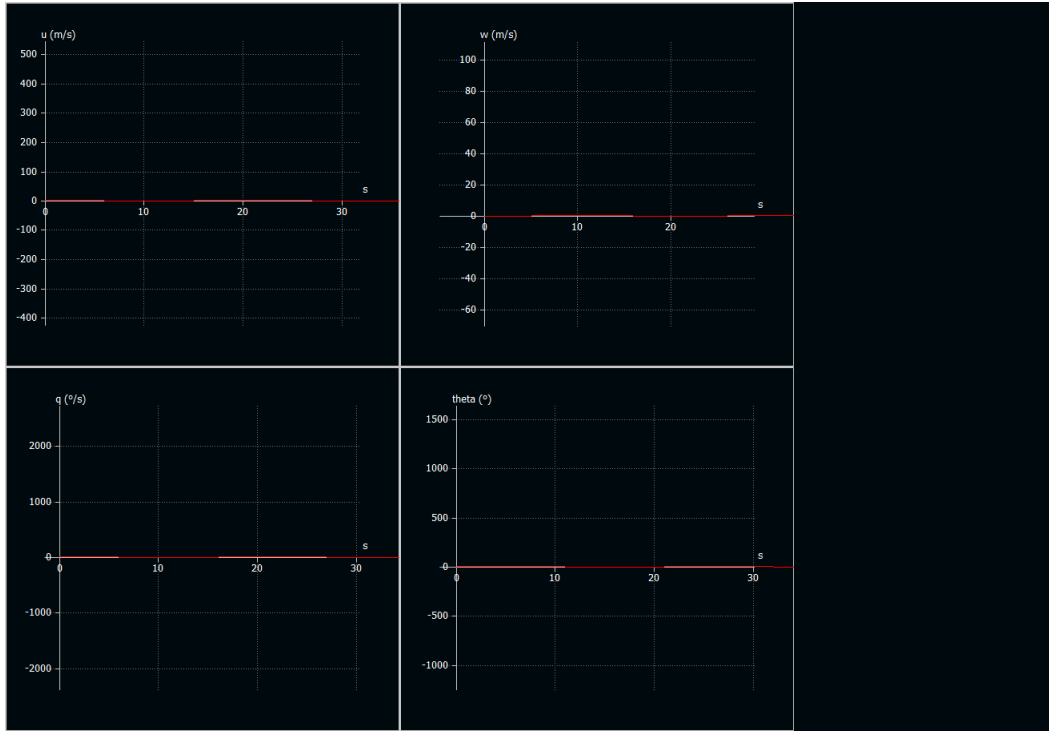


Figure 2.18: Long period motion error on Xflr5

Using Xflr5 to get the long period motion produced an error. The error that it produced is a system that is too stable. The system should have a general plot that is either a decaying sinusoidal shape or a close to exact sinusoidal shape. Although the short period motion produced was acceptable, the long period motion was not.

2.7.3 AVL short period motion

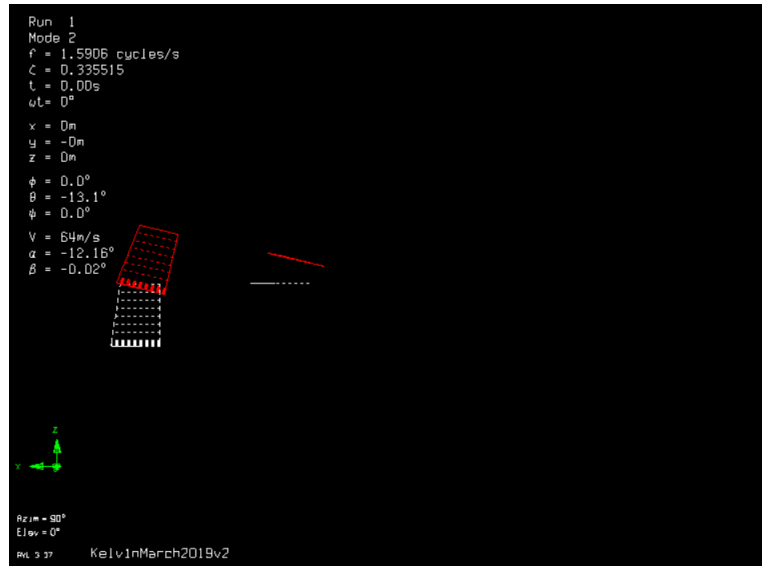


Figure 2.19: Short period motion Position 1 AVL



Figure 2.20: Short period motion Position 2 AVL

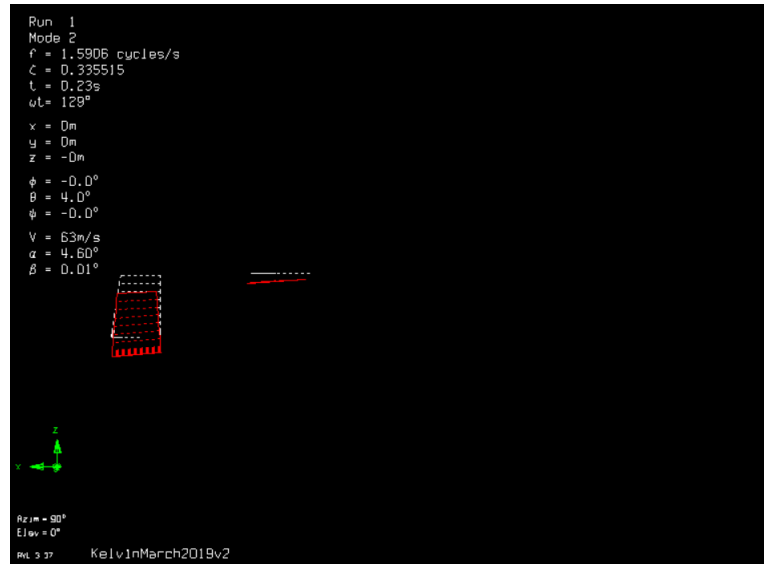


Figure 2.21: Short period motion Position 3 AVL



Figure 2.22: Short period motion Position 4 AVL

2.19 through 2.22 show the short period motion produced by AVL. After an initial disturbance of approximately -12 degrees, the aircraft returns to steady state after approximately 1.4 seconds. This is similar to Xflr5's results.

2.7.4 AVL long period motion

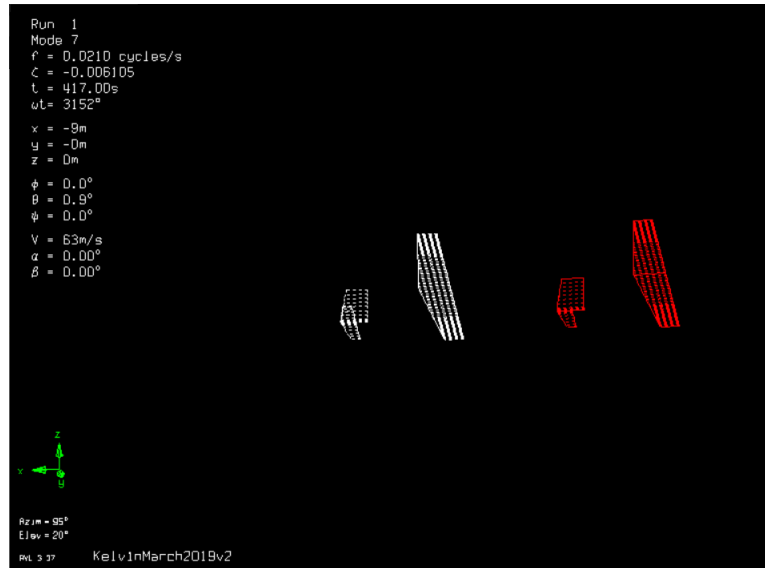


Figure 2.23: Long period motion Position 1 AVL



Figure 2.24: Long period motion Position 2 AVL

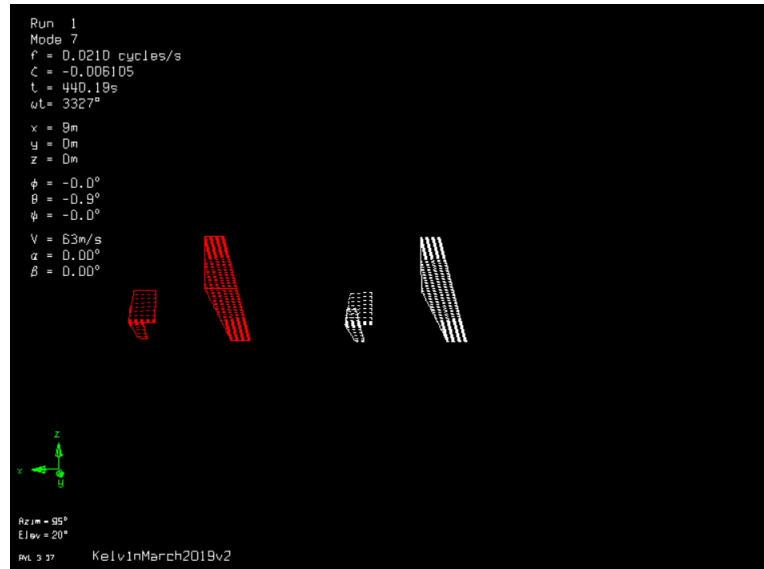


Figure 2.25: Long period motion Position 3 AVL

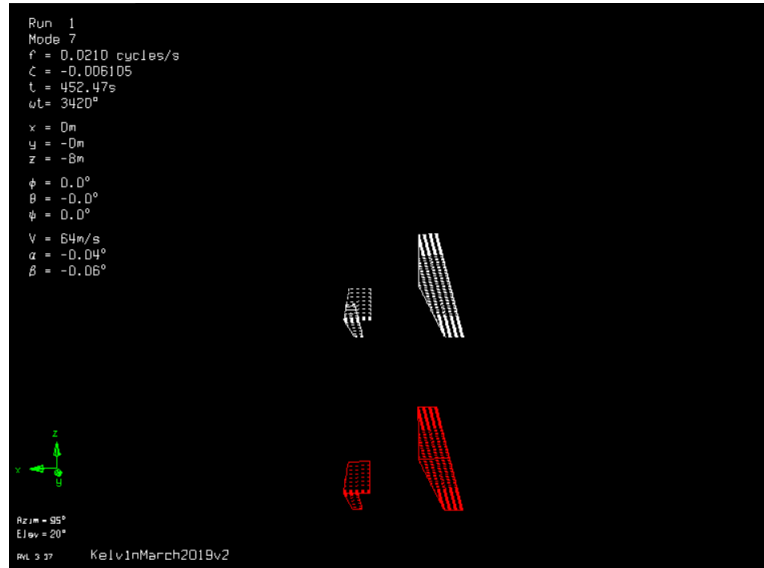


Figure 2.26: Long period motion Position 4 AVL

2.23 through 2.26 show the long period motion produced by AVL. 2.23 shows the aircraft starting at -9 meters behind the steady state reference point, shifting upwards to 9m but also shifting forward to 0 meters seen in 2.24. 2.25 shows the aircraft continuing its translation to 9 meters forward but on the horizontal reference point and 2.26 shows the aircraft on its final translation of -8 meters below the horizontal reference point before completing the cycle that is 2.23.

AVL produced better results overall than Xflr5 for both motions especially long period motion. Long period motion is a sinusoidal motion, it is not stable because it needs to be a decaying sinusoidal motion. This might be an error in the programming and an error in inputting certain

parameters. MATLAB calculations show that the static longitudinal stability is in the acceptable range of stability.

3 Stability Conclusion

By changing the V_y, V_h and the Aspect ratios, the team obtained different geometries with different stability values. Shifting the CG through several conditions and configurations produce different tail designs. The final tail design accounts for all the configurations. The stability values are acceptable but the size of most of the iterated geometries are not feasible due to added mass and cost. The final iterated values are displayed in 2.9. The overall stability of the aircraft is stable. Approaching stall and beyond, stability of the aircraft decreases. AVL and XFLR5 produced a stable short period motion but both of their long period motions were unacceptable, although AVL was better at producing the long period motion. Tail design and optimization is an important factor in aircraft design. The tail is responsible for two major functions, pitching the aircraft nose up or down and trimming the aircraft. Aircraft trimming is an important aspect of tail design due to keeping the aircraft in steady state.

Part VII

Book VII: Airworthiness

1 Subpart B – Flight

1.1 Performance

1.1.0.1 Weight and center of gravity Limits for weights and centers of gravity that provide safety were considered. All specifics were considered and mentioned within the report using section 23.2100.

1.1.0.2 Performance data Performance of the aircraft have been represented in several conditions including still air, ambient atmospheric within the flight envelope, within airport altitude ranges, different temperatures and different takeoff and landing conditions

1.1.0.3 Stall speed Stall speed was determined following the regulation rules of idle/zero thrust for propulsion systems and nominal thrust for propulsion systems.

1.1.0.4 Takeoff performance Takeoff performance conditions where accounted for, including stall speed safety margins, minimum control speeds and climb gradients. Clearing the climb distance of 15 meters above takeoff distance was also considered.

1.1.0.5 Climb requirements With the engine operating and in the initial climb configuration, the aircraft must have a climb gradient of 8.3 percent.

1.1.0.6 Climb information Climb performance was determined at different conditions such as different weights, altitudes and ambient temperature within the envelope. Gliding performance was determined after the loss of propulsion.

1.1.0.7 Landing Distance required to land starting from a height of 15 meters above the landing surface was considered to a complete stop. A pilot with average skill can land the aircraft within the determined landing distance consistently without damage and injury.

1.2 Flight Characteristics

1.2.0.1 Controllability The airplane is controllable and maneuverable without exceptional piloting skill. The aircraft is controllable at all loading conditions, during all phases of flight,

during propulsion failure and during configuration changes. The aircraft must land safely on the steepest approved approached landing strip.

1.2.0.2 Trim The airplane maintains lateral and directional trim without further force upon the primary flight controls in cruise. Longitudinal trim is maintained during climb, level flight, descent and approach. Control forces do not fatigue or distract the pilot during normal operations and emergency operations.

1.2.0.3 Stability The aircraft has static longitudinal, lateral and directional stability in normal operations. Dynamic short period and Dutch roll stability in normal operations is considered. Stable control force feedback is available for the pilot.

1.2.0.4 Stall characteristics, stall warning and spins The aircraft exhibits controllable stall characteristics in several conditions based on section 23.2150.

1.2.0.5 Ground and water handling characteristics During taxi, the aircraft exhibits a controllable longitudinal and directional handling characteristic.

1.2.0.6 Vibration, buffeting and highspeed characteristics Vibrations are within acceptable ranges throughout several conditions.

1.2.0.7 Performance and flight characteristics requirements for flight in icing conditions Icing conditions are mentioned and considered throughout the report. Icing conditions are considered during several flight conditions such as different speeds and different temperatures.

2 Subpart B-Structures

2.1 Structure design envelope

This section is part of the FAR 23.22 that highlights the loads and limits for which all structures have to be designed for. All the structures in the airplane were designed for a load factor of +3.8g. The highest speeds were used which is experienced at dive. The structures were designed for this as well.

2.2 Interaction of systems and structures

One system that interacts with the structures is the battery frame that is attached inside the fuse. The fuselage was designed accordingly to handle the frame as well as any other mounting points.

2.3 Structural loads

All critical combinations were accounted for. These are extreme cases that the airplane is expected to experience in flight.

2.3.1 Flight load conditions

Gust loads were accounted for and deemed to be less extreme when compared to the manoueving loads.

2.3.2 Ground Load conditions

All ground load conditions were calculated in accordance with the landing gear design. Canadian Aviation Regulations, Part V - Airworthiness Manual Chapter 523 is used to derive the ground loads of the landing gear.

2.3.3 Level Landing Conditions:

"For a level landing, the nose and main wheels contact the ground simultaneously; and the main wheels contact the ground and the nose wheel is just clear of the ground." [33]

2.3.4 One-wheel Landing Conditions:

"The aircraft is assumed to be in the level attitude and to contact the ground on one side of the main landing gear. The ground reactions must be the same the ground load obtained on 523.479." [33]

2.3.5 Side Load Conditions:

"The aircraft is assumed to be in a level attitude with only the main wheels contacting the ground and with the shock absorbers and tires in their static positions." [33]

- The limit vertical load factor must be 1.33, with the vertical ground reaction divided equally between the main wheels. [33]
- The limit side inertia factor must be 0.83, with the side ground reaction divided between the main wheels so that $0.5(W)$ is acting inboard on one side and $0.33(W)$ is acting outboard on the other side. [33]

For side load condition, the main landing gear was tested in ANSYS to ensure the main landing gear can withstand the condition. [33]

Please refer to appendix for the results of 1.33 limit vertical load factor , with the vertical ground reaction divided by two between the main gear.

2.3.6 Braked Roll Conditions

"Under braked roll conditions, with the shock absorbers and tires in their static positions, the following apply": [33]

- The limit vertical load factor must be 1.33
- The attitudes and ground contacts must be those described in 523.479 for level landings.
- A drag reaction equal to the vertical reaction at the wheel multiplied by a coefficient of friction of 0.8 must be applied at the ground contact point of each wheel with brakes, except that the drag reaction need not exceed the maximum value based on limiting brake torque.

Since both landing gear met the requirements in 523.499 and 523.485, therefore it met the braked roll conditions as well.

2.3.7 Supplementary Conditions for Nose Wheels

"In determining the ground loads on nose wheels and affected supporting structures, and assuming that the shock absorbers and tires are in their static positions, the following conditions must be met:" [33]

1. For aft loads, the limit force components at the axle:
 - A vertical component of 2.25 times the static load on the wheel.
 - A drag component of 0.8 times the vertical load.
2. For forward loads, the limit force components at the axle:
 - A vertical component of 2.25 times the static load on the wheel.
 - A forward component of 0.4 times the vertical load.
3. or side loads, the limit force components at ground contact:
 - A vertical component of 2.25 times the static load on the wheel.
 - A side component of 0.7 times the vertical load.

The above conditions of the axle were tested in ANSYS.³

³Refer to Appendix D for calculation regarding ANSYS results

2.3.8 Towing Loads

The towing loads must be applied to the design of tow fittings and the immediate attaching structure. [33]

Tow Point	Position	Load		
		Magnitude	No.	Direction
Main gear		0.225 W per main gear unit	1 2 3 4	Forward, parallel to drag axis. Forward, at 30° to drag axis. Aft, parallel to drag axis. Aft, at 30° to drag axis.
Auxiliary gear	Swivelled forward	0.3 W	5 6 7 8	Forward Aft Forward Aft
	Swivelled aft			
	Swivelled 45° from forward	0.15W	9 10	Forward, in plane of wheel
	Swivelled 45° from aft	0.15W	11 12	Aft, in plane of wheel Forward, in plane of wheel Aft, in plane of wheel

Figure 2.1: Prescribed Towing Loads Given by CAR

The tow point of the aircraft is at the nose landing gear. Therefore 0.3W load and 0.15W load condition is applied and the following figures are the analysis result from ANSYS.⁴

2.4 Structural performance

2.4.1 Structural strength

The structure was designed to handle limit loads without: 1) Interference to safe flight 2) Permanent Deformation of materials as well as ultimate loads

⁴Refer to Appendix D for calculation regarding ANSYS results

3 Subpart D–Design and Construction

3.1 Flight control systems

The Flight Control Systems were designed to provide easy operation and smooth performance for the pilots

3.2 Landing gear systems

The Landing Gear was designed to handle static as well as landing loads

3.3 Fire protection

Protective fire proof layers were added to surround each battery pack. Firewalls were also installed both fore and aft to protect the passengers from any fire.

3.3.1 Lightning protection

The airframe is fitted with lightning discharge rods to redirect the voltage through the airframe, thus keeping the occupants safe.

4 Subpart E–Powerplant

4.1 Powerplant installation

1. Electrical Power Plant is simple with minimum components
2. Propulsive Units are separated and redundant
3. Operating Altitude is within limits
4. Power Plant unit is easily accessed via hinges on the hood
5. Engine cowls and nacelles are easily opened for inspection by the pilot
6. Does not Apply
7. Engine installation complies with engine type certificate
8. Engine Installation complies with chapter 523.901 Installation
9. Does not Apply

4.2 Powerplant installation hazard assessment

- a) In the case of engine failure continued flight for landing is possible using engine 2. If double engine failure is to occur gliding for short distance will allow for safe landing.
- b) multiple redundancies to prevent serious injury.
- c) immediate action is not required but must be taken soon.

4.3 Powerplant ice protection

- a) Not applicable for electric airplane.
- b) Powerplant installation design will prevent any accumulation of ice or snow.

4.4 Reversing systems

- a) No unsafe condition will result during normal operation of the system (multiple redundancies are enforced).
- b) Airplane is capable of continued safe flight in the event of single failure.

4.5 Powerplant operational characteristics

- a) The installed powerplant operates without any hazardous characteristics during normal and emergency operation within the range of operating limitations for the airplane and the engine.
- b) Pilot has capability to stop and restart engines during flight.

5 Subpart F – Equipment

5.1 Airplane level systems requirements

The equipment should be able to operate safely during the day, night, and IFR conditions. More specifically for night time, required lights on the exterior and interior of the plane are properly placed and with the correct colours.

5.2 Function and installation

No modifications are made to the purchased equipment, meeting the requirements of installation.

5.3 Equipment, systems and installations

Equipment such as the glass cockpits are not connected to each so if one fails, the others can continue to operate and are able to perform the same tasks as the one that fails. If there is a power outage there are multiple redundancies throughout the equipment bay to ensure the plane is able to operate after any failure.

5.4 System power generation, storage and distribution

Many electrical systems have their own back up battery or batteries, along with the plane having its own back-up batteries to supply both engine and equipment.

5.5 External and cockpit lighting

The appropriate lighting for both internal and external lights have met the requirements along with an additional nose light.

5.6 Safety equipment

An ELT can be activated with a push of a button in a case of an emergency.

5.7 Equipment containing high energy rotors

All rotary components are placed far away from any passengers and have minimal to no chance of injuring the passengers in case of malfunction.

6 Subpart G – Flightcrew Interface and Other Information

6.1 Flightcrew interface

All required instruments have been installed, along with fully electrical power plant instruments. All instruments come with adjustable lighting and the cabin has lighting itself, that allow for the least amount of fatigue for eyes and body.

6.2 Installation and operation

There is a fully programmable annunciator that indicates and notifies the pilots and passengers of any problems within the plane. Each instrument also has labels for it to be easily identifiable and as to its minimum and max readings/capacities.

6.3 Instrument markings, control markings, and placards

Each instrument clearly defines their function and displays its capabilities.

6.4 Flight, navigation, and powerplant instruments

The glass cockpit that is installed along with their compatible autopilot system are of the latest technology available that indicate various systems and provides a clear display of the current readings for flight navigation and autopilot.

Part VIII

Book VIII: Cost and Budgeting

1 Project Development Costs

In order to estimate development and overall costs for DACION, the DAPCA-IV cost estimation model was referred upon in 'General Aviation Aircraft Design' by Snorri Gudmundsson [20]. The following areas were analyzed for cost related estimates.

- Avionics & System Cost
- Propulsion System Cost
- Structural Raw Material Cost
- Project Development & Manufacturing Cost
- Operational Cost
- Maintenance Cost

This model utilizes an experience effectiveness factor that accounts for learning curve in staff at DACION. This factor increases productivity in manufacturing and labour when staff become more experienced in the future. Beginning with an experience effectiveness of 0.8, a quantity discount factor is determined.

$$QDF = F_{exp}^{1.4427 * \ln * N} \quad (1.1)$$

The following expressions outline the aircraft's engineering cost, where the consumer price index rate was converted for the range of 1968 to 2018. Factors such as the general aviation aircraft type and, simplicity of design, and material selection costs are factored into this method. The following expressions take into consideration that the FALCO E-1 is certified as a 14 CFR Part 23 aircraft, has a simple flap system, does not utilize composite materials, has a tapered wing, and has an unpressurized cabin. Details of the parameters and numbers used are shown in the MATLAB code in the Appendices.

The following were used to determine the number of engineering man hours and cost of engineering:

$$H_{ENG} = 0.0396 * W_{airframe}^{0.791} * V_H^{1.526} * N^{0.183} * F_{CERT} * F_{CF} * F_{COMP} * F_{Press} \quad (1.2)$$

$$C_{ENG} = 2.0969 * H_{ENG} * R_{ENG} * CPI_{2018} \quad (1.3)$$

Cost required for man hours used to design tools and fixtures is outlined as follow:

$$H_{TOOL} = 1.0032 * (W_{airframe}^{0.764}) * (V_H^{0.899}) * (N^{0.178}) * Q_m^{0.066} * (F_{Taper}) * (F_{CF}) * (F_{COMP}) * (F_{Press}) \quad (1.4)$$

$$C_{TOOL} = H_{TOOL} * R_{TOOL} * CPI_{2018} \quad (1.5)$$

Manufacturing cost estimation for the assembly of the aircraft is as follow:

$$H_{MFG} = 9.6613 * (W_{airframe}^{0.74}) * (V_H^{0.543}) * (N^{0.524}) * (F_{CF}) * (F_{COMP}) * (F_{Press}) \quad (1.6)$$

$$C_{MFG} = 2.0969 * H_{MFG} * R_{MFG} * CPI_{2018} \quad (1.7)$$

The following expression outlines the cost for company development support such as administrations, human resources and logistics:

$$C_{DEV} = 0.06458 * (W_{airframe}^{0.873}) * (V_H^{1.89}) * (N_P^{0.346}) * (F_{CF}) * (F_{COMP}) * (F_{Press}) * (F_{CERT}) * CPI_{2018} \quad (1.8)$$

Total cost of flight testing is as follow:

$$C_{FT} = 0.009646 * (W_{airframe}^{1.16}) * (V_H^{1.3718}) * (N_P^{1.281}) * (F_{CERT}) * CPI_{2018} \quad (1.9)$$

Quality control ensures authenticity of the final product which protects the client and the seller. The cost to maintain quality control is as follow:

$$C_{QC} = 0.13 * C_{MFG} * F_{CERT} * F_{COMP} \quad (1.10)$$

Total cost of materials is,

$$C_{MAT} = 24.896 * (W_{airframe}^{0.689}) * (V_H^{0.624}) * (N^{0.792}) * (F_{CERT}) * (F_{Press}) * (F_{CF}) * CPI_{2018} \quad (1.11)$$

Total cost of certification is the summation of cost in development, testings, tooling productions and prototyping:

$$C_{CERT} = C_{ENG} + C_{DEV} + C_{FT} + C_{TOOL} \quad (1.12)$$

A cost analysis was done for all aspects of the avionics system from the instrument panel, to the lights on the exterior of the plane. As shown below in the table, the total cost of all avionics comes to a total of 108 026.85CAD. Not all products were originally in CAD so at the time of creating of this cost analysis, the exchange rate between USD, and Euro to the Canadian dollar was used. The grey highlighted areas signifies that the information for the manufacturer, distributor, or country of origin is not available.

Table 1.1: Avionics System Cost Analysis

Section	Component	Number of units	Price (CAD)	Manufacturer	Distributor	Country of Origin	Cost of All Units (CAD)
Instrument Panel	Glass cockpit	3	6,568.25	Aspen Avionics		USA	19,704.75
	Autopilot	1	32,841.25	Genesys Aerosystems		USA	32,841.25
	Yoke (Steering Wheel)	2	141.75	ACS Products co.	Aircraft Spruce Canada	USA	283.5
	Standard Switch Panel	1	1,033.00	Composite Design Inc.	Aircraft Spruce Canada	USA	1,033.00
	Trim Switch	1	347	Cygnet Aerospace	Aircraft Spruce Canada	USA	347
	Speed Brake	1	104.75		Aircraft Spruce Canada		104.75
	Master Switch	1	60.75	Carling Technologies	Aircraft Spruce Canada	Mexico	60.75
	Micro Relay	1	175		Aircraft Spruce Canada		175
	Ignition Switch	1	260.95	ACS Products co.	Aircraft Spruce Canada	USA	260.95
	Rocker Switches Mount (Backup Battery)	1	654	Control Vision	Aircraft Spruce Canada	USA	654
	Throttle	1	170.75		Aircraft Spruce Canada		170.75
	Flap Switch	1	125.75	Aircraft Specialty	Aircraft Spruce Canada	USA	125.75
	Panel Dimming Rheostat (No Knob, 0-15 Ohm)	1	79.75	Ohmite	Aircraft Spruce Canada	USA	79.75
	Knob	1	6.85		Aircraft Spruce Canada		6.85
	Cabin Heater	1	277.95	DC Thermal	Aircraft Spruce Canada	USA	277.95
	Cabin Heater Rheostat	1	141.75	C & D Associates inc.	Aircraft Spruce Canada	Canada	141.75
	Cabin Temperature Screen	1	333	Davtron Instruments	Aircraft Spruce Canada	USA	333
	LXNAV FES Unit	1	1,787.86	LZ Design Compnay/LXNAV	LXNAV	Slovenia	1,787.86
	Chronometer (Digital Clock)	1	260.1	Davtron Instruments	Pacific Coast Avionics Corporation	USA	260.1
	Programmable Annunciator	1	1,445.01	Aero Safety Systems	Pacific Coast Avionics Corporation	UK	1,445.01
	Hour Meter	1	41.5	Honeywell	Aircraft Spruce Canada	USA	41.5
	Transponder	1	2,358.00	Garmin	Pacific Coast Avionics Corporation	USA	2,358.00
	Flap Angle Indicator	1	256.16	U.M.A. Instruments	Pacific Coast Avionics Corporation	USA	256.16
	Cabin Pressure Indicator	1	798	U.M.A. Instruments	Aircraft Spruce Canada	USA	798
	Rudder pedals, 2 place	2	399		Aircraft Spruce Canada		798
	Parking Brake, pull	1	79.75		Aircraft Spruce Canada	USA	79.75
	NAVCOM	2	3,284.13	Garmin	Pacific Coast Avionics Corporation	USA	6,568.26
	iPad mount	1	74.75	Delkin Devices	Aircraft Spruce Canada	USA	74.75
	ELT	1	1,351.75	Artex	Sarasota Avionics and Maintenance	USA	1,351.75
Lights	Wing tip light	2	591.14	Whelen Engineering	Pacific Coast Avionics Corporation	USA	1,182.28
	Tail and Nose Lights	3	505.76	Whelen Engineering	Pacific Coast Avionics Corporation	USA	1,517.28
	Cabin Lights (with dimmer)	1	198.75	Superior Panel Technology	Aircraft Spruce Canada	USA	198.75
Other	Flight Management System	1	19,573.38				19,573.38
	Custom Instrument Panel	1	4,597.77				4,597.77
Hydraulics	Brake Valve	2	615	Parker Hannifin	Aircraft Spruce Canada	USA	1,230.00
	Lining (Cost per foot, units = length in feet)	25	1.1		Aircraft Spruce Canada		27.5
BMS	ORION 2 cell	180	1,680.00	Orion		USA	1,680.00
	Motor Controller	2	2,800.00	MGM COMPRO		Czech Republic	5,600.00
TOTAL COST							108,026.85

Initial cost breakdown of structures was completed based on raw materials. The table below lists the various components for raw material

Table 1.2: Structural Raw Material Cost Breakdown

Component	Manufacturer	Weight (kg)	Cost/kg	Total Cost
Outer Skin	Online Metals	30.62	\$ 55.60	\$ 572.68
Inner Skin	Online Metals	10.3	\$ 55.60	\$ 1,702.47
Structural Components (Stringers, Bulkheads, Ribs)	Online Metals	380.17	\$ 55.60	\$ 21,072.40
Interiors	Outsourced		N/A	\$ 8000.00
	Total Weight	210.09	Total Cost	\$ 31,347.55

Propulsion system cost breakdown per unit is listed below in Table 1.3.

Table 1.3: Propulsion System Cost Breakdown

Component	Number of Units	Cost of All Units (CAD)
Battery Packs	28	-
Battery Housing	2	1966.54
Alternator	1	2000
Emrax 268 Motor	2	18400
Propeller Blade and Hub	2	20000
Firewall	2	1000
Wiring (Cost per feet)	60	85.8

2 Operational Costs

Though the FALCO E-1 is built with quality components, maintenance and care is also an integral part of this family. As this is a pure electric aircraft, the cost per flight is significantly reduced. Annual fuel cost, a usual parameter in this domain shall be replaced with the cost for battery charging. The following parameters were considered for operational costs:

- Annual Maintenance Cost
- Storage Cost
- Annual Insurance Cost
- Annual Inspection Cost
- Electrical Cost per Flight Hour
- Total Operating Yearly Cost
- Recharge Cost

The annual maintenance cost of an aircraft is largely dependent on the complexity of the aircraft and the amount of flight hours per year flown. For the FALCO E-1, as a general aviation aircraft used as a trainer, the flight hours are extensive. An average annual flight time of 1040 hours was estimated [20].

$$C_{AP} = F_{MF} * R_{AP} * Q_{FLGT} \quad (2.1)$$

Maintenance to flight hour ratio below outlines specific variables to determine the ease of maintenance with the GA aircraft configuration. F1 is a parameter that offers a maintenance choice for the client to be supplied a mechanic. F2 determines the ease accessibility of the engine. F3 outlines the aircraft's landing gear configuration (fixed or retractable). F4 and F5 determines the type of radios installed (VFR or IFR). F6 determines the presence of integrated fuel tanks. F7 for flap systems selection (simple or complex system) and F8 for certification identifications.

$$F_{MF} = 0.3 + F_1 + F_2 + F_3 + F_4 + F_5 + F_6 + F_7 + F_8 + F_9 \quad (2.2)$$

Annual renewal costs include insurance, inspection and storage. If private owners choose to purchase a FALCO E-1 without a private hanger, rental spaces can be annually renewed at around 250\$

$$C_{STOR} = 12 * R_{STOR} \quad (2.3)$$

The annual insurance cost of an aircraft is dependant on the insured value of the aircraft which in often times is the purchasing cost of the aircraft.

$$C_{INS} = 500 + 0.015 * C_{AC} \quad (2.4)$$

Aircraft will at often times require regular inspection of their components. For the FALCO E-1, the motor, batteries, and composite propeller will require inspection and maintenance. Inspection costs are generally in the range of \$500 [20].

The FALCO E-1 utilizes a fully electrical propulsion system. The usual cost of fuel burned for gas turbine engine is more expensive than the FALCO E-1's electrical flight costs. The cost to fully recharge the battery is shown in Equation 2.5 below.

$$C_{batt} = \epsilon m_{batteries} * (\text{cost to recharge batteries (\$ per KWhr)}) \quad (2.5)$$

Assuming 1040 hours of flight annually with a given endurance of 2.35 hours, the number of recharges necessary per year can be found. By multiplying the cost of recharging the battery and the number of recharges required yearly, the annual cost of the FALCO E-1's electrical consumption is found.

$$C_{batt,annual} = C_{batt} * \frac{Q_{flgt}}{\text{Endurance}} \quad (2.6)$$

3 Master Cost Structure for FALCO E-1

With the analysis above, total cost breakdown can be separated into two categories: Project development cost and operational cost. This analysis model used a cost estimation based on a five year period. Each formula above yields a cost parameter that can be summed to a five year company cost estimation. The total project development cost divided by the number of aircrafts produced within five years will equate the unit cost of the FALCO E-1. To adhere to a profit margin, a ten percent increase in the FALCO E-1 unit cost. Using the operational cost analysis, the final cost per flight hour rate was also calculated.

Table 3.1: DACION Project Development Cost Analysis

Project Development Cost Type	Total Cost Over 5 Years [CAD]
Engineering	45,762,000
Development Support	1,928,000
Flight Test Operations	377,410
Manufacturing	283,050,000
Quality Control	36,797,000
Materials	45,108,000
Certify	48,067,000
Fixed Landing Gear Discount	7,500,000
Total Project Development Cost	453,590,000
Aircraft Unit Cost	450,000
Aircraft Sale Price	495,000

Table 3.2: DACION Operational Cost Analysis

Air Speed [m/s]	64
Air Density [kg/m^3]	0.9268
Wing Area [m^2]	13.975
Angle of Attack [deg]	12
Flap Deflection [degree + Down]	30
Lift Force [N]	64607.3
Drag Force [N]	7052.32
Lift Coefficient	2.4356
Drag Coefficient	0.2658
Aerodynamic Efficiency	0.6475

Part IX

Book X: Marketing

1 Electric Aircraft Market Overview

The global electric aircraft market size is projected to observe an extensive growth in the coming years due to increasing strict emission norms related to aircraft industry coupled with increased investment in more efficient power electronics and high energy density batteries, and the requirement for new aircraft to meet the global air traffic demand. In addition, lower cost of ownership for the electric aircraft, is expected to boost the market in the near future ("Electric Aircraft Market Size, Share | Industry Report, 2025", 2019). Governments' initiatives to increase the adoption of solar power and/ or electric aircrafts to decrease air pollution encourages new market entrants. This consequently reduces prices of electric aircrafts as the prices of solar cells and/or batteries are expected to decrease in near future across the globe. Additionally, all-electric aircraft is expected to increase steadily in near future owing to growing usage of autonomous systems, improved aircraft performance, reduced gas emissions, airport noise, and reduced maintenance and operational costs. Furthermore, the demand for fuel-efficient and eco-friendly aircraft is anticipated to be the fundamental driving factor that forces the shift to the production of electrically propeller aircrafts.

2 Marketing Strategy

This section of the report aims to outline the team's marketing strategy towards the FALCO E-1. The section will give insight on the product, place, promotion and price.

3 The Product

The FALCO E-1 is to be one of the world's first electric regional passenger plane. The aircraft designed is to accommodate four passengers for commercial, private and flight school purposes. The FALCO E-1 has a stunning world class cabin and a luxurious interior; nevertheless, capable of an impressive three-hour flight time and two and a half hour of air time whilst cruising at 250 km/hr. Our aircraft has the best in class range of 349 nm exceeding the MR&O by 39 nm. The FALCO E-1 is to equip an innovative design of a single electric engine with a deployable emergency motor. This innovative design addresses the world's biggest concern when flying a single engine aircraft.

4 Location & Place

Often you will hear marketers saying that marketing is about putting the right product, at the right price, at the right place, at the right time. It's critical then, to evaluate what the ideal locations are to convert potential clients into actual clients. Today, even in situations where the actual transaction doesn't happen on the web, the initial place potential clients are engaged and converted is online. For that reason, DACION will insure a dedicated 360-degree visualizer for its FALCO E-1. The visualizer can inherit BMW's Build and Price concept for different sub model lines and features. Interims of manufacturing, an ideal location would be GMC's plant in Oshawa. This would restore many Canadian jobs that were taken away with GMC's closure. The plant is at an ideal location with 10 million square feet of factory floor.

5 Promotion

DACION team will participate in air shows to gain brand exposure. In addition, social media such as Facebook, Instagram, twitter and YouTube will be used at launch. The team also is preparing an ad video alongside a poster for the FALCO E-1 that will be presented to bombardier on the 4th of April 2019; this could encourage word of mouth. The target audience includes aviation enthusiasts, private pilots, regional small scale airlines and flight schools.

6 Price

The pricing strategy used is Price skimming. The product will be listed at a high price as it is first introduced to the market, and then lowering the price later when the product has reached maturity in the life cycle. This will give the funding needed to produce more planes. In addition, DACION will seek the government for subsidy and support as DAICON is Canadian based and aims to reduce emissions by being a fully electric plane. The FALCO E-1's is yet to be determined after the economics sub team finalize total costs.

References

- [1] Recreational Flying. How do you choose the best wing tip device, 2014.
- [2] National Aeronautics and Space Administration. Winglets. NASA, 2015.
- [3] Gregg Stansbery. 767-400 Raked Wingtips, 2003.
- [4] VMS Racing. VORTEX GENERATOR NASA ROOF FIN KIT VERSION BLACK. THE REAL DEAL! VMS Racing, 2017.
- [5] Pipistrel-USA. Pipistrel Virus LSA Aircraft NASA CAFE Record Holder. Online, 2019.
- [6] Norman S. Currey. *Aircraft Landing Gear Design: Principles and Practices*. American Institute of Aeronautics and Astronautics, Inc, 1988.
- [7] Goodyear. *Global Aviation Tires*. The Goodyear Tire and Rubber Company, June 2018.
- [8] Hodge Flight Services. *Instrument Panel Instruments Cessna 172*. Hodge Flight Services, 2019.
- [9] TRC Simulators. *Dimensions*. TRC Simulators, 2019.
- [10] Aspen Avionics. *Glass Cockpit*. Aspen Avionics, 2019.
- [11] Genesys Aerosystems. *System 55X Autopilot*. Genesys Aerosystems, 2019.
- [12] AVIDYNE. *Flight Management System*. AVIDYNE, 2018.
- [13] Aircraft Spruce. *Rocker Panel*. Aircraft Spruce, 2019.
- [14] COMPRO. *Motor Controller*. COMPRO, 2019.
- [15] Aircraft Spruce. *Brushless Cabin Heater*. Aircraft Spruce, 2019.
- [16] *Contra Rotating Propeller for Light Aircraft*. CONTRA ELECTRIC PROPULSION LTD., 2018.
- [17] Asm.matweb.com. ASM Material Data Sheet. Online, 2019.
- [18] Evonik Industries. Plexiglas Reference Sheet. Online, 2019.
- [19] Heys USA. Smart luggage® 21. Online, 2019.
- [20] Snorri Gudmundsson. *General Aviation Aircraft Design - Applied Methods and Procedures*. Elsevier, 2014.
- [21] United States. *Aircraft Propeller*. Bureau of Naval Personnel, 1954.
- [22] Canadian Aviation Regulations (CARs). Part V - Airworthiness Manual Chapter 523 - Normal, Utility, Aerobatic And Commuter Category Aeroplanes. Government of Canada, 2019.
- [23] Flight Level Engineering. ProAdvice 3: AILERON SIZING . Great Owl Publishing, 2011.

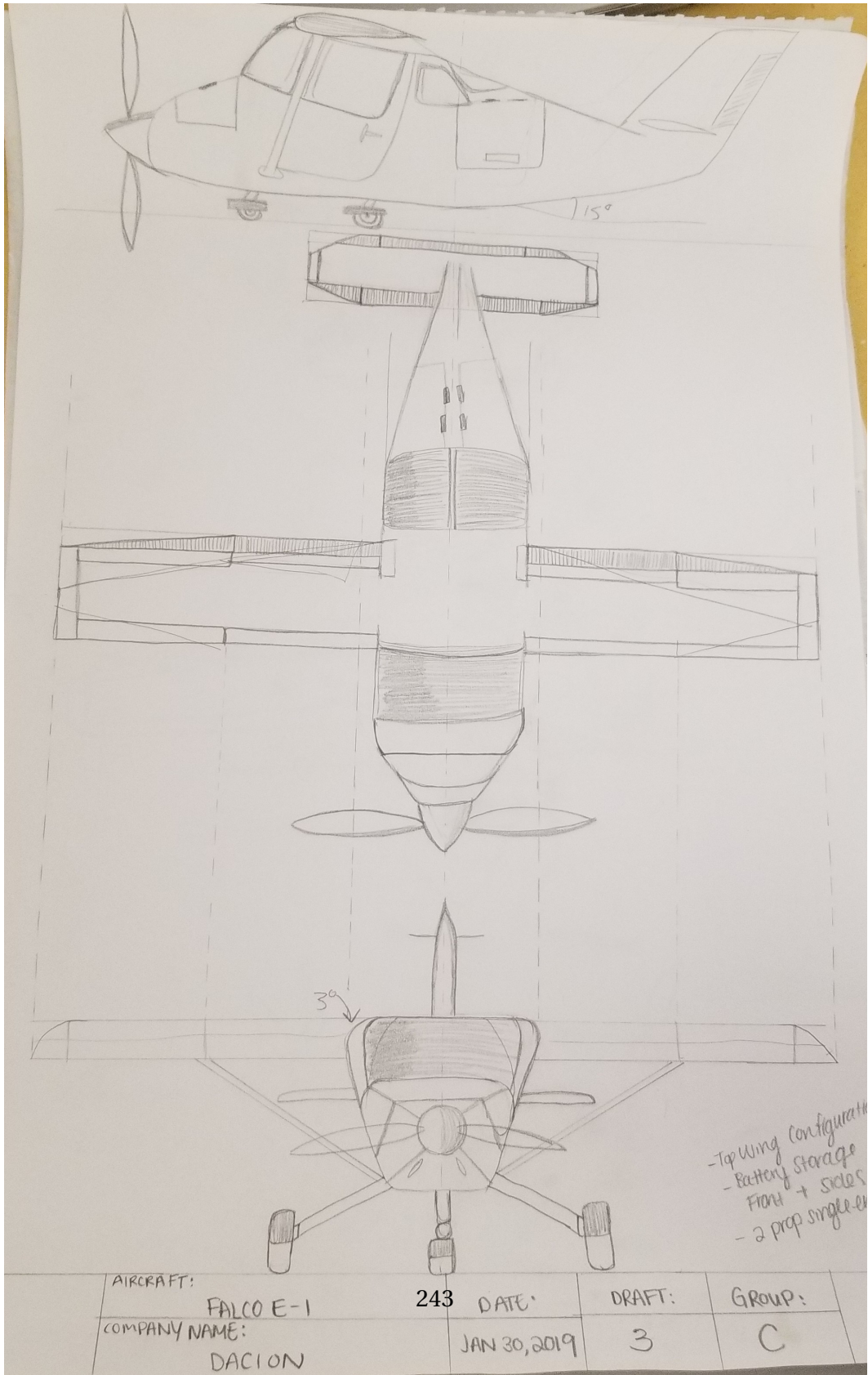
- [24] David L. Kohlman. FLIGHT TEST DATA FOR A CESSNA CITATION. University of Kansas Center for Research, 1974.
- [25] LEAP CFD Team. Tips Tricks: Estimating the First Cell Height for correct Y. LEAP Australia Pty Ltd, 2019.
- [26] Daniel P. Raymer. *Aircraft Design: A Conceptual Approach*. American Institute of Aeronautics and Astronautics, Inc, 1992.
- [27] William Ching Hin Lo. *AER621, Aircraft Structure Design: Landing Gear*. William Ching Hin Lo, April 2018.
- [28] ASM Aerospace Specification Metals Inc. *Aluminum 7075-T6*. ASM Aerospace Specification Metals Inc., 2018.
- [29] AZO Materials. *AISI 4340 Alloy Steel*. AZoM, 2018.
- [30] ASM Aerospace Specification Metals Inc. *Titanium Alloy Ti-10V-2Fe-3Al*. ASM Aerospace Specification Metals Inc., 2018.
- [31] Cessna Aircraft Company. *C172s POH*. Cessna Aircraft Company, December 2007.
- [32] Grove. *RV Nose Wheel*. Grove Aircraft Landing Gear Systems Inc., 2018.
- [33] Canadian Aviation Regulations. *Part V - Airworthiness Manual Chapter 523 - Normal, Utility, Aerobatic And Commuter Category Aeroplanes*. Canadian Aviation Regulations, 2019.
- [34] Grove. *600x6 Wheel and Brake Kit*. Grove Aircraft Landing Gear Systems Inc., 2018.
- [35] Confor Foam. *CONFOR FOAM SEAT CUSHION*. Confor Foam., 2018.
- [36] MIT. *Flight Thrust, Power, and Energy Relations*. MIT Publishing, 2014.
- [37] NASA. *Friction Characteristics of Three 30 x 11.5-14.5, Type VIII, , Aircraft Tires With Various Tread Groove Patterns and Rubber Compounds*. NASA Publishing.
- [38] Chris Dubuque Ingrid Wakefield. *Exceeding Tire Speed Rating During Takeoff*. The Boeing Company.
- [39] Sion Power. *Licerion Modular Power Pack Specifications*. Sion Power Corporation, 2018.
- [40] Matt Pressman. *Understanding Tesla's Lithium Ion Batteries*. Evannex, 2017.
- [41] Tadiran Lithium Batteries. *MODEL TL-5930 DATASHEET*. Digi-Key, 2018.
- [42] Cadex Electronics. *Basics about Discharging*. Battery University, 2012.
- [43] Environment Canada. *Sunshine in Canadian Cities: Average Hours & Days a Year*. Current Results Publishing Ltd., 2019.
- [44] Cessna Aircraft. *CESSNA MODEL 172P Section 8: Airplane Handling, Service & Maintenance*. Cessna Aircraft, 1982.

- [45] U.S. Standard Atmosphere. *U.S. Standard Atmosphere Air Properties - Imperial*. Engineering Toolbox, 2003.
- [46] Sion Power. *Graphenano and Grabat launch graphene-based batteries*. Graphenano Technologies, 2018.
- [47] EV & More. *PRODUCTION OF REVOLUTIONARY GRAPHENE BATTERIES BEGINS IN SPAIN*. Graphenano Technologies, 2016.
- [48] Sion Power. *Licerion Battery Pack Datasheet*. Sion Power Marketing Servicess, 2018.
- [49] *The History of Aluminum Propeller*. Hartzell Propeller., 2017.
- [50] B. D. Rutkay. *A Process for the Design and Manufacture of Propellers for UAV*. 2014.
- [51] *How a Composite Propeller Blade is Made*. Hartzell Propeller, 2016.
- [52] David R. Greatrix. *Powered Flight - The Engineering of Aerospace Propulsion*. Springer, 2012.
- [53] Professor Chung. *Stability and Control*. Ryerson University, January 2018.
- [54] unknown. *Lab 8 Notes- Basic Aircraft Design Rules*. April 2006.
- [55] John McIver B.Eng.(Aero). *Cessna Skyhawk II / 100 Performance Assessment*. Temporal, January 2003.
- [56] Aircraft Spruce. *Power Panel*. Aircraft Spruce, 2019.
- [57] Aircraft Spruce. *ACS Control Wheel*. Aircraft Spruce, 2019.
- [58] Aircraft Spruce. *Trim Switch*. Aircraft Spruce, 2019.
- [59] Aircraft Spruce. *Speed Brake*. Aircraft Spruce, 2019.
- [60] Aircraft Spruce. *Mini Fuse and Micro Relay*. Aircraft Spruce, 2019.
- [61] Aircraft Spruce. *Split Master Switch*. Aircraft Spruce, 2019.
- [62] Aircraft Spruce. *Key Ignition Switch*. Aircraft Spruce, 2019.
- [63] Aircraft Spruce. *Flap Switch*. Aircraft Spruce, 2019.
- [64] Aircraft Spruce. *Temperature Rheostat*. Aircraft Spruce, 2019.
- [65] Aircraft Spruce. *Cabin Tmeprature Screen*. Aircraft Spruce, 2019.
- [66] LXNAV. *LXNAV FES Unit*. LXNAV, 2017.
- [67] Aircraft Spruce. *Panel Light Dimming Rheostat*. Aircraft Spruce, 2019.
- [68] Garmin. *Digital Transponder*. Pacific Coast Avionics, 2019.
- [69] U.M.A. Instruments. *Flap Position Indicator*. Pacific Coast Avionics, 2019.

- [70] U.M.A. Instruments. *Cabin Pressure Indicator*. Aircraft Spruce, 2019.
- [71] Aircraft Spruce. *Rudder Pedals*. Aircraft Spruce, 2019.
- [72] Honeywell. *Hour Meter*. Aircraft Spruce, 2019.
- [73] PS Engineering. *NAVCOM*. PS Engineering, 2019.
- [74] Fat Gecko. *iPad Mount*. Aircraft Spruce, 2019.
- [75] Artex. *ELT*. Sarasota Avionics and Maintenance, 2015.
- [76] Superior Panel Technology. *Cabin Lighting*. Aircraft Spruce, 2019.
- [77] Cleveland. *Brake Valve*. Aircraft Spruce, 2019.
- [78] Aircraft Spruce. *Lining*. Aircraft Spruce, 2019.

7 Appendices

A Preliminary Designs



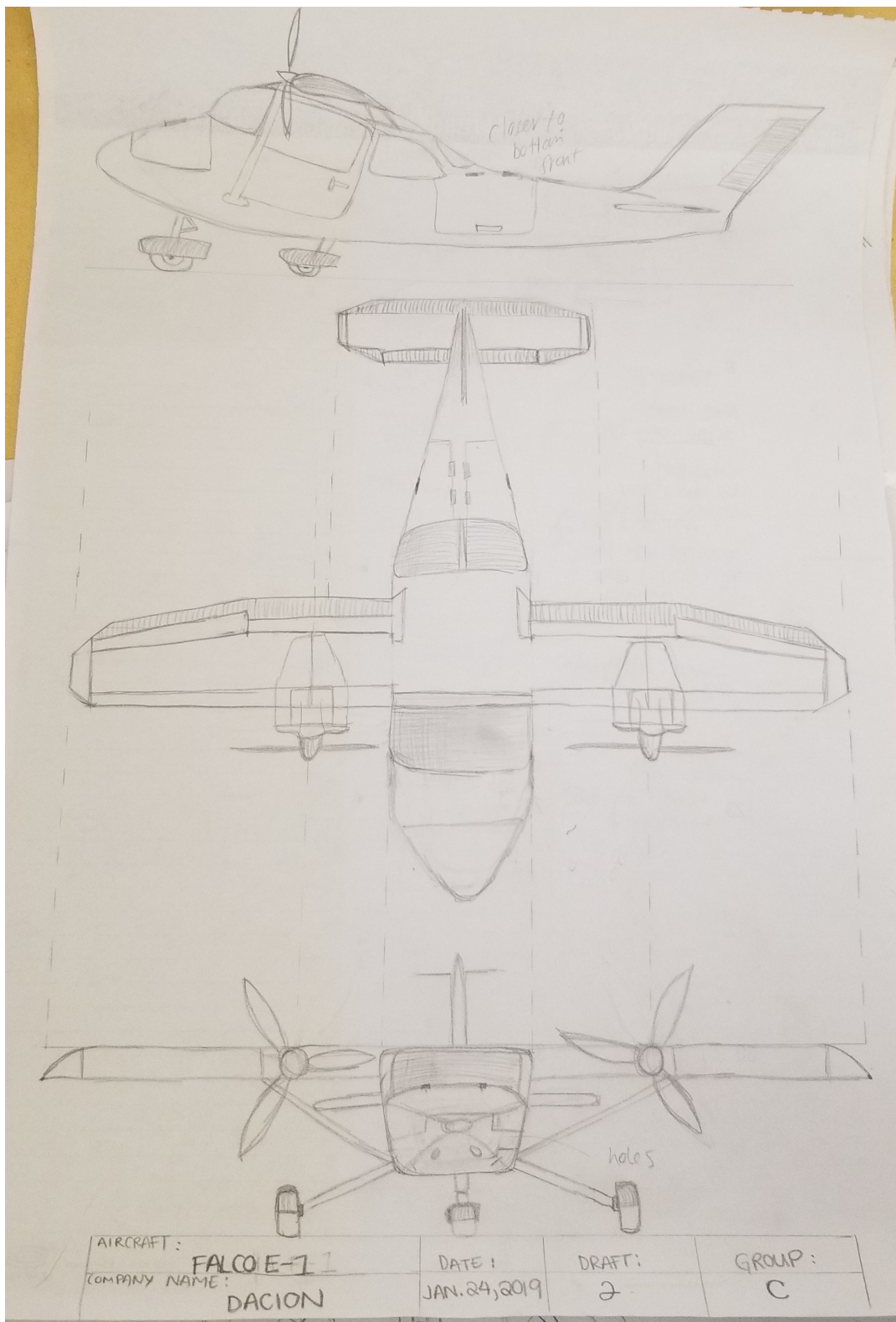


Figure A.2: Concept Design 2

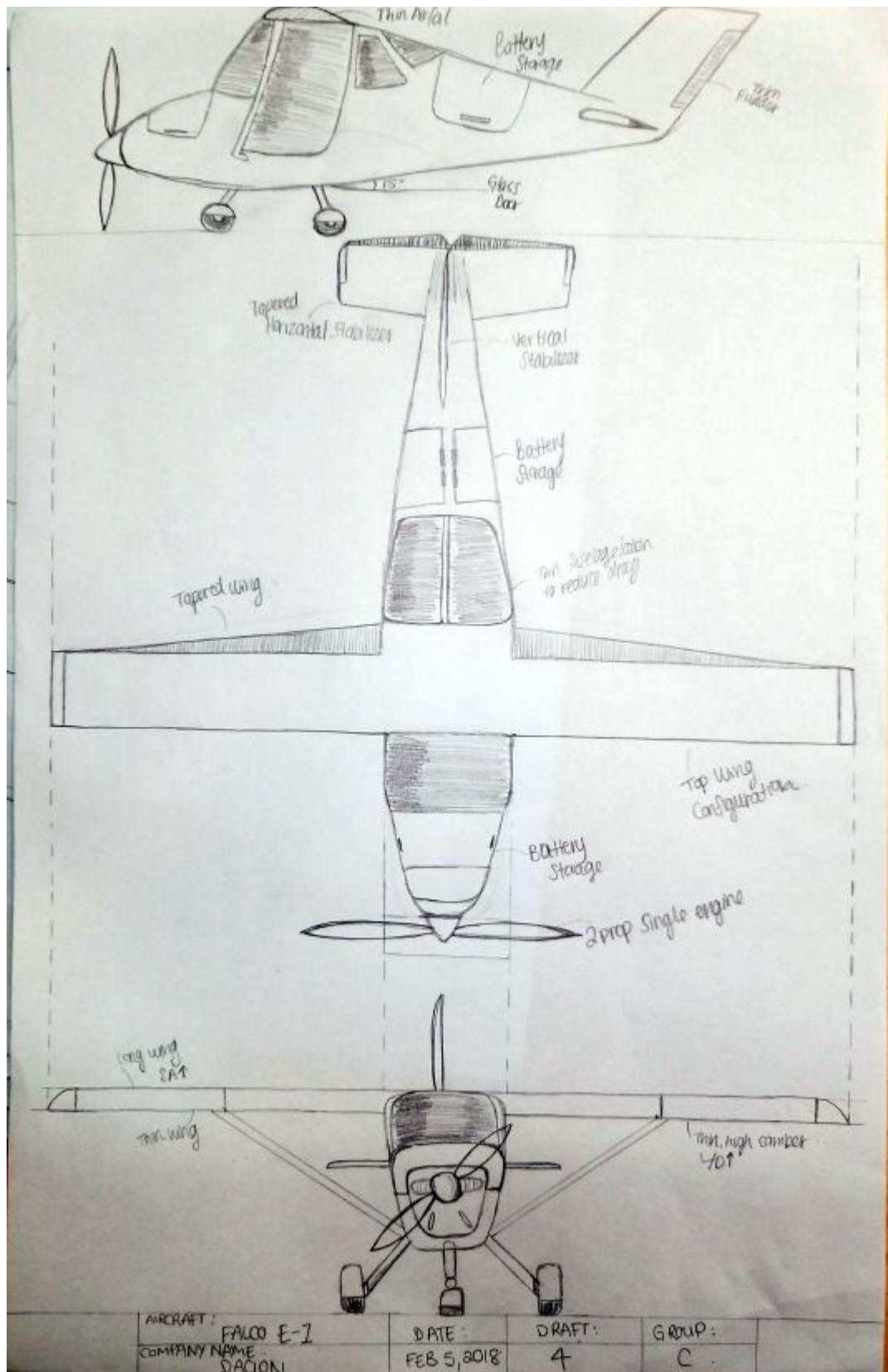


Figure A.3: Final Preliminary Sketch

B Avionics



(a) Glass Cockpit[10]



(b) Autopilot[11]



(a) Switch Panel [56]



(b) Yoke[57]



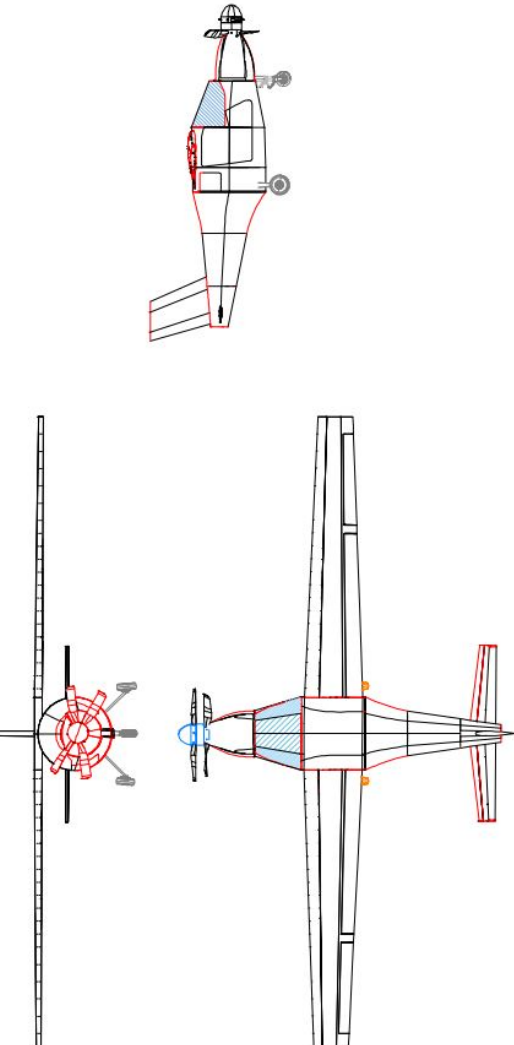
(a) Trim Switch[58]



(b) Speed Brake[59]

REV.	DATE	BY	REVISION DESCRIPTION

		TITLE: Falco E-1	
		DACION	
		MATERIAL: Composites	
			
FALCO E-1 NOTICE : This drawing is the exclusive property of DACION INC. & is disclosed to you in strict confidence & with the understanding that it is not to be reproduced, copied, or used except for the purpose of producing tools or products exclusively for DACION INC. Copies of this drawing are to be made only when necessary for the purpose stated above & all copies must contain this notice.		SCALE: FULL	SHEET: 1 of 1
		PREPARED BY: NASEH NAYEM	WORK ORDER: CDD 1.23
		DESIGN BY: NASEH NAYEM	DATE: Apr-4-2019
		DRAWING/PART NUMBER:	





(a) Micro Relay[60]



(b) Master Switch[61]



(a) Ignition Switch[62]



(b) Flap Switch[63]



(a) Cabin Heater Rheostat[64]



(b) Cabin Temperature Screen[65]

Rheostat.PNG Rheostat.PNG



(a) LXNAV FES Unit[66]



(b) Dimming Rheostat[67]



(a) Transponder[68]



(b) Flap Indicator[69]



(a) Cabin Pressure Indicator[70]



(b) Rudder Pedals[71]



(a) Hour Meter[72]



(b) NAVCOM[73]



(a) iPad Mount[74]



(b) ELT[75]



(a) Flight Management System[12]



(b) Cabin Lights (with dimmer)[76]



(a) Brake Valve[77]



(b) Hydraulic Fluid Lining[78]

C Aerodynamics

C.1 Additional Graphs

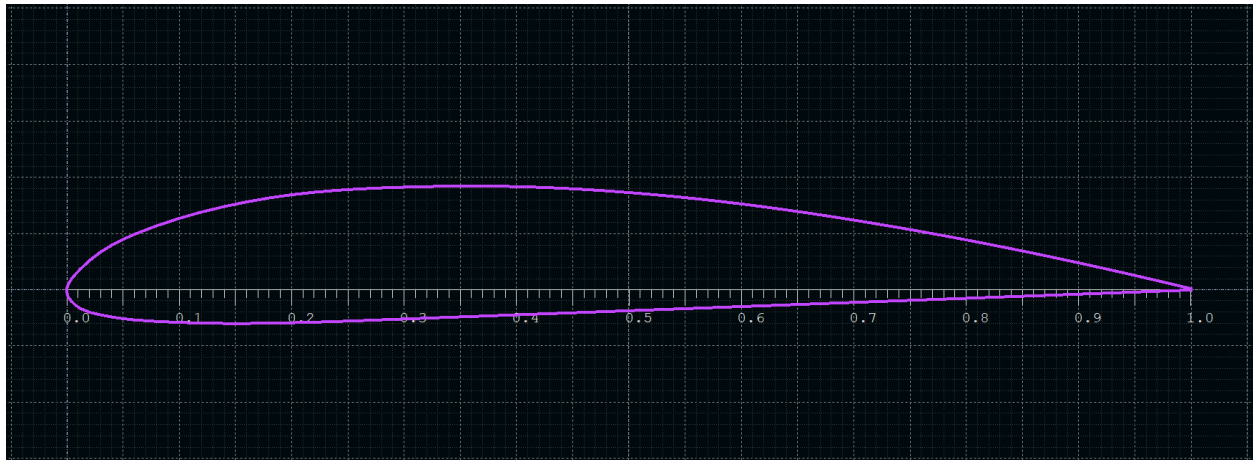


Figure C.1: Clark Y Airfoil Geometry

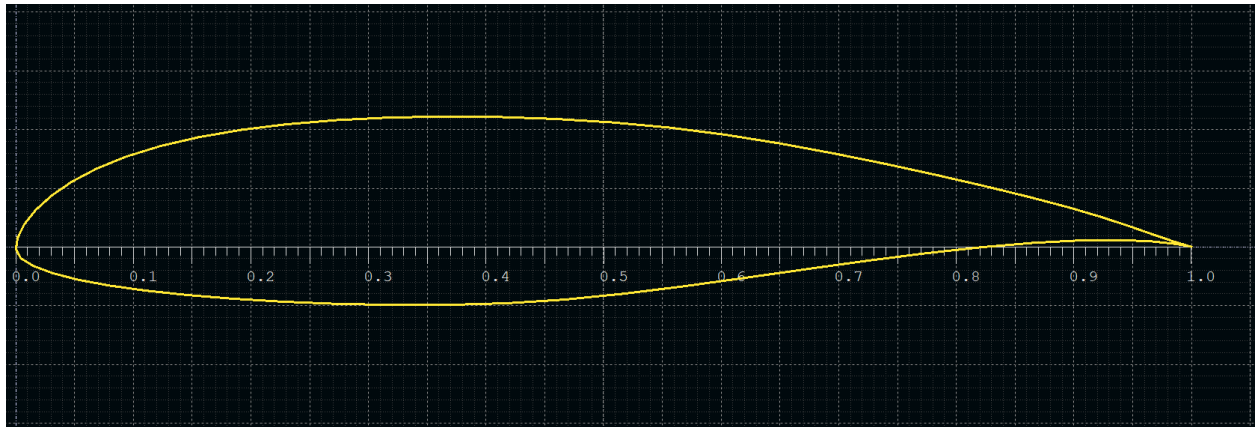


Figure C.2: Airfoil Outlines of

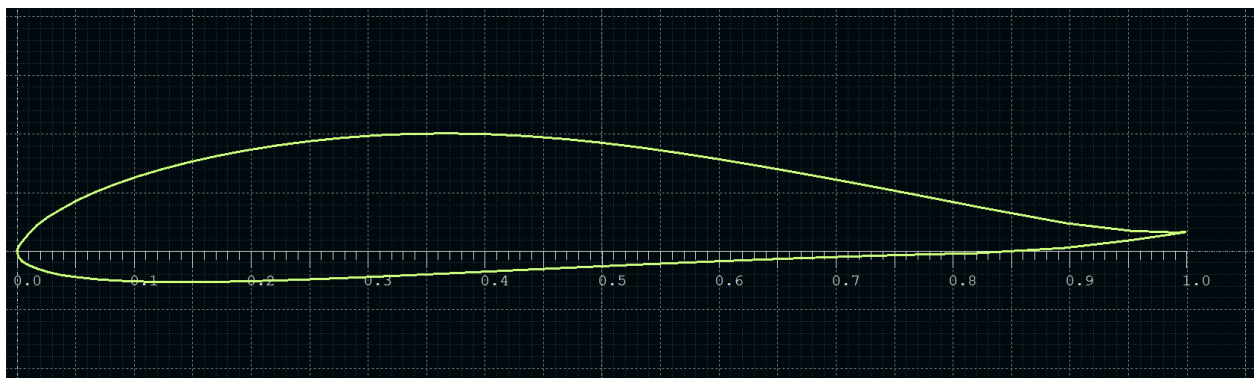


Figure C.3: Airfoil Outlines of

D Propulsion

D.1 Motor Technical Data

Technical data	Type														
	EMRAX 268 / 268 VHML High Voltage			EMRAX 268 / 268 VHML Medium Voltage			EMRAX 268 / 268 VHML Low Voltage								
Air cooled = AC Liquid cooled = LC Combined cooled = Air + Liquid cooled = CC	AC	LC	CC	AC	LC	CC	AC	LC	CC						
Ingress protection	IP21	IP65	IP21	IP21	IP65	IP21	IP21	IP65	IP21						
Cooling medium specification (Air Flow = AF; Inlet Water/glycol Flow = WF; Ambient Air = AA) If inlet WF temperature and/or AA temperature are lower, then continuous power is higher.	AF=20m/s ; AA=25°C	WF=8l/mi n at 50°C; AA=25°C	WF=8l/mi n at 50°C; AA=25°C	AF=20m/s ; AA=25°C	WF=8l/mi n at 50°C; AA=25°C	WF=8l/mi n at 50°C; AA=25°C	AF=20m/s ; AA=25°C	WF=8l/mi n at 50°C; AA=25°C	WF=8l/mi n at 50°C; AA=25°C						
Weight [kg]	19,9	20,3	20,3	19,9	20,3	20,3	19,9	20,3	20,3						
Diameter ø / width [mm]					268/91										
Maximal battery voltage [Vdc] and full load/no load RPM	700 Vdc (3200/3800 RPM)			680 Vdc (4700/5500 RPM)			130 Vdc (2300/2900 RPM) 250 Vdc (4500/5500 RPM)								
Peak motor power at max RPM (few min at cold start / few seconds at hot start) [kW]	160			230			115 (at 2300 RPM load); 220 (at 4500 RPM load)								
Continuous motor power (at 2000-4000 RPM) depends on the motor RPM [kW]	40 - 75	40 - 80	50 - 85	40 - 80	40 - 90	50 - 110	40 - 75	40 - 80	50 - 90						
Maximal rotation speed [RPM]	4500 RPM (5500 RPM peak for a few seconds)														
Maximal motor current (for 2 min if it is coded as described in Manual) [Arms]	270			400			1000								
Continuous motor current [Arms]	125			190			500								
Maximal motor torque (for a few seconds) [Nm]	500														
Continuous motor torque [Nm]	250														
Torque / motor current [Nm/1Aph rms]	2,0			1,4			0,5								
Maximal temperature of the copper windings in the stator and max. temperature of the magnets [°C]	120														
Motor efficiency [%]	92 - 98														
Internal phase resistance at 25 °C [mΩ]	26			11,5			1,7								
Input phase wire cross-section [mm²]	10,2			15,2			38								
Wire connection	star														
Induction in Ld/Lq [μH]	292/273			126/118			17/15,9								
Controller / motor signal	sine wave														
AC voltage between two phases [Vrms/1RPM]	0,2320			0,1520			0,0560								
Specific idle speed (no load RPM) [RPM/1Vdc]	5,4			8,2			22,2								
Specific load speed (depends on the controller settings) [RPM/1Vdc]	4,5 - 5,4			7 - 8,2			18 - 22,2								
Magnetic field weakening (for higher RPM at the same power and lower torque) [%]	up to 100														
Magnetic flux - axial [Vs]	0,1014			0,0664			0,0245								
Temperature sensor in the motor	qty 81/210														
Number of pole pairs	10														
Rotor inertia (mass dia=195mm, m=9,8kg) [kg*cm²]	932														
Bearings (front:back) – SKF/FAG	6206:6206 (for radial forces) or 6206:7206 (for axial-radial forces; for pull mode; e.g. for air propeller) or 6206:3206 (for axial-radial forces; for pull-push mode; »O« orientation, $\alpha=25^\circ$); other bearings are possible (exceptionally)														
EMARX 268 Very High Mechanical Loads (VHML)	stronger motor shaft and bearings (6207:6207 for radial forces)			stronger motor shaft and bearings (6207:3207 for radial-axial; for pull-push mode; »O« orientation, $\alpha=25^\circ$ and for pull mode; e.g. for air propeller)											

*EMRAX 268 VHML Low Voltage version always has 2 sequences of phase connectors (2x UWV).

**Controller for EMRAX 268 Low Voltage motor should have very high peak and continuous motor current (1000 Arms peak and 500 Arms continuous). It is difficult to find such a high current controller in the global market. The most suitable is emDrive 500 from the Emsiso Company, which has 500 Arms continuous and 800 Arms peak motor current. Another possibility to get a high enough motor current is to

Figure D.1: EMRAX268 Technical Data Table

Type	EMRAX 228 High Voltage			EMRAX 228 Medium Voltage			EMRAX 228 Low Voltage								
Technical data	AC	LC	CC	AC	LC	CC	AC	LC	CC						
Air cooled = AC Liquid cooled = LC Combined cooled = Air + Liquid cooled = CC	AC	LC	CC	AC	LC	CC	AC	LC	CC						
Ingress protection	IP21	IP65	IP21	IP21	IP65	IP21	IP21	IP65	IP21						
Cooling medium specification (Air Flow = AF; Inlet Water/glycol Flow = WF; Ambient Air = AA) If inlet WF temperature and/or AA temperature are lower, then continuous power is higher.	AF=20m/s ; AA=25°C	WF=8l/min at 50°C; AA=25°C	WF=8l/min at 50°C; AA=25°C	AF=20m/s ; AA=25°C	WF=8l/min at 50°C; AA=25°C	WF=8l/min at 50°C; AA=25°C	AF=20m/s ; AA=25°C	WF=8l/min at 50°C; AA=25°C	WF=8l/min at 50°C; AA=25°C						
Weight [kg]	12,0	12,3	12,3	12,0	12,3	12,3	12,0	12,3	12,3						
Diameter ø / width [mm]	228/86														
Maximal battery voltage [Vdc] and full load/no load RPM	670 Vdc (5300/6500 RPM)			470 Vdc (5170/6500 RPM)			130 Vdc (4400/5200 RPM)								
Peak motor power at max RPM (few min at cold start / few seconds at hot start) [kW]	100														
Continuous motor power (at 3000-5000 RPM) depends on the motor RPM [kW]	28 - 42	28 - 42	35 - 55	28 - 42	28 - 42	35 - 55	28 - 42	28 - 42	35 - 55						
Maximal rotation speed [RPM]	5500 (6500 RPM peak for a few seconds)														
Maximal motor current (for 2 min if cooled as described in Manual) [Arms]	240			340			900								
Continuous motor current [Arms]	115			160			450								
Maximal motor torque (for a few seconds) [Nm]	240														
Continuous motor torque [Nm]	125														
Torque / motor current [Nm/1Aph rms]	1,1			0,75			0,27								
Maximal temperature of the copper windings in the stator and max. temperature of the magnets [°C]	120														
Motor efficiency [%]	92 – 98														
Internal phase resistance at 25 °C [mΩ]	18			8,0			1,12								
Input phase wire cross-section [mm²]	10,2			15,2			38								
Wire connection	star														
Induction in Ld/Lq [μH]	177/183			76/79			10,3/10,6								
Controller / motor signal	sine wave														
AC voltage between two phases [Vrms/1RPM]	0,0730			0,0478			0,0176								
Specific idle speed (no load RPM) [RPM/1Vdc]	9,8			14			40								
Specific load speed (depends on the controller settings) [RPM/1Vdc]	8 – 9,8			11 – 14			34 – 40								
Magnetic field weakening (for higher RPM at the same power and lower torque) [%]	up to 100														
Magnetic flux – axial [Vs]	0,0542			0,0355			0,0131								
Temperature sensor in the motor	kty 81/210														
Number of pole pairs	10														
Rotor inertia (mass dia=175mm, m=5,5kg) [kg*cm²]	421														
Bearings (front:back) - SKF/FAG	6206:6206 (for radial forces) or 6206:7206 (for axial-radial forces; for pull mode; e.g. for air propeller) or 6206:3206 (for axial-radial forces; for pull-push mode; »O« orientation, $\alpha=25^\circ$); other bearings are possible (exceptionally)														

Figure D.2: EMRAX228 Technical Data Table

E MATLAB

E.1 Aerodynamics

Contents

- Criteria

- Wing Geometry and Weight Characteristics
- Aerodynamic Coefficients
- Aileron Sizing Determination

```
clc; clear all;
```

Criteria

Plane must have a minimum roll rate of 60deg/4s for landing and 60deg/5s for takeoff

Wing Geometry and Weight Characteristics

```
MTOW = 1157;           % [kg]
Vstall = 20.5778; %16.9767;           % [m/s]

b = 13;
S = 13.975;           % [m^2]
AR = 12.093;
Sht = 0.107*S;         % [m^2]
Svt = 0.202*S;         % [m^2]

Cr = 1.35;           % [m]
Ct = 0.8;             % [m]
Cbar = (Cr+Ct)/2;       % [m]
lambda = Ct/Cr;

delta_a = 20;          % [deg]

% Aileron chord is initially placed at 25% chord
% Based on sectional moment distribution b2 is placed at 5.5m half span
y2 = 6;               % [m]

% Estimated using Cessna 172
% Ixx = 948;           % [slugs*ft^2]
Ixx = 1285.3154166; % [kg*m^2]
```

Aerodynamic Coefficients

```
% Approximated using XFLR5 assuming linear slope 0-10 deg
a_w = ((1.72-0.409)/15)*180/pi;      % [/rad]
cd0 = 0.005;
```

```
% Estimated from XFLR5 airfoil analysis using 10deg deflection
% Approximating using a linear slope
cl_del_a = ((1.439-0.919)/10)*180/pi;      % [/rad]
```

Aileron Sizing Determination

syms y1

y1 = 4;

```
% Roll Dampening Coefficient
Cl_p = -(((a_w+cd0)*Cr*b)/(24*S))*(1+3*lambda);
```

```
% Roll Authority Coefficient
```

```
Cl_del_a = ((cl_del_a*Cr)/(S*b))*((y2^2-y1^2)+(4*(lambda-1)/(3*b))*(y2^3-y1^3));
```

```
% Approach Speed
```

```
Vapp = 1.3*Vstall;
```

```
% Roll Rate
```

```
p = -(Cl_del_a/Cl_p)*delta_a*(2*Vapp/b)
```

```
% y1 = double(solve(p==12.5,y1))
```

```
% y1 = y1(2)
```

p =

34.1376

E.2 Stability

```
1 %X = NOSE GEAR FORCE
2 %Y = MAIN GEAR FORCE
```

3

```
4 cg = PositionCG;
```

```
5 xn = 1.05;
```

```
6 xm = 3.4;
```

```
7 ncg = cg-xn;
```

```
8 mcg = xm-cg;
```

9

```
10 syms x y
```

```

11 eqn1 = x + y == 1156.62*9.81; %FORCES
12 eqn2 = (x*ncg) - (y*mcg) == 0; %MOMENTS
13
14 [A,B] = equationsToMatrix([eqn1, eqn2], [x, y]);
15 result = linsolve(A,B);
16
17 if paxNo == 4;
18     fprintf('4 PAX Case \n')
19 else if paxNo == 3;
20     fprintf('3 PAX Case \n')
21 else if paxNo == 2;
22     fprintf('2 PAX Case \n')
23 else if paxNo == 1;
24     fprintf('1 PAX Case \n')
25 end
26 end
27 end
28 end
29
30 fprintf(' CG = %.2f m \n', cg)
31 fprintf(' Wing CG = %.2f m \n', cg-(cg-WingA))
32 fprintf(' Nose Gear = %.2f m \n', xn)
33 fprintf(' Tail Gear = %.2f m \n', xm)
34 fprintf(' %.2f \n', result(1))
35 fprintf(' %.2f \n', result(2))
36
37 if result(1)> (1156.62*9.81*0.36)
38
39     fprintf('sevag is poopoo head \n\n')
40
41 end

```

1 % 2 PAX Case
2 paxNo = 2;
3 %Parameters meters
4 A= 1.35 %Root Chord Wing
5 AA= 0.9 %Root Chord Tail
6 B= 0.8 %Tip Chord Wing
7 BB= 0.86 %Tip Chord Tail
8 S= 0.138 %Sweep Distance Wing
9 SS= 0.018 %Sweep Distance Tail
10 Y= 6.5 %Half Span Wing
11 YY= 1.1 %Half Span Tail
12 D= 4.4 %Wing root to Tail root LE
13 SM= 0.12 %Desired Static Margin

```

14
15 %Weights in kilograms
16 MainGear=24.673;
17 NoseGear=30.085;
18
19 Pilot=60.7185;
20 Passenger1=60.7185;
21 Passenger2=0;
22 Passenger3=0;
23
24 Bag1=30;
25 Bag2=30;
26 Bag3=0;
27 Bag4=0;
28
29 BatteryNose=123.25*1.25
30 BatteryFuse=200.606*1.25
31
32 Avionics=40.0454
33 Motor=20.3*1.75
34 Tails=25
35 Wing=125
36 TotalWt=1089*9.81
37
38 MotorEm=12.3
39 MechEm=20
40
41 %Arm Distances
42 MainGearA=xm
43 NoseGearA=xn
44 PilotA=1.189;
45 Passenger1A=1.189;
46 Passenger2A=2.059;
47 Passenger3A=2.059;
48
49 Bag1Arm=2.1;
50 Bag2Arm=2.1;
51 Bag3Arm=2.1;
52 Bag4Arm=2.1;
53
54 BatteryNoseA=-0.708;
55 BatteryFuseA=4.106;%+0.5;
56
57 AvionicsA=0.5;
58 MotorsA=-0.814;

```

```

59 MotorEmA=5.6;
60 MechEmA=5.6;
61 TailsA=6;
62 WingA=1.1375+0.5;
63
64
65 %Equations
66 C=(S*(A+2*B)) / (3*(A+B)); %wing sweep
67
68 MAC=A-(2*(A-B)*(0.5*A+B)/(3+(A+B)));
69 MAClocation=Y*((A-MAC)/(A-B));
70
71 WA=Y*(A+B); %wing area
72 TA=YY*(AA+BB); %tail area
73
74 ARw=((Y*2)^2)/WA; %wing aspect ratio
75 ART=((YY*2)^2)/TA; %tail aspect ratio
76 wingAC=A*0.25;
77 tailAC=AA*0.25;
78 TailArm=(D-wingAC)+tailAC;
79 Vbar=(TA/WA)*(TailArm/MAC); %tail volume
80
81
82 NP=0.25+(0.25*sqrt(sqrt(ARw)))*Vbar
83 idealCG=NP-SM
84 Moment=9.81*((MotorEm*MotorEmA)+(MainGear*MainGearA)+(NoseGear*NoseGearA)
+(Pilot*PilotA)+(Passenger1*Passenger1A)+(Passenger2*Passenger2A)+(
Passenger3*Passenger3A)+(BatteryNose*BatteryNoseA)+(BatteryFuse*
BatteryFuseA)+(Avionics*AvionicsA)+(Motor*MotorsA)+(Tails*TailsA)+(Wing*WingA))
85 Datum2LE=1
86 actualCG=((Moment/TotalWt)-(Datum2LE+C))/MAC
87 AcutalSM=NP-actualCG
88 Length=7.76 %meters
89 PositionCG=actualCG*Length

```

```

1 % 4 PAX Case
2 paxNo = 4;
3 %Parameters meters
4 A= 1.35 %Root Chord Wing
5 AA= 0.9 %Root Chord Tail
6 B= 0.8 %Tip Chord Wing
7 BB= 0.86 %Tip Chord Tail
8 S= 0.138 %Sweep Distance Wing
9 SS= 0.018 %Sweep Distance Tail

```

```

10 Y= 6.5 %Half Span Wing
11 YY= 1.1 %Half Span Tail
12 D= 4.4 %Wing root to Tail root LE
13 SM= 0.12 %Desired Static Margin
14
15 %Weights in kilograms
16 MainGear=24.673;
17 NoseGear=30.085;
18
19 Pilot=60.7185;
20 Passenger1=60.7185;
21 Passenger2=60.7185;
22 Passenger3=60.7185;
23
24 Bag1=30;
25 Bag2=30;
26 Bag3=30;
27 Bag4=30;
28
29 BatteryNose=106.8*1.25
30 BatteryFuse=160.2*1.25
31
32 Avionics=40.0454
33 Motor=20.3*1.75
34 Tails=25
35 Wing=125
36
37 MotorEm=12.3
38 MechEm=20
39
40 ActualWT=MainGear+NoseGear+MotorEm+MechEm+Pilot+Passenger1+Passenger2+
    Passenger3+Bag1+Bag2+Bag3+Bag4+BatteryNose+BatteryFuse+Avionics+Motor+
    Tails+Wing
41 TotalWt=1156*9.81
42
43
44 %Arm Distances
45 MainGearA=xm
46 NoseGearA=xn
47 PilotA=1.189;
48 Passenger1A=1.189;
49 Passenger2A=2.059;
50 Passenger3A=2.059;
51
52 Bag1Arm=2.2;

```

```

53 Bag2Arm=2.2;
54 Bag3Arm=2.2;
55 Bag4Arm=2.2;
56
57
58 BatteryNoseA=-0.5;
59 BatteryFuseA=3.106;
60
61 AvionicsA=0.25;
62 MotorsA=-0.814;
63 MotorEmA=5.6;
64 MechEmA=5.6;
65 TailsA=6;
66 WingA=1.1375+0.5;
67
68
69 %Equations
70 C=(S*(A+2*B)) / (3*(A+B)); %wing sweep
71
72 MAC=A-(2*(A-B)*(0.5*A+B)/(3+(A+B)));
73 MAClocation=Y*((A-MAC)/(A-B));
74
75 WA=Y*(A+B); %wing area
76 TA=YY*(AA+BB); %tail area
77
78 ARw=((Y*2)^2)/WA; %wing aspect ratio
79 ART=((YY*2)^2)/TA; %tail aspect ratio
80 wingAC=A*0.25;
81 tailAC=AA*0.25;
82 TailArm=(D-wingAC)+tailAC;
83 Vbar=(TA/WA)*(TailArm/MAC); %tail volume
84
85
86 NP=0.25+(0.25*sqrt(sqrt(ARw)))*Vbar
87 idealCG=NP-SM
88 Moment=9.81*((MotorEm*MotorEmA)+(MainGear*MainGearA)+(NoseGear*NoseGearA)
+ (Pilot*PilotA)+(Passenger1*Passenger1A)+(Passenger2*Passenger2A)+(
Passenger3*Passenger3A)+(BatteryNose*BatteryNoseA)+(BatteryFuse*
BatteryFuseA)+(Avionics*AvionicsA)+(Motor*MotorsA)+(Tails*TailsA)+(
Wing*WingA))
89 Datum2LE=1
90 actualCG=((Moment/TotalWt)-(Datum2LE+C))/MAC
91 AcutalSM=NP-actualCG
92 Length=7.76 %meters
93 PositionCG=actualCG*Length

```

Stroke Calculation

```
clear all
clc
g=9.81; %m/s^2
Wlmax = (1156.661*g*1.5*0.15)/cos((7/180)*pi) %a/c weight x gravity lbf

MinNoseGearLoad=1156.661*0.1*1.07 %kg
MaxNoseGearLoad=1156.661*0.15*1.07 %kg

N=3;

Wnose= (2550*32.2*1.5*0.15)/ cos((7/180)*pi)
ns= 1 %number of struts on Nose Landing Gear
Pm=Wnose/ns

%Diameter of strut
ds=0.041+0.0025*sqrt(Pm); %ft
dscm=ds*30.48 %ft to cm
%Diameter of the piston rod in cm
dpistonrod= dscm/1.3 %ext. diameter is typically 30% greater than piston rod

% Stroke Determination

% Vv sink speed
Vv=3.05; %m/s

St=0.03; %m
n=0.8;
nt=0.47;
% Landing Assumed L=2/3Wl
L=(2/3)*Wlmax;
S=((0.5*(Wlmax/g)*Vv.^2-St*(Wlmax*(1+nt*N)-L))/(Wlmax*(-1+n*N)+L))*100
Ssafety= S+3

% Landing Assumed L=Wl
Snew=((Vv.^2/(2*g*n*N))-((nt/n)*St))*100
Ssafetynew=Snew+3
%Strut Length
ls=3*Ssafety
lss=3*Ssafetynew
```

```

nlglength = (lss+Ssafetynew)/100 %m
Hcg = 1.1745 %nlglength*(sin(83*pi/180))
Hg= 0.65 %0.2m fuselage to cg

Base=2.35
dynamicload= (3.048*Hcg*1156.661)/(g*2.35)

Wlmax = 2.5722e+03
MinNoseGearLoad = 123.7627
MaxNoseGearLoad = 185.6441
Wnose = 1.8613e+04
ns = 1
Pm = 1.8613e+04
dscm = 11.6457
dpistonrod = 8.9583
S = 20.4113
Ssafety = 23.4113
Snew = 17.9931
Ssafetynew = 20.9931
ls = 70.2339
lss = 62.9792
nlglength = 0.8397
Hcg = 1.1745
Hg = 0.6500
Base = 2.3500
dynamicload = 179.6128

% Ev=0.5*(Wl/g)*Vv^2+(Wl-L)*(S-St)
% Ev=n*N*Wl*S+nt*N*Wl*St
Ev=(ns*N*Wlmax*Ssafetynew)+(nt*N*Wlmax*St)

Ev = 1.6210e+05

Area = 13.975; %Wing surface area m2
cl_max = 1.740;
density = 1.225;

Vstall = sqrt((2*Wlmax)/(density*Area*cl_max))
KE_Breaking = 0.5*(Wlmax/g)*Vstall^2

KE_Breaking_EachWheel= KE_Breaking/2
Vstall = 13.1416

```

```
KE_Breaking = 2.2642e+04
```

```
KE_Breaking_EachWheel = 1.1321e+04
```

Steel Leaf Spring MLG

```
%Stroke
```

```
NS = 0.5 %shock absorber efficiency for steel leaf spring
```

```
Ss= (((Vv^2)/(2*g*N))-(nt*0.045 ))/NS)+0.03
```

```
%Ss=((0.5*((Vv^2)/g)/N)/0.5)*100)+3 %add 3 cm for safety
```

```
ETi = 107*(10^9)%GPa Ti10v2Fe3Al
```

```
Gearleglength = (Hg)/(cos(40*pi/180))
```

```
Wmlg=1156.661*g*0.85*1.5
```

```
MaxMainGearLoad=(1156.661*0.9*1.07)/2 %lb
```

```
MinMainGearLoad=(1156.661*0.85*1.07)/2 %lb
```

```
Fs=(Wmlg*N)/2
```

```
F = Fs*sin(40*pi/180)
```

```
y= Ss/sin(40*pi/180)
```

```
I=(F*Gearleglength^3)/(3*ETi*y)
```

```
%wheel track
```

```
Wheeltrack= (Hg*tan(40*pi/180)*2)+1.27
```

```
% The Beam Width Parameter
```

```
b=(0.0067*2550*((2550/150.47947)^0.5))/(Gearleglength*39.37)
```

```
% From the Leaf Spring Sizing Graph
```

```
% b =2.1053, WR=4.5in and WB=1.7131in
```

```
WR= 4.5/39.37 %m
```

```
WB=1.7131/39.37 %m
```

```
ThicknessMLG = WR/8 %m
```

```
BendingRadius = ThicknessMLG*3
```

```
ApN=2.3*((4.95*13.25)^0.5)*((13.25/2)-5.7)
```

```
ApM=2.3*((6.3*17.5)^0.5)*((17.5/2)-6.9)
```

```
NS = 0.5000
```

```
Ss = 0.3038
```

```

ETi = 1.0700e+11
Gearleglength = 0.8485
Wmlg = 1.4467e+04
MaxMainGearLoad = 556.9323
MinMainGearLoad = 525.9916
Fs = 2.1701e+04
F = 1.3949e+04
y = 0.4726
I = 5.6171e-08
Wheeltrack = 2.3608
b = 2.1053
WR = 0.1143
WB = 0.0435
ThicknessMLG = 0.0143
BendingRadius = 0.0429
ApN = 17.2298
ApM = 44.6775

```

E.3 Landing Gear Stroke MATLAB Code

Stroke Calculation

```

clear all
clc
g=9.81; %m/s^2
Wlmax = (1156.661*g*1.5*0.15)/cos((7/180)*pi) %a/c weight x gravity lbf

MinNoseGearLoad=1156.661*0.1*1.07 %kg
MaxNoseGearLoad=1156.661*0.15*1.07 %kg

N=3;

Wnose= (2550*32.2*1.5*0.15)/ cos((7/180)*pi)
ns= 1 %number of struts on Nose Landing Gear
Pm=Wnose/ns

%Diameter of strut
ds=0.041+0.0025*sqrt(Pm); %ft
dscm=ds*30.48 %ft to cm
%Diameter of the piston rod in cm
dpistonrod= dscm/1.3 %ext. diameter is typically 30% greater than piston rod

% Stroke Determination

```

```

% Vv sink speed
Vv=3.05; %m/s

St=0.03; %m
n=0.8;
nt=0.47;
% Landing Assumed L=2/3Wl
L=(2/3)*Wlmax;
S=((0.5*(Wlmax/g)*Vv.^2-St*(Wlmax*(1+nt*N)-L))/(Wlmax*(-1+n*N)+L))*100
Ssafety= S+3

% Landing Assumed L=Wl
Snew=((Vv.^2/(2*g*n*N))-((nt/n)*St))*100
Ssafetynew=Snew+3
%Strut Length
ls=3*Ssafety
lss=3*Ssafetynew

nlglength = (lss+Ssafetynew)/100 %m
Hcg = 1.1745 %nlglength*(sin(83*pi/180))
Hg= 0.65 %0.2m fuselage to cg

Base=2.35
dynamicload= (3.048*Hcg*1156.661)/(g*2.35)

Wlmax = 2.5722e+03
MinNoseGearLoad = 123.7627
MaxNoseGearLoad = 185.6441
Wnose = 1.8613e+04
ns = 1
Pm = 1.8613e+04
dscm = 11.6457
dpistonrod = 8.9583
S = 20.4113
Ssafety = 23.4113
Snew = 17.9931
Ssafetynew = 20.9931
ls = 70.2339
lss = 62.9792
nlglength = 0.8397
Hcg = 1.1745
Hg = 0.6500
Base = 2.3500

```

```

dynamicload = 179.6128

% Ev=0.5*(Wl/g)*Vv^2+(Wl-L)*(S-St)
% Ev=n*N*Wl*S+nt*N*Wl*St
Ev=(ns*N*Wlmax*Ssafetynew)+(nt*N*Wlmax*St)

Ev = 1.6210e+05

Area = 13.975; %Wing surface area m2
cl_max = 1.740;
density = 1.225;

Vstall = sqrt((2*Wlmax)/(density*Area*cl_max))
KE_Breaking = 0.5*(Wlmax/g)*Vstall^2

KE_Breaking_EachWheel= KE_Breaking/2
Vstall = 13.1416

KE_Breaking = 2.2642e+04

KE_Breaking_EachWheel = 1.1321e+04

Steel Leaf Spring MLG

%Stroke
NS = 0.5 %shock absorber efficiency for steel leaf spring

Ss= (((Vv^2)/(2*g*N))-(nt*0.045 ))/NS)+0.03
%Ss=((0.5*((Vv^2)/g)/N)/0.5)*100)+3 %add 3 cm for safety

ETi = 107*(10^9)%GPa Ti10v2Fe3Al
Gearleglength = (Hg)/(cos(40*pi/180))
Wmlg=1156.661*g*0.85*1.5
MaxMainGearLoad=(1156.661*0.9*1.07)/2 %lb
MinMainGearLoad=(1156.661*0.85*1.07)/2 %lb
Fs=(Wmlg*N)/2
F = Fs*sin(40*pi/180)
y= Ss/sin(40*pi/180)
I=(F*Gearleglength^3)/(3*ETi*y)

%wheel track
Wheeltrack= (Hg*tan(40*pi/180)*2)+1.27

```

```

% The Beam Width Parameter
b=(0.0067*2550*((2550/150.47947)^0.5))/(Gearleglength*39.37)

% From the Leaf Spring Sizing Graph
% b =2.1053, WR=4.5in and WB=1.7131in

WR= 4.5/39.37 %m
WB=1.7131/39.37 %m
ThicknessMLG = WR/8 %m

BendingRadius = ThicknessMLG*3

ApN=2.3*((4.95*13.25)^0.5)*((13.25/2)-5.7)
ApM=2.3*((6.3*17.5)^0.5)*((17.5/2)-6.9)

NS = 0.5000
Ss = 0.3038
ETi = 1.0700e+11
Gearleglength = 0.8485
Wmlg = 1.4467e+04
MaxMainGearLoad = 556.9323
MinMainGearLoad = 525.9916
Fs = 2.1701e+04
F = 1.3949e+04
y = 0.4726
I = 5.6171e-08
Wheeltrack = 2.3608
b = 2.1053
WR = 0.1143
WB = 0.0435
ThicknessMLG = 0.0143
BendingRadius = 0.0429
ApN = 17.2298
ApM = 44.6775

```

E.4 Landing Gear Tire Clearance MATLAB Code

Aircraft Tire Dimensioning Calculations

```
clear all;
clc;

Vs=46; %kts
Gw = 1.04; % Section Width Growth Factors
speed= 1.3*Vs;
```

BIAS TYPE III 5.00-5

```
Do_1= 14.2; %in
D_1= 5; %in
Ds_1= 12.55 %in
Df_1= 6.5;
Fh_1= 0.75;
W_1= 4.95; %in
Ws_1= 4.2; %in
AR_1 = 0.93;

a=Do_1-Ds_1

% Growth
Gh_1 = 1.115-(0.75*AR_1) % Section Height Growth Factors
H_1=(Do_1-D_1)/2
Hs_1=(Ds_1-D_1)/2
Wg_1=Gw*W_1
Dg_1=D_1+(2*Gh_1*Hs_1)
Wsg_1=Gw*Ws_1

%Used Inflated Tire
UsedInflatedTire_1= Wsg_1/2
% New Inflated Tire
%NewInflatedTire= Ws_1/2

% Radial Clearance
Cr_1= ((17.02+(2.61*((speed/100)^3.348)))/1000)*Wg_1+0.4
% Lateral Clearance
Cw_1= (0.019*Wg_1)+0.23

% Radial Distance From Axle Centerline To Adjacent Part
```

```

Rxmin_1= (Dg_1/2)+Cr_1
% Lateral Distance rom Tire Centerline To Adjacent Part
Wxmin_1= (Wg_1/2)+Cw_1
% Clearance allowed Between Tire Shoulder Area And Adjacent Part
Sxmin_1= (Cw_1+Cr_1)/2

% Deflection
% Deflection In Percentage = 35
deflection_1= ((Do_1-Df_1)*(35/100))/2)*2.54

Ds_1 = 12.5500
a = 1.6500
Gh_1 = 0.4175
H_1 = 4.6000
Hs_1 = 3.7750
Wg_1 = 5.1480
Dg_1 = 8.1521
Wsg_1 = 4.3680
UsedInflatedTire_1 = 2.1840
Cr_1 = 0.4900
Cw_1 = 0.3278
Rxmin_1 = 4.5661
Wxmin_1 = 2.9018
Sxmin_1 = 0.4089
deflection_1 = 3.4226

```

BIAS TYPE III 6.00-6

```

Do_2= 17.5;
D_2= 6;
Ds_2= 15.45;
Df_2= 7.5;
Fh_2= 0.75
W_2= 6.3;
Ws_2= 5.35;
AR_2 = 0.91;

% Growth
Gh_2 = 1.115-(0.075*AR_2); % Section Height Growth Factors
H_2= (Do_2-D_2)/2
Hs_2= (Ds_2-D_2)/2
Wg_2= Gw*W_2
Dg_2= D_2+(2*Gh_2*Hs_2)

```

```

Wsg_2= Gw*Ws_2

% Used Inflated Tire
UsedInflatedTire_2= Wsg_2/2
% New Inflated Tire
%NewInflatedTire= Ws_2/2

% Radial Clearance
Cr_2= ((17.02+(2.61*((speed/100)^3.348)))/1000)*Wg_2+0.4
% Lateral Clearance
Cw_2= (0.019*Wg_2)+0.23
% Radial Distance From Axle Centerline To Adjacent Part
Rxmin_2= (Dg_2/2)+Cr_2
% Lateral Distance rom Tire Centerline To Adjacent Part
Wxmin_2= (Wg_2/2)+Cw_2
% Clearance allowed Between Tire Shoulder Area And Adjacent Part
Sxmin_2= (Cw_1+Cr_1)/2

% Deflection
deflection_2= (((Do_2-Df_2)*(35/100))/2)*2.54

Fh_2 = 0.7500
H_2 = 5.7500
Hs_2 = 4.7250
Wg_2 = 6.5520
Dg_2 = 15.8918
Wsg_2 = 5.5640
UsedInflatedTire_2 =n2.7820
Cr_2 = 0.5146
Cw_2 = 0.3545
Rxmin_2 =8.4605
Wxmin_2 = 3.6305
Sxmin_2 = 0.4089
deflection_2 = 4.4450

```

E.5 Wing Boom Idealization and Stresses Code

```

1 clc
2 clear
3 %root
4 b1=340; %Front
5 b2=40; b3=b2; b4=b3;
6 b5=100; b6=130; %Rear

```

```

7 b7=60; b8=b7; b9=b7;
8 b10=530; %Front
9 % 2m
10 % b1=243; %Front
11 % b2=40; b3=b2; b4=b3;
12 % b5=80; b6=130; %Rear
13 % b7=60; b8=b7; b9=b7;
14 % b10=420; %Front
15 %3.8m
16 % b1=155; %Front
17 % b2=40; b3=b2; b4=b3;
18 % b5=45; b6=130; %Rear
19 % b7=60; b8=b7; b9=b7;
20 % b10=300; %Front
21 tD = 1.1;
22 % tD = 0.8;
23 boom_area = [b1 b2 b3 b4 b5 b6 b7 b8 b9 b10];
24 k=1;
25 for j=0.25:0.1:0.65
26 %root
27 q(k)=(j - 0.25)*1.35*1000; %X-Distance
28 t(k)=(-0.0486*j+0.1077)*1.35*1000; %Y-Top
29 b(k)=(0.0495*j - 0.046475)*1.35*1000; %Y-Bottom
30 % %2m
31 % q(k)=(j - 0.25)*1.18*1000;
32 % t(k)=(-0.0486*j+0.1077)*1.18*1000; %Y-Top
33 % b(k)=(0.0495*j - 0.046475)*1.18*1000; %Y-Bottom
34 %t3.8m
35 % q(k)=(j - 0.25)*1.028*1000;
36 % t(k)=(-0.0486*j+0.1077)*1.028*1000; %Y-Top
37 % b(k)=(0.0495*j - 0.046475)*1.028*1000; %Y-Bottom
38 end
39
40 for i = 2:(length(boom_area)/2)-1
41 boom_area(i) = boom_area(i) + ((tD*0.1*1.35*1000/6)*(2+(t(i+1)/t(i)))) +
42 ((tD*0.1*1.35*1000/6)*(2+(t(i-1)/t(i)))); 
43 end
44 k=4;
45 for i = ((length(boom_area)/2)+2):(length(boom_area)-1)
46 boom_area(i) = boom_area(i) + ((tD*0.1*1.35*1000/6)*(2+(b(k+1)/b(k)))) +
47 ((tD*0.1*1.35*1000/6)*(2+(b(k-1)/b(k)))); 
48 k=k-1;
49 end
50 boom_area(1)=boom_area(1) + ((tD*0.1*1.35*1000/6)*(2+(t(2)/t(1)))) + ((3*(t(1)-b(1))/6)*(2+(b(1)/t(1))));
```

```

49 boom_area(5)=boom_area(5) + ((tD*0.1*1.35*1000/6)*(2+(t(4)/t(5)))) + ((3*(t(5)-b(5))/6)*(2+(b(5)/t(5))));  

50 boom_area(6)=boom_area(6) + ((tD*0.1*1.35*1000/6)*(2+(b(4)/b(5)))) + ((3*(t(5)-b(5))/6)*(2+(t(5)/b(5))));  

51 boom_area(10)=boom_area(10) + ((3*(t(1)-b(1))/6)*(2+(t(1)/b(1)))) + ((tD*0.1*1.35*1000/6)*(2+(b(2)/b(1))));  

52 denom = sum(boom_area);  

53 numerator = [];  

54 xnumerator = [];  

55 %% Y_Bar  

56  

57 for i=1:(length(boom_area)/2)  

58     numerator(i) = boom_area(i)*t(i);  

59 end  

60 k=5;  

61 for i=((length(boom_area)/2)+1):length(boom_area)  

62     numerator(i) = boom_area(i)*b(k);  

63     k=k-1;  

64 end  

65 numerator_sum = sum(numerator);  

66 y_bar = numerator_sum/denom  

67 %% X_Bar  

68 for z=1:(length(boom_area)/2)  

69     xnumerator(z) = boom_area(z)*q(z);  

70 end  

71 k=5;  

72 for z=((length(boom_area)/2)+1):length(boom_area)  

73     xnumerator(z) = boom_area(z)*q(k);  

74     k=k-1;  

75 end  

76 xnumerator_sum = sum(xnumerator);  

77 x_bar = xnumerator_sum/denom  

78  

79 %% Moment of Inertia Calculations  

80 %%Ixx  

81 Ixx = [];  

82  

83 for i=1:(length(boom_area)/2)  

84     Ixx(i) = boom_area(i)*(t(i)-y_bar)^2;  

85 end  

86 k = 5;

```

```

91  for i=((length(boom_area)/2)+1):length(boom_area)
92
93      Ixx(i) = boom_area(i)*(b(k)-y_bar)^2;
94      k = k-1;
95  end
96  I_xx = sum(Ixx)

97
98 %Iyy
99 Iyy = [];
100 for z=1:(length(boom_area)/2)
101     Iyy(z) = boom_area(z)*(q(z)-x_bar)^2;
102 end
103 k = 5;
104 for i=((length(boom_area)/2)+1):length(boom_area)
105
106     Iyy(z) = boom_area(z)*(q(k)-x_bar)^2;
107     k = k-1;
108 end
109 I_yy = sum(Iyy)

110
111 %Ixxy
112 Ixy = [];
113 for i=1:(length(boom_area)/2)
114
115     Ixy(i) = boom_area(i)*(q(i)-x_bar)*(t(i)-y_bar);
116 end
117 k=5;
118 for i=((length(boom_area)/2)+1):length(boom_area)
119
120     Ixy(i) = boom_area(i)*(q(k)-x_bar)*(b(k)-y_bar);
121     k=k-1;
122 end
123 I_xy = sum(Ixy)

124
125 %% Stress Calculations
126 % Stress in Booms
127 Mx = -58471*1000;
128 Mz = -12918*1000;
129 sigmaz = [];

130
131 for i=1:(length(boom_area)/2)
132     sigmaz(i) = (((Mz*I_xx-Mx*I_xy)/(I_xx*I_yy-I_xy^2))*(q(i)-x_bar) + (((Mx*I_yy-Mz*I_xy)/(I_xx*I_yy-I_xy^2))*(t(i)-y_bar)));
133 end
134 k=5;

```

```

135 for i=((length(boom_area)/2)+1):length(boom_area)
136     sigmaz(i) = (((Mz*I_xx-Mx*I_xy)/(I_xx*I_yy-I_xy^2))*(q(k)-x_bar) + (((Mx*I_yy-Mz*I_xy)/(I_xx*I_yy-I_xy^2))*(b(k)-y_bar)));
137     k=k-1;
138 end
139
140 sigmaz
141 boom_area

```

E.6 Range MATLAB Code

```

1 %% Variable Definitions
2 % MTOW = max takeoff mass in kg = 1159.91 2550lb [kg]
3 % battPc = battery mass percentage [percent]
4 % battMass = battery total mass [kg]
5 % battCap = battery capacity [Wh/kg]
6 % battAv = total energy available from batteries [kWh]
7 % motorPwr = avg shaft power output (~0.8Pmax) [kW]
8 % motormass = 19.9 based on emrax 268 air cooled(120 kW) [kg]
9 % PAXmass = 362.87 for max passengers and bags [kg]
10 % fltime = flight time target [hrs]
11 Pmax = 110E3;
12 MTOW = 1156.69; %2550lb =1156.69 2400=1088.62
13 rhoto = 1.225;
14 dacWA = 14; %minimum wing area from aero team
15 dacCd = 0.016*1.33; %assuming 33% flaps drag increase
16 dacVto = 27.75;
17 dacVbc = 31.90; %best climb speed
18
19 %used best climb speed as worst case drag i.e. conservative power estimation
20 dacTto = dacDrag;
21 Rp = 1.91/2;
22 dacPropEff = 0.80;
23
24 %%
25
26 %-----TAKEOFF CALCS-----
27
28 fprintf('-----TAKEOFF & CLIMB CONDITION-----\n\n')
29
30
31 tot = 34; %target takeoff time in seconds
32
33 TOFL = 518.16; %takeoff field length to 50 ft alt in m

```

```

34 ato = (dacVto - 0)/tot;
35 %Treqto = (MIOW*ato)*DragFactor; %takeoff thrust required
36 Vavg = TOFL/tot;
37 % if Vavg < 0.66*dacVto
38 %     fprintf('Uh oh, takeoff speed not reached in time!!! \n\n')
39 % end
40
41
42 MIOW = MIOW;
43 m = MIOW;
44 a = ato;
45 mu = 0.2; %mu tire at 55knots
46
47 rhoto = 1.225;
48 dacWA = 13.975; %minimum wing area from aero team
49 dacCd = 0.016*1.33; %assuming 33% flaps drag increase
50 dacVto = 27.75;
51 dacVbc = 31.90; %best climb speed
52 dacDrag = 0.5*rhoto*(0.66*dacVbc.^2)*dacCd*dacWA*2; %1.5 factor for total
      drag 15% drag increase from flaps
53
54
55 %Calculating minimum takeoff power required
56
57 Fairdrag = dacDrag;
58 Ftiredrag = mu*m*9.81;
59 Feng = (m*a)+Fairdrag+Ftiredrag; %thrust to exceed various drags
60 Treqto = Feng;
61
62 fprintf('---Ground Roll--- \n')
63 fprintf('Tire friction coefficient = %.2f \n', mu);
64 fprintf('Air Resistance Force = %.2f N \n', Fairdrag);
65 fprintf('Tire Resistance Force = %.2f N \n', Ftiredrag);
66 fprintf('Thrust Required for takeoff acceleration = %.2f N \n\n', Feng);
67
68 %TOFL exceed checker
69 syms x
70 eqn = ato*x == dacVto; %dynamic equation of velocity wrt acceleration
71 t = solve(eqn,x);
72 if (ato/2)*(t*t) > TOFL %dynamic equation of position wrt velocity
73
74 fprintf('---Field Length Performance--- \n')
75 fprintf('Takeoff time = %.2f sec \n', tot)
76 fprintf('Calculated TOFL = %.2f m \n', (ato/2)*(t*t));
77 fprintf('Maximum Allowable TOFL = %.2f m \n', TOFL);

```

```

78 SM = (TOFL - ((ato/2)*(t*t)))/TOFL;
79 fprintf('TOFL Exceeded! Reduce takeoff time!\n');
80 return
81
82 else
83
84 fprintf('---Field Length Performance--- \n')
85 fprintf('Takeoff time = %.2f sec \n',tot)
86 fprintf('Calculated TOFL = %.2f m \n', (ato/2)*(t*t));
87 fprintf('Maximum Allowable TOFL = %.2f m \n', TOFL);
88 SM = (TOFL - ((ato/2)*(t*t)))/TOFL;
89 fprintf('Safety Margin = %.2f%% \n',SM*100);
90 end
91
92
93 PshReq = (((Treqto)^(3/2))/sqrt(2*pi*rphoto))*(1/Rp)*(1/dacPropEff);
94 fprintf('Minimum Shaft Power req @ takeoff = %.2f kW \n', PshReq/1000)
95 fprintf('Maximum Shaft Power available = 115 kW \n') %115kW E268 max
96 continuous @ 2300RPM
97 fprintf('Takeoff acceleration = %.2f m/s^2. \n',ato)
98 fprintf('Takeoff thrust = %.2f N \n\n',Treqto)
99
100
101 %Calculating energy consumed from takeoff to cruise alt
102 %calculating best angle of climb
103 vbc = 31.89; %v best angle of climb 62 kts = 31.89m/s
104 D = 0.5*rphoto*(dacVbc.^2)*dacCd*dacWA*2; %drag best climb speed
105 T = Treqto*0.8; %prop efficiency 80%
106 W = MIOW*9.81;
107 Hcr = 2438.4;
108 fprintf('---Climb Performance--- \n')
109
110 syms A
111 eqn = sin(A) == (T-D)/W;
112 angle = solve(eqn,A, 'PrincipalValue', true);
113 fprintf('Angle of climb for Vbestclimb = %.2f deg \n',angle*(180/pi));
114
115 vvert = vbc*sin(angle); %vertical velocity at v best climb
116 fprintf('Vertical speed for Vbestclimb = %.2f m/s \n',vvert);
117
118 ttc = Hcr/vvert/3600; %takeoff to cruise time in hours
119 fprintf('Takeoff to cruise time = %.2f min \n',ttc*60)
120
121 Wtoc = PshReq * ttc;

```

```

122 %Wtoc = 8000;
123
124 fprintf('Energy used for takeoff and climb = %.2f Wh \n\n', Wtoc)
125 %%%
126
127 %-----LANDING PERFORMANCE CALCS-----
128 fprintf('-----LANDING & GROUND ROLL CONDITION----- \n')
129 angleAp = 3; %approach angle in degrees
130 Vs0 = 16.98; %Vs0 = 33kts = 16.98 m/s
131 Vapp = 1.3*Vs0;
132 Vhoriapp =Vapp*cos((180-angleAp)*(180/pi)); %ground speed on approach
133 Vvertapp =(-1)* Vapp*sin((180-angleAp)*(180/pi)); %sink rate on approach
134 Lapp = 9656.06; %approach distance in meters (6 miles)
135 timeapp = (Lapp/Vhoriapp)/60; %approach time in minutes
136 Happ = Vvertapp*timeapp*(-60);
137 Dapp = 0.5*rho*(Vapp.^2)*dacCd*1.33*dacWA*2; %33% drag increase due to
   flaps 1.5 ratio wing to total drag
138 Tapp = Dapp; %weight from the approach angle reduces the thrust required
139 Papp = Tapp*Vapp*(1/dacPropEff); %thrust required to maintain approach
   angle at approach speed
140 PCapp = (Papp/Pmax); %approach power percentage
141 fprintf('Power Output Required during approach = %.2f kW \n',Papp/1000)
142 fprintf('Power percentage = %.2f%% Pmax \n',(PCapp)*100)
143 fprintf('Approach speed = %.2f m/s \n',Vapp)
144 fprintf('Approach ground speed = %.2f m/s \n',Vhoriapp)
145 fprintf('Approach sink speed = %.2f m/s \n',Vvertapp)
146 fprintf('Initial approach altitude = %.2f m \n',Happ)
147 fprintf('Approach time = %.2f min \n\n',timeapp)

148
149 %%%
150 %-----CRUISE AND RANGE CALCS-----
151 fltime = 2.9;
152
153 Pmax = 110E3;
154 CruisePc = 0.75;           %percent of Pmax required for Pcruise
155 prevtime = fltime;         %saves prev run estimation to compare it to
   current
156 ctl = timeapp/60;          %cruise to landing time in hours
157 PowerAv = ((ttc*1)+(ctl*PCapp)+((fltime-(ttc+ctl))*CruisePc))/fltime;
158 fltime = fltime + (3.0-fltime); %this begins iterations at high flight
   time before converging down to the real time
159 counter = 0;
160 while (fltime > 0.5)
161 %Battery life calculation
162 MIOW = MIOW;

```

```

163 motormass = 19.9;
164 Emotormass = 12; %Emergency Motor Mass in kg, EMRAX 228
165 PAXmass = 226.79; %800lbs = 362.87 500=226.79 900=408.23
166 aframeSys = 387.61;
167 emptywt = MOW - PAXmass - motormass-Emotormass; %Cessna172 empty weight =
168 634.48kg
169 %battPC = 0.35;
170 battCap = 1000;
171 packEff = 0.80;
172 %battMass = emptywt-aframeAl-aframeCF;
173 battMass = 200;%battPC*emptywt; % only 80% of battery pack weight is
174 actually batteries from Sion Power original=272.72kg
175 %battPC = (emptywt-aframeSys)/emptywt ;
176 battPC = battMass/emptywt ;
177 ToffClimbEnergy = Wtoc; %power consumed for takeoff & climb
178 PowerAv = ((ttc*1)+(ctl*0.45)+((fltime-(ttc+ctl))*CruisePc))/fltime ;
179 battAv = (battMass * battCap * packEff)-ToffClimbEnergy;
180 motorPwr = (battAv/fltime);
181
182 %Power required calculation
183
184 %CRUISE
185
186 %Cessna 172 cruise conditions
187 %Power Output = 140 HP = 104.4 kW
188 %Vcr = 350 kph = 97.22 m/s @75% power
189 %Pcr = 104.4 * 0.75 = 78.3 kW
190 %Hcr = 8000 ft = 2438.4 m
191 %rhocr = 0.9642 kg/m3
192 %Wing area = 16.17 m2
193 %Total Cd = 0.032
194 %Prop efficiency = 73.5%
195
196 %DACION FALCO cruise conditions
197 %Power Output = motorPwr/0.8
198 %Vcr = 125ktas = 64.31 m/s @75% power 120kts =61.73
199 %Pcr = (motorPwr/PowerAv)*0.75 @75% power
200 %Hcr = 10000 ft = 3048 m
201 %rhocr = 0.9629 kg/m3 8000Ft
202 %Wing area = 16.17 m2
203 %Total Cd = 0.032
204 %Prop efficiency = 80% (minimum target)
205 %GearR = 1.2 based on Cessna shaft to prop power ratio
206 Hcr = 2438.4;

```

```

206 dacRhoCr = 0.905; %accurate based on reference book at OBJECTIVE 10 000 ft
207 dacWA = 13.975; %Assuming 10 minimum
208 dacCd = 0.016; %Cd from Aerodynamics Team
209 dacVcr = 64.31; %64.31 original
210 %dacDrag = 0.5*dacRhoCr*(dacVcr.^2)*dacCd*dacWA*3; %1.5 wing to total drag
   factor
211 dacDrag = 799;
212 dacTcr = dacDrag;
213 dacPropEff = 0.80;
214 dacPreq = dacTcr*dacVcr*(1 / dacPropEff);
215 CruisePc = CruisePc; %percent of Pmax required for Pcruise
216 dacPcr = (motorPwr/PowerAv)*CruisePc;
217
218
219
220 %%%
221 %-----EMERGENCY POWER CALCS-----%
222 Emotormass = 12; %Emergency Motor Mass in kg, EMRAX 228
223 EPmax = 100E3; %Emergency motor max power instantaneous in W
224 EPmaxCont = 55E3; %Emergency motor max power continuous in W
225 EdacPreq = dacTcr*dacVcr*(1 / dacPropEff); %Emergency power required at
   cruise
226 VlowAlt = dacVcr*0.7; %Speed at low altitude , loiter speed
227 DragLowAlt = 0.5*rho0*(VlowAlt.^2)*dacCd*dacWA*2;
228 TLowAlt = DragLowAlt;
229 EPreqLowAlt = TLowAlt*(VlowAlt);
230 AbortAccel = (VlowAlt - Vapp) / 9; %Acceleration required to go from
   approach speed to loiter speed in 9 seconds
231 Tabort =(TLowAlt) + (MOW*AbortAccel); %Thrust required to abort a landing
232 Pabort = Tabort*(VlowAlt*0.66); %Power required to abort a landing
233
234
235
236
237 if Pmax < PshReq
238   fprintf( 'Pmax %.2f kW is too low for takeoff!\n', Pmax/1000)
239   fprintf( 'Reduce initial flight time guess or change aircraft specs
      !\n')
240   break
241 end
242
243
244 if dacPcr > dacPreq
245   time = fltime -0.5; %-0.5 hrs allocated to emergency & taxi
   battery

```

```

246 range = ((ttc*3600*vbc)+(timeapp*60*Vhoriapp)+((fltime-(ttc+ctl))*  

247     dacVcr*3600)); %range in meters  

248 fprintf('----CRUISE CONDITION & FLIGHT TIME ESTIMATE---- \n')  

249 fprintf('MTOW = %.2f kg = %.2f lb\n',MTOW, floor(MTOW*2.20462262)  

250     )  

251 fprintf('PAX = %.2f kg = %.2f lb\n\n',PAXmass, ceil(PAXmass  

252     *2.204))  

253 fprintf('Battery Mass = %.2f kg (%.2f%% Usable Weight @%.0f%%  

254     Packing Efficiency)\n',battMass,battPC*100,packEff*100)  

255 fprintf('Airframe & Systems Mass = %.2f kg (%.2f%% Usable Weight)\n  

256     ,(1-battPC)*emptywt,(1-battPC)*100)  

257 fprintf('Battery Capacity = %.0f Wh/kg\n\n',battCap)  

258 fprintf('Avg power output = %.1f%% Pmax\n',PowerAv*100)  

259 fprintf('Preq @ cruise = %.2f kW\n',dacPreq/1000)  

260 fprintf('Poutput @ cruise = %.2f kW \n',dacPcr/1000)  

261 fprintf('Cruise thrust output = %.2f N \n\n',dacTcr)  

262 fprintf('Cruise Altitude = %.0f m = %.0f ft\n',Hcr, Hcr/0.3048)  

263 fprintf('Cruise Speed = %.2f m/s = %.1f kts\n',dacVcr, ceil(dacVcr  

264     *1.943))  

265 fprintf('PMax available = 110 kW\n\n')  

266 lasttime = prevtime;  

267  

268 fprintf('Flight time = %.2f hrs \n',fltime)  

269 fprintf('Last run flight time = %.2f hrs\n',lasttime)  

270 fprintf('Range = %.2f nm\n',range*0.00054)  

271 fprintf('Takeoff to cruise time = %.2f min \n',ttc*60)  

272 fprintf('Cruise to land time = %.2f min \n\n',ctl*60)  

273  

274 fprintf('----EMERGENCY POWER CONDITION---- \n\n')  

275 fprintf('Emergency Motor PMax (for a few seconds) = %.2f kW \n',  

276     EPmax/1000')  

277 fprintf('Emergency Motor PMax (continuous) = %.2f kW \n',  

278     EPmaxCont/1000')  

279 fprintf('Main Motor Power Available (continuous) = 90 kW \n')  

280 fprintf('Cruise Power Required = %.2f kW \n',EdacPreq/1000)  

281 fprintf('Low Altitude Power Required = %.2f kW (@%.0f kts) \n',  

282     EPreqLowAlt/1000, VlowAlt*1.94)  

283 fprintf('Abort Landing Power Required = %.2f kW \n',Pabort/1000)  

284 fprintf('\n')  

285  

286     if Pmax < Pmax/1000  

287         fprintf('Pmax required exceeds Pmax engine \n')  

288         end  

289  

290     if Pmax < 90

```

```

282     fprintf('with this power, you cant even takeoff dumbass \n')
283
284     end
285
286     break
287
288 else
289     fltime = fltime - 0.01;
290     counter = counter + 1;
291     if counter > 300
292         disp 'it overlooped, fix the code'
293         break
294     end
295
296
297 %disp 'done'
```

E.7 Battery Sizing and Positioning MATLAB Code

```

1 %Battery Sizing Calcs Side Flow
2
3 frontPC = 0.40;           %percentage of battery mass in the front
4 rearPC = 1 - frontPC;    %percentage of battery mass in the rear
5
6 frontmass = battMass*frontPC;
7 %front battery mass + casing/wiring weight(10% battery mass) [kg]
8
9 rearmass = battMass*rearPC;
10 %front battery mass + casing/wiring weight(10% battery mass) [kg]
11
12 %-----Battery Pack Sizing Begins-----
13 %Volume = width x height x depth
14 width = 149;             %Pack width [mm]
15 height = 149;            %Pack width [mm]
16 depth = 153;             %Pack width [mm]
17 Vcell = (149*149*153)*0.001; %Cell Volume [cm3]
18 Mcell = 2.8;              %Pack mass [kg]
19 tbs = 1; %space above/below ea. cell [mm]
20 fbs = 1; %space in front/behind ea. cell [mm]
21 ss = 1; %side to side space ea. cell [mm]
22 Vreal = (width+ss)*(height+tbs)*(depth+ss)*(0.1^3);
23 vperkg = Vreal/Mcell; %Cell Specific Volume [cm3/kg]
24
25 VbattF = (frontmass*vperkg); %Total Battery Volume + Containment/Wiring
FRONT
```

```

26 EdgeLF = VbattF^(1/3); %perfect cube edge length in cm FRONT
27 CellNoF = ceil(frontmass/Mcell); % number of cells FRONT
28 CellEdgeHF = floor(EdgeLF/((depth+ss+ss)*0.1)); %batteries across face
    horizontal
29 FaceAcrossF = CellEdgeHF*((depth+ss+ss)*0.1);
30 CellEdgeVF = floor(EdgeLF/((height+tbs+tbs)*0.1)); %batteries across face
    vertical
31 FaceHeightF = CellEdgeVF*((height+tbs+tbs)*0.1);
32 CellFaceF = CellEdgeHF * CellEdgeVF; % number of cells per face
33 FaceNoF = ceil(CellNoF/CellFaceF); %number of faces needed
34 FaceDepthF = (width + fbs +fbs)*0.1; %face depth [cm]
35 BattDepthF = FaceDepthF*FaceNoF;
36
37
38 VbattR = (rearmass*vperkg); %Total Battery Volume + Containment/Wiring
    REAR
39 EdgeLR = VbattR^(1/3); %perfect cube edge length in cm REAR
40 CellNoR = ceil(rearmass/Mcell); % number of cells REAR
41 CellEdgeHR = floor(EdgeLR/((depth+ss+ss)*0.1)); %batteries across face
    horizontal REAR
42 FaceAcrossR = CellEdgeHR*((depth+ss+ss)*0.1);
43 CellEdgeVR = floor(EdgeLR/((height+tbs+tbs)*0.1)); %batteries across face
    vertical
44 FaceHeightR = CellEdgeVR*((height+tbs+tbs)*0.1);
45 CellFaceR = CellEdgeHR * CellEdgeVR; % number of cells per face
46 FaceNoR = ceil(CellNoR/CellFaceR); %number of faces needed
47 FaceDepthR = (width + fbs +fbs)*0.1; %face depth [cm]
48 BattDepthR = FaceDepthR*FaceNoR;
49
50
51 fprintf('---BATTERY CELL CONFIGURATION AND PACK SIZE CALCULATIONS--- \n'
    );
52 fprintf('Total packs required = %.0f cells \n', CellNoF + CellNoR);
53 fprintf('Battery pack module dimensions = %.0f x %.0f x %.0f mm \n', width
    , depth, height);
54 fprintf('Front packs required = %.0f cells \nRear cells required = %.0f
    cells\n\n', CellNoF, CellNoR);
55
56 fprintf('Battery pack spacing \n');
57 fprintf('Side spacing = %.0f mm \n', ss);
58 fprintf('Front and back spacing = %.0f mm \n', fbs);
59 fprintf('Top and Bottom spacing = %.0f mm \n\n', tbs);
60
61 fprintf('Packs per battery section row FRONT = %.0f cells (%.0f X %.0f) \n
    ', CellFaceF, CellEdgeHF, CellEdgeVF);

```

```

62 fprintf('Number of section rows FRONT = %.0f sections \n',FaceNoF);
63 fprintf('Battery section depth FRONT = %.2f cm \n', BattDepthF);
64 fprintf('Battery Pack face area FRONT = %.2f cm X %.2f cm \n\n',
65   FaceAcrossF, FaceHeightF);

66 fprintf('Packs per battery section REAR= %.0f cells (%.0f X %.0f) \n',
67   CellFaceR, CellEdgeHR, CellEdgeVF);
68 fprintf('Number of section rows REAR = %.0f sections \n',FaceNoR);
69 fprintf('Battery section depth REAR = %.2f cm \n', BattDepthR);
70 fprintf('Battery Pack face area REAR = %.2f cm X %.2f cm \n\n',
71   FaceAcrossR, FaceHeightR);

72 fprintf('Total Pack Volume (incl. casing and wiring) FRONT = %.2f cm3 \n',
73   VbattF);
74 fprintf('Total Pack Volume (incl. casing and wiring) REAR = %.2f cm3 \n\n',
75   VbattR);

76
77 frontPC = 0.40;           %percentage of battery mass in the front
78 rearPC = 1 - frontPC;    %percentage of battery mass in the rear

79
80 frontmass = battMass*frontPC;
81 %front battery mass + casing/wiring weight(10% battery mass) [kg]

82
83 rearmass = battMass*rearPC;
84 %front battery mass + casing/wiring weight(10% battery mass) [kg]

85
86 frontcg = 1.06; %distance from nose to front battery pack CG [m]
87 rearCG = 6.37;  %distance from nose to rear battery pack CG [m]

88
89 if frontcg > rearCG || frontcg == rearCG %prevents impossible CGs
90   fprintf('Your CG locations are incorrect! Fix them and run again! \n')
91   ;
92 end

93
94 battCG = ((frontmass*frontcg) + (rearmass*rearCG))/(frontmass + rearmass);
95 oldCG = battCG;
96 %distance from nose to combined battery pack CG [m]

97
98 %Iteratively move battery packs to achieve desired battery CG target
99 Ltot = 7.5; %total aircraft length in m
100 targetcg = 2; %sets the CG target [m]

```

```

101 newcg = 2.03; %initial newcg guess [m]
102 n = 1; %CG slider
103 %
104 %-----CG Recalculation Begins-----
105
106 if frontcg > targetcg %checks if target is fore of Fcg
107     while frontcg > 0.40 + (BattDepthF/2) %limits frontcg position due to
108         structural obstacles
109     frontcg = targetcg - (0.01*n); %starts pulling front cg forward first
110     %newcg = ((frontmass*frontcg) + (rearmass*rearcg))/(frontmass +
111         rearmass);
112     %recalculates avg cg
113     if abs(newcg-targetcg)<0.02
114         break
115     end
116
117
118 elseif rearcg < targetcg %checks if target is aft of Rcg
119
120     while rearcg < 9-(BattDepthR/2) %limits rearcg position due to
121         structural obstacles
122     rearcg = targetcg + (0.01); %starts pulling rear cg aft first
123     newcg = ((frontmass*frontcg) + (rearmass*rearcg))/(frontmass +
124         rearmass);
125     %recalculates avg cg
126     if abs(newcg-targetcg)<0.02
127         break
128     end
129
130
131 else %only option left is that the target is between the two
132
133 if (frontmass*frontcg)>(rearmass*rearcg) %determines which pack is
134     more critical
135     while frontcg < targetcg %keeps Fcg in front of Tcg
136         frontcg = frontcg + (0.01);
137         newcg = ((frontmass*frontcg) + (rearmass*rearcg))/(frontmass +
138             rearmass);
139         %recalculates avg cg
140         if abs(newcg-targetcg)<0.02
141             break

```

```

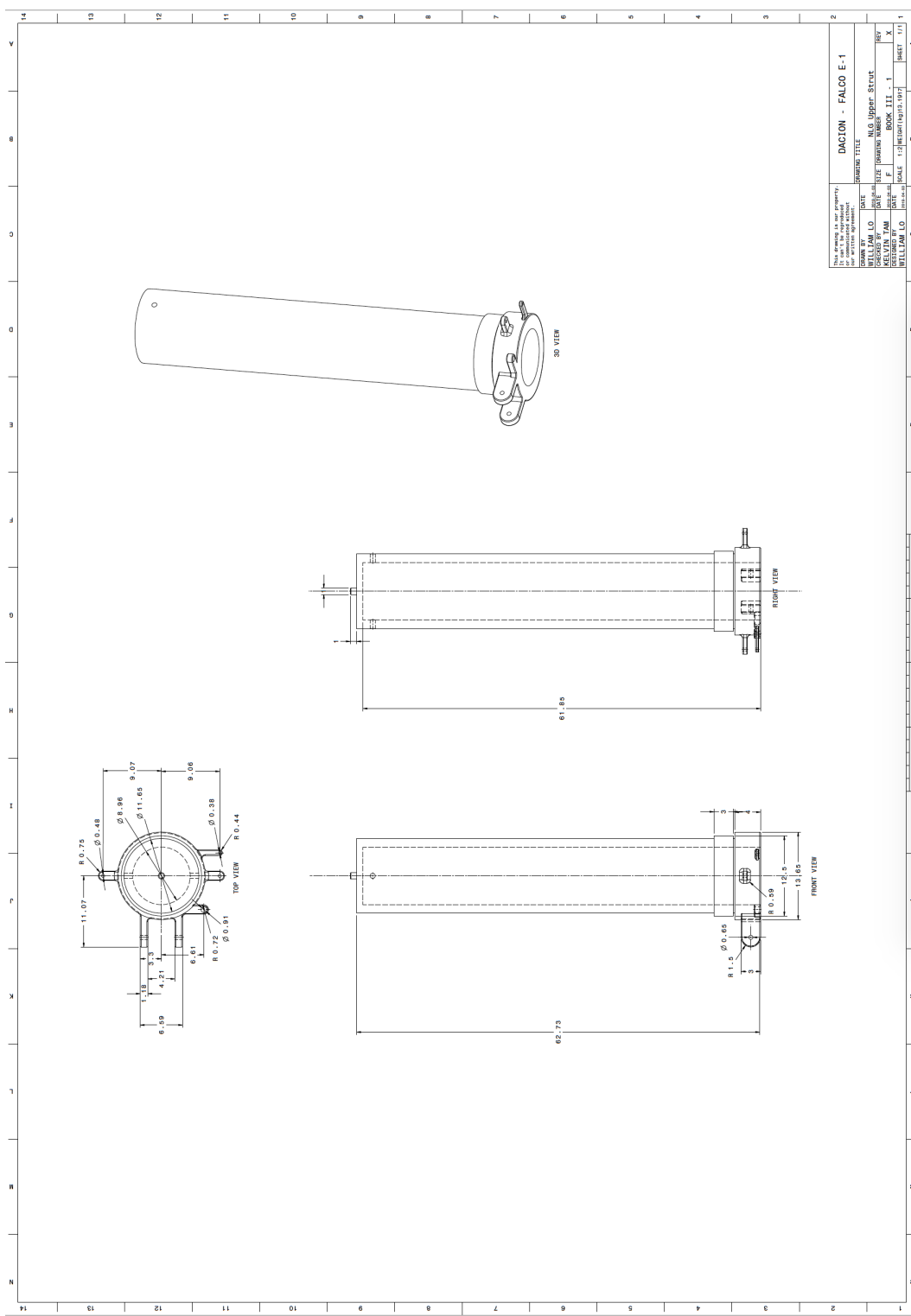
140 end
141
142 end
143 elseif (frontmass*frontcg)<(rearmass*rearcg) %determines which pack is
144     more critical
145
146     while rearcg > targetcg %keeps Rcg behind Tcg
147         rearcg = rearcg - (0.01);
148         newcg = ((frontmass*frontcg) + (rearmass*rearcg)) / (frontmass +
149             rearmass);
150         %recalculates avg cg
151         if abs(newcg-targetcg)<0.02
152             break
153         end
154     end
155 end
156
157 fprintf('----BATTERY DISTRIBUTION AND CG CALCULATIONS---- \n');
158 fprintf('Battery mass = %.2f kg (%.0f%% empty weight) \n', battMass,
159     battPC*100);
160 fprintf('Distribution = %.2f%% Front (%.2f kg) %.2f%% Rear (%.2f kg) \n',
161     frontPC*100,frontmass,rearPC*100,rearmass);
162 fprintf('Original CG = %.2f m --- Recalculated CG = %.2f m --- Target CG
163     =%.2f m \n', oldCG,newcg,targetcg);
164 fprintf('Front CG = %.2f m Rear CG = %.2f m \n\n\n', frontcg,rearcg);

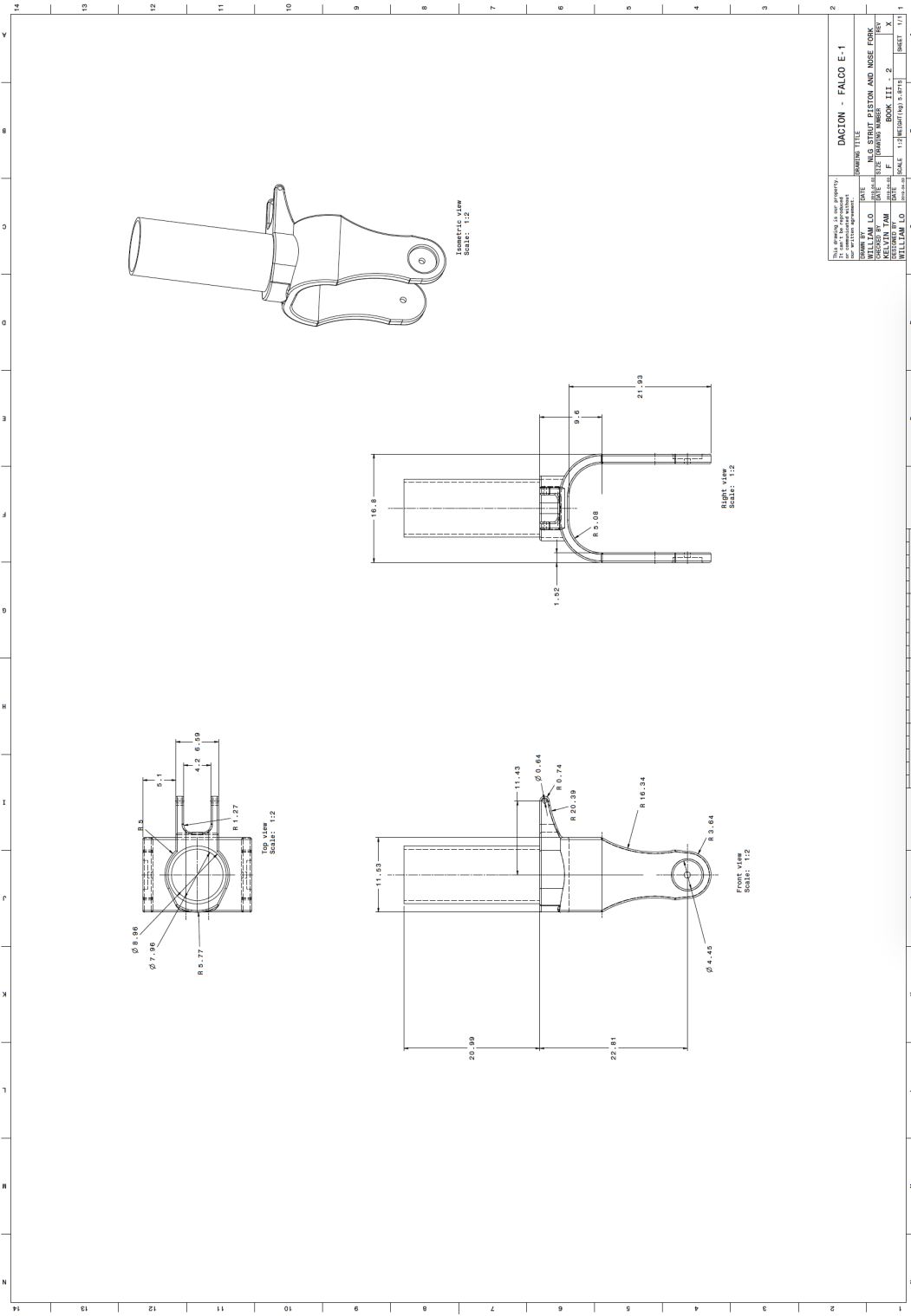
```

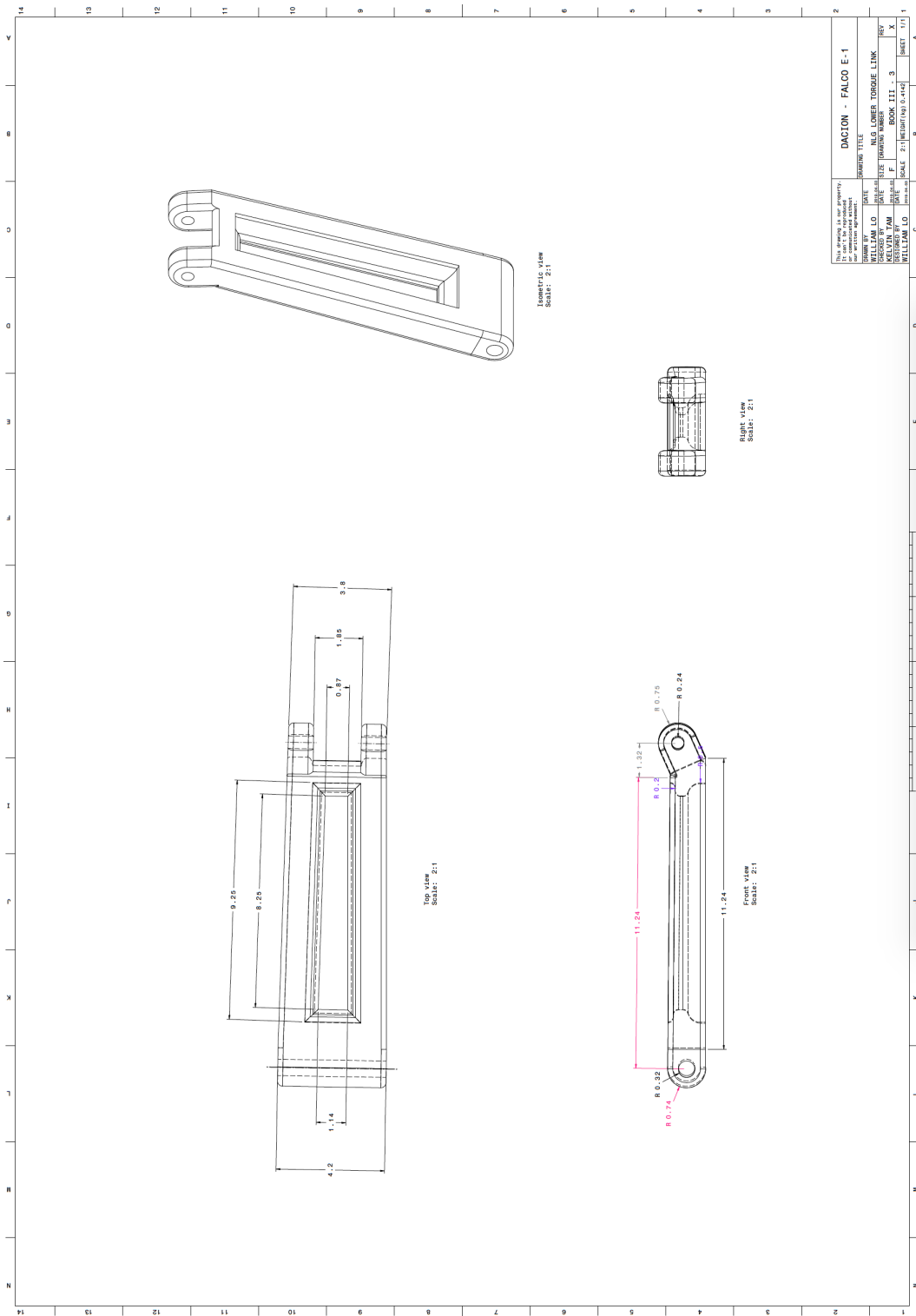
F CATIA Drawings

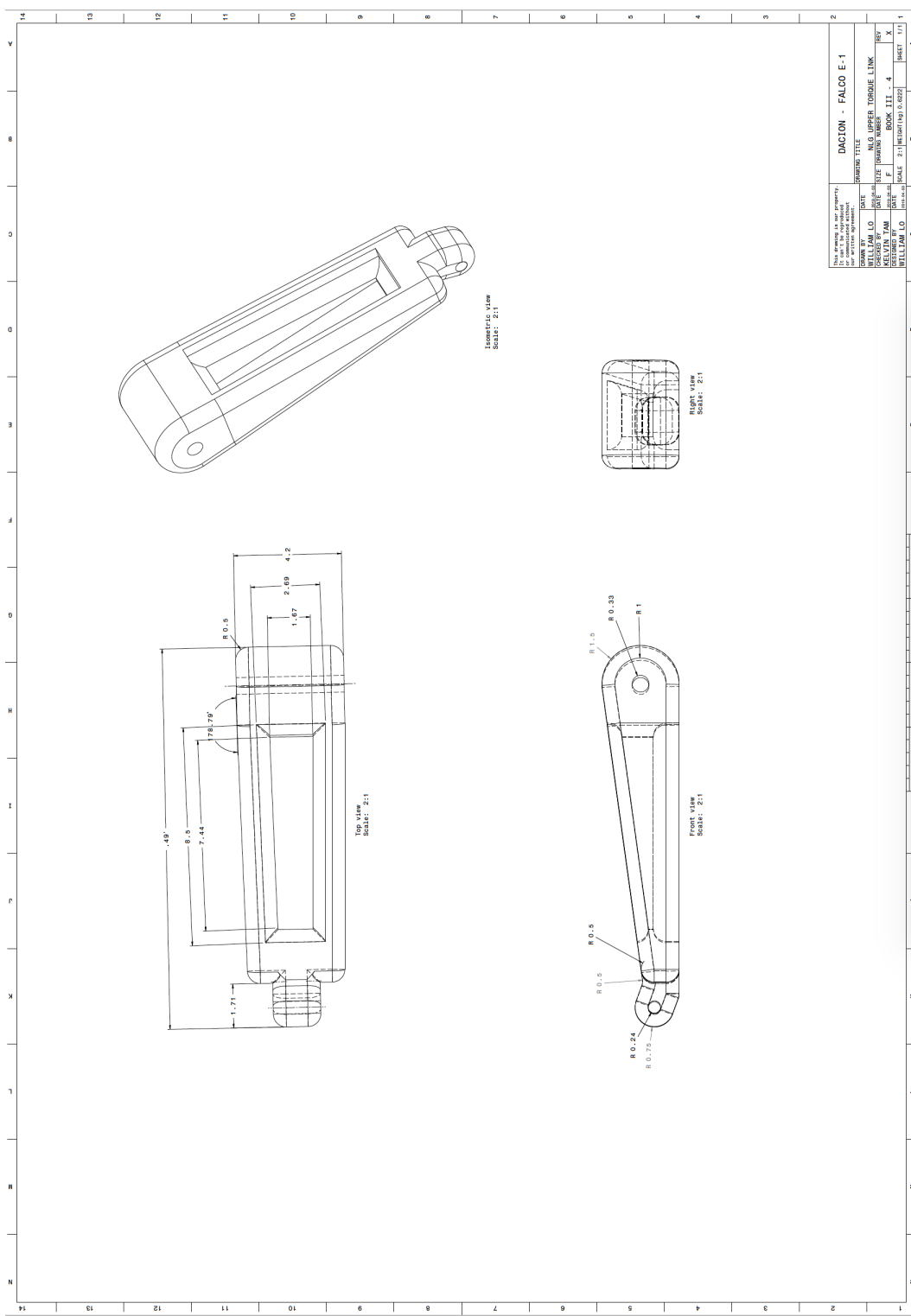
E.1 Landing Gear Drawings

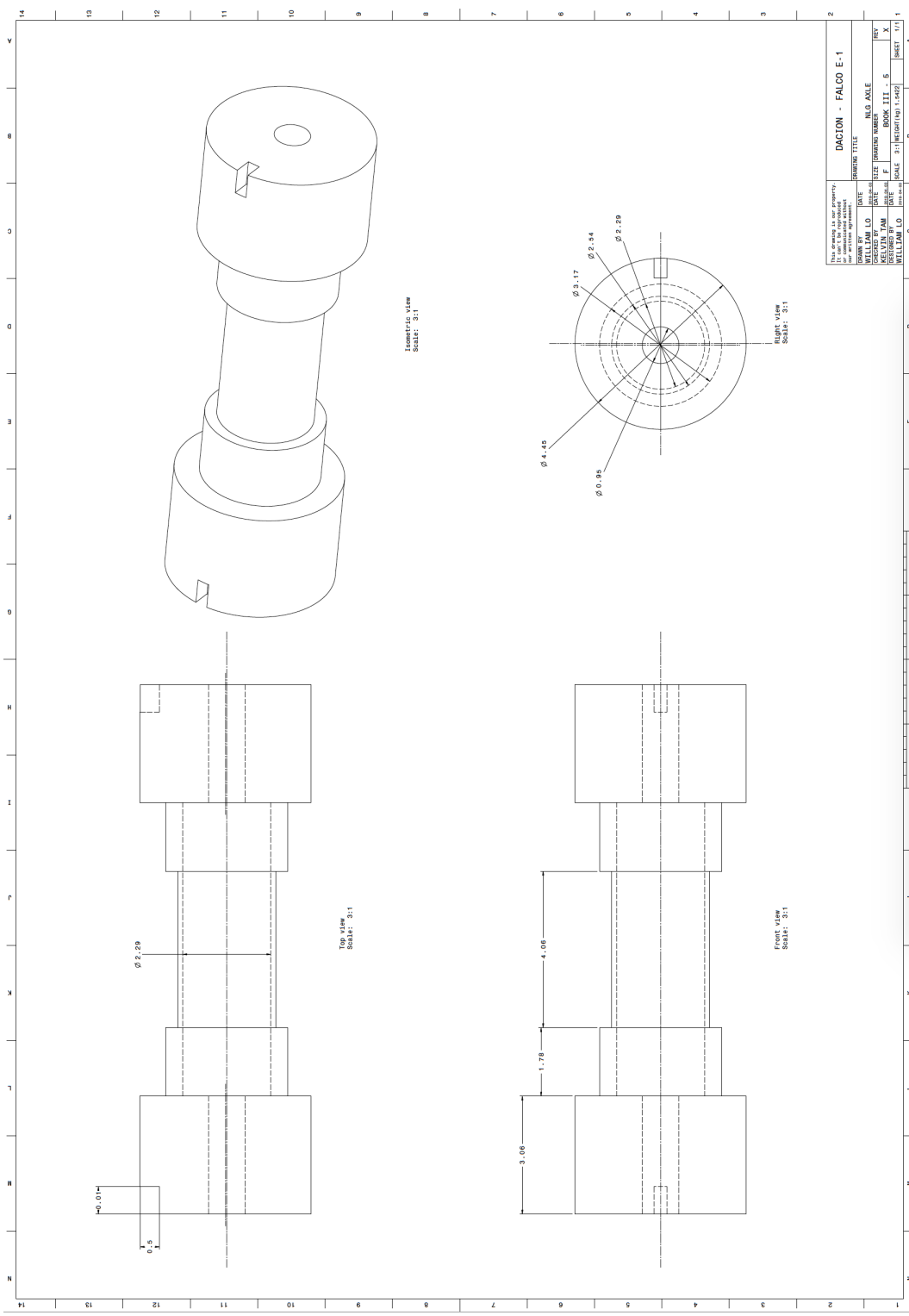
All dimensions in the CATIA drawings are in centimeter.

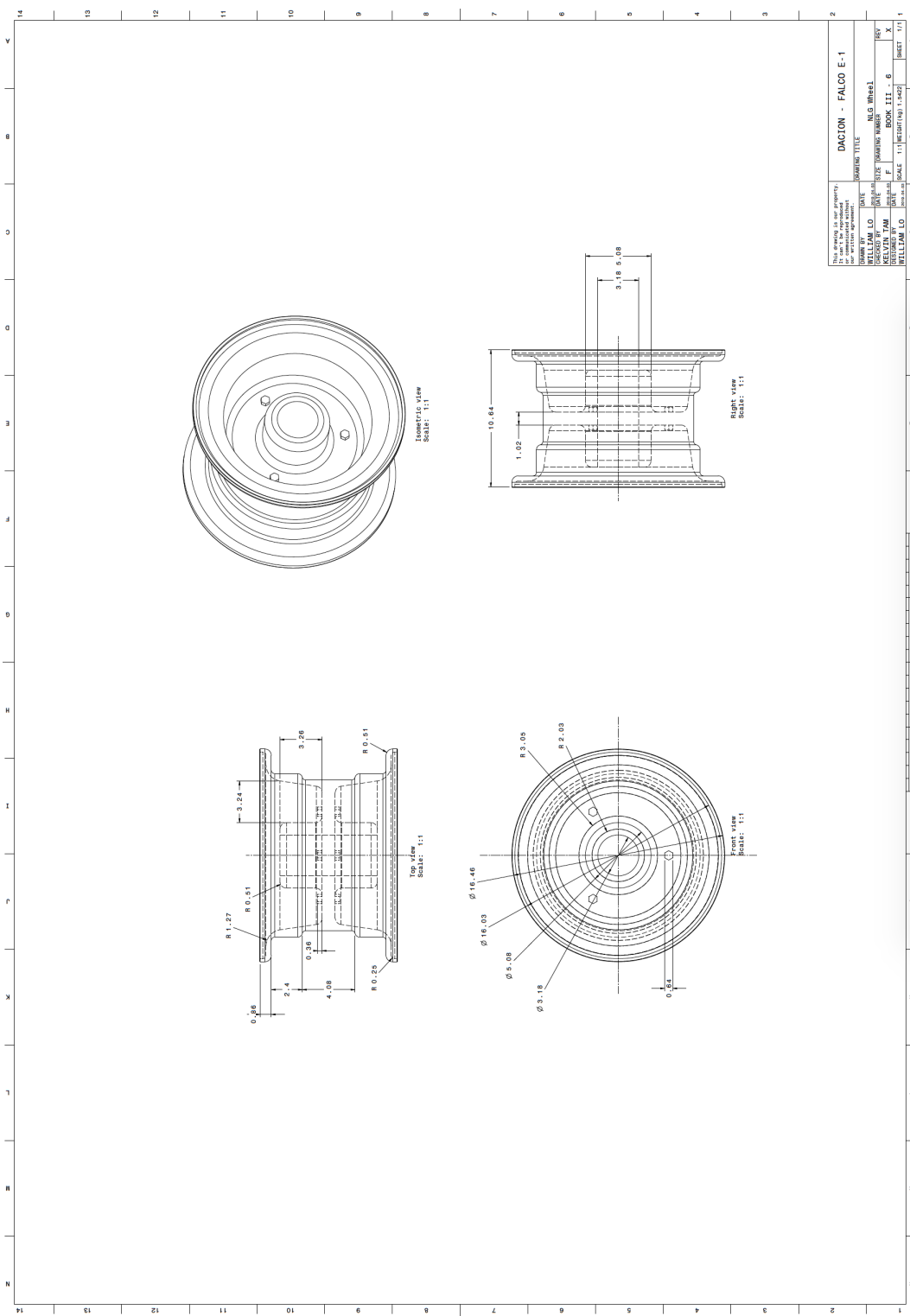


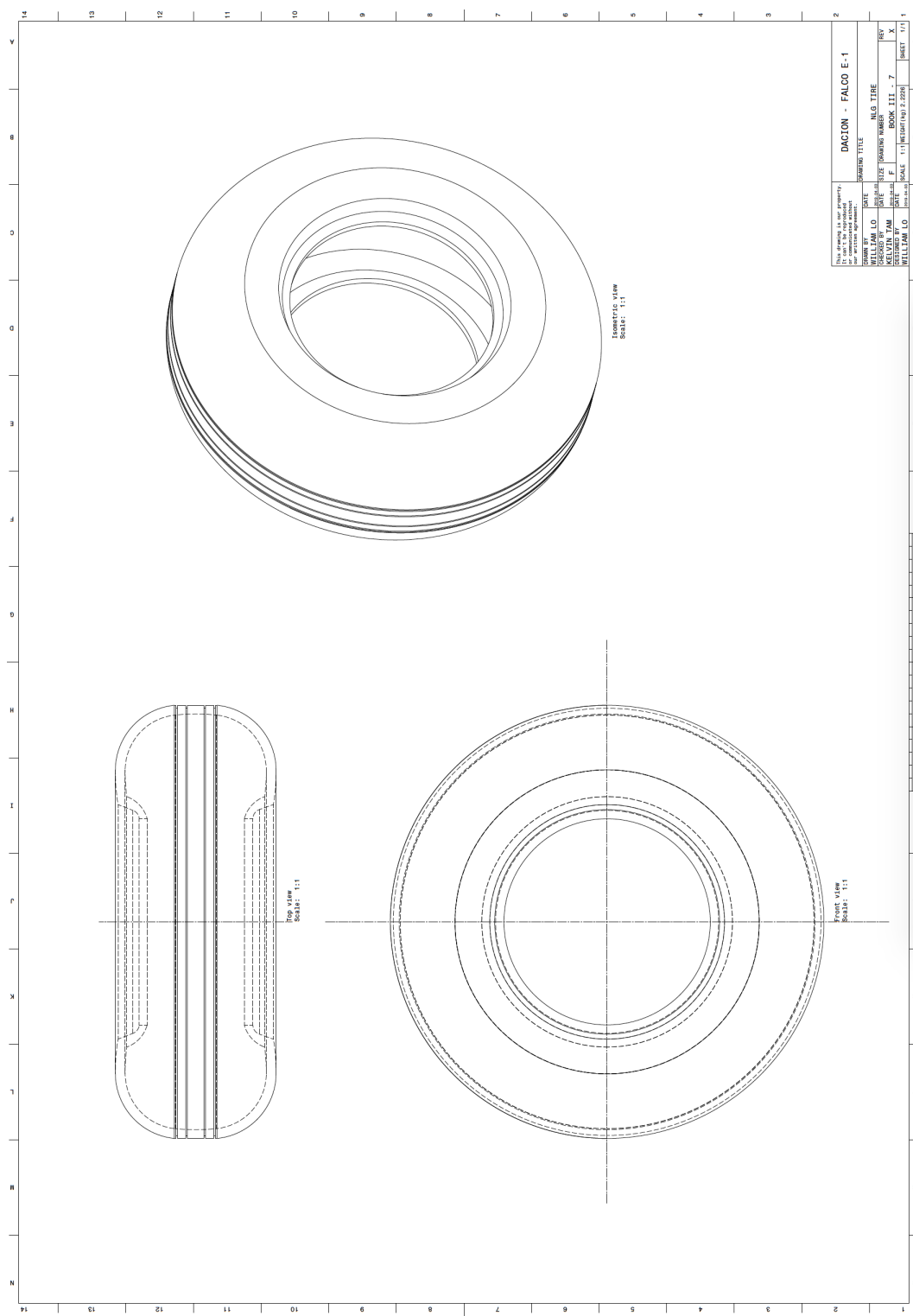


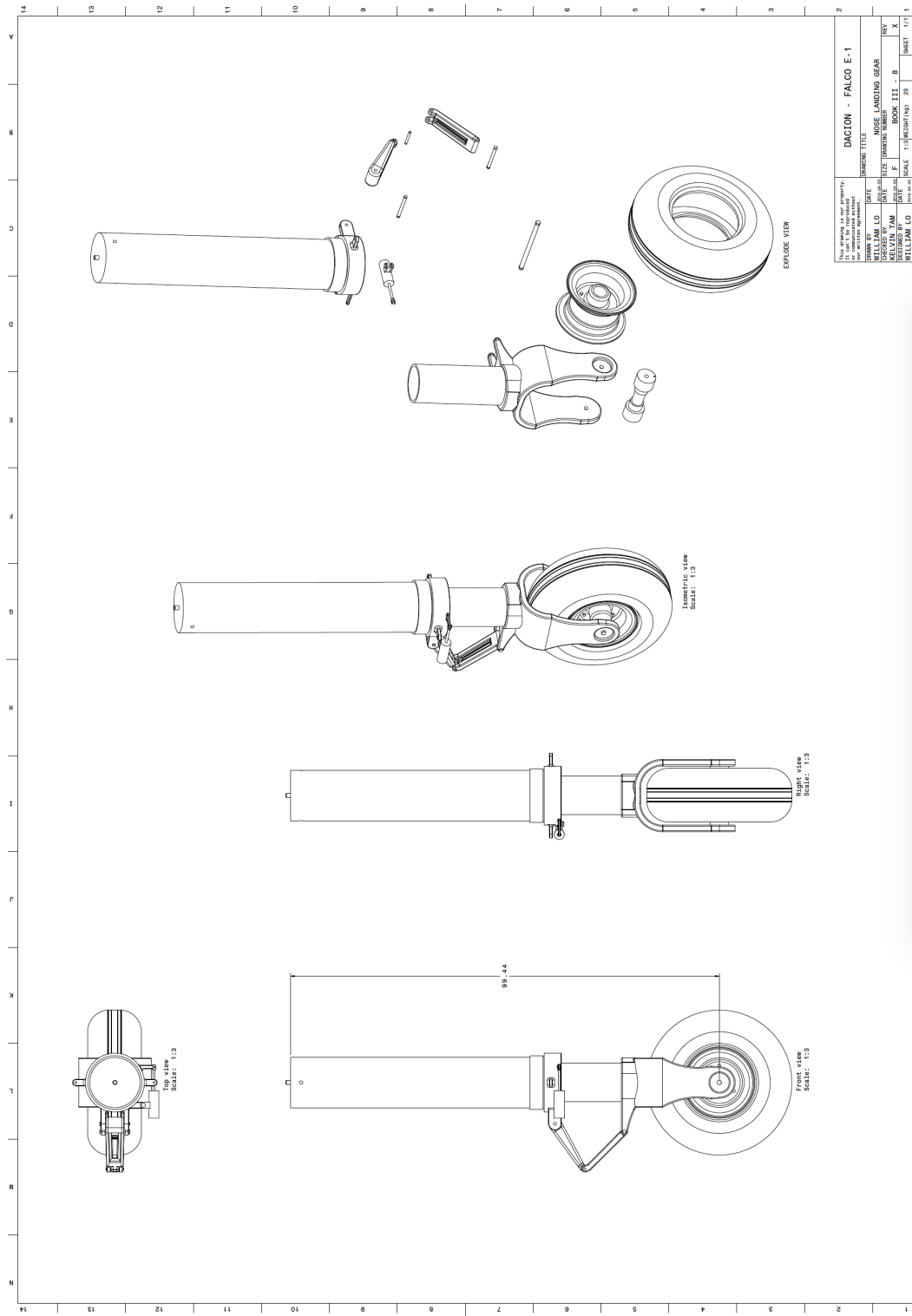


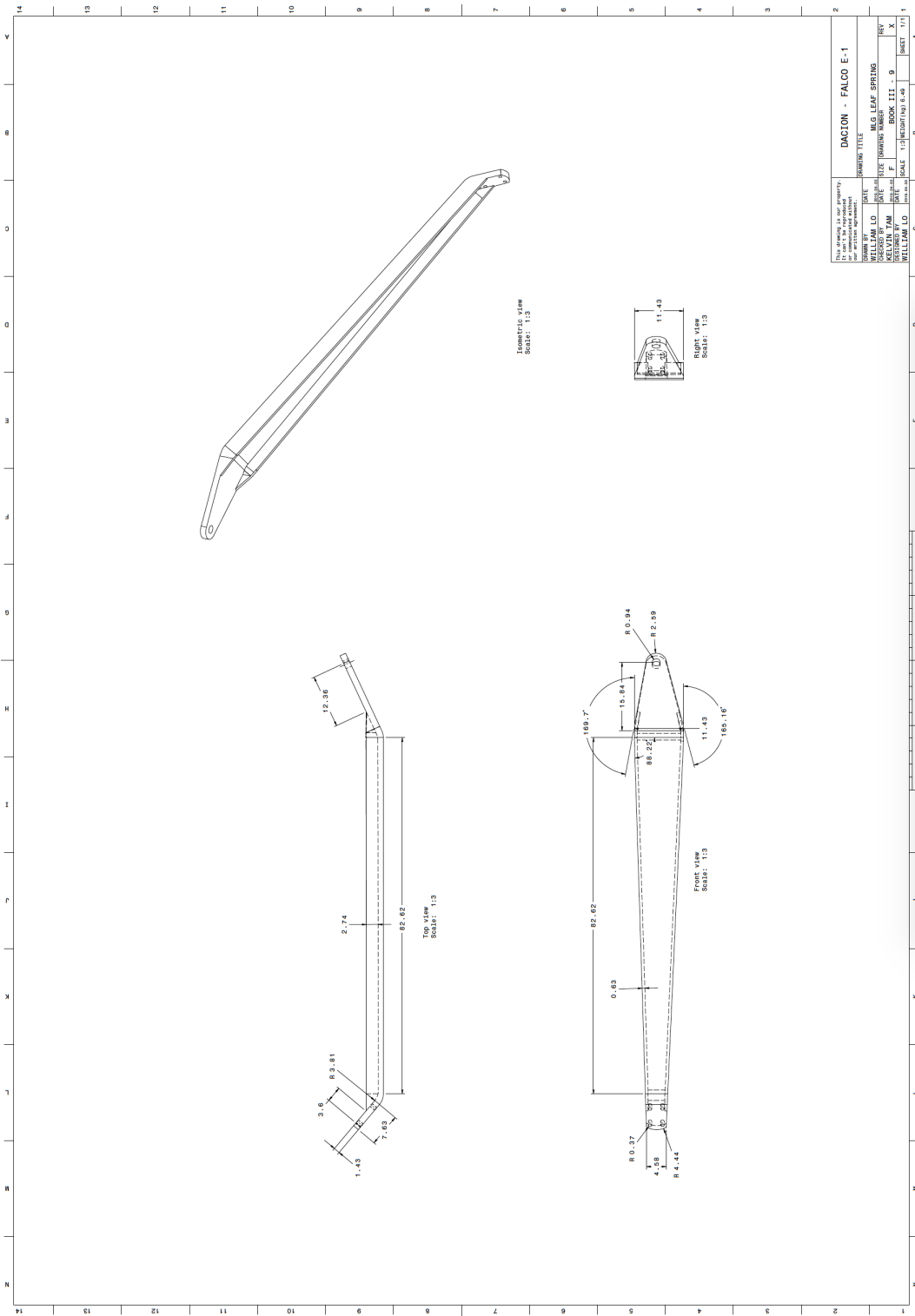


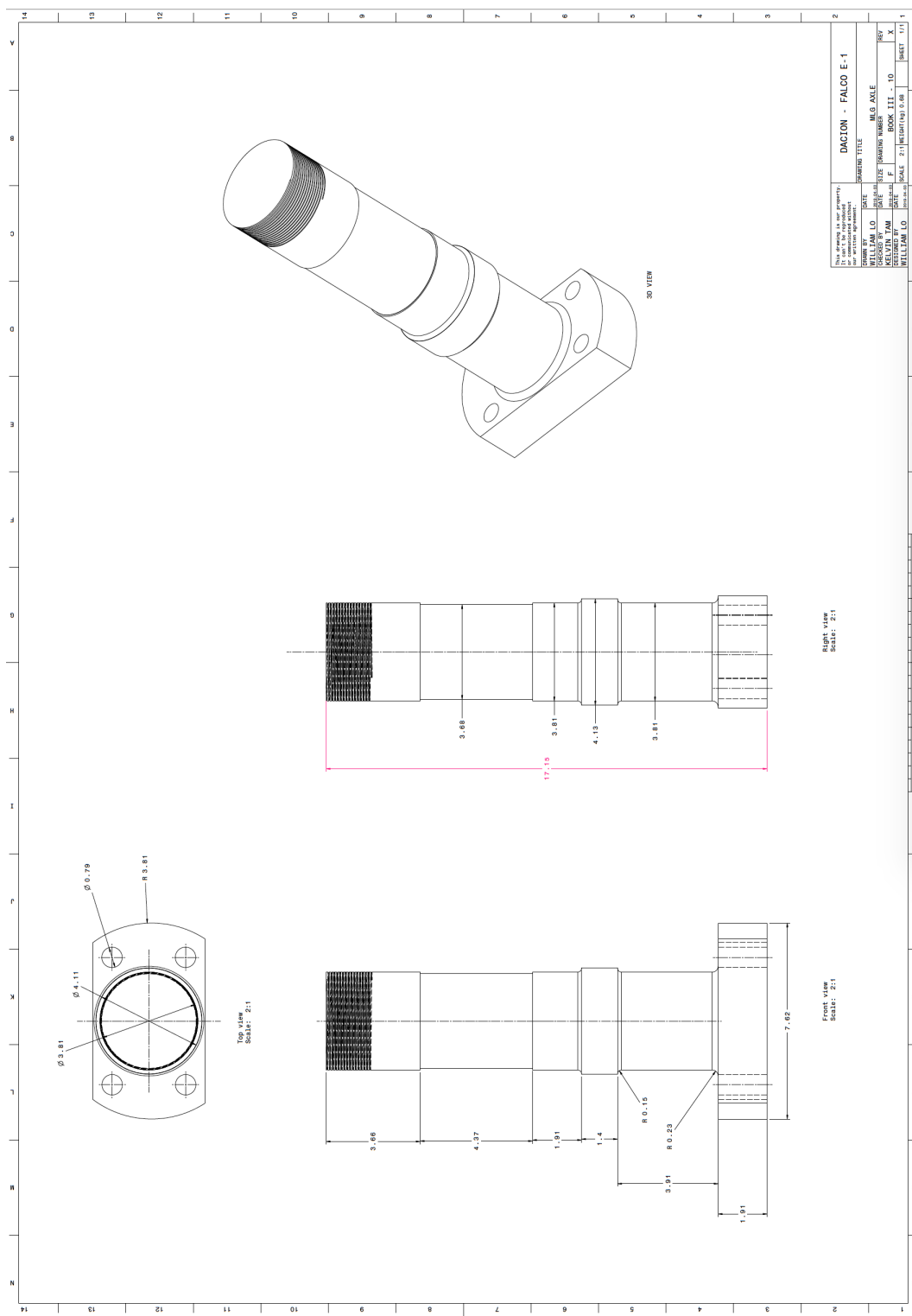


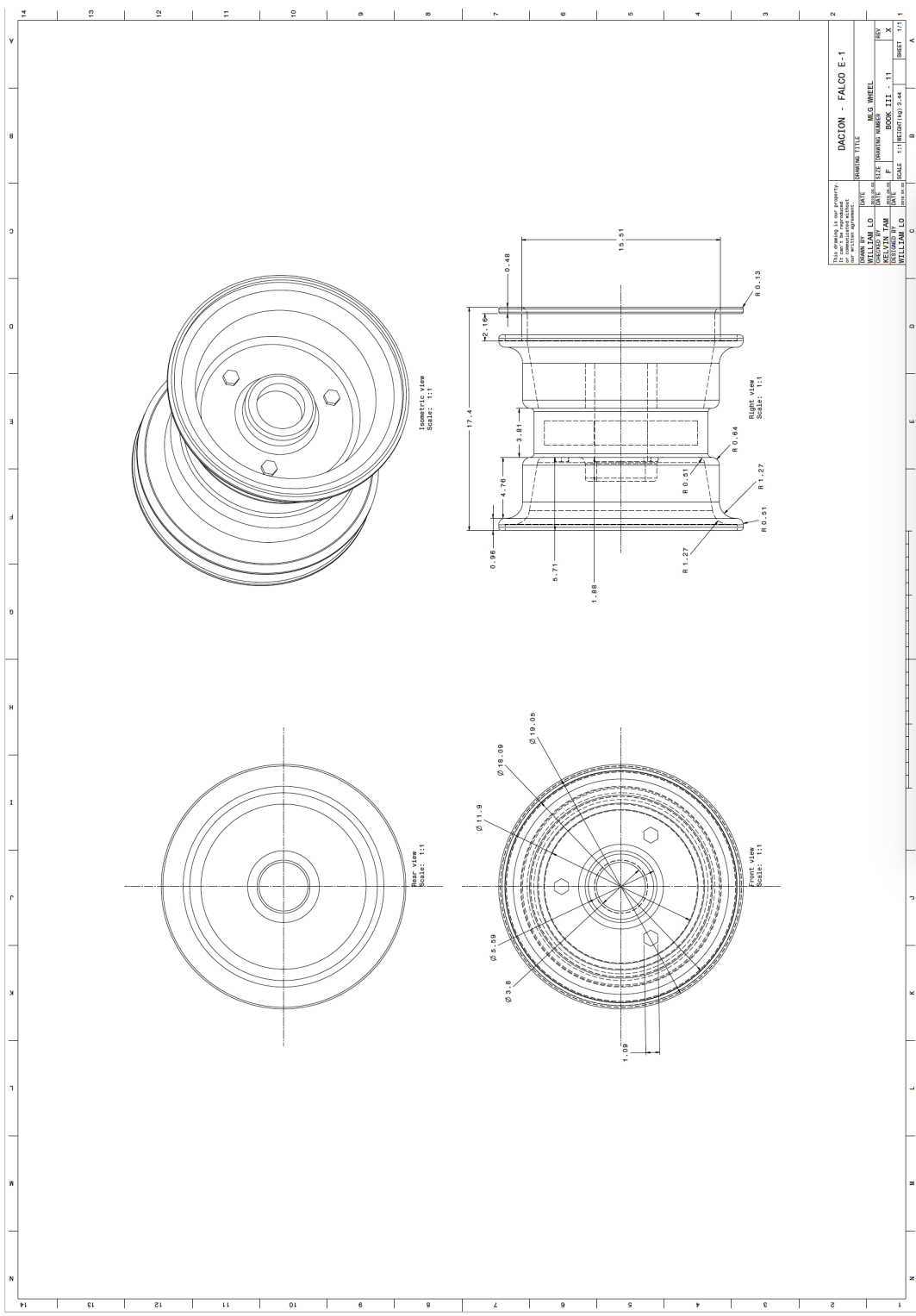


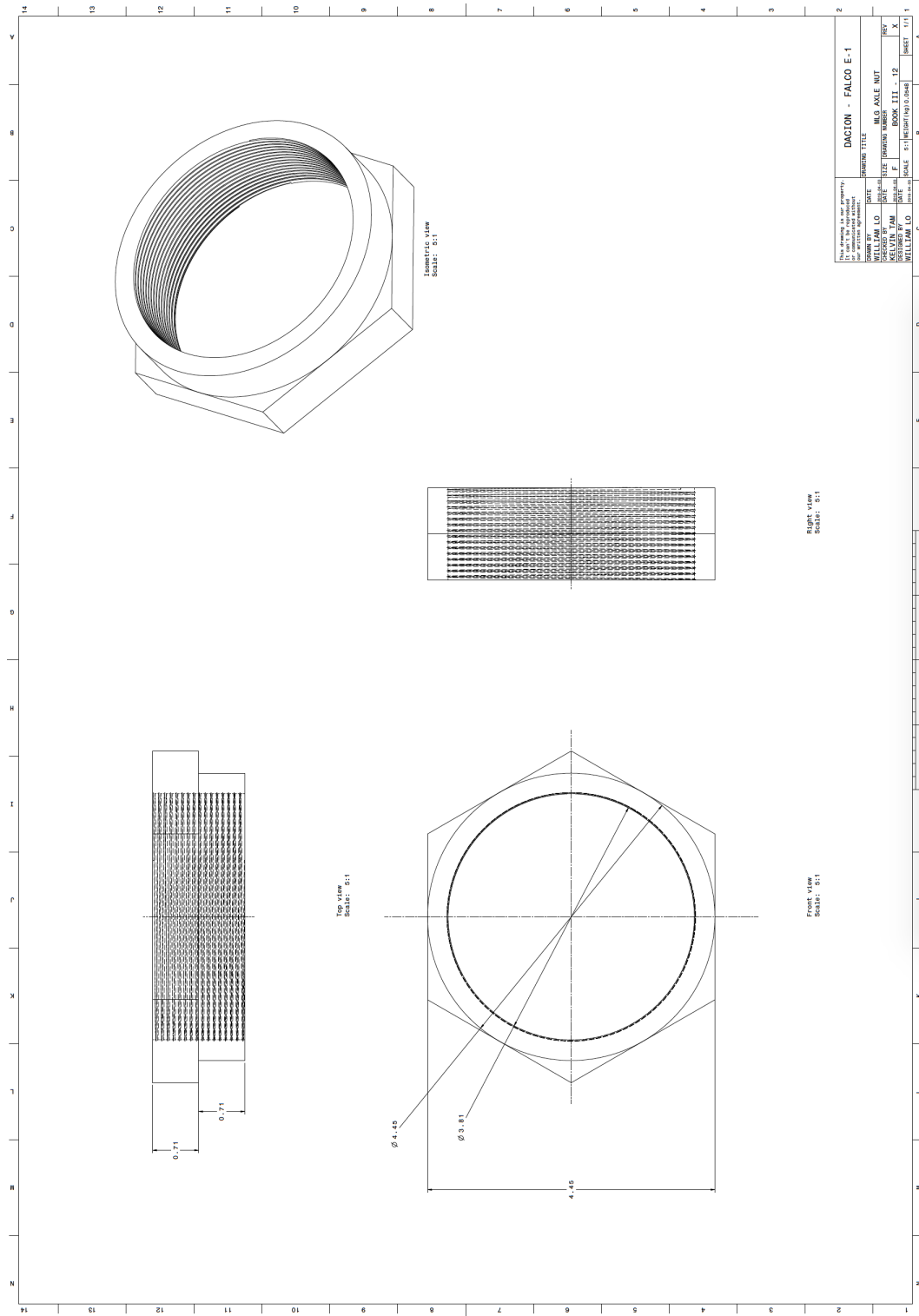


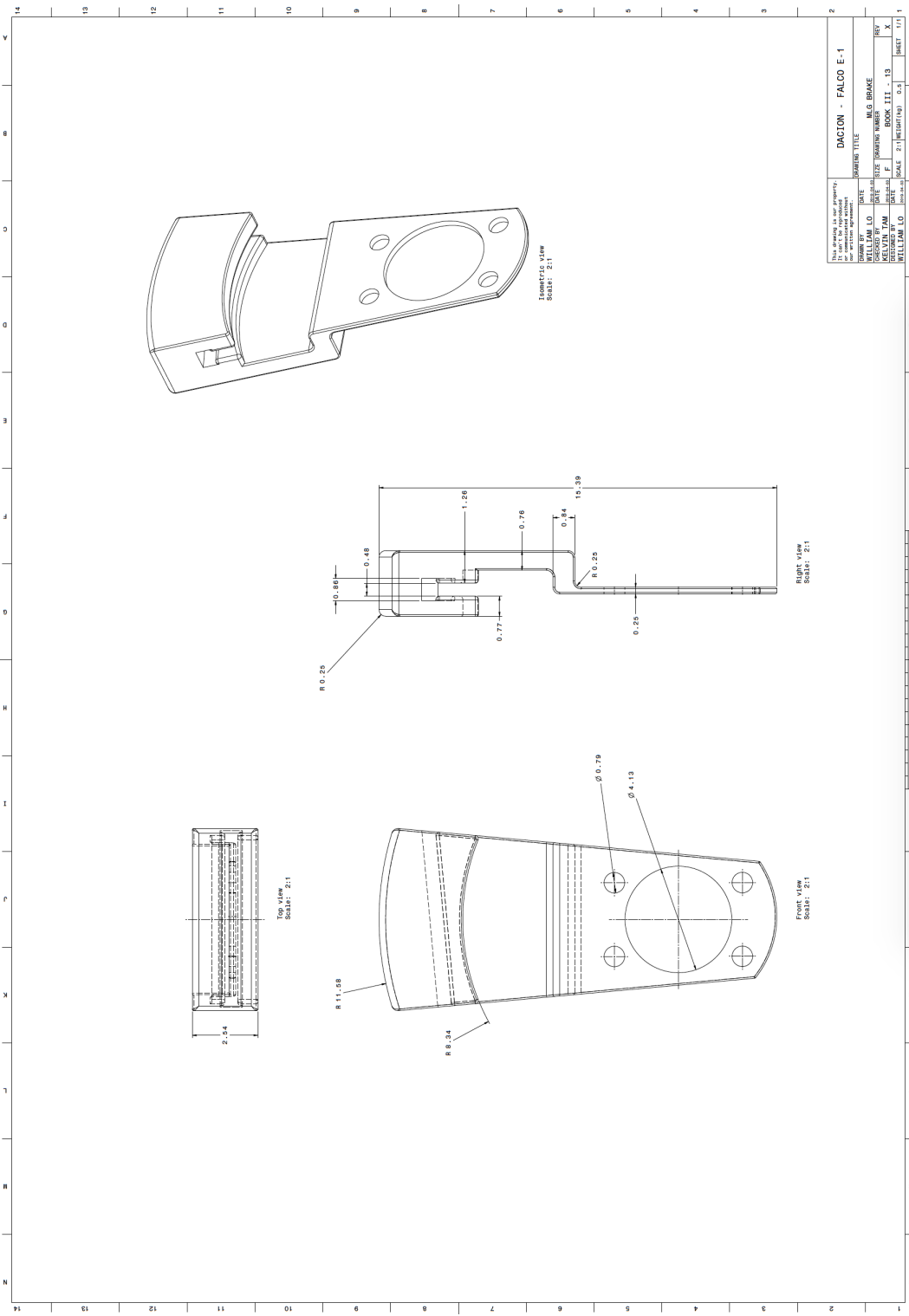


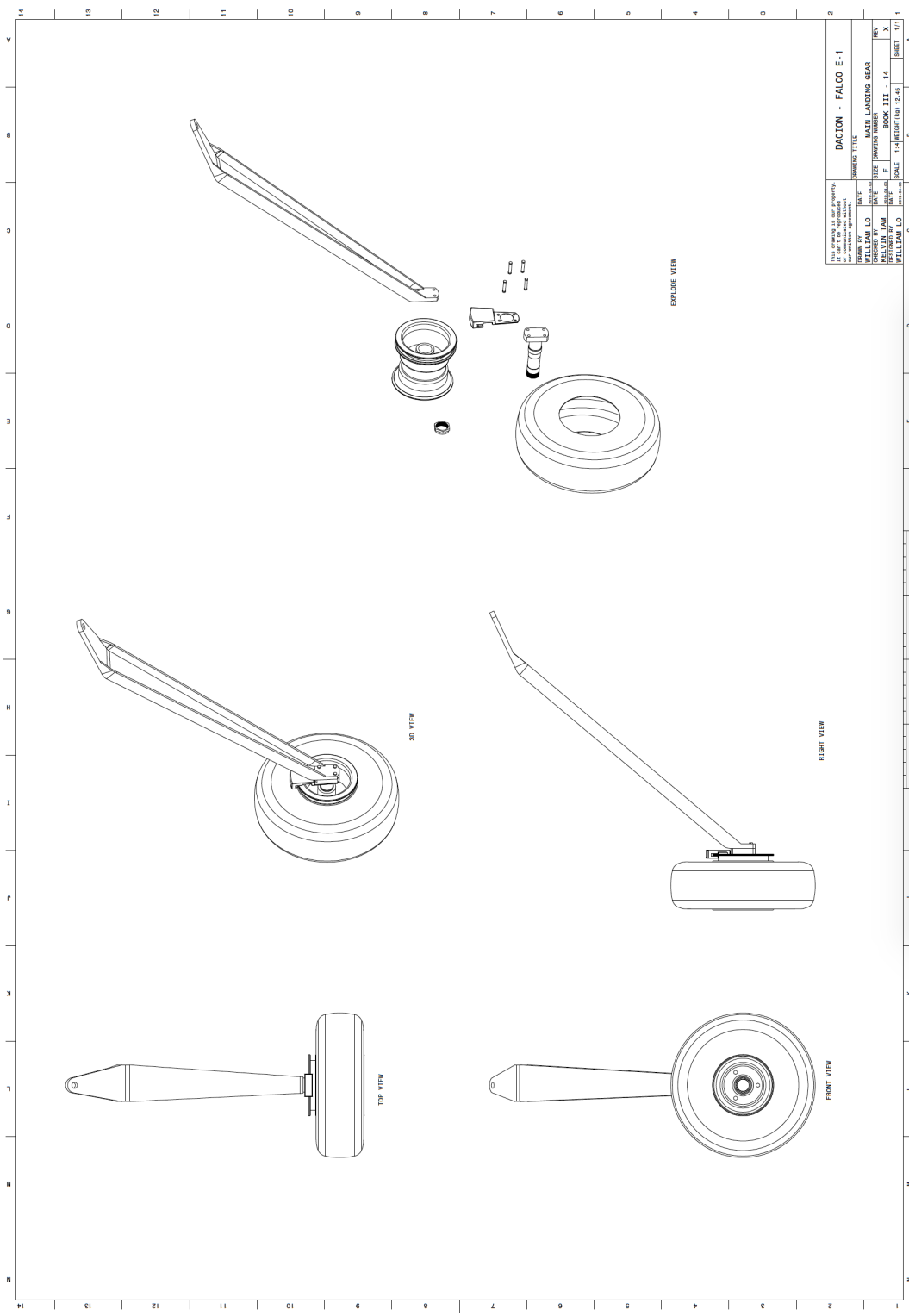


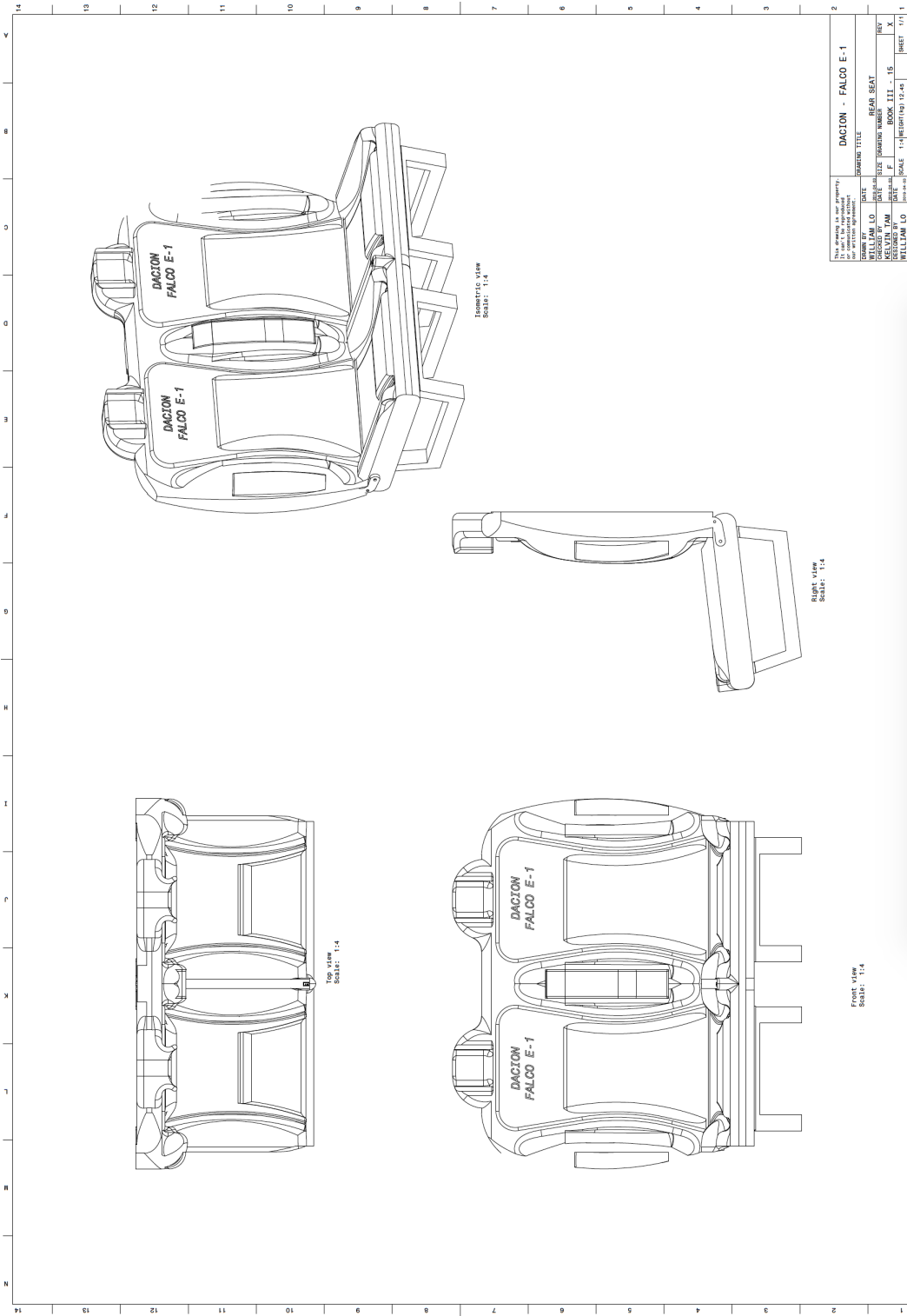


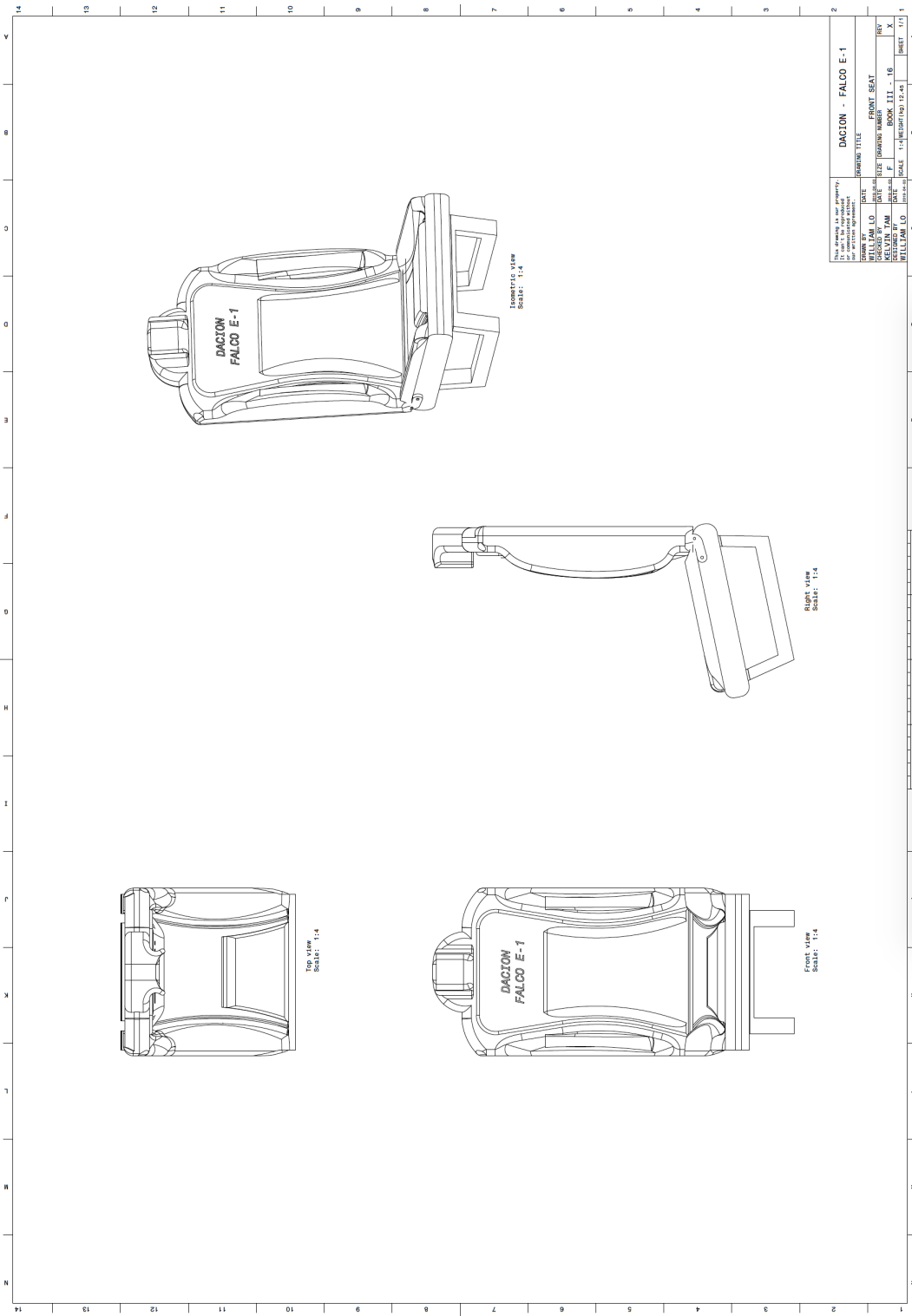






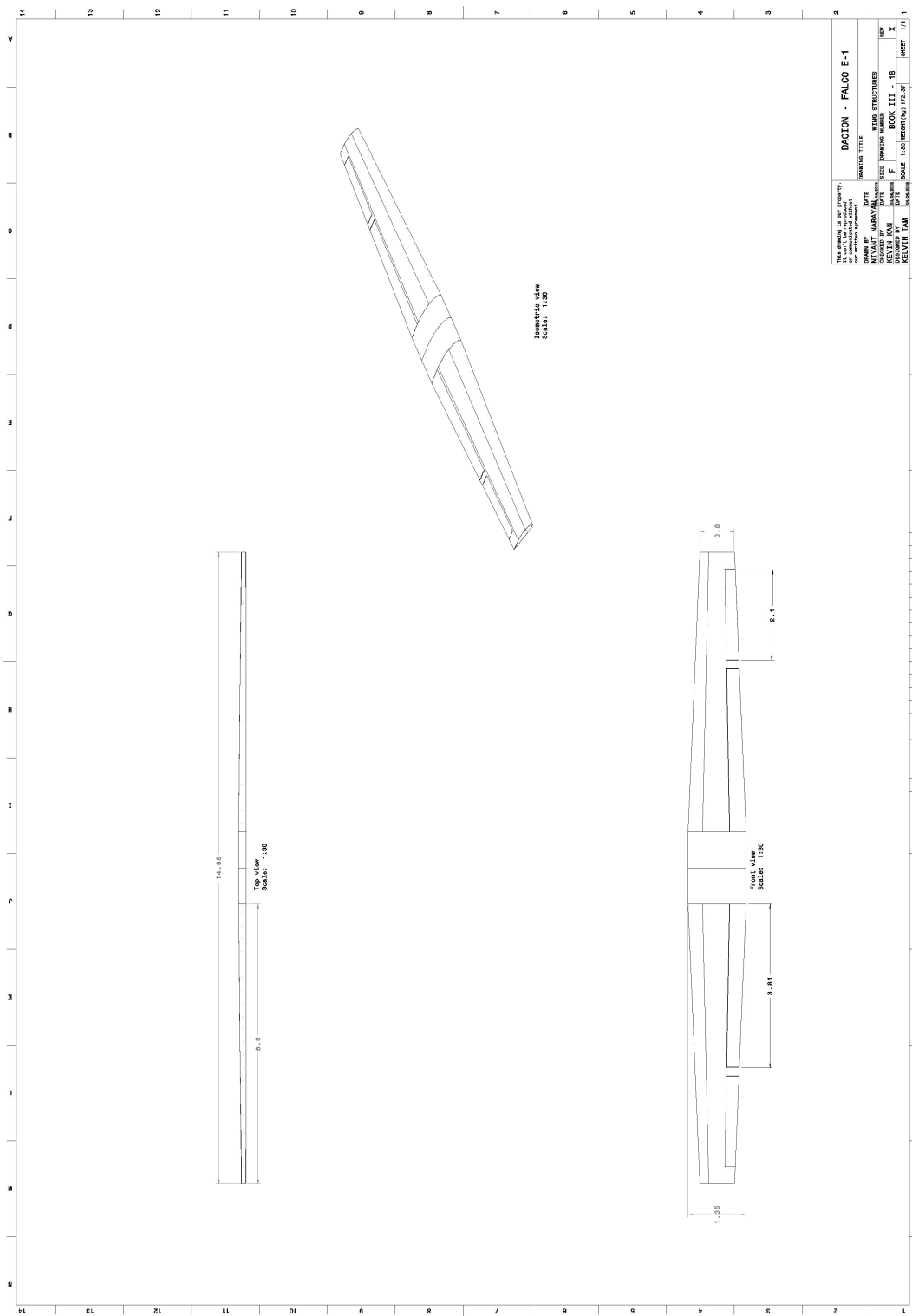






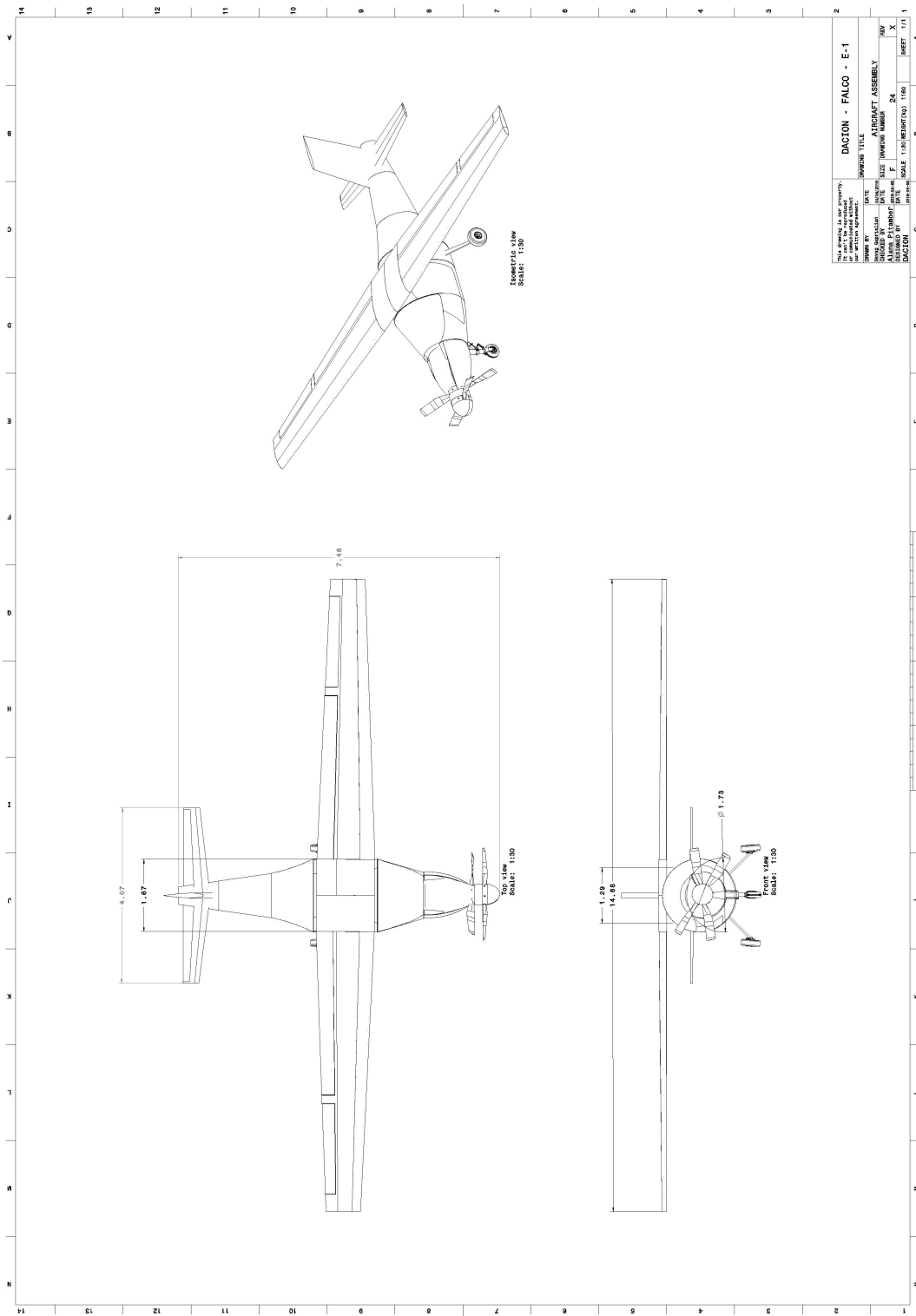
E.2 Wing Structure Drawing

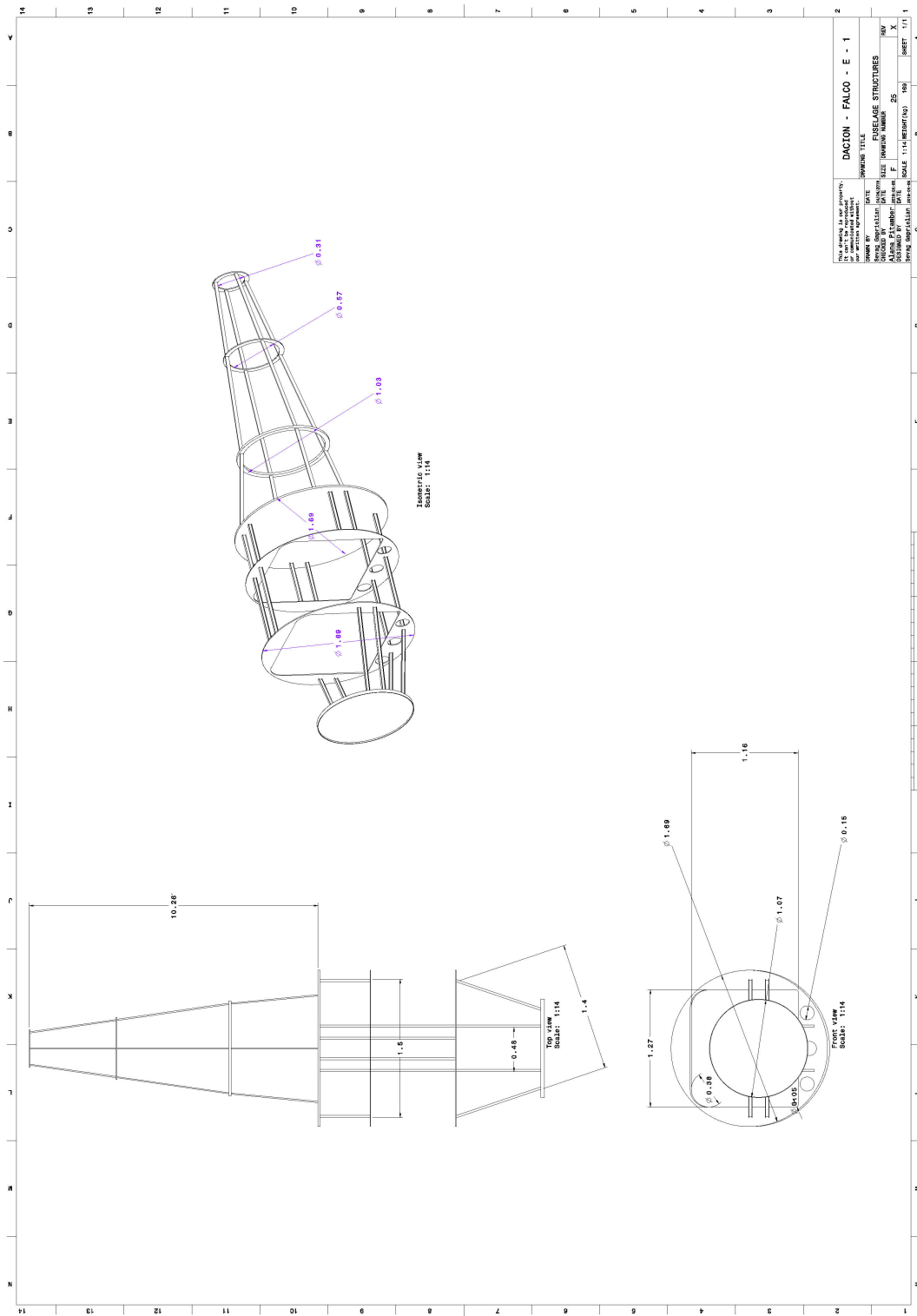
Wing Drawing units are in meters.



F.3 Fuselage Structure and Assembly Drawings

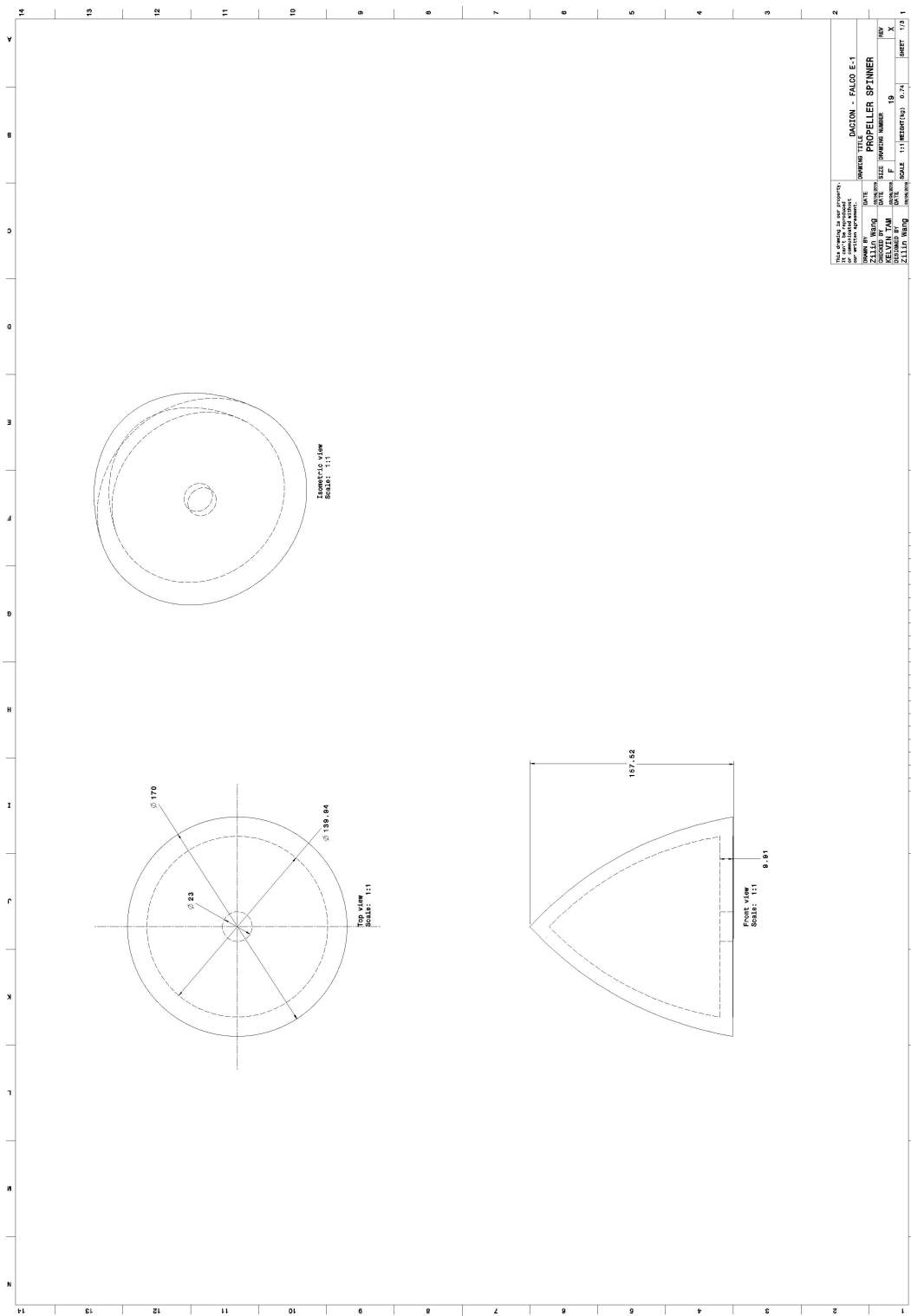
Drawing units are in meters.

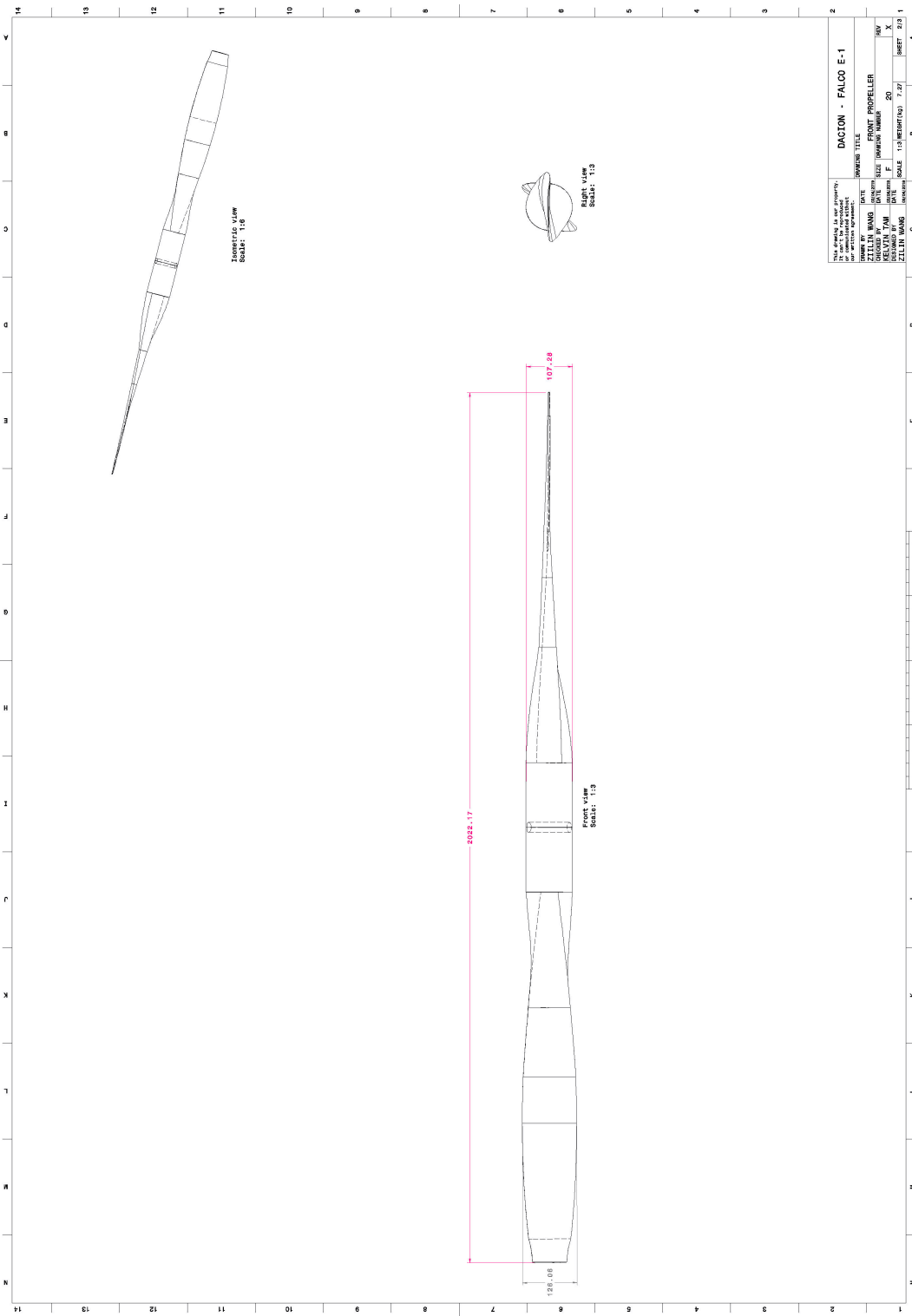


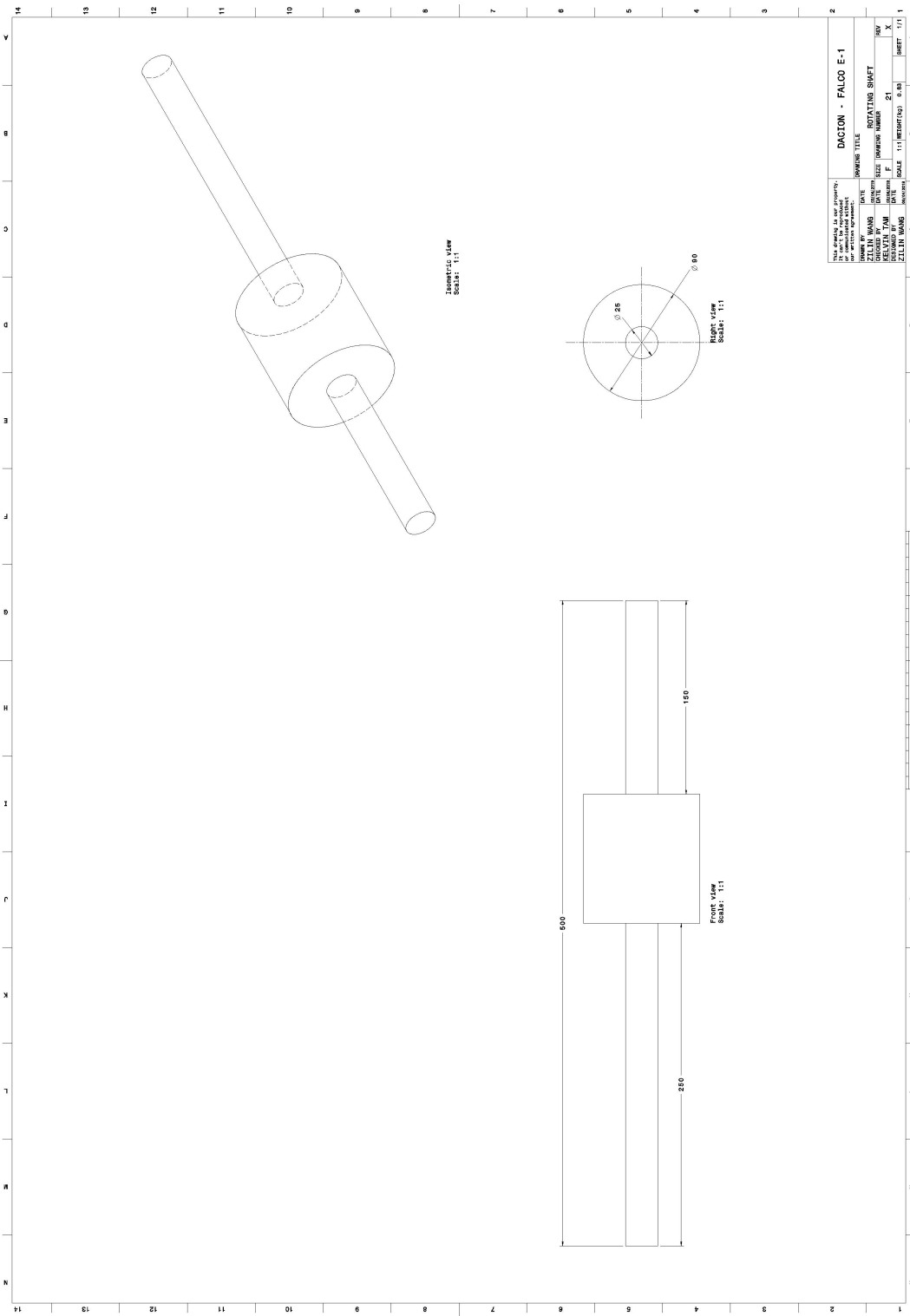


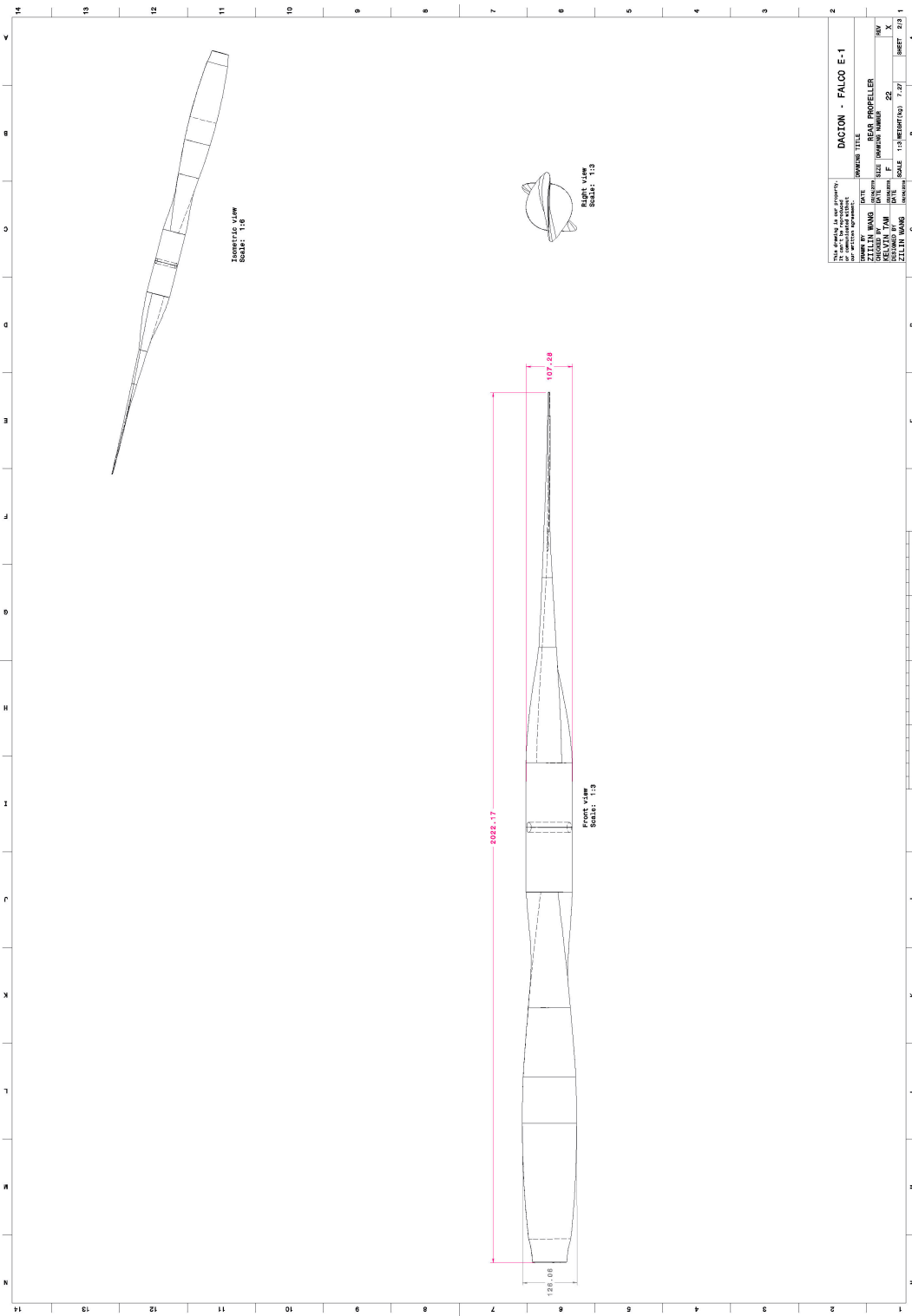
F.4 Propeller Drawing

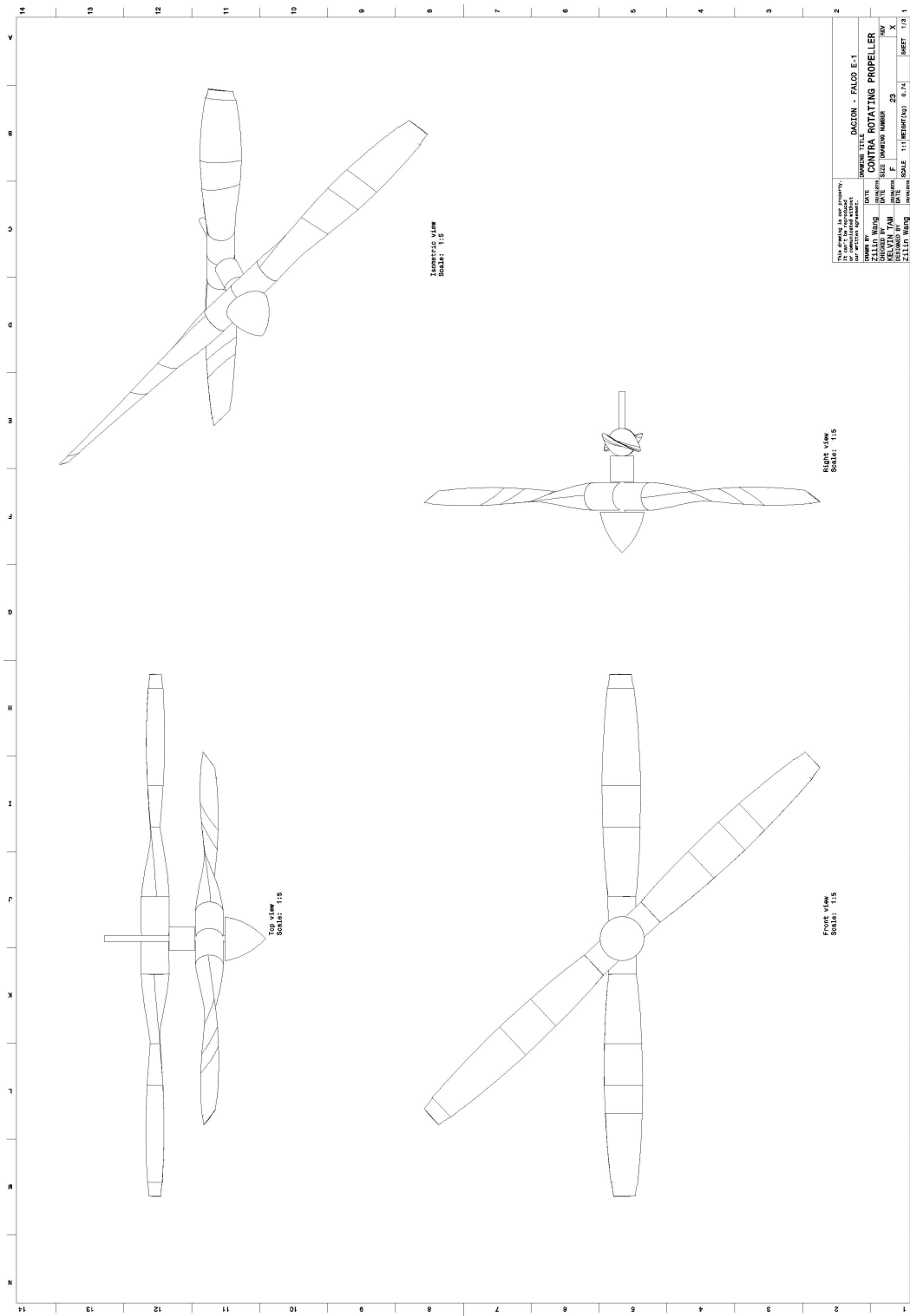
Propeller Drawing units are in millimeters.











G ANSYS Results

G.1 Landing Gear

523.485 Side Load Conditions:

The following figures are the results of 1.33 limit vertical load factor , with the vertical ground reaction divided by two between the main gear.

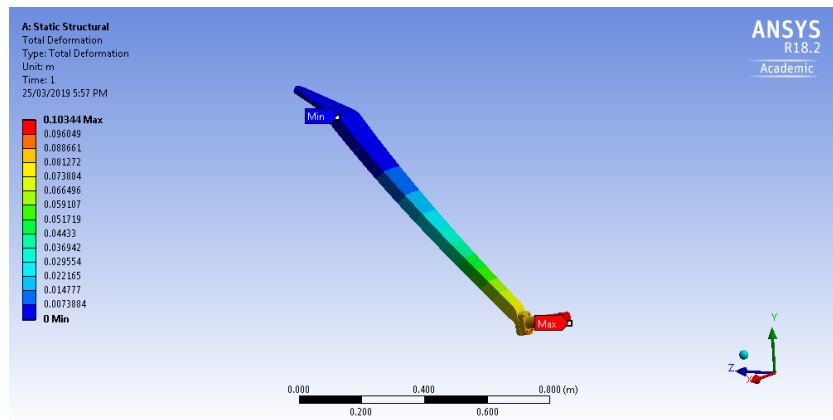


Figure G.1: MLG Total Deformation with 1.33 limit vertical load factor

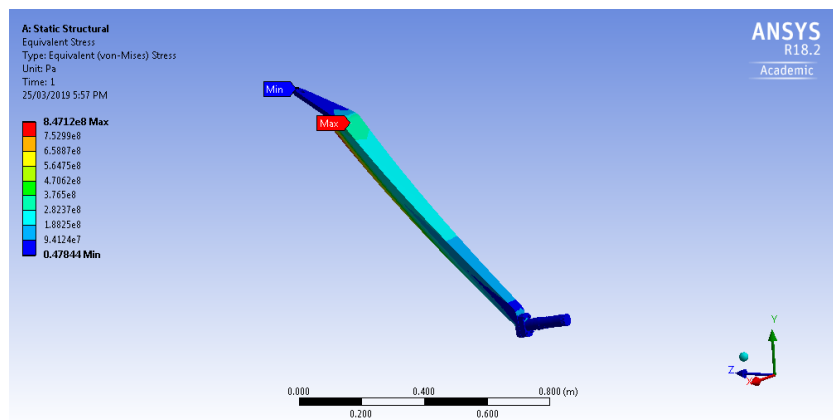


Figure G.2: MLG Equivalent Stress with 1.33 limit vertical load factor

The following figures are the results of 0.5W is acting inboard on one side.

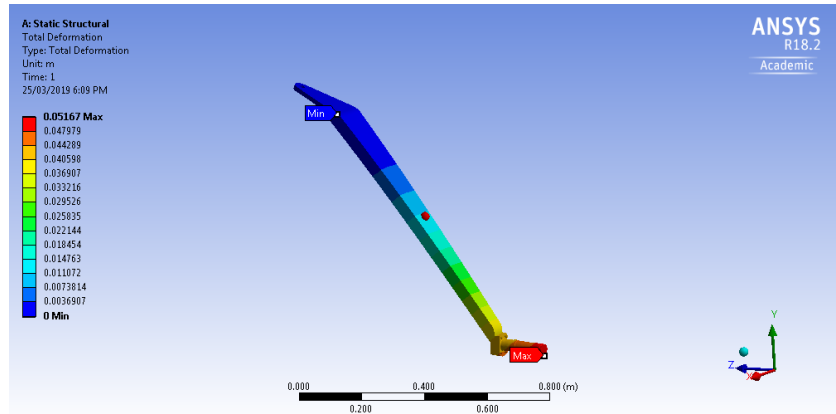


Figure G.3: MLG Total Deformation with 0.5W on one side

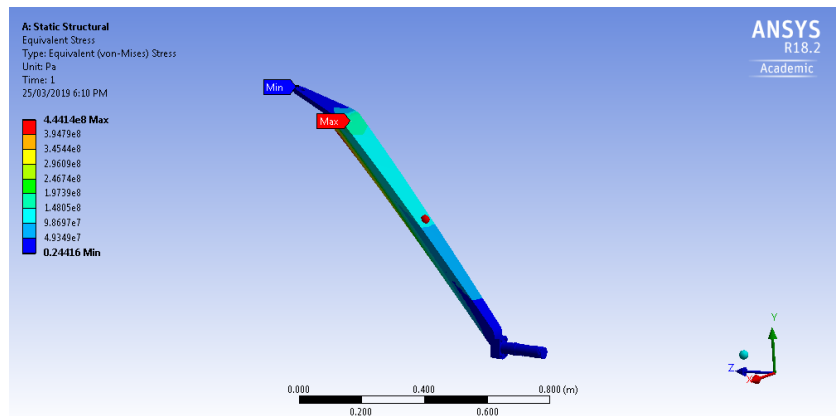


Figure G.4: MLG Equivalent Stress with 0.5W Acting on One Side

The following figures are the results of 0.33W is acting outboard on one side.

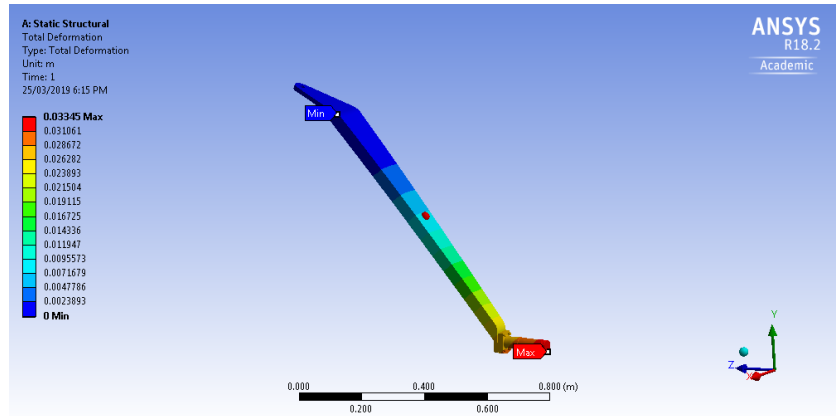


Figure G.5: MLG Total Deformation with 0.33W Acting Outboard on On Side

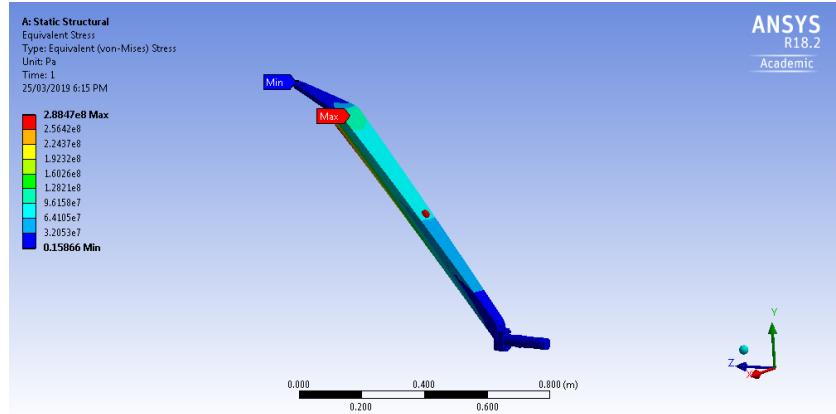


Figure G.6: MLG Equivalent Stress with 0.33W Acting Outboard on On Side

523.499 Supplementary Conditions for Nose Wheels The following figures are the results of the limit force components at the axle for aft loads.

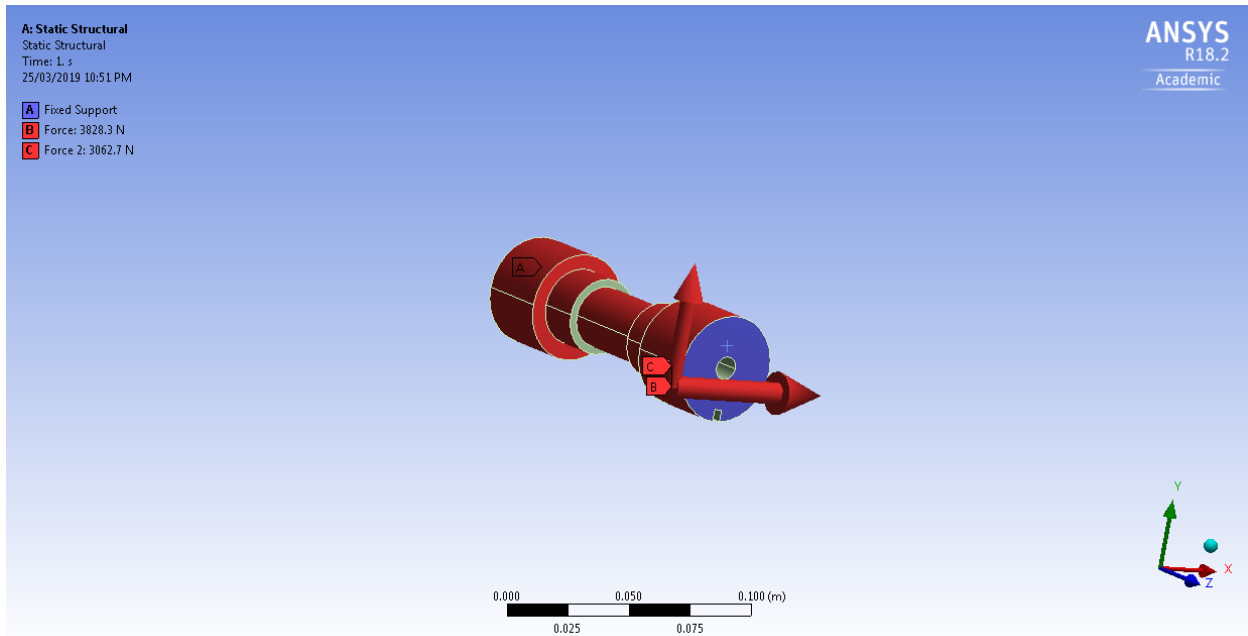


Figure G.7: NLG Layout with 0.8 Drag Component

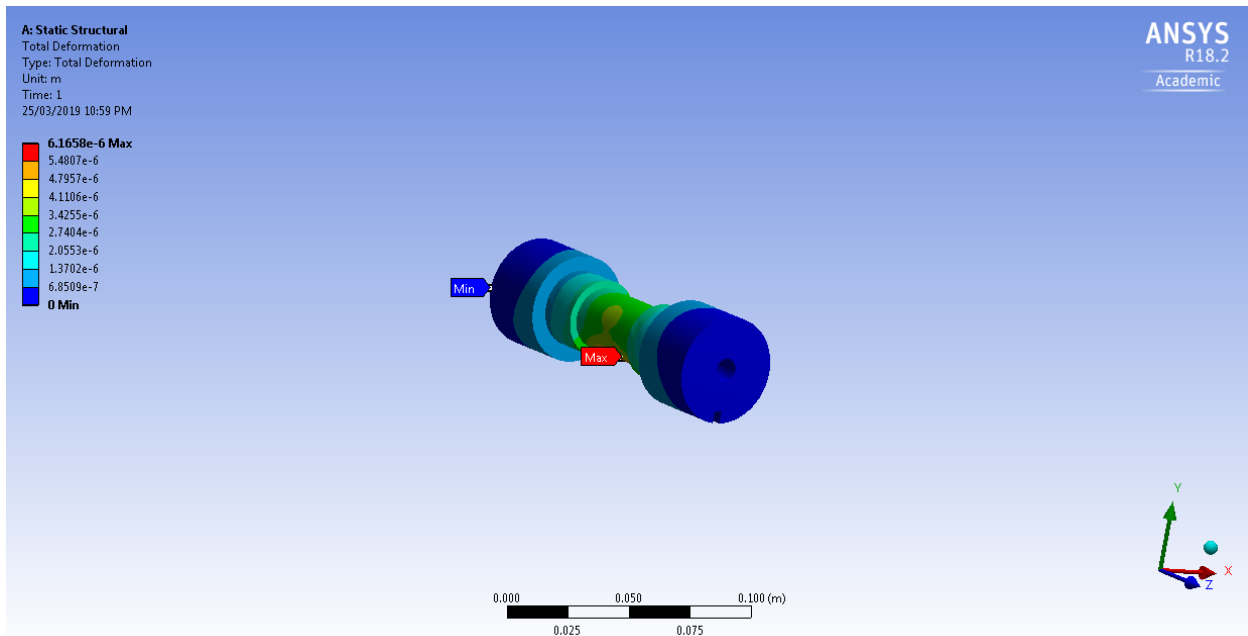


Figure G.8: NLG Total Deformation with 0.8 Drag Component

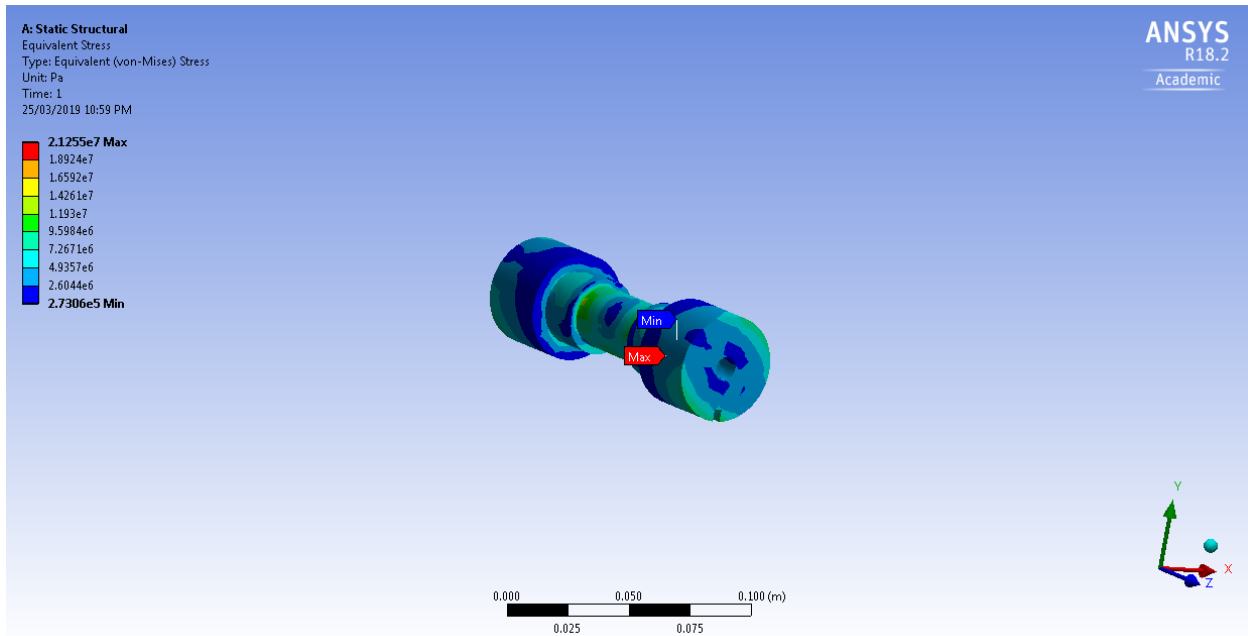


Figure G.9: NLG Equivalent Stress with 0.8 Drag Component

The following figures are the results of the limit force components at the axle for forward loads.

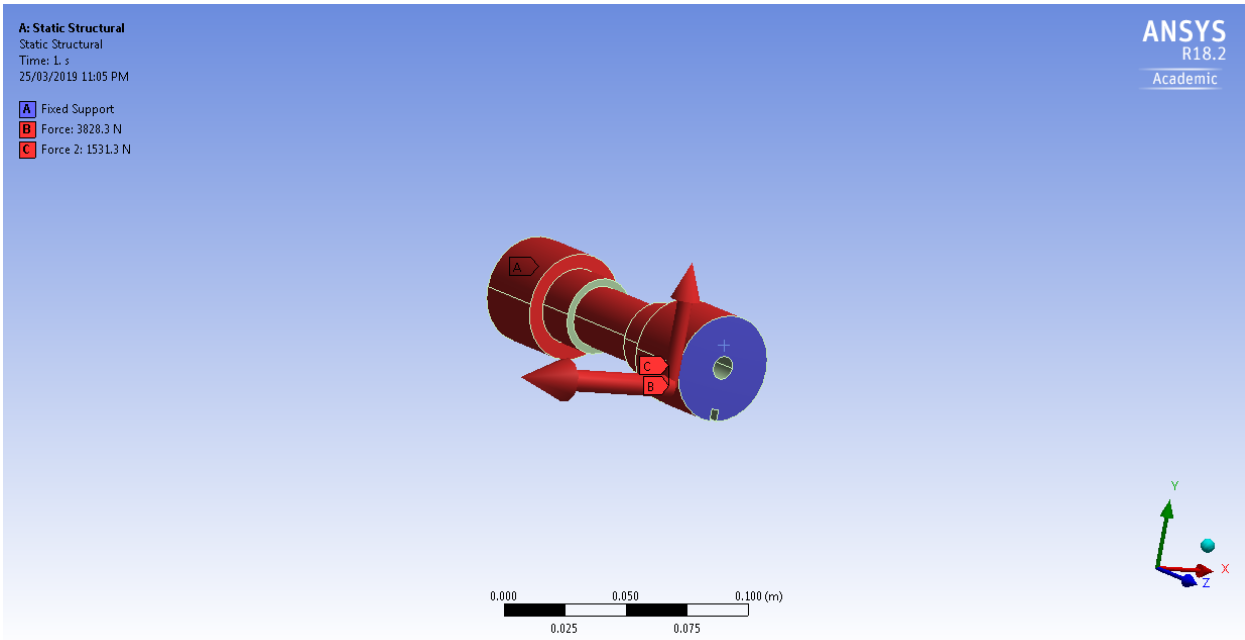


Figure G.10: NLG Layout with Foward Component of 0.4

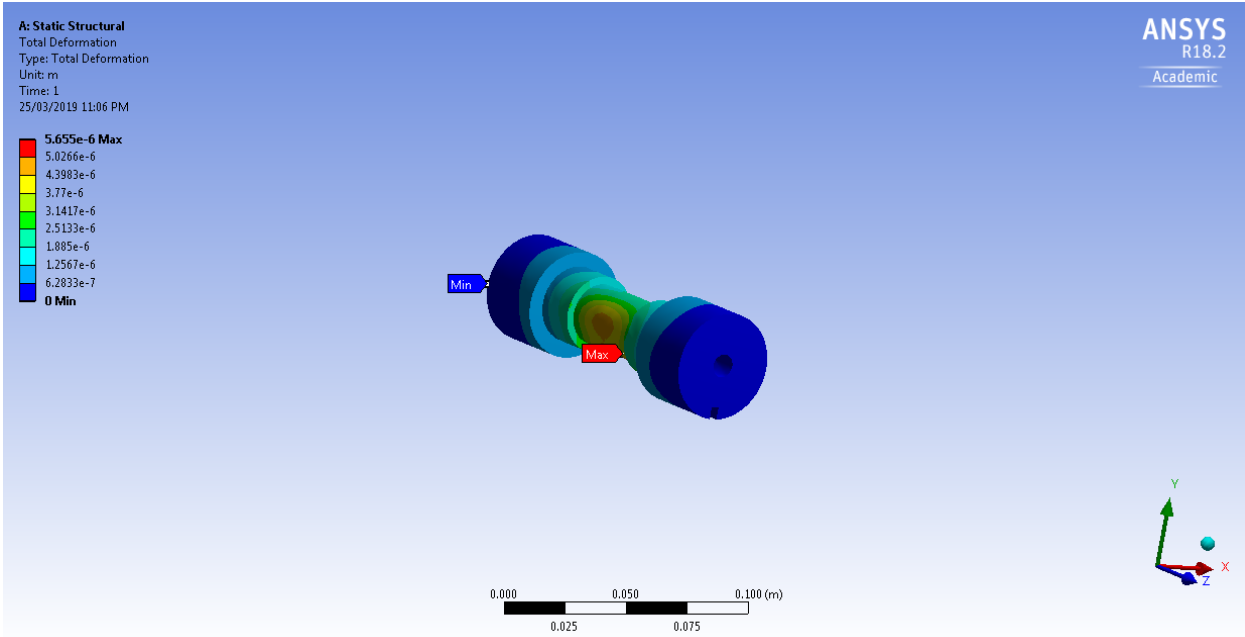


Figure G.11: NLG Total Deformation with Foward Component of 0.4

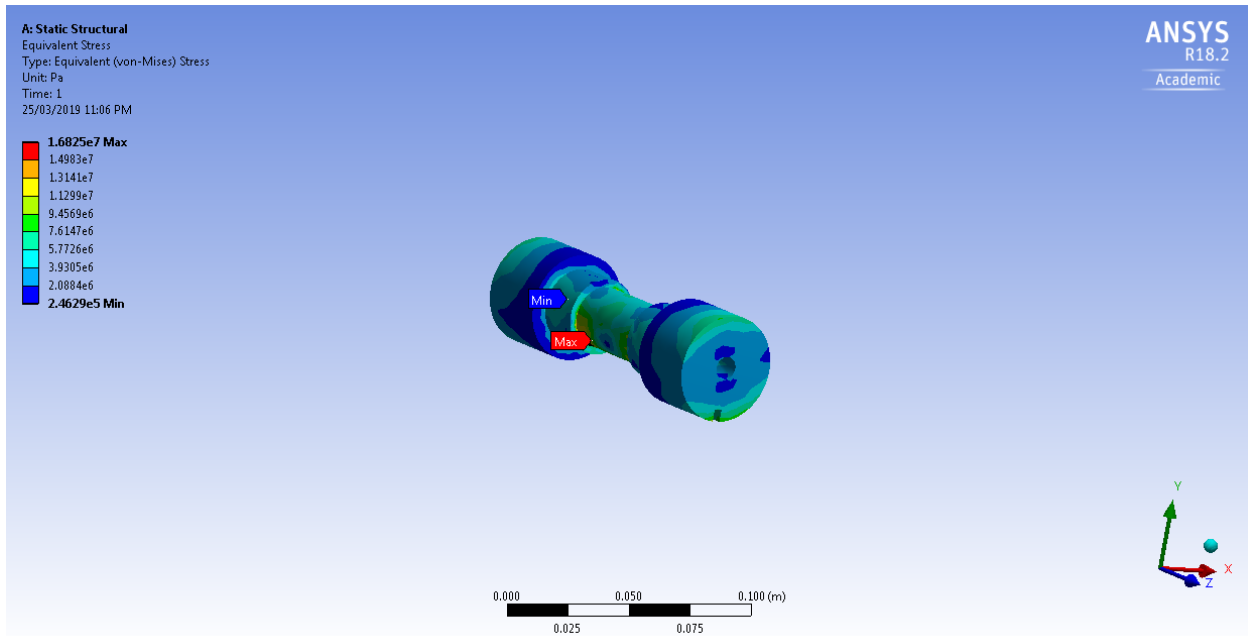


Figure G.12: NLG Equivalent Stress with Foward Component of 0.4

The following figures are the results of the limit force components at the axle for side loads.

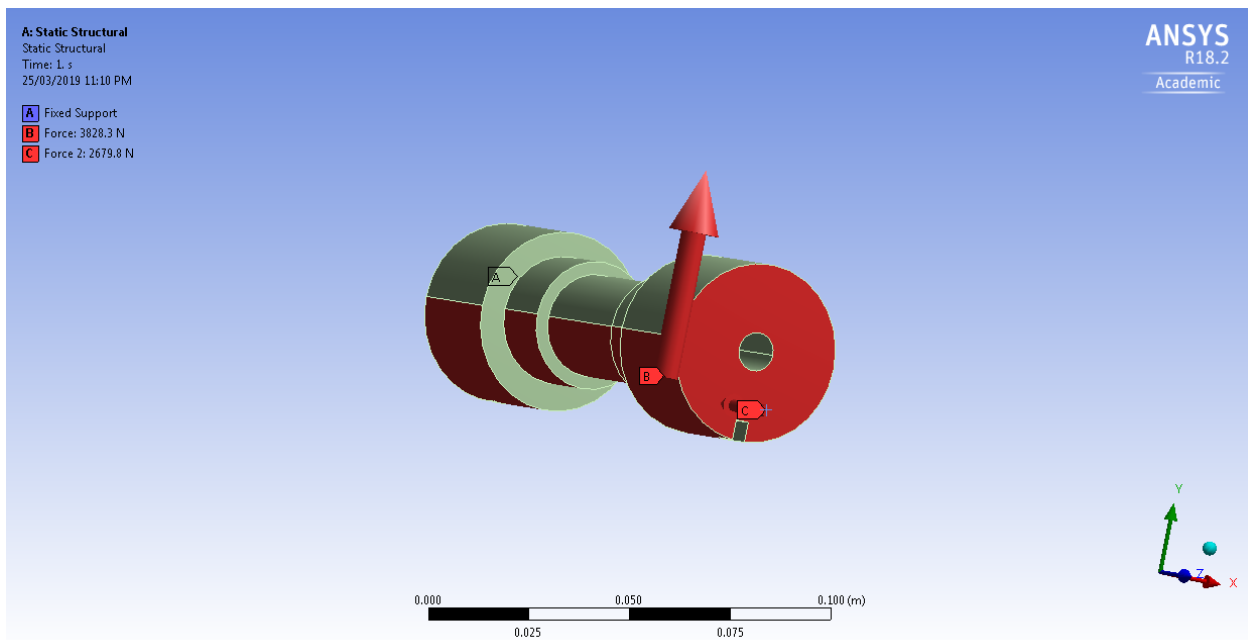


Figure G.13: NLG Layout with Side Component of 0.7

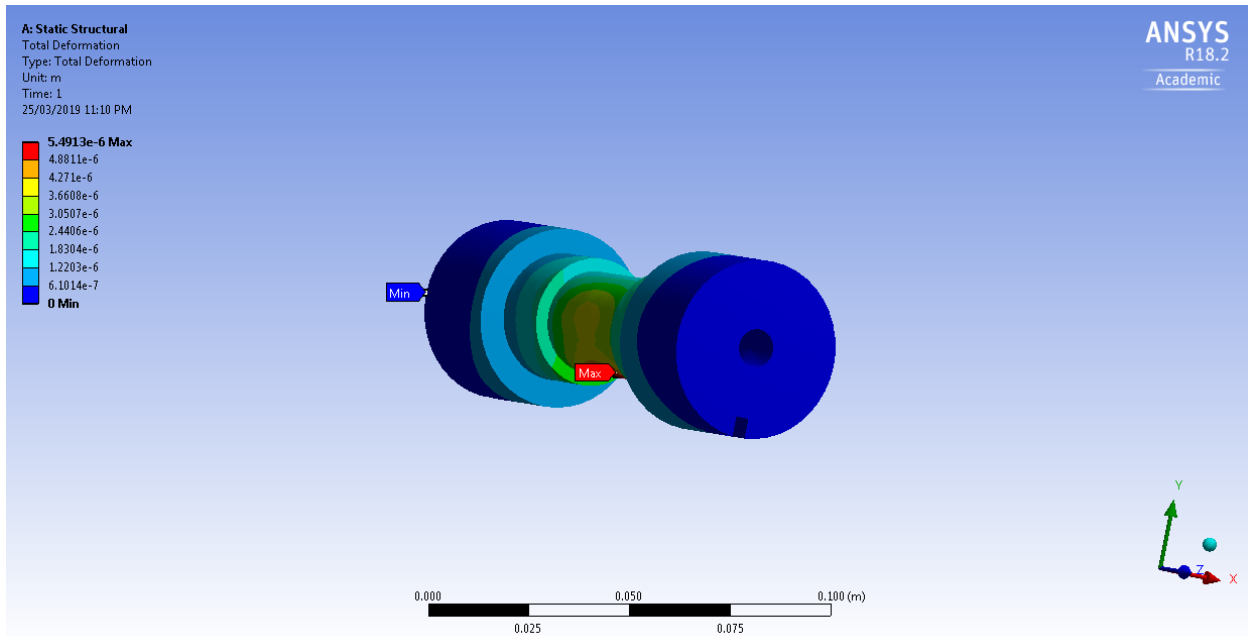


Figure G.14: NLG Total Deformation with Side Component of 0.7

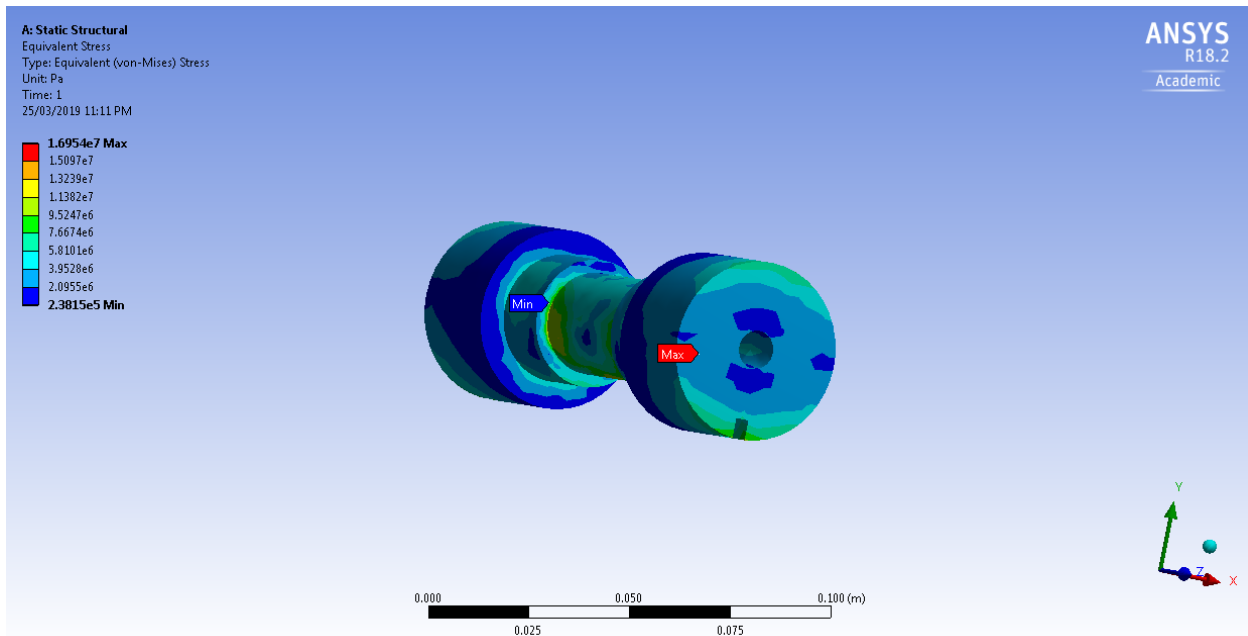


Figure G.15: NLG Equivalent Stress with Side Component of 0.7

523.509 Towing Loads:

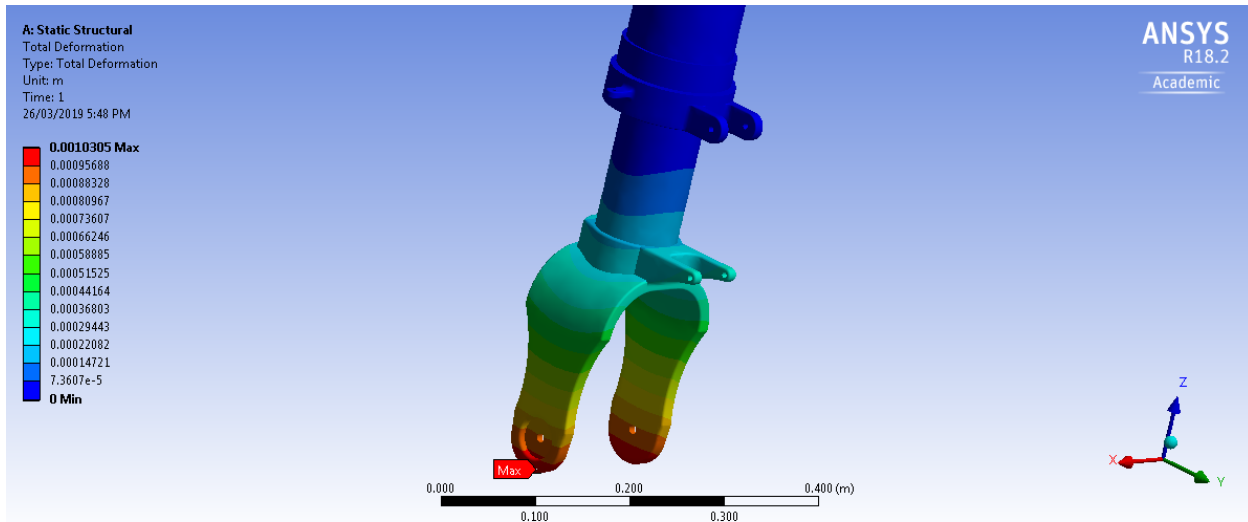


Figure G.16: Total Deformation of Swivelled Forward with 0.3W Load

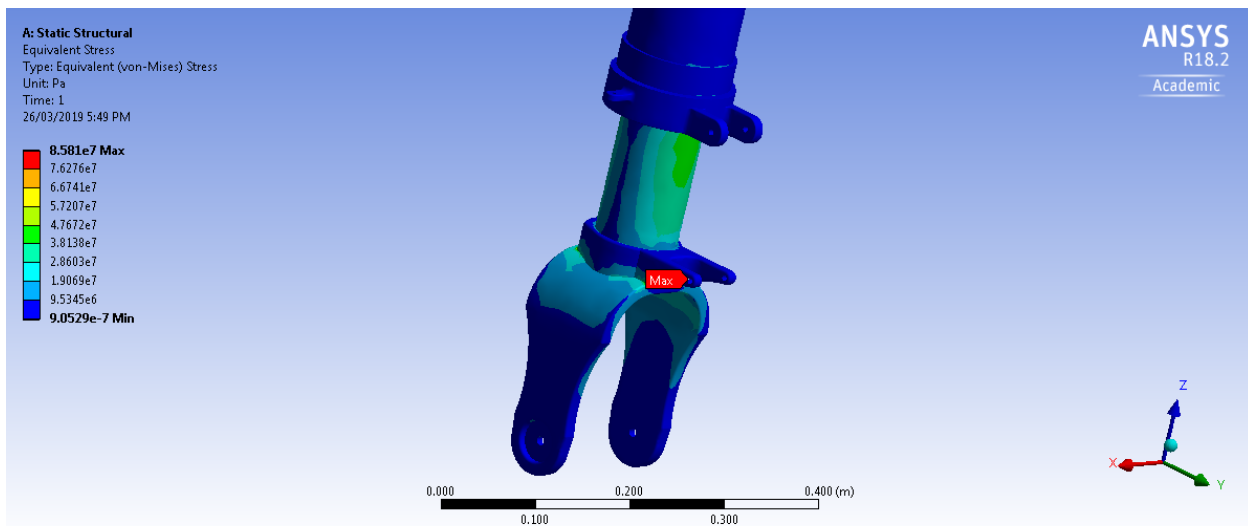


Figure G.17: Equivalent Stress of Swivelled Forward with 0.3W Load

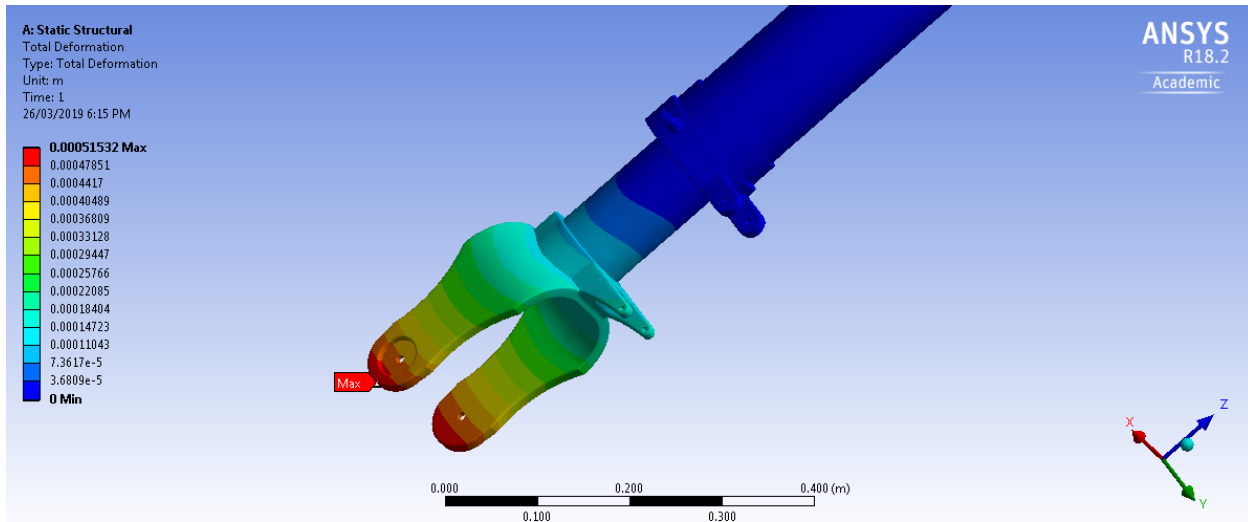


Figure G.18: Total Deformation of Swivelled 45 deg Forward with 0.15W Load

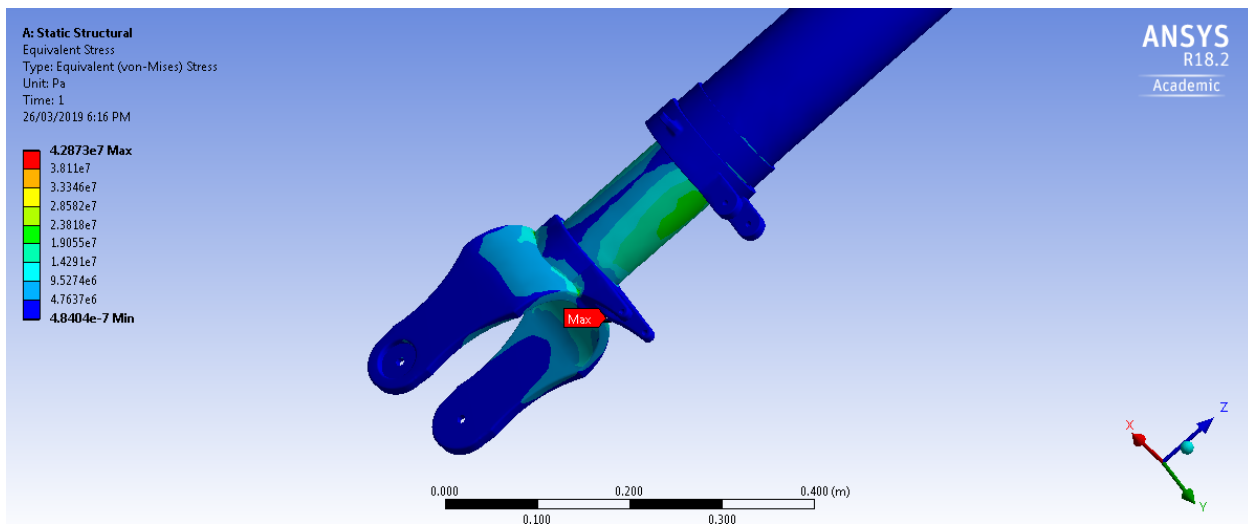


Figure G.19: Equivalent Stress of Swivelled 45 deg Forward with 0.15W Load